UNIVERSITA' VITA-SALUTE SAN RAFFAELE

CORSO DI DOTTORATO DI RICERCA INTERNAZIONALE IN MEDICINA MOLECOLARE

CURRICULUM IN BIOLOGIA CELLULARE E MOLECOLARE

THE ROLE OF THE POLYCYSTINS AND CILIA IN REGULATION OF MITOCHONDRIA AND METABOLISM

DoS: Dott.ssa Alessandra Boletta Alessandra Boletta

Second Supervisor: Prof.ssa Lotte Bang Pedersen

Tesi di DOTTORATO di RICERCA di Maria Elena Steidl

matr. 015602

Ciclo di dottorato XXXV

SSD BIO/13 – Biologia Applicata

Anno Accademico 2021/2022

CONSULTAZIONE TESI DI DOTTORATO DI RICERCA

Il/la sottoscritto/I **Maria Elena Steidl**

Matricola / registration number **015602**

nata a/ born at **Varese**

il/on **10/01/1994**

autore della tesi di Dottorato di ricerca dal titolo / author of the PhD Thesis titled

THE ROLE OF THE POLYCYSTINS AND CILIA IN REGULATION OF MITOCHONDRIA AND METABOLISM

☐ AUTORIZZA la Consultazione della tesi / AUTHORIZES *the public release of the thesis*

✓ NON AUTORIZZA la Consultazione della tesi per **12** mesi /DOES NOT AUTHORIZE *the public release of the thesis for 12 months*

a partire dalla data di conseguimento del titolo e precisamente / *from the PhD thesis date, specifically*

Dal / *from* **28/02/2023** Al / *to* **28/02/2024**

Poiché /*because*:

□ l'intera ricerca o parti di essa sono potenzialmente soggette a brevettabilità/ *The whole project or part of it might be subject to patentability;*

✓ ci sono parti di tesi che sono già state sottoposte a un editore o sono in attesa di pubblicazione/ *Parts of the thesis have been or are being submitted to a publisher or are in press;*

□ la tesi è finanziata da enti esterni che vantano dei diritti su di esse e sulla loro pubblicazione/ *the thesis project is financed by external bodies that have rights over it and on its publication.*

Si rende noto che parti della tesi sono indisponibili in relazione all'utilizzo di dati tutelati da segreto industriale **(da lasciare solo se applicabile)** /*Please Note: some parts of the thesis are not available in relation to the norm of the use of information protected by trade secret* ***(To leave only if relevant)***

Data /Date ....27/01/2023. Firma /Signature ....Maria Elena Steidl

DECLARATION

This thesis has been:

- composed by myself and has not been used in any previous application for a degree. Throughout the text I use both 'I' and 'We' interchangeably.

- has been written according to the editing guidelines approved by the University.

Permission to use images and other material covered by copyright has been sought and obtained. For the following image/s (specify), it was not possible to obtain permission and is/are therefore included in thesis under the "fair use" exception (Italian legislative Decree no. 68/2003).

All the results presented here were obtained by myself, except for:

1) ***NMR exometabolomics and LC-MS targeted metabolomics.***

NMR exometabolomics (Results, chapter 3.2, figure 3.2.4, 3.2.5, 3.2.6 and table 3.1, 3.2) were performed in collaboration with Dr. V. Mannella, Biomolecular Nuclear Magnetic Resonance Unit, Division of Genetics and Cell Biology, San Raffaele Scientific Institute, Milan, Italy. Current address: Center for Omics Sciences, San Raffaele Scientific Institute, Milan, Italy

LC-MS targeted metabolomics (Results, chapter 3.2, figure 3.2.7, 3.2.8; chapter 3.5, figure 3.5.1; chapter 3.6, figure 3.6.1, 3.6.2; chapter 3.7, figure 3.7.2, 3.7.3) were performed in collaboration with Dr.M. Yang MRC, Cancer Unit Cambridge, University of Cambridge, Hutchison/MRC Research Centre, Box 197, Cambridge Biomedical Campus, Cambridge, CB2 0XZ, United Kingdom. Current address: CECAD Research Center, Cologne, Germany, Division of Cell Biology Department, San Raffaele Scientific Institute, Milan, Italy.

2) ***Subcellular fractionation analysis.***

Subcellular fractionation analysis (Results, chapter 3.9, figure 3.9.1) was performed by Dr. E.A. Nigro, Molecular Basis of Cystic Kidney Disorders, Division of Genetics and Cell Biology, San Raffaele Scientific Institute, Milan, Italy.

1) ***Hematoxylin-eosin analysis of Ift88$^{flox/flox}$;KspCre mice at P35.***

Hematoxylin-eosin analysis of Ift88$^{flox/flox}$;KspCre (Results, chapter 3.6, figure 3.6.4) was performed by A. Fiocchi, UniSR Facility - Animal Histopathology, San Raffaele Scientific Institute, Milan, Italy. Mouse handling and bright-field imaging was performed by M. Chiaravalli Molecular Basis of Cystic Kidney Disorders, Division of Genetics and Cell Biology, San Raffaele Scientific Institute, Milan, Italy.

All sources of information are acknowledged by means of reference. Parts of the thesis have been published on the scientific journal Nature Metabolism (Steidl ME, Nigro EA, Nielsen AK, Pagliarini R, Cassina L, Lampis M, Podrini C, Chiaravalli M, Mannella V, Distefano G *et al* (2023) Primary cilia sense glutamine availability and respond via asparagine synthetase. *Nat Metab*).

AKNOWLEDGEMENTS

I would like to particularly thank my Director of Studies Dr. Alessandra Boletta for giving me the opportunity to scientifically grow in her group and for supervising my PhD training as my mentor. I also want to thank all my colleagues for the support and help in proceeding with my scientific training. Furthermore, I am grateful to my Second Supervisor Prof. Lotte Bang Pedersen for giving her feedback on my project of PhD thesis. Finally, I want to thank all our collaborators for both scientific discussions and experimental support to proceed with this thesis: in particular Dr. Giovanna Musco (my PhD tutor) and Dr. Valeria Mannella for NMR spectroscopy analysis, Prof. Christian Frezza and Dr. Ming Yang for LC-MS analysis, Dr. Angela Bachi and Dr. Laura Tronci for scientific discussions about the project, and also the ALEMBIC staff for the technical support for imaging and Amleto Fiocchi for hematoxylin and eosin staining. I am grateful to Fronzaroli family for the funding of my PhD bursary. This research was supported by fundings of Dr. Alessandra Boletta's lab.

ABSTRACT

Investigating the still not completely uncovered role of cilia could shed light on their function both in physiological and in pathological contexts. Primary cilia are solitary organelles that protrude from most mammalian cells and are considered as “antennae” that could regulate cellular responses to different *stimuli*. Their dysfunction leads to a wide range of disorders called ciliopathies, frequently characterized by polydactyly, blindness, obesity, and renal cystogenesis. In my thesis we found that primary cilia respond to nutrient availability and facilitate glutamine utilization through anaplerosis by asparagine synthetase (ASNS). In particular, our analyses revealed that cilia elongate upon a metabolic stress such as nutrient deprivation and that glutamine, but not glucose, is able to shorten cilia, by driving mitochondrial respiration and, as a consequence, ATP production. Our results show that cilia-deficient cells display impaired nutrient utilization and energy production. Indeed, the absence of cilia induces decreased energy charges and impairs fatty acid oxidation upon nutrient deprivation. Furthermore, cilia-deficient cells are less able to utilize glutamine to drive mitochondrial respiration. The absence of cilia induces the decrease of asparagine levels, suggesting that ASNS could mediate the ciliary response to glutamine. Indeed, while asparagine supplementation and degradation by asparaginase (ASNase) does not dramatically affect cilia length in response to glutamine, interfering with *Asns* significantly elongates cilia and impairs the capability of the cell to respond to glutamine in terms of ciliary shortening and mitochondrial respiration. These results suggest that cilia facilitate glutamine usage into mitochondrial respiration through its ASNS-driven conversion into glutamate. Importantly, we found that ASNS localizes at the centrosome-cilium complex, strengthening its role in the ciliary regulation of glutamine usage. In conclusion, this thesis reveals a new role of cilia as sensors of nutrient availability and regulators of cellular metabolism by driving glutamine usage through ASNS to fuel mitochondrial respiration and, as a consequence, energy production. These findings could be relevant not only to understand the cilia role in physiology, but also to possibly find new therapeutic approaches to treat ciliopathies.

I TABLE OF CONTENTS

I TABLE OF CONTENTS

II ACRONYMS AND ABBREVIATIONS

2,3-BPG	2,3-biphosphoglycerate
2-DG	2-deoxy-D-glucose
5HTR6	Serotonin receptor 6
AC	Adenylyl cyclase
ACLY	ATP citrate lyase
ACSLs	acyl-CoA synthases
ADPKD	Autosomal dominant polycystic kidney disease
AgRP	Agouti-related peptide
ALDO	Aldolase
ALMS	Alström syndrome
AMPK	AMP-activated protein kinase
ARL13B	ADP-ribosylation factor-like protein 13 B
ARPKD	Autosomal recessive polycystic kidney disease
ASNase	Asparaginase
ASNS	Asparagine synthetase
ATG16L1	Autophagy related 16 like 1 protein
BBIP10	BBSome interacting protein 10
BGP	Biphosphoglycerate;
BPGM	Biphosphoglycerate mutase (gene);
CAMK1D	Calcium/calmodulin dependent protein kinase 1D
cAMP	Cyclic AMP
CDCA	Cilia-dependent cyst activation
CEP290, 97	Centrosomal protein
CKD	Chronic kidney disease
CKI	Casein kinase I
CP110	Centriolar coiled coil protein 110
CPT1-2	Carnitine palmitoyl transferase 1-2
CUX1	Cut-like homeobox 1
CV	Ciliary vesicle
DAs	Distal appendages

DHA	Docosahexaenoic acid
DHAP	Dihydroxyacetone phosphate
DHH	Desert hedgehog
DRD1	Dopamine receptor 1
DVL	Dishevelled
DZIP1L	DAZ-interacting protein 1-like protein
ECAR	Extracellular acidification rate
eIF2α	Eukaryotic translation elongation 2 subunit α
ENO	Enolase
EPAC	Exchange protein directly activated by cAMP
ESCRT	Endosomal sorting complex required for transport
ESRD	End-stage renal disease
ELOVL	Fatty acid elongases
F	The Frizzled family of GPCRs
FAO	Fatty acid oxidation
FAS	Fatty acid synthesis
FASN	Fatty acid synthetase
FBP	Fructose-1,6-biphosphate
FFAR4	Free fatty acid receptor 4
FLCN	Folliculin
FTO	Fat Mass and Obesity-Associated gene
G6P	Glucose-6-phosphate
GADP	Glyceraldehyde-3-phosphate
GAPDH	Glyceraldehyde-3-phosphate dehydrogenase
GCN2	General control non derepressable 2
GDH	Glutamate dehydrogenase
GLI	Glioma-associated family
GLS	Glutaminase
GPCRs	G protein-coupled receptors
Gpi	Glucose phosphate isomerase
GPR161	G protein coupled receptor 161
GSK3	Glycogen synthase kinase

HH	Hedgehog
HK	Hexokinase
HK1	Hexokinase 1
hRPE	Human retinal pigment epithelium
HSP90	Heat shock protein 90
IF	Immunofluorescence
IFT	Intraflagellar transport
IGF-1R	Insulin-like growth factor receptor
IHH	Indian
INPP5E/OCRL	Inositol polyphosphate-5-phosphatases
IPPs	Polyphosphoinositides
IR	Insulin receptor
JBN	Jouberin
JS	Joubert syndrome
JSRD	JS related diseases
KAP3	KIF associated protein 3
KIF3a, b	Kinesin-like protein 3a, b
KISS1R	Kiss-peptin receptor 1
LDH	Lactate dehydrogenase
LDHA	Lactate dehydrogenase
LPR	Lipoprotein receptor-related protein
MCHR1	Melanin-concentrating hormone receptor 1
MDCK	Madin Darby Canine Kidney cells
MEF	Mouse Embryonic Fibroblasts
mIMCD3	Mouse Inner Medullary Collecting Duct cells 3
MKS	Meckel syndrome
MRI	Magnetic Resonance Imaging
mTOR	Mechanistic target of rapamycin
MTS	Molar tooth sign
MYH9	Myosin heavy chain 9
NPHP	Nephrocystin
OCR	Oxygen consumption rate

OFD1	Oral-facial-digital type 1
OXPHOS	Oxidative phosphorylation
PCP	Planar cell polarity
PCVs	Preciliary vesicles
PDGFRα	Platelet-derived growth factor receptor α
PDH	Pyruvate dehydrogenase
PDK	Pyruvate dehydrogenase kinase
PEP	Phosphoenolpyruvate
PERK	PRK–like endoplasmic reticulum kinase
PFK	Phosphofructokinase
PGK	Phosphoglycerate kinase
PGM	Phosphoglycerate mutase
PI(3,4,5)P3	Phosphatidylinositol-3,4,5-bisphosphate
PI(4)P	Phosphatidylinositol-4-phosphate
PI(4,5)P2	Phosphatidylinositol-4,5-bisphosphate
PI3K	Phosphoinositide 3 kinase
PIK3R4/VPS15	Phosphoinositide-3-kinase regulatory subunit 4
PK	Pyruvate kinase
PKA	Protein kinase A
PKHD1	Polycystic kidney and hepatic disease 1
PKM2	Pyruvate kinase muscle isoform M2
PLD	Phospholipase D
POMC	Propiomelanocortin
PPARα	Peroxisome proliferator-activated receptor α
PPARγ	Peroxisome proliferator-activated receptor γ
PTCH1	Patched-1
ROS	Reactive oxygen species
RTKs	Receptor tyrosine kinases
SARA	SMAD anchor for receptor activation
SCD	Stearoyl-CoA desaturase
SHH	Sonic Hedgehog
SLC2A	Solute carrier family 2A

SMO	Smoothened
SSTR3	Somatostatin receptor 3
STK11/LKB1	Serine-threonine kinase 11
SUFU	Suppressor of FUSED
TCF	T-cell factor
TGFβ/BMP	Transforming factor β/bone morphogenetic pathway
TMEM67	Transmembrane protein
Tpi	Triose phosphate isomerase
TUB	Tubby family protein
TULP3	TUB like protein 3
TZ	Transition zone
VEGF	Vascular endothelial growth factor
α-KG	α-ketoglutarate

III LIST OF FIGURES AND TABLES

1. INTRODUCTION

1.1 Primary cilium at a glance

Cilia are cellular organelles protruding from the surface of cells of both unicellular organism, such as *Chlamydomonas* and *Trypanosoma*, and multicellular organisms, as vertebrates (Satir & Christensen, 2008). Cilia emanate from cells when they are non-dividing. Some examples of cilia in different tissues are reported in **Figure 1.1**, where cilia of cells of the oviduct, brain ventricle, kidney, limb bud, node, and chondrocytes are shown. (Barnes, 1961; Grillo & Palay, 1963; Marshall & Nonaka, 2006; Sorokin, 1962). These organelles show a diameter around 200 nm and variable length, usually between 2-10 μm, but with some exceptions about 200 μm in olfactory neurons. They could be divided into two main cathegories: motile cilia and immotile (primary) cilia (Reiter & Leroux, 2017; Satir & Christensen, 2008). Motile cilia (or flagella) could be multiple on the surface of a single cell and are able to drive the movement of the cell (such as spermatozoa) or of extracellular fluid (such as mucus in the airways) (Reiter & Leroux, 2017). Primary (or sensory) cilia are immotile and solitary on the surface of cells. They have been considered for a long time as a *vestigium* and only quite recently have been revealed to regulate the response of the cell to different *stimuli* both outside and inside the cell (Marshall & Nonaka, 2006). In general, ciliary sensing functions comprise mechanosensation, chemosensation, light sensation, and signalling. Indeed, they are defined as cellular “antennas” and their dysfunction leads to a wide range of disorders named ciliopathies, which affect a plethora of tissues and organs frequently leading to neurodevelopmental abnormalities, obesity, and renal cystogenesis (Reiter & Leroux, 2017). The following chapters will describe the ciliary structure and machineries, the ciliary membrane, the ciliogenesis process, the main ciliary signalling pathways, and the role of these organelles in pathology.

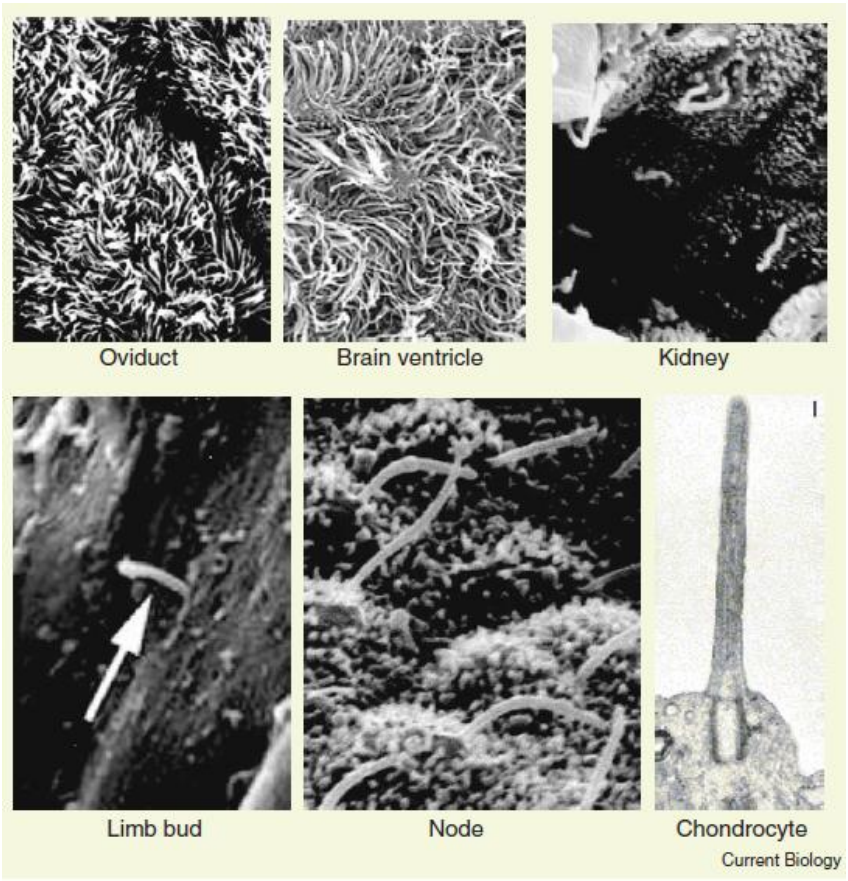

Figure 1.1 Cilia are present in different tissues and organs. *Images showing cilia present in oviduct, brain ventricles, kidneys, limb bud, node, and chondrocytes (Marshall & Nonaka, 2006).*

1.1.1 Structure and machineries

1.1.1.1 The basal body, the axoneme, and the transition zone

Cilia display three main components: the basal body, the axoneme, and the transition zone. The basal body is a specialized form of the mother centriole that allows the growth of the axoneme to build the cilium. The basal body is composed by triplets of microtubules and structures called sub-distal and distal appendages (DAs) (or transition fibers), which allow the docking of the basal body to the plasma membrane (Carvalho-Santos *et al*, 2011; Fisch & Dupuis-Williams, 2011). During the process of generation of the cilium (named ciliogenesis) the basal body allows the growth of the doublets of microtubules (each composed by a complete A tubule and an incomplete B tubule), which form the axoneme. Post-translational modified forms of tubulin, such as acetylated tubulin, have been found in cilia (Piperno & Fuller, 1985). Of note, also a role of axonemal glutamylation in the regulation of ciliary structure and function has been uncovered quite recently (Yang *et al*, 2021). One of the main differences in the structure of motile cilia compared to primary cilia is represented by a different axoneme structure. Indeed, motile cilia are characterized by 9 doublets of microtubules and 2 central microtubules named as the central doublet, leading to a 9+2 axonemal structure (**Fig. 1.2**) (Reiter *et al*, 2012; Reiter & Leroux, 2017; Satir & Christensen, 2008). Furthermore, in contrast with primary cilia, motile cilia display inner and outer dynein arms to lead to the ciliary bending. Differently, primary cilia lack the central doublet, giving rise to a 9+0 axonemal structure (**Fig. 1.2**) (De Robertis, 1956; Porter, 1955; Reiter & Leroux, 2017). However, the structure of primary cilia is already controversial, since some recent studies by cryo-electron tomography show that primary cilia present the 9+0 structure only at the cilium base (Kiesel *et al*, 2020). Cilia are characterized by a transition zone (TZ), which consists of Y-shaped structures that connect the microtubules doublets of the axoneme with the ciliary membrane and is composed by about 30 proteins that assemble into protein complexes, such as nephrocystin (NPHP), CEP290, RPGRIP1L, and Meckel Syndrome (MKS) complexes, whose dysfunction causes ciliopathy-associated phenotypes as nephronophthisis, Meckel and Joubert Syndromes (**Fig. 1.2**) (Reiter & Leroux, 2017; Williams *et al*, 2011). The TZ is considered as a gate that regulates the entry and exit of proteins at cilium and defines the protein content of cilia. The TZ function is crucial, since cilia do not have ribosomes and consequently the ciliary proteins

need to reach the cilium from the cytoplasm (Garcia-Gonzalo *et al*, 2011; Najafi *et al*, 2012). One of the key factors that discriminate the proteins that will access the cilium through the TZ is the molecular weight. Indeed, proteins in the range of 50-100 kDa can pass through the TZ to enter into the cilium. This leads to consider the TZ as a diffusion barrier for membrane proteins, due to the presence of septins, such as Septin-2 (Awata *et al*, 2014; Breslow *et al*, 2013; Garcia *et al*, 2018; Hu *et al*, 2010). Indeed, mutations in components of the TZ cause the leakage of several ciliary proteins (Jensen *et al*, 2015; Nachury & Mick, 2019; Williams *et al.*, 2011). Since the TZ displays binding sites, this ciliary component functions also as binding/pausing waypoint for ciliary membrane proteins, such as Smoothened, which has been found to pause at the TZ of the cilium (Milenkovic *et al*, 2015; Shi *et al*, 2017). However, the complexity of the process of entry and exit of ciliary proteins into the cilium is still not fully understood and seems to require other machineries than the TZ. Three other sub-compartments of the cilium are represented by the ciliary matrix, which is a fluid phase of the cilium between the axoneme and the ciliary membrane containing proteins of the intraflagellar transport (IFT) (described in **Chapter 1.1.1.2**), by the ciliary membrane (described in **Chapter 1.1.1.3**), and by the ciliary tip, which has been found as a site for extracellular vesicle budding for excess signalling molecules removal and cilium length regulation (Long *et al*, 2016; Marshall & Nonaka, 2006; Nager *et al*, 2017; Phua *et al*, 2017). Another important component of the cilium is represented by a specialized plasma membrane compartment near the cilium and characterized by a peculiar lipid and protein composition, named as ciliary pocket.

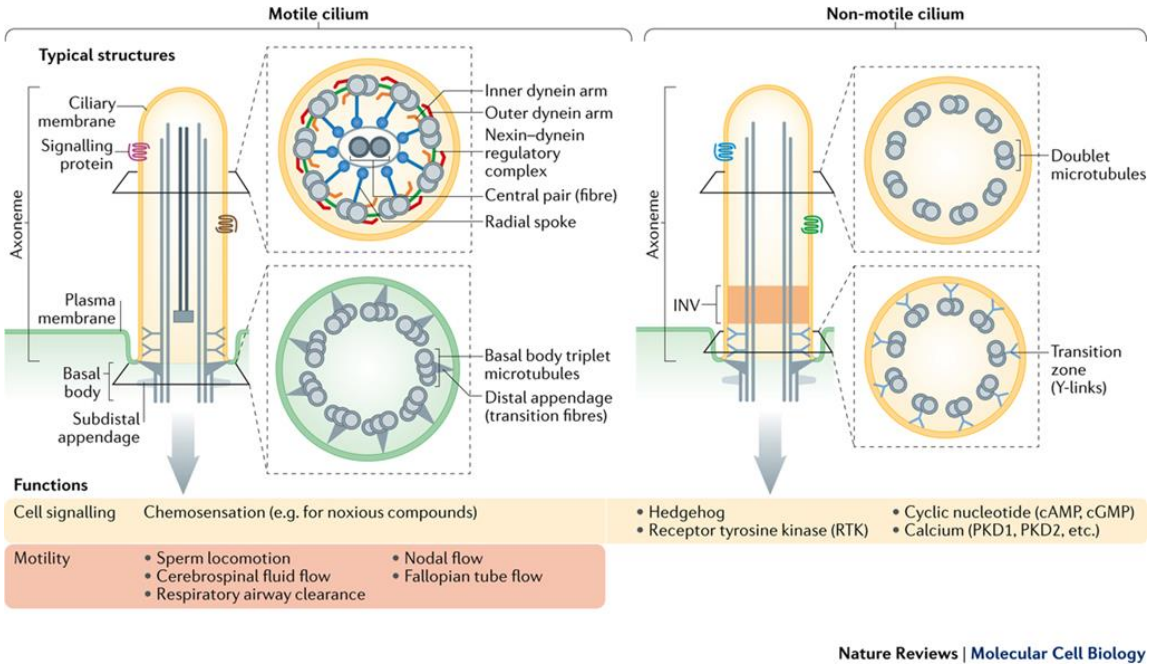

Figure 1.2 Schematic representation of motile and non-motile cilia structures. *Motile cilia are characterized by a 9+2 axonemal structure: their function is related to motility and chemosensation. Non-motile cilia are characterized by a 9+0 axoneme. These immotile cilia display sensory functions primarily through Hedgehog, receptor tyrosine kinase (RTK), cyclic nucleotide (cAMP, cGMP, and calcium (PKD1, PKD2) signalling pathways (Reiter & Leroux, 2017).*

1.1.1.2 The intraflagellar transport and the BBSome

The intraflagellar transport (IFT) is a complex ciliary machinery that allows the trafficking of different kinds of protein cargoes on the ciliary axoneme and it is responsible for the assembly and maintenance of cilia (Kozminski *et al*, 1993; Lechtreck, 2015). IFT was discovered in *Chlamydomonas reinhardtiii* in 1993, when movement of particles from the base to the tip of flagella was observed (Kozminski *et al.*, 1993). Indeed, this trafficking system is bidirectional, since it can move cargoes from the base to the tip of primary cilia (anterograde) and from the tip to the base (retrograde). The building blocks of IFT are the IFT trains, complexes of proteins formed by IFT-particles and IFT motors, which propel IFT particles on the axoneme (**Fig. 1.3**) (Jekely & Arendt, 2006; Lechtreck, 2015; van Dam *et al*, 2013). The assembly of IFT particle proteins, which are divided into IFT-A and IFT-B proteins, leads to the generation of IFT-A and IFT-B subcomplexes, which together form IFT-particles. The latter together with IFT motors form IFT-A complexes and IFT-B complexes (Pigino *et al*, 2009). IFT-A complexes are responsible for the retrograde transport by binding cytosolic dynein, while IFT-B complexes are involved in the anterograde transport by binding to the plus-end directed kinesin-2 (**Fig. 1.3**) (Cole, 1999; Gibbons *et al*, 1994; Lechtreck, 2015).

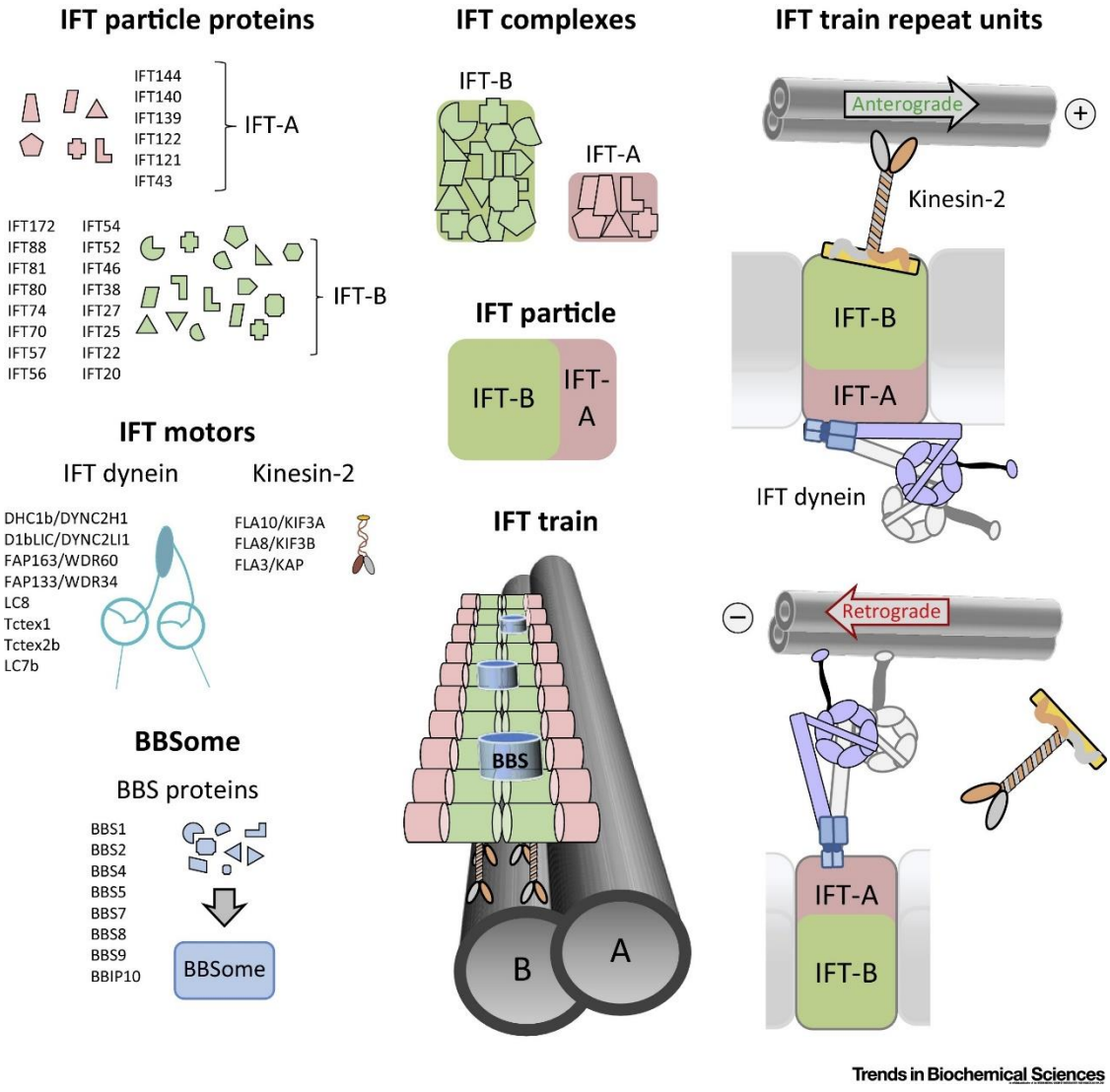

Figure 1.3 Intraflagellar transport components. *IFT particle proteins are classified in IFT-A and IFT-B proteins, leading to IFT-A and IFT-B complexes formation, respectively. IFT-A and IFT-B complexes form IFT particles. IFT motors are IFT dynein (anterograde transport) and kinesin-2 (retrograde transport). The BBSome is composed by BBS proteins. IFT trains consist of IFT particles, IFT motors and the BBSome (Lechtreck, 2015).*

Cytosolic dynein responsible for the retrograde transport is minus-end directed and composed by a heavy chain, an intermediate chain, an intermediate light chain, and multiple light chains (Asante *et al*, 2014; Criswell *et al*, 1996). Kinesin-2 responsible for the anterograde transport is plus-end directed and is a heterotrimeric complex composed by the motor subunits kinesin-like protein 3 a (KIF3a) and b (KIF3b), and the non-motor subunit KIF associated protein 3 (KAP3) (Cole *et al*, 1993). Examples of IFT cargoes are tubulin and axonemal dyneins. Since their loading on anterograde IFT is high in growing cilia and low in assembled cilia, this suggests that IFT loading is regulated by the length of cilia. Interestingly, tubulin can diffuse through the assembled cilium without need to be transported by anterograde IFT. Another key player in IFT is the BBSome, whose name derives from the Bardet-Biedl Syndrome, since mutations in genes encoding for its proteins lead to this disease, characterized by polydactyly, cognitive retardation, retinal degeneration, renal cystogenesis, and usually obesity (Asante *et al.*, 2014; Criswell *et al.*, 1996; Sheffield, 2010; Wingfield *et al*, 2018). The BBSome consists of 8 subunits (BBS1, BBS2, BBs4, BBS5, BBS7, BBS8, BBS9, BBS18/BBIP10), which are considered as the core BBS machinery. The BBSome is considered as an adapter of the transport of ciliary membrane proteins and a key regulator of ciliary retrieval cooperating with the retrograde IFT (Jin *et al*, 2010; Liu & Lechtreck, 2018; Loktev *et al*, 2008; Nachury *et al*, 2007). In particular, the BBSome is responsible for the removal from the cilia of β-arrestin 2-recognized G-protein coupled receptors (GPCRs), like GPR161, by transporting them through the TZ (Ye *et al*, 2018) and leading them to undergo lateral diffusion through the plasma membrane or endocytosis at the level of the periciliary membrane/ciliary pocket (**Fig. 1.4**) (Lechtreck *et al*, 2009; Nachury & Mick, 2019; Wingfield *et al.*, 2018).

Other then GPCRs, the BBSome retrieval machinery is also responsible for the removal from cilia of non-resident proteins, like phospholipase D (PLD).

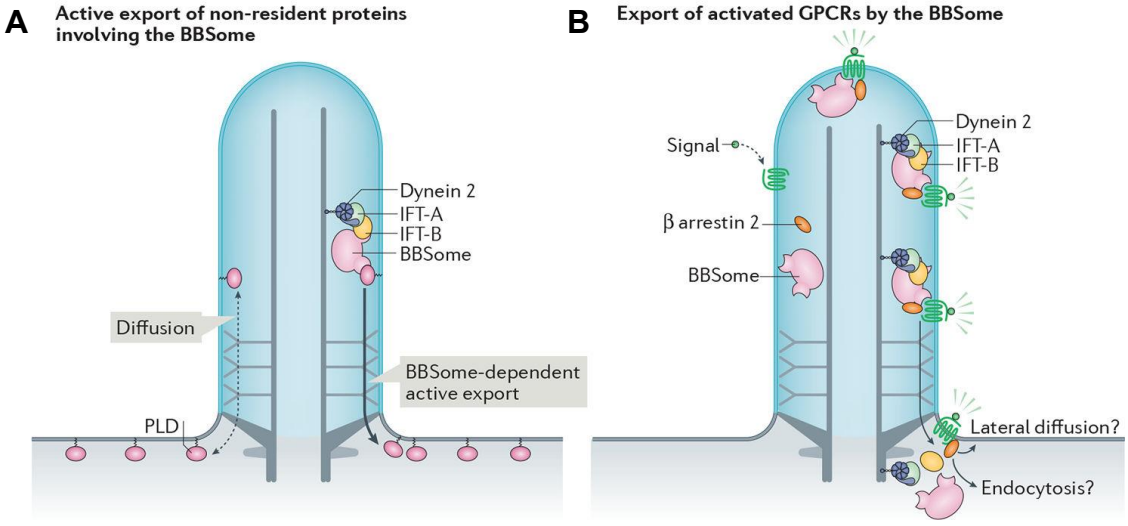

Figure 1.4 Schematic representation of protein export by the BBSome*. The BBSome mediates the export of both non-resident proteins (A) and activated GPCRs (B). The alatter involves β-arrestin 2 and results in later diffusion or endocytosis. Adapted from (Nachury & Mick, 2019).*

Another way of the cilia to remove ciliary content is represented by ectocytosis, which is the process by which extracellular vesicles (ectosomes) bud from the tip of the cilium mediated by the endosomal sorting complex required for transport (ESCRT) (Hurley, 2015; Long *et al.*, 2016). Even GPCRs that are reported to be retrieved by the BBSome, such as GPR161, could undergo ectocytosis when the BBSome retrieval machinery is defective. Furthermore, since ectocytosis is dramatically efficient compared to the BBSome retrieval machinery, the removal of excess of ciliary component possibly occurs through ectocytosis rather than the BBSome machinery **Figure 1.5** (Nachury & Mick, 2019).

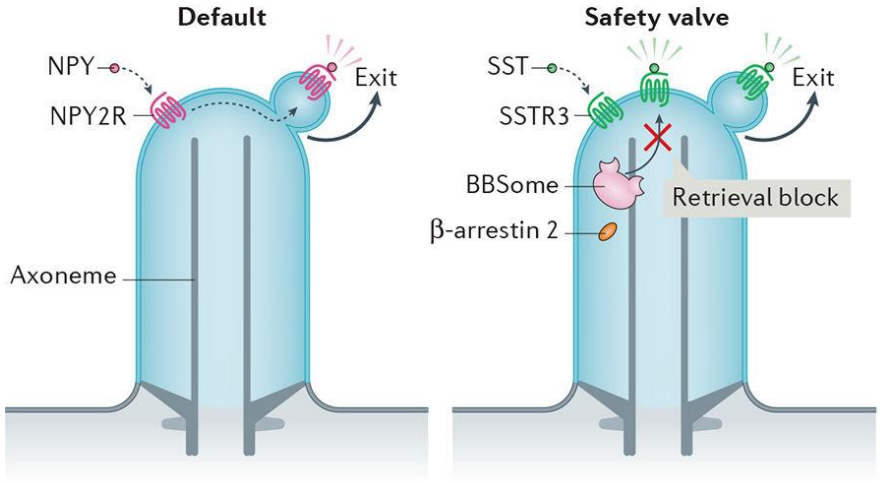

Figure 1.5 Ectocytosis*. Removal of excess content from cilia through ectosomes budding from the ciliary tip. When the BBSome retrieval machinery is blocked, the ectocytosis represents a safety valve for removal of ciliary components. Adapted from (Nachury & Mick, 2019).*

1.1.1.3 The ciliary membrane

Another feature of cilia is their specialized membrane, which is continuous with the plasma membrane and show peculiar protein and lipid composition. In particular the ciliary membrane is enriched in GPCRs (Hilgendorf *et al*, 2016) and proteins associated with Polycystic Kidney Disease, such as fibrocystin, whose mutations lead to Autosomal Recessive Polycystic Kidney Disease (ARPKD) (Ward *et al*, 2003), and polycystins-1 and -2, whose mutations cause Autosomal Dominant Polycystic Kidney Disease (ADPKD) (Pazour *et al*, 2002; Yoder *et al*, 2002). Lipid biosynthetic enzymes that are enriched in sub-ciliary compartments are responsible for the regulation and mainteinance of the lipid composition in the ciliary membrane. Polyphosphoinositides (PPIs), which are signalling lipids involved into the activation of ciliary pathways such as the Sonic Hedgehog, are highly represented into the ciliary membrane. In particular, in mammals phosphatidylinositol-4-phosphate (PI(4)P) is enriched in the ciliary membrane, while phosphatidylinositol-4,5-bisphosphate (PI(4,5)P2) and phosphatidylinositol-3,4,5-trisphosphate (PI(3,4,5)P3) are depleted in the ciliary membrane, but enriched in the TZ (Chavez *et al*, 2015; Dyson *et al*, 2017; Garcia-Gonzalo *et al*, 2015; Nechipurenko, 2020). This peculiar distribution is due to the activity of inositol polyphosphate-5-phosphatases (INPP5E and OCRL), which localize in mammalian cilia and are responsible for the conversion of PI(4,5)P2 or PI(3,4,5)P3 in PI(4)P and PI(3,4)P2 (**Fig. 1.6**) (Zhang *et al*, 2022).

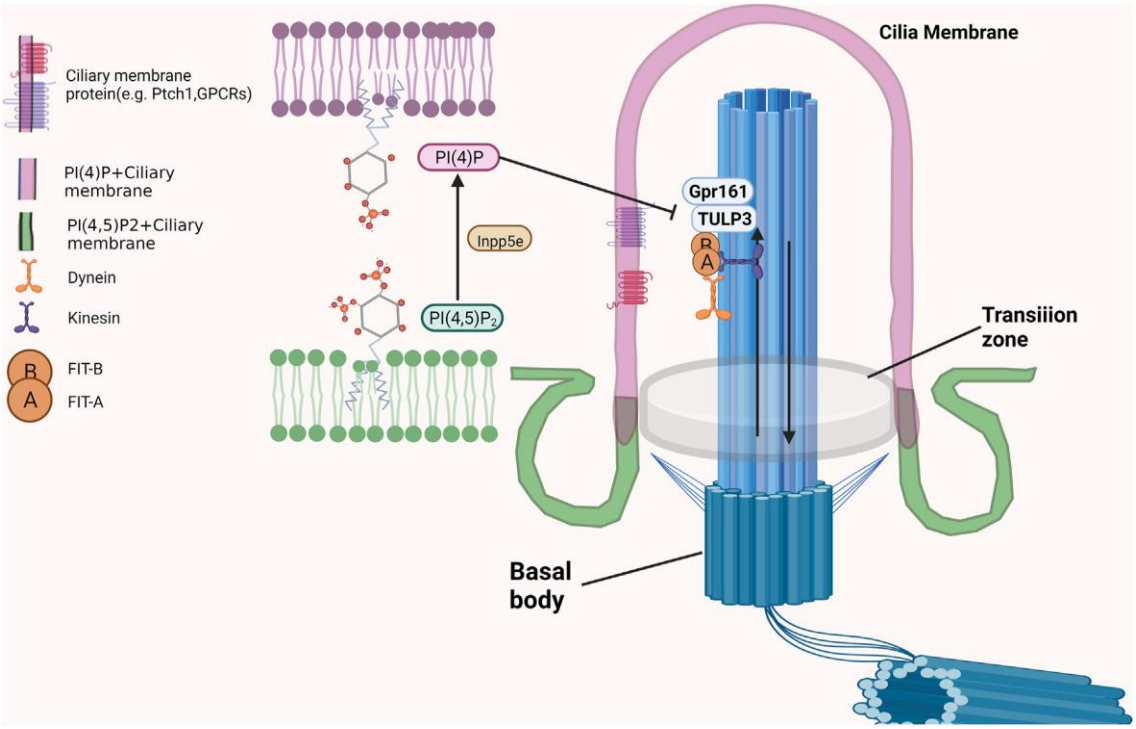

Figure 1.6 Schematic representation of polyphosphoinositides composition of the ciliary membrane*. Phosphatidylinositol-4-phosphate (PI(4)P) is enriched in the ciliary membrane, while phosphatidylinositol-4,5-bisphosphate (PI(4,5)P2) is enriched in the transition zone (TZ). Inositol polyphosphate-5-phosphatases (Inpp5e) converts of PI(4,5)P2 in PI(4)P. The activity of Inpp5e regulates TULP3 activation (Zhang et al, 2022).*

Indeed, *INPP5* mutations lead to Joubert and MORM syndrome, and *OCRL* mutations cause Lowe syndrome, due to accumulation of PI(4,5)P2 and depletion of PI(4)P in the ciliary membrane (**Fig. 1.7**) (Chavez *et al.*, 2015; Garcia-Gonzalo *et al.*, 2015; Jacoby *et al*, 2009; Prosseda *et al*, 2017; Zhang *et al.*, 2022).

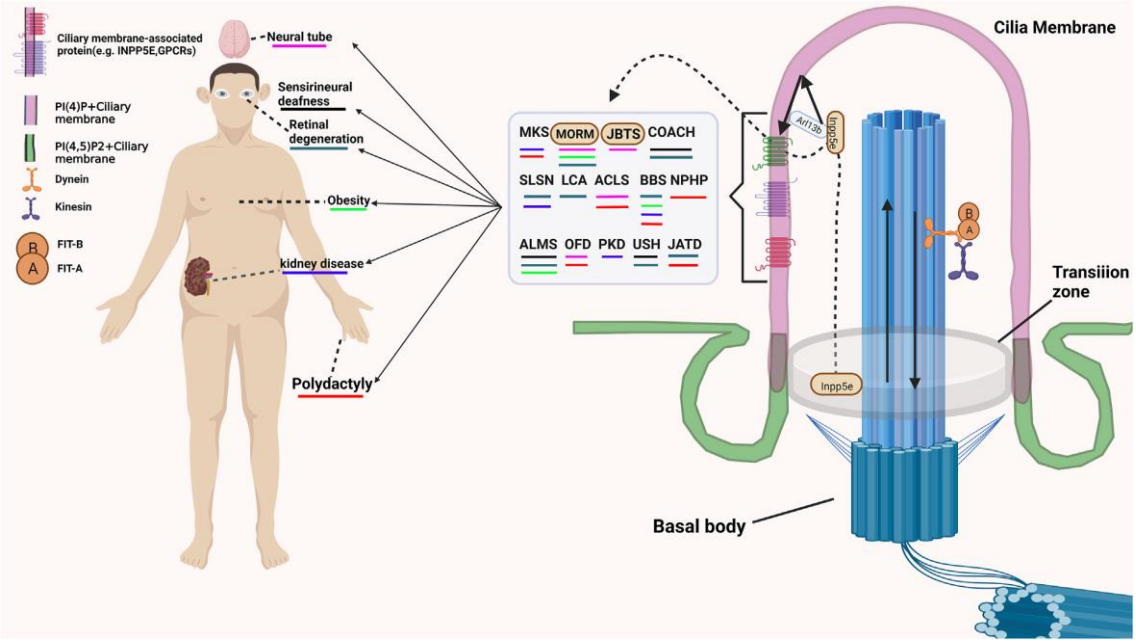

Figure 1.7 INPP5E and ciliopathies. *Mutations in Inpp5e cause Joubert (JBTS) and MORM syndromes, characterized by neurological defects, sensory abnormalities, retinal degeneration, obesity, kidney disease, and polydactyly (Zhang et al, 2022).*

PPIs cooperate to the trafficking of GPCRs and channels into the cilia through their interactions with tubby family proteins TUB/TULP3 (which are adapters for ciliary membrane proteins trafficking) to facilitate their association with the transmembrane proteins that are then delivered into the cilium (**Fig. 1.6**) (Badgandi *et al*, 2017; Mukhopadhyay *et al*, 2010). Furthermore, ciliary membrane displays the presence of lipid rafts, which are characterized by high levels of sphyngolipids and sterols (Kaneshiro *et al*, 1984; Montesano, 1979), which play a central role in the regulation of the Hedgehog (HH) pathway (Raleigh *et al*, 2018).

1.1.1.4 Ciliogenesis

Ciliogenesis is a process requiring multiple steps that lead to the biogenesis of cilia. It occurs when cells exit from the cell cycle (G0/G1 phase), when the centrioles are not involved in the formation of the mitotic spindle for cell division. The process of ciliogenesis could differ depending on the cell type and whether membrane remodeling events occur (Garcia *et al.*, 2018). The presence of two main processes of ciliogenesis have been described so far: the intracellular pathway, which is peculiar of fibroblasts, mesenchymal cells, and retinal pigment epithelium (hRPE1) cells, and the extracellular pathway, which is associated with polarized epithelial cells, such as Madin Darby Canine Kidney (MDCK) cells and multiciliated cells (Zhao *et al*, 2023). Interestingly it seems that murine Inner Medullary Collecting Ducts (mIMCD3) cells undergo both intracellular and extracellular ciliogenesis pathways, depending on cell density (Stuck *et al*, 2021; Wu *et al*, 2018). These data suggest that possibly also other cell types could display both ciliogenesis processes. The intracellular pathway is characterized by the docking of preciliary vesicles (PCVs) of about 50 nm of diameter to the distal appendages (DAs) leading to the formation of distal appendages vesicles (DAVs) (**Fig. 1.8 A**) (Zhao et al., 2023). These vesicles lead to the generation of the ciliary vesicle (CV) of about 300 nm. The growing axoneme is encased by a double membrane ciliary sheath, which subsequently fuses with the plasma membrane to generate the ciliary pocket. During the fusion of the outer face of the ciliary sheath to the plasma membrane, extracellular membrane tubules form and connect the ciliary membrane with the extracellular environment (Insinna *et al*, 2019). Alternatively, the extracellular pathway is characterized by the migration and docking of the mother centriole through the DAs to the plasma membrane before the cilium formation (**Fig. 1.8 B**) (Zhao et al., 2023). For multiciliated cells, centrioles duplicate through the deuterosome and then DAs and sub-distal appendages form during the migration towards the plasma membrane. Once DAs dock to the plasma membrane, several motile cilia originate (**Fig. 1.8 C**) (Zhao et al., 2023). Most of the knowledge about ciliogenesis belongs to the intracellular pathway, while the extracellular pathway is still to be uncovered. During both the processes of the mother centriole undergoes to uncapping through the removal of centriolar coiled coil protein 110 (CP110) and CEP97 by ubiquitin proteasomal cascade. The TZ assembly occurs before the axoneme and ciliary membrane growth, which involves IFT-B complex

and ciliogenesis regulators, such as ADP-ribosylation factor-like protein 13 B (ARL13B), which associates with the axoneme through tubulin, and RAB8 (Li *et al*, 2010).

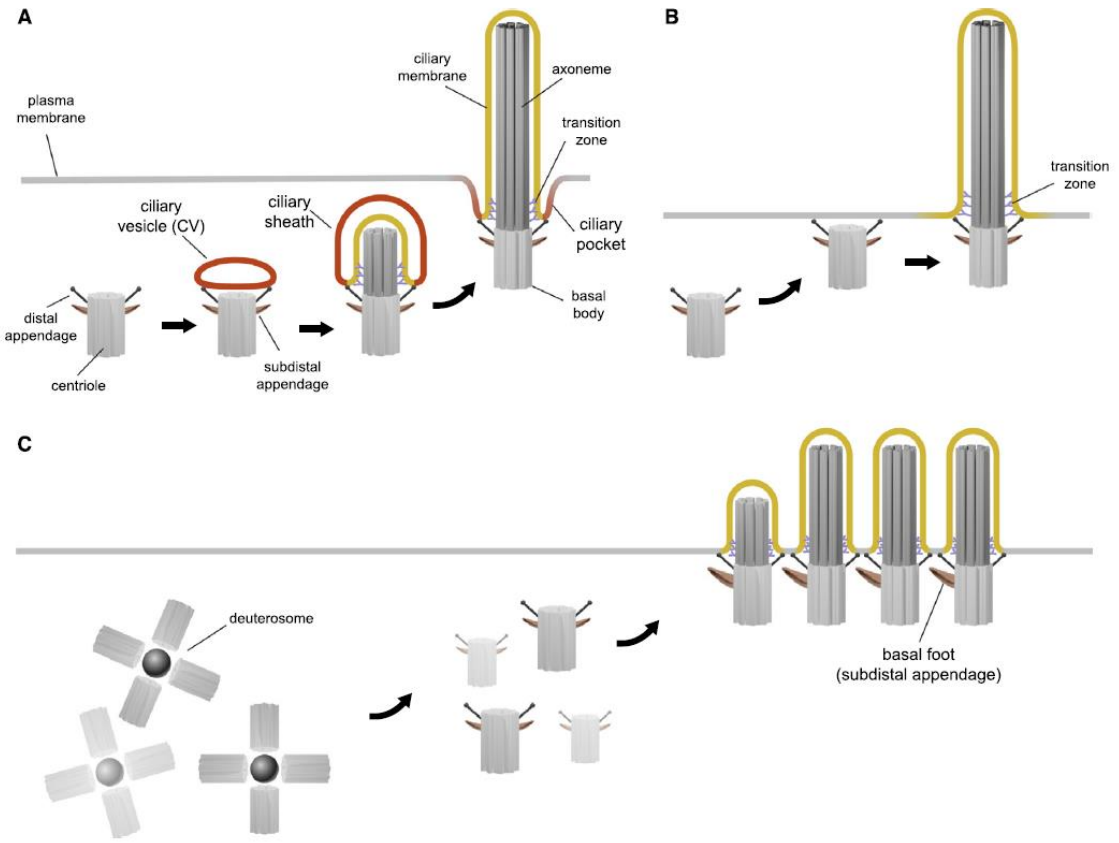

Figure 1.8 Scheme of different mechanisms of ciliogenesis. *A) The intracellular pathway involves the formation of the ciliary vesicle (CV), axoneme and ciliary sheath formation, which fuses with the plasma membrane to generate the ciliary pocket. B) The extracellular pathway consists of the docking of the distal appendages with the plasma membrane to generate the cilium. C) Multiciliated ciliogenesis mediated by deuterosomes Multiple centrosomes form and during the migration to the plasma membrane distal and subdistal appendages generate. After the docking to the plasma membrane several cilia assembly (Zhao et al., 2023).*

1.1.2 Cilia and signalling

1.1.2.1 Hedgehog signalling pathway

The Hedgehog signalling pathway is evolutionarily conserved and responsible for the development and homeostasis of tissues and organs. It owes its name to the phenotype induced by *Hh* mutations in larvae of *Drosophyla* that led to the lack of development of the segmented anterior-to-posterior body plan and to the generation of denticles resembling a Hedgehog (Nusslein-Volhard & Wieschaus, 1980). The activation of the pathway is due to the binding of HH ligand to the 12 transmembrane domains receptor Patched-1 (PTCH1). Three different HH ligands have been identified in mammals: Sonic (SHH), Indian (IHH), and Desert (DHH) Hedgehog, which differ principally for their tissue specificity. SHH is important for the specification of cell types in the nervous system and in patterning of the limbs; IHH is crucial in skeletal development; DHH is expressed in the gonads and promotes the differentiation of fetal Leydig cells and specification of adult Leydig cells and germ cells survival and spermatogenesis (Bangs & Anderson, 2017; Nygaard *et al*, 2015). The Hedgehog signalling pathway has been considered as a ciliary pathway since it has been found that the *wimple* (wim) and *flexo* (fxo) mouse mutants induced by ethylnitrosurea led to the loss of ventral neural cell types (whose specification depended on SHH) together with the disruption of IFT proteins (Huangfu *et al*, 2003). This discovery uncovered the essential role of the IFT machinery in the transduction of the HH signal (Huangfu *et al.*, 2003). In the absence of HH ligand, the HH pathway is kept off by the HH ligand receptor PTCH1, which is located in the membrane of the primary cilium due to its carboxyl terminal region of the last transmembrane domain (Kim *et al*, 2015). PTCH1 prevents the ciliary translocation of the 7 transmembrane domains receptor Smoothened (SMO), which belongs to the Frizzled (F) family of GPCRs (Bangs & Anderson, 2017). Interestingly, *Ptch1* loss induces the abnormal cell specification of all neural progenitors, irrespectively of the activation of the pathway, demonstrating PTCH1 role as a negative regulator of the HH pathway (Huangfu *et al.*, 2003). In the absence of the HH ligand, SMO does not translocate to the cilium and GPR161, which is a GPCR translocated at cilia by its binding to TULP3 and IFT-A, increases cyclic AMP (cAMP) levels through adenylyl cyclase (AC) activation via G proteins (Gαs) (**Fig. 1.9**) (Bangs & Anderson, 2017; Han *et al*, 2019; Mukhopadhyay *et al.*, 2010; Mukhopadhyay *et al*, 2013). When *Inpp5e* is

inactivated, PI(4,5)P_2, accumulate leading to the recruitment of TULP3, IFT-A, and GPR161 at cilia and, as a consequence, to the HH pathway inactivation irrespectively of the presence of HH ligand or SMO at cilia (Garcia-Gonzalo *et al.*, 2015). Among nine ACs that catalyze the conversion of ATP into cAMP, three have been identified at cilia (AC3, AC5, AC6), suggesting the importance of local production of cAMP at cilia to promote the transduction of signals (Bishop *et al*, 2007; Mick *et al*, 2015; Vuolo *et al*, 2015).

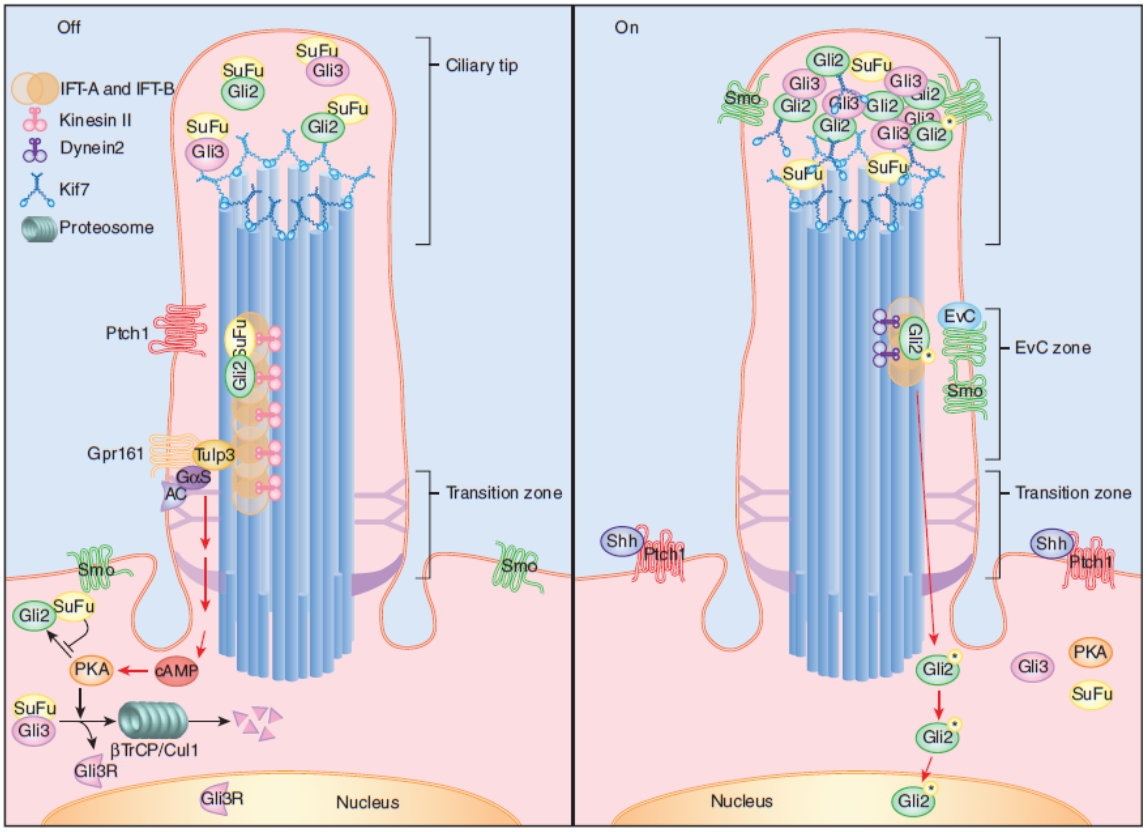

Figure 1.9 Hedgehog signalling pathway. *When the Hedgehog pathway is off, Patched1 (Ptch1) remains in the ciliary membrane. Gpr161 promotes the activation of adenylyl cyclase (AC) through GαS. This increases cAMP that activates protein kinase A (PKA) leading to proteolitical processing of Gli3, which is retained in the cytoplasm by Suppressor of FUSED (SuFu), to generate transcriptional repressor Gli3R. When Sonic Hedgehog (Shh) binds to Ptch1, the latter translocates to the plasma membrane. Smoothened (Smo) moves to the ciliary membrane and converts GLI2 into GLIA to the expression of target genes. Kif7 is enriched at ciliary tip where it binds Gli2 and Gli3. (Bangs & Anderson, 2017).*

Increased cAMP levels lead to the activation of protein kinase A (PKA). This conserved component of the HH signalling pathway is responsible of the phosphorylation of GLI3, a transcription factor belonging to the glioma-associated (GLI) family, which undergoes proteolitical processing becoming a repressor (GLIR) of the expression of HH target genes (**Fig. 1.10**) (Niewiadomski *et al*, 2014). In this context, the Suppressor of FUSED (SUFU) display a crucial role by keeping GLI3 in the cytoplasm and by inducing its proteolitical processing to convert it into GLI3R (Humke *et al*, 2010; Jia *et al*, 2009). Alternatively, when HH ligand binds to PTCH1, the latter is translocated outside the cilium and, at the same time, SMO is translocated to the cilium, converting full length GLI2 transcription factor to transcriptional activator (GLIA) able to drive the transcription of HH target genes (**Fig. 1.10**) (Niewiadomski *et al.*, 2014). When HH pathway is activated, GPR161 is removed from the cilium in a β-arrestin/IFT-A dependent manner.

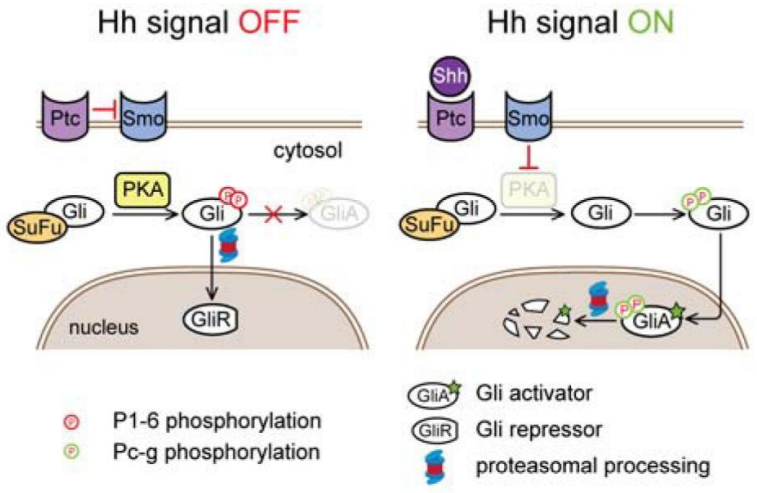

Figure 1.10 Schematic representation of HH signalling pathway. *When Hh signal is off, Ptch inhibits Smo translocation at cilium and SuFu retains Gli in the cytosol to undergo proteolytical processing to generate the repressor form GliR. When Hh signal is on, Smo tranlocates to cilia and full length Gli becomes an activator (GliA) of target gene ecpression. Adapted from (Niewiadomski et al., 2014).*

During the activation of the HH pathway, the enrichment of KIF7 in the ciliary tip occurs. KIF7 preferentially binds at the plus-end microtubules to the GTP-tubulin promoting the arrest of growth of the cilium (**Fig. 1.11 A**) (He *et al*, 2014). Indeed, cells lacking KIF7 show unstable cilia, due to overgrowth of the axoneme (**Fig. 1.11 B**) (He et al., 2014). Thus, KIF7 displays a crucial role in the organization of the ciliary tip and the regulation both positively and negatively of the HH signalling by its capability to bind to both GLI2 and GLI3 (Cheung *et al*, 2009; He *et al.*, 2014; Liem *et al*, 2009).

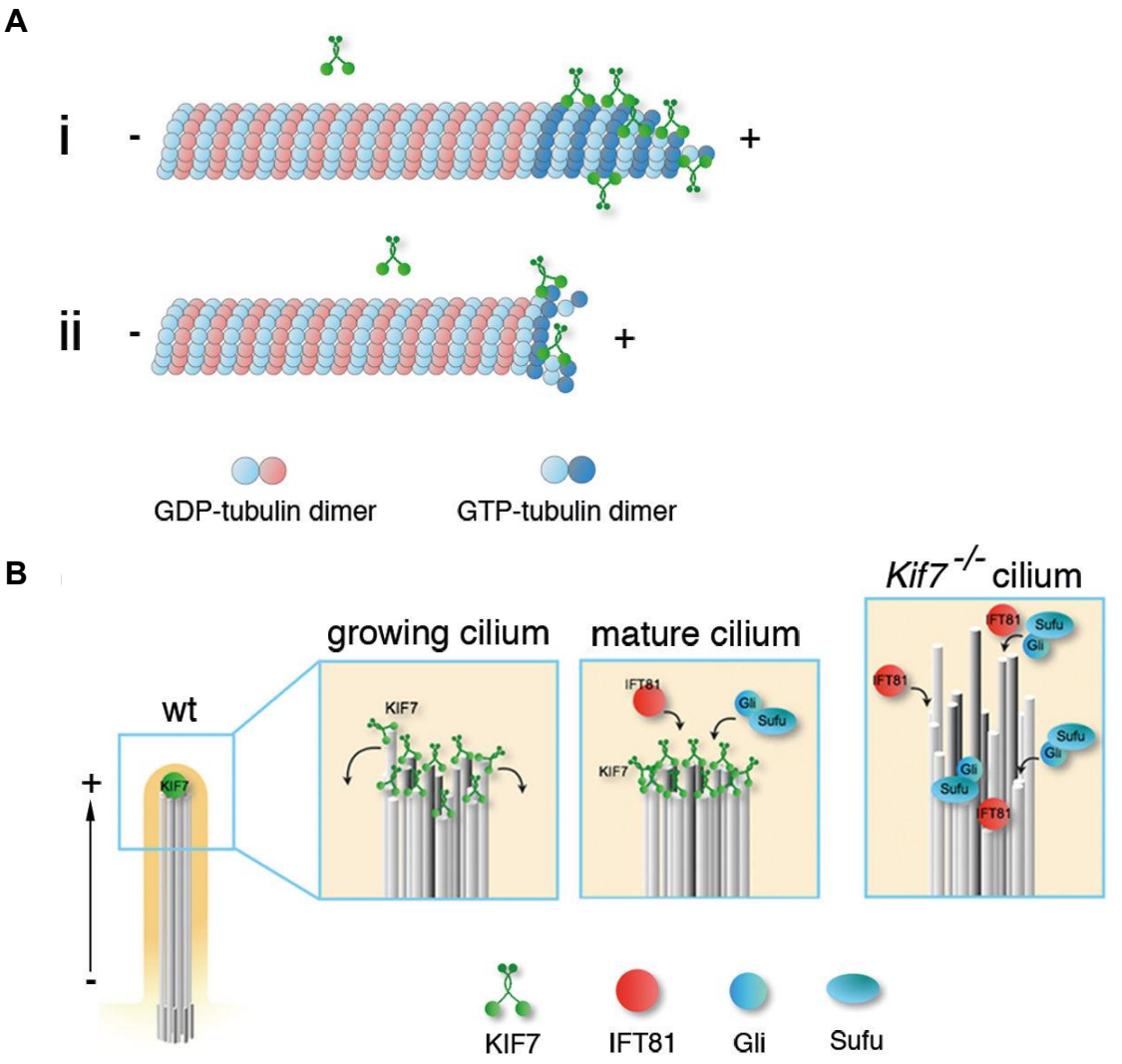

Figure 1.11 KIF7 activity at the ciliary tip. *A) KIF7 preferentially binds to GTP-tubulin inhibiting microtubules growth by blocking the adding of tubulin dimers (i) or by inducing the destabilization of GTP-tubulin cap (ii). B) KIF7 prevents overgrowth of microtubules of the growing cilium. In mature cilium, KIF7 form a ciliary tip compartment together with IFT81 and Gli-SuFu. In Kif7$^{-/-}$ cilium, microtubule growth is not controlled and synchronized generating long, unstable cilia. Adapted from (He et al., 2014)*

Interestingly, sterols have been reported to regulate the HH signalling pathway. Indeed, HH ligands are bound to a palmitoyl moiety at the N terminus and a cholesterol moiety at the C terminus, and oxygenated metabolites of cholesterol named oxysterols are able to bind to SMO and to induce its accumulation at cilia, driving HH pathway activation. Thus, since PTCH1 and SMO do not directly interact, a model where PTCH1 is the transporter of the sterol (second messenger) that activates SMO has been proposed (**Fig. 1.12**) (Radhakrishnan *et al*, 2020).

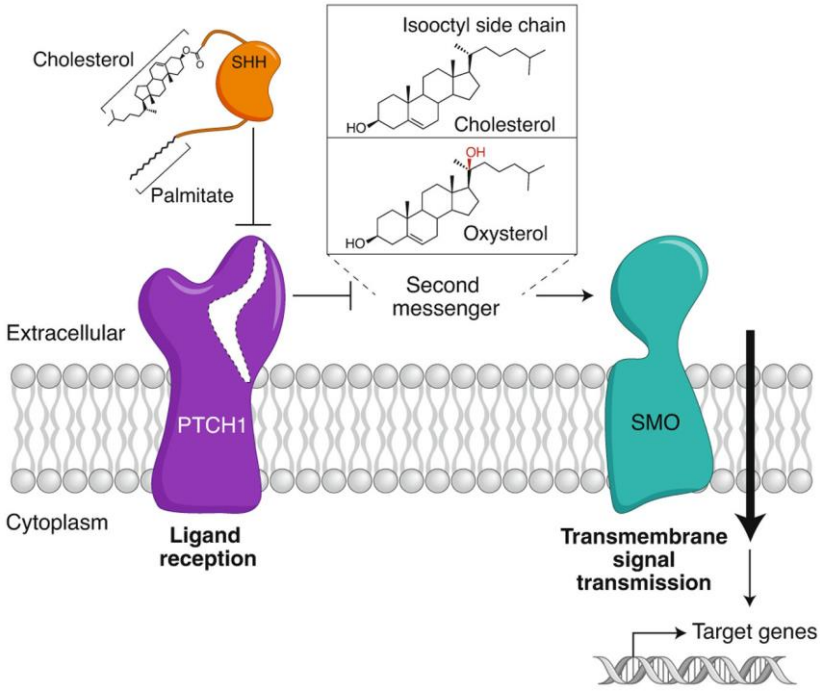

Figure 1.12 Schematic representation of the proposed model of interaction of Patched1 and Smoothened. *Since Patched1 (PTCH1) and Smoothened (SMO) are not able to directly interact, a model where PTCH1 is the transporter of the second messenger (represented by a sterol) that drives the activation of SMO has been proposed (Radhakrishnan et al, 2020).*

Furthermore, an important role in the regulation of HH pathway is related to the accessibility of cholesterol. Indeed, depletion of sphingomyelin, which leads to increase of cholesterol, is sufficient to induce the activation of HH signalling in the absence of the HH ligand (Kinnebrew *et al*, 2019). Thus, it has been proposed that PTCH1 negatively regulates HH signalling by reducing the accessibility of cholesterol to SMO in the ciliary membrane. By contrast, in the presence of HH ligand, PTCH1 is inhibited and this causes an increase in the accessible cholesterol in the ciliary membrane inducing the activation of SMO and the transduction of HH pathway (**Fig. 1.13**) (Radhakrishnan *et al.*, 2020) .

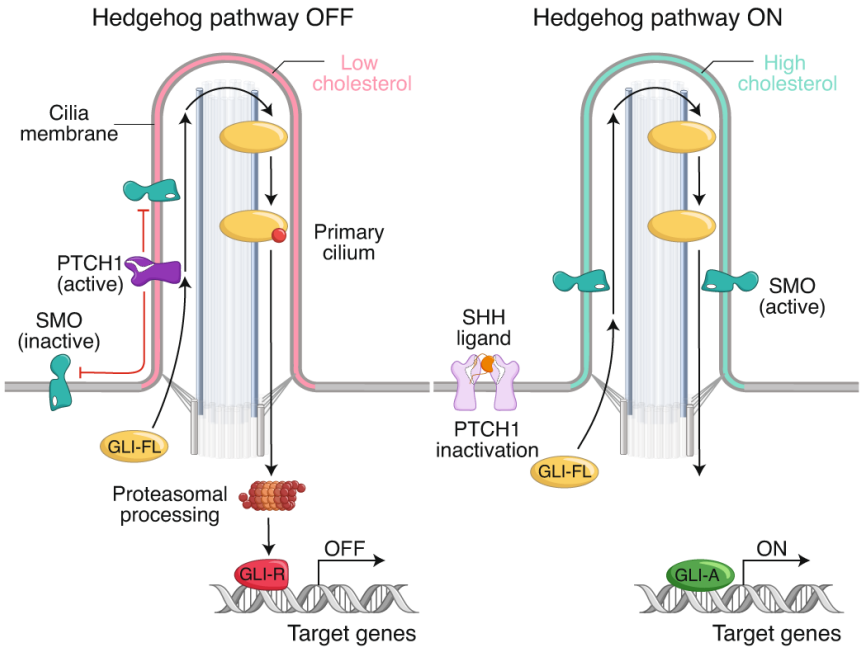

Figure 1.13 Hedgehog signalling pathway and cholesterol accessibility. *When the Hedgehog pathway is off, Patched1 (PTCH1) reduces the accessibility of cholesterol in the ciliary membrane to keep Smoothened inactive. Consequently, full length GLI (GLI-FL) undergoes proteosomal processing to become a repressor (GLI-R) of Hedgehog target genes transcription. When the Hedgehog pathway is on, PTCH1 is inactivate upon Sonic Hedgehog (SHH) binding. Thus, cholesyerol is highly accessible in the ciliary membrane and activates SMO. GLI-FL becomes an activator (GLI-A) of Hedgehog target genes transcription. Adapted from (Radhakrishnan et al, 2020).*

1.1.2.2 WNT signalling pathway

The WNT signalling pathway comprises two main branches: the canonical WNT-β-catenin and the non-canonical WNT-planar cell polarity (PCP) pathways (Anvarian *et al*, 2019). When WNT ligand is absent, the canonical WNT-β-catenin pathway is kept off by the formation of a complex of proteins (including Axin, casein kinase I (CKI), glycogen synthase kinase (GSK3), and Dishevelled (DVL)) that mediate the phosphorylation and ubiquitination by E3 ubiquitin ligase βTrCP of β-catenin, which undergoes proteosomal degradation. This prevents β-catenin to drive the expression of target genes. By contrast, the activation of the pathway requires the binding of WNT to Frizzled receptor, which leads to association of Axin with phosphorylated lipoprotein receptor-related protein (LPR). This leads to the stabilization of β-catenin, which binds to the T-cell factor (TCF) to drive target gene expression (**Fig. 1.14**) (Nusse & Clevers, 2017).

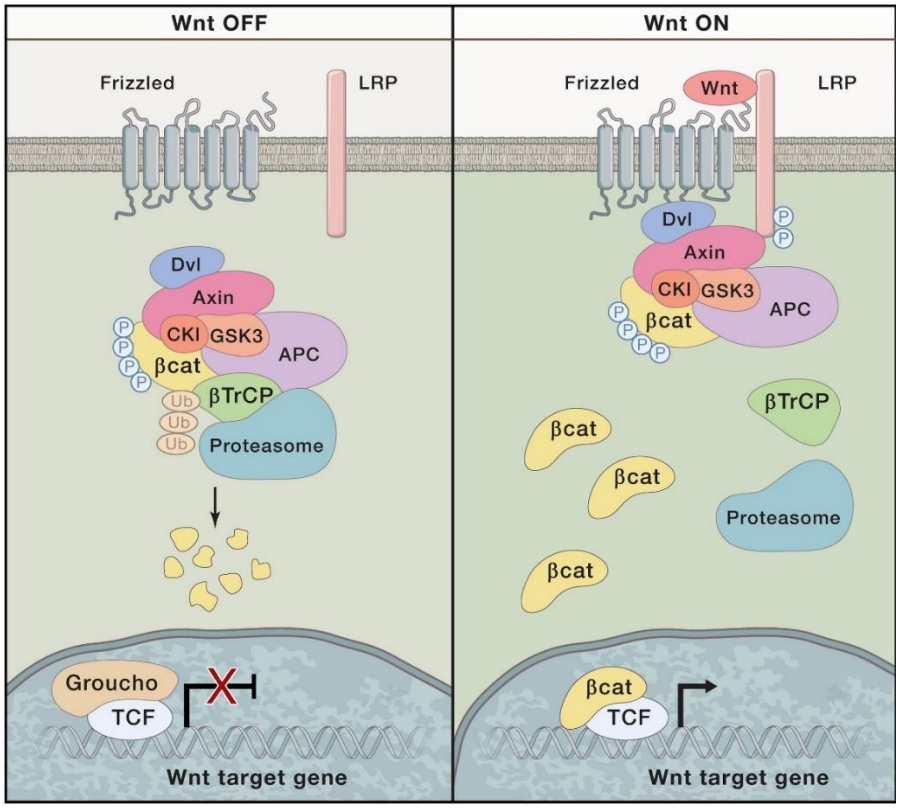

Figure 1.14 Canonical Wnt-β-catenin signalling pathway. *When the Wnt-β-catenin signalling pathway is off, a complex of proteins (including Axin, CKI, GSK3, Dvl) forms to drive the phosphorylation and ubiquitination of β-catenin. This promotes its proteasomal degradation that does not activate the Wnt target gene expression. When Wnt-β-catenin signalling pathway is activated by Wnt ligand binding to Frizzled, Axin associates with lipoprotein receptor-related protein (LPR). Therefore, stabilization of β-catenin occurs and its binding to T-cell factor drives the Wnt target gene expression. Adapted from (Nusse & Clevers, 2017).*

The non-canonical WNT-PCP pathway is activated by the non-canonical WNT5a or WNT11 ligands, which drives the recruitment of DVL. The latter activates the downstream effectors RHO family GTPases and JNK, which mediate the organization of the cytoskeleton and cell migration (**Fig. 1.15**) (VanderVorst *et al*, 2019).

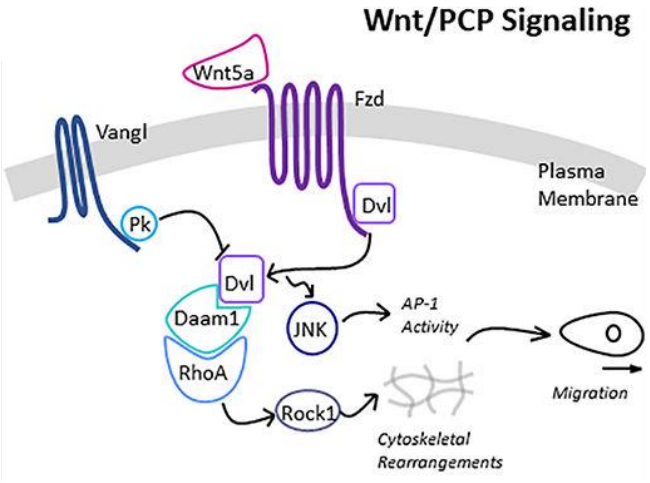

Figure 1.15 Non-canonical Wnt-PCP pathway. *When Wnt5e ligand binds to frizzled (Fzd), Dishvelled (Dvl) is recruited to activate the downstream effectors: GTPases of the RHO family (RhoA and Rock1) and JKN. The latter modulate cytoskeleton rearrangements and cell migration. Adapted from (VanderVorst et al., 2019).*

The role of the cilium in the WNT signalling pathway is still to be elucidated. Indeed, several components of it have been identified in the cilium. For example, nephrocystin 2 (NPHP2, also called Inversin), as also NPHP4, has been shown to modulate the WNT signalling pathways by affecting DVL (Borgal *et al*, 2012; Lienkamp *et al*, 2010; Simons *et al*, 2005). Some proteins of the MKS complex at the transition zone such as Jouberin (JBN) and transmembrane protein 67 (TMEM67) display a role in the regulation of the WNT pathway. In particular, JBN positively regulate the pathway by facilitating the β-catenin localization in the nucleus in the absence of cilium, while negatively modulate the pathway by promoting the localization of β-catenin in the cilium when the latter is present (Lancaster *et al*, 2009; Oh & Katsanis, 2013). TMEM67 recruits ROR2 to activate RHOA in presence of WNT5A to drive the WNT non-canonical pathway in the morphogenesis of epithelial cells (Abdelhamed *et al*, 2015). Furthermore, the link between the cilium and the WNT signalling has been investigated in studies where ciliary genes were inactivated or mutated. One study shows that the loss of *Kif3a* in mouse

embryonic fibroblasts (MEFs) leads to hyperactivation of the WNT pathway (Corbit *et al*, 2008). By contrast, another study demonstrates that mutations in *Kif3a* does not affect this signalling pathway (Ocbina *et al*, 2009). Furthermore, normal WNT target gene expression and convergent extension have been found in *ift88* mutants in Zebrafish that display impaired HH signalling (Huang & Schier, 2009). Taken together, all these findings suggest that the role of cilia in WNT signalling should be further clarified.

1.1.2.3 RTK signalling pathways

Receptor tyrosine kinases (RTKs) represent a family of receptors that includes several members and mediate cell proliferation, migration, metabolism, death, and cell-cycle progression. RTKs are characterized by an extracellular region with ligand binding domain, a single transmembrane helix domain, a cytoplasmic region with a tyrosine kinase domain, and several regulatory regions. Generally, RTKs dimerize after ligand binding and auto-phosphorylate their own tyrosine residues to recruit a platform of proteins required to drive the signal transduction via phosphoinositide 3 kinase (PI3K)-AKT, mitogen-activated protein kinase (MAPK), and phospholipase PLC-γ pathways (Hubbard, 2013; Lemmon & Schlessinger, 2010). The plethora of signalling pathways transduced by RTKs could be related to the timing, duration, and magnitude of the signal, as well as to the capability of these receptors to homodimerize or heterodimerize promoting the formation of different species characterized by peculiar properties in binding and signalling (Vasudevan *et al*, 2015). Among RTKs, platelet-derived growth factor receptor α (PDGFRα) has been identified at cilia in several cell types starting from NIH3T3 and MEFs to human embryonic stem cells (Awan *et al*, 2010). PDGFRα signalling pathway display a crucial role in embryogenesis to mediate the development of the neural system as well as mesenchymal derived structures. Indeed, the lack of PDGFRα is embryonic lethal in mouse and mutations in humans cause a wide range of developmental issues (Rattanasopha *et al*, 2012; Soriano, 1997). A study revealed that cells where cilia formation was impaired by inactivation of *Ift88* and *Kif3a* displayed altered PDGFRα signalling, strengthening the finding that PGFRα signalling is regulated by cilia (**Fig. 1.16**) (Christensen *et al*, 2017; Schneider *et al*, 2010; Schneider *et al*, 2005). Another relevant RTK whose function is deeply related to cilia is represented by insulin (IR) and insulin-like growth factor (IGF-1R) receptors. After ligand binding, a conformational change and autophosphorylation of the tyrosine residues occur, leading to the signal transduction through insulin receptor substrate 1 (IRS-1), which activates the PI3K-AKT pathway (**Fig. 1.16**) (Cabail *et al*, 2015; Christensen *et al.*, 2017). IGF-1R mediates the regulation of adipogenesis, the process of differentiation of preadipocytes to mature adipocytes, through cilia. Indeed, the ablation of cilia through downregulation of *Ift88* or *Kif3a* in 3T3-L1 preadipocytes has been revealed to impair the capability of preadipocytes to respond to insulin due to reduced phosphorylation of IGF-1R and AKT

and decreased transcriptional expression of adipogenic genes such as CEBPα and peroxisome proliferator-activated receptor γ (PPARγ) (Zhu *et al*, 2009). Furthermore, IGF-1R signalling pathways was found to be implicated in the cell cycle progression and cilia resorption, as found in MEFs, RPE and neuronal progenitor cells (Li *et al*, 2011; Yeh *et al*, 2013). All these findings revealed the role of cilia in the regulation of signal transduction through RTKs as PGFRα and IR/IGF-1R.

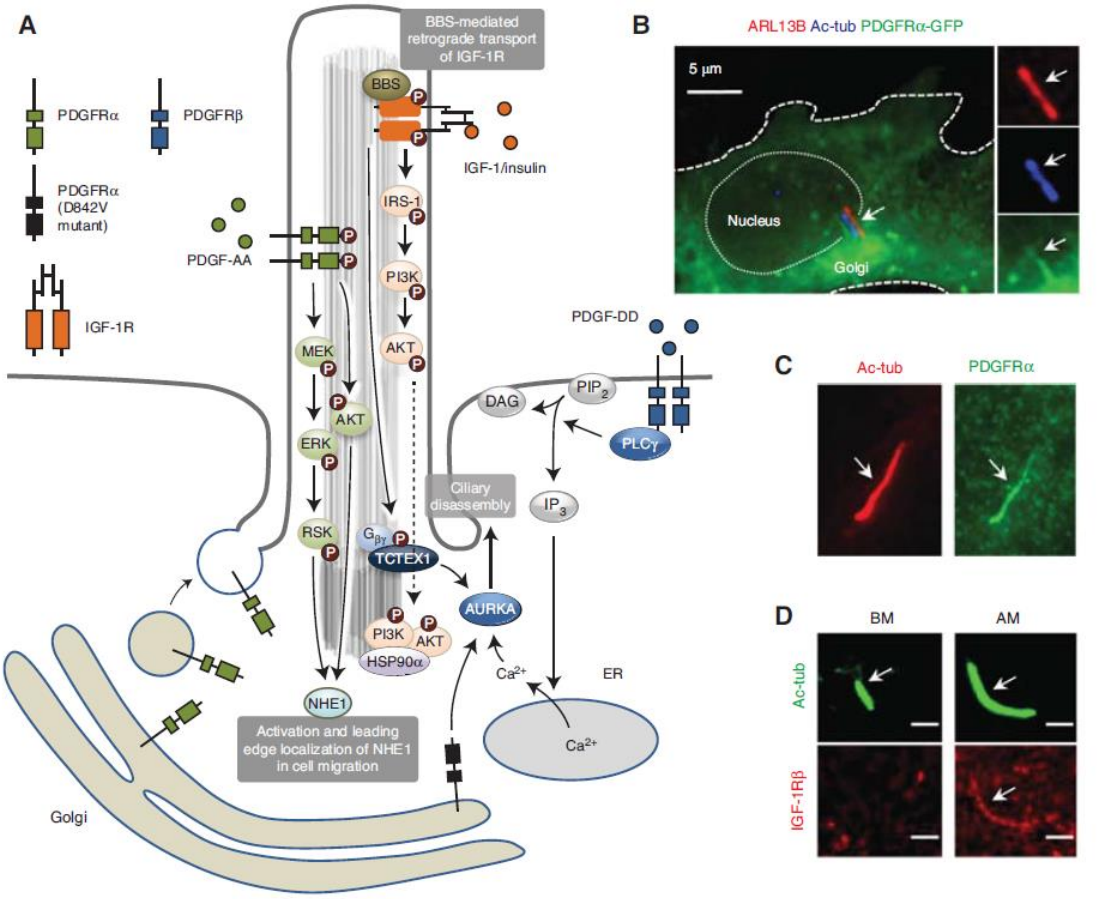

Figure 1.16 Receptor tyrosine kinases signalling*. A) Schematic representation ciliary and extra-ciliary signalling of platelet-derived growth factor receptor α (PGFRα) and insulin-like growth factor (IGF-1R) receptor involving phosphoinositide 3 kinase (PI3K)-AKT, mitogen-activated protein kinase (MAPK), and phospholipase PLC-γ pathways to promote signal transduction. B) Fluorescent image of PDGFRα-GFP localization in the Golgi and in primary cilia. Cilia: ARL13B (red), Acetylated tubulin (Ac-tub) (blue); PDGFRα-GFP (green). C) Fluorescence image of colocalization of cilia (Ac-tub, red) and endogenous PDGFRα (green). D) Fluorescence images of cilium length and ciliary localization of IGF-1Rβ upon basal medium (BM), and adipogenic medium (AM) in mesenchymal stem cells. Cilia: Ac-tub (green); IGF-1Rβ (red) (Christensen et al., 2017)*

1.1.2.4 TGF-β signalling pathways

The transforming factor β/bone morphogenetic protein (TGF-β/BMP) signalling consists of canonical and non-canonical signalling caused by more than 30 pleiotropic ligands belonging to TGF-β–activin–Nodal and BMP subfamilies. This signalling pathway mediates the regulation of several cellular processes, including cell proliferation, survival, and differentiation (Massague, 2012). TGF-β and BMP superfamily ligands activate receptor serine/threonine kinases of type I (RI) and II (RII) to induce the phosphorylation of transcription factors for target gene expression. In canonical signalling, transcription factors of R-SMAD family, which includes SMAD2/3 for TGF-β or SMAD1/5/8 for BMP signalling, are phosphorylated by RI receptors and form a complex with SMAD4 for translocation into the nucleus and other ligands transcription factors (activated by HH, WNT, RTK signalling) to promote the transcription of target genes (**Fig. 1.17**) (Anvarian *et al.*, 2019; Christensen *et al.*, 2017; Clement *et al*, 2013). Of interest, ligands of growth and differentiation factor (GDF) could propagate signalling through R-SMADs, while other ligands could inhibit it. These findings suggest the complexity of the regulation of TGF-β/BMP signalling. In the non-canonical signalling, RI and RII receptor kinases activate non-R-SMAD pathways, including PI3K/AKT, MAPK (such as ERK1/2 and JNK), Rho-like GTPases, and NF-kB signalling (Guo & Wang, 2009; Zhang *et al*, 2016). These pathways could participate in larger signalling networks and crosstalk with R-SMAD transcription factors to mediate the regulation of several cellular processes depending on different contexts. Of note, internalization through clathrin-mediated endocytosis of receptors plays a crucial role in the regulation of TGF-β/BMP signalling (**Fig. 1.17**) (Balogh *et al*, 2013; Clement *et al.*, 2013; Ehrlich, 2016). In this context, upon compartimentalization of activated receptors in early endosomes by clathrin-mediated endocytosis, SMAD anchor for receptor activation (SARA) is reported to enhance the SMAD2/3 signalling by anchoring to the PI3P-enriched membrane of the endosomes and facilitating the association between the receptor RI and R-SMADs (Sorkin & von Zastrow, 2009). Nevertheless, SARA activity on the regulation of TGF-β/BMP signalling is reported to be dispensable and dependent on the cell type (Bakkebo *et al*, 2012). Caveolin-mediated endocytosis mediates the proteosomal degradation of TGF-β/BMP receptor-ligand complex, leading to a negative regulation of the signalling (Heldin & Moustakas, 2016). The first evidence that led to

hypothesize a role of cilium in TGF-β/BMP signalling regulation is represented by the finding that the ciliary pocket is a crucial site for clathrin-mediated endocytosis (Clement *et al.*, 2013). Indeed, upon ligand activation, TGF-β RI and RII accumulation was observed at the ciliary base, where SMAD4 was enriched, in cultured mouse and human fibroblasts. Furthermore, internalization of receptors was reported to occur through clathrin-mediated endocytosis at the ciliary pocket to promote SMAD2/3 signalling (**Fig. 1.17**) (Clement *et al.*, 2013). ERK1/2 activation at the base of cilia was observed as well, although it was not dependent on clathrin-mediated endocytosis (Clement *et al.*, 2013). Another evidence that revealed the relevance of cilia in TGF-β/BMP signalling consists of the localization at the centrosome-cilium complex of some of TGF-β/BMP signalling components, such as TGF-β RI/II and SMAD2/3, SMAD4, and SMAD7 (Christensen et al., 2017). These results obtained in fibroblasts have been strengthen by the identification of SMAD2/3 and SMAD4, as well as ERK1/2, Rho GTPases, and AKT, by proteomics of cilia through proximity-labelling (Mick *et al.*, 2015). Cilia-mediated regulation of TGF-β/BMP signalling plays a fundamental role in bone formation and heart development. Indeed, ciliary localization of TGF-β and BMP receptors has been reported to mediate human bone mesenchymal stem cells migration to bone and osteogenesis *in vitro* and *in vivo* (Labour *et al*, 2016; Xie *et al*, 2016; Zhang *et al*, 2017a). The relevance of ciliary regulation of TGF-β signalling in heart development has been uncovered by several findings. First, nodal cilia are able to generate a fluid flow at the embryonic node to establish the lateral asymmetry (Hirokawa *et al*, 2012). Therefore, dysfunction of nodal cilia causes heterotaxy and congenital heart disease (Shiratori & Hamada, 2014). Furthermore, ciliary-mediated TGF-β signalling has been reported to drive differentiation of mouse cancer stem cells and human mesenchymal stem cells to cardiomyocytes, since TGF-β temporal accumulation and SMAD2/3 activation occurs at the base of cilia (Clement *et al.*, 2013). Another study reported that endothelial cilia prevent endothelial-to-mesenchymal transition induced by shear stress by reducing the SMAD2/3-driven signalling in the endocardial cushion area (Egorova *et al*, 2011). Other evidence of cilia involvement in the regulation TGF-β signalling is that *Tg737*^{orpk} mutant fibroblasts, carrying an hypomorphic mutation in the *Ift88* gene, show reduced SMAD2/3 signalling and decreased clathrin-mediated endocytosis at the base of cilia. From the other side, TGF-β signalling is reported to be involved in the regulation of ciliary length and in TZ

function in sensory and motile cilia. As an example, TGF-β signalling was found to lead to decreased expression of IFT88 and consequently shortening of cilia in chondrocytes. (Kawasaki *et al*, 2015). Furthermore, *Smad1/5*^{cko} mice show an impaired orientation of primary cilia in the growth plate (Ascenzi *et al*, 2011). Deficiency of primary cilia driven by TGF-β signalling has been reported to induce epithelial-to-mesenchymal transition of kidney epithelial cells (Han *et al*, 2018). Furthermore, alteration of mechanosensation and maturation in human osteoblasts has been reported to be associated with TGFβ1 via HDAC6-driven shortening of cilia (Ehnert *et al*, 2017). The importance of TGF-β signalling ciliary regulation has been strengthen by the finding that loss of the subdistal appendage protein CEP128 impairs TGF-β signalling by reducing the phosphorylation of R-SMADs and causes defective organ development in zebrafish morphants. Loss of ciliary recruitment by CEP128 of RAB11, which is responsible for TGF-β receptors endosomal recycling, and defects in vescicular trafficking are likely the causes of the phenotype observed in *cep128* morphants (Monnich *et al*, 2018). Primary cilia are also shown to be involved in the differentiation of human adipose progenitors to myofibroblasts (Arrighi *et al*, 2017). SMAD7 and SMURF1, localized at cilia, inhibit the TGF-β signalling. SMAD7 has been reported to limit the ciliary localization of TGF-β receptors and to reduce the migration and the invasion of tumor cells by supressing the crosstalk between TGF-β receptors and SMO in HH signalling pathway (Gencer *et al*, 2017). The E3 ubiquitin ligase SMURF1 inhibits SMAD1/5/8 phosphorylation at cilia to regulate cell type specification during heart development *in vivo* (Koefoed *et al*, 2018).

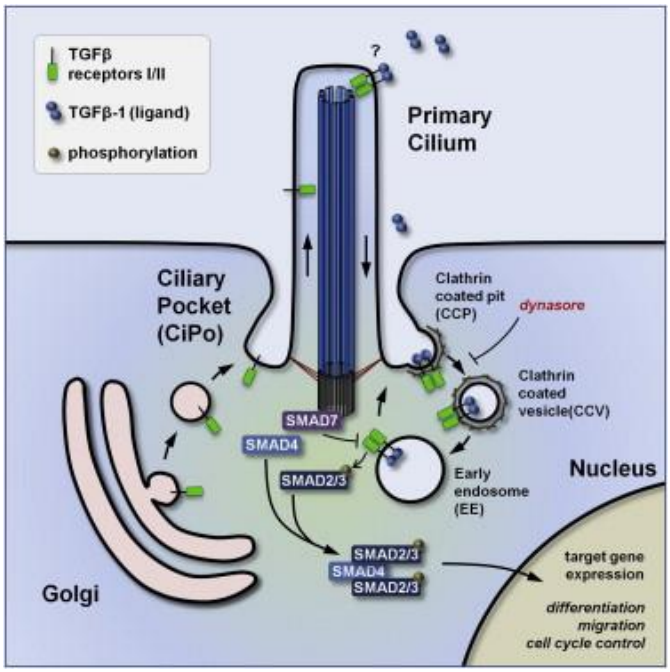

Figure 1.17 TGF-β signalling. *TGF-β signalling is involved in the regulation of several cellular processes, including cell differentiation, migration, and cell cycle control. TGF-β receptor kinases of type I and type II (RI/II) are activated by more than 30 pleiotropic ligands to promote target gene expression through R-SMAD transcription factors (SMAD2/3 for TGF-β or SMAD1/5/8 for BMP signalling - canonical pathway) or non-R-SMAD pathways (PI3K/AKT, MAPK, Rho-like GTPases, and NF-kB signalling – non-canonical pathways). Internalization of TGF-β receptor-ligand complex is mediated by clathrin-mediated endocytosis at the ciliary pocket. SMAD4 interacts with R-SMADs for translocation into the nucleus, while SMAD7 negatively regulates TGF-β signalling (Clement et al., 2013).*

1.1.3 Cilia and Autophagy

Autophagy is a degradative process that promotes the incorporation of cellular components into double-membrane vesicles called autophagosomes. Consequently, autophagy regulates the maintenance of cellular energy homeostasis upon nutrient deprivation. A crosstalk between cilia and autophagy has been uncovered during the last decades, starting from the observation that autophagy driven by serum starvation promotes ciliogenesis (Tang *et al*, 2013). This effect has been shown to be caused by the removal of oral-facial-digital type 1 (OFD1) protein, which is located at the basal body and is necessary for cilia formation and left-right asymmetry during development (**Fig. 1.18 A**) (Morleo *et al*, 2023). Indeed, its dysfunction leads to the OFD1 syndrome, classified as a ciliopathy. By contrast, another study has been published showing that in MEFs basal autophagy (not induced by serum starvation) inhibits ciliogenesis through the removal of IFT20 (**Fig. 1.18 A**) (Morleo *et al.*, 2023; Pampliega *et al*, 2013). Thus, basal autophagy has been proposed to inhibit ciliogenesis through IFT20 degradation, while serum starvation-induced autophagy to the removal of OFD1. Furthermore, other studies show that the degradation of other proteins such as CP110 (Liu *et al*, 2021), myosin heavy chain 9 (MYH9) (Yamamoto *et al*, 2021), and kinesin family member 19 (KIF19) (Arora *et al*, 2020) through serum starvation-driven autophagy promotes ciliogenesis (**Fig. 1.18 A**) (Morleo *et al.*, 2023). Furthermore, other proteins involved in the regulation of both autophagy and ciliogenesis are represented by phosphoinositide-3-kinase regulatory subunit 4 (PIK3R4/VPS15), which localizes at the cilia and is involved in the formation and release of IFT20-positive vesicles from the cis-Golgi to cilia (Stoetzel *et al*, 2016), and by PIK3CA, which localizes at the basal body and is responsible for the synthesis of the ciliary pool of PI(3)P (**Fig. 1.18 A**) (Franco *et al*, 2014; Morleo *et al.*, 2023). The autophagy related 16 like 1 protein (ATG16L1), which belongs to the ATG proteins responsible for the autophagosome biogenesis, is reported to drive the INPP5E-IFT20 trafficking to cilia to promote ciliogenesis (**Fig. 1.18 A**) (Boukhalfa *et al*, 2021; Morleo *et al.*, 2023). As autophagy can influence cilia, it has been proven that also cilia can affect autophagy. Indeed, upon shear stress primary cilia are able to mediate the activation of the AMP-activated protein kinase (AMPK), which is a master regulator of the energy homeostasis of the cell (Mihaylova & Shaw, 2011), through serine-threonine kinase 11 (STK11/LKB1). As a consequence, the mechanistic

target of rapamycin (mTOR), which is a key regulator of cell growth, metabolism, and survival, is inhibited leading to reduction of the cell size (**Fig. 1.18 B**) (Boehlke *et al*, 2010; Morleo *et al.*, 2023; Orhon *et al*, 2016). During shear stress, also the upregulation of ciliary component Folliculin (FLCN) occurs upstream to AMPK activation (**Fig. 1.18 B**) (Morleo *et al.*, 2023; Zemirli *et al*, 2019). Other than fluid flow-induced shear stress, also mechanical forces can induce autophagy through cilia. Indeed, primary cilia of trabecular meshwork cells, which are localized in the anterior part of the eye, sense mechanical stress and activate autophagy through AKT1 and SMAD2-SMAD3 signalling pathways to regulate the homeostasis of the intraocular pressure (**Fig. 1.18 B**) (Morleo *et al.*, 2023; Shim *et al*, 2021). Another evidence that cilia can affect autophagy is the involvement of HH signalling pathway in the regulation of autophagy. Indeed, HH ligands activate autophagy, while HH antagonists inhibit it. To reinforce this finding, it is reported that cells with ciliary defects display an impaired autophagy activation (**Fig. 1.18 B**) (Morleo *et al.*, 2023; Pampliega *et al.*, 2013). Taken together, these findings show that cilia and autophagy interplay each other.

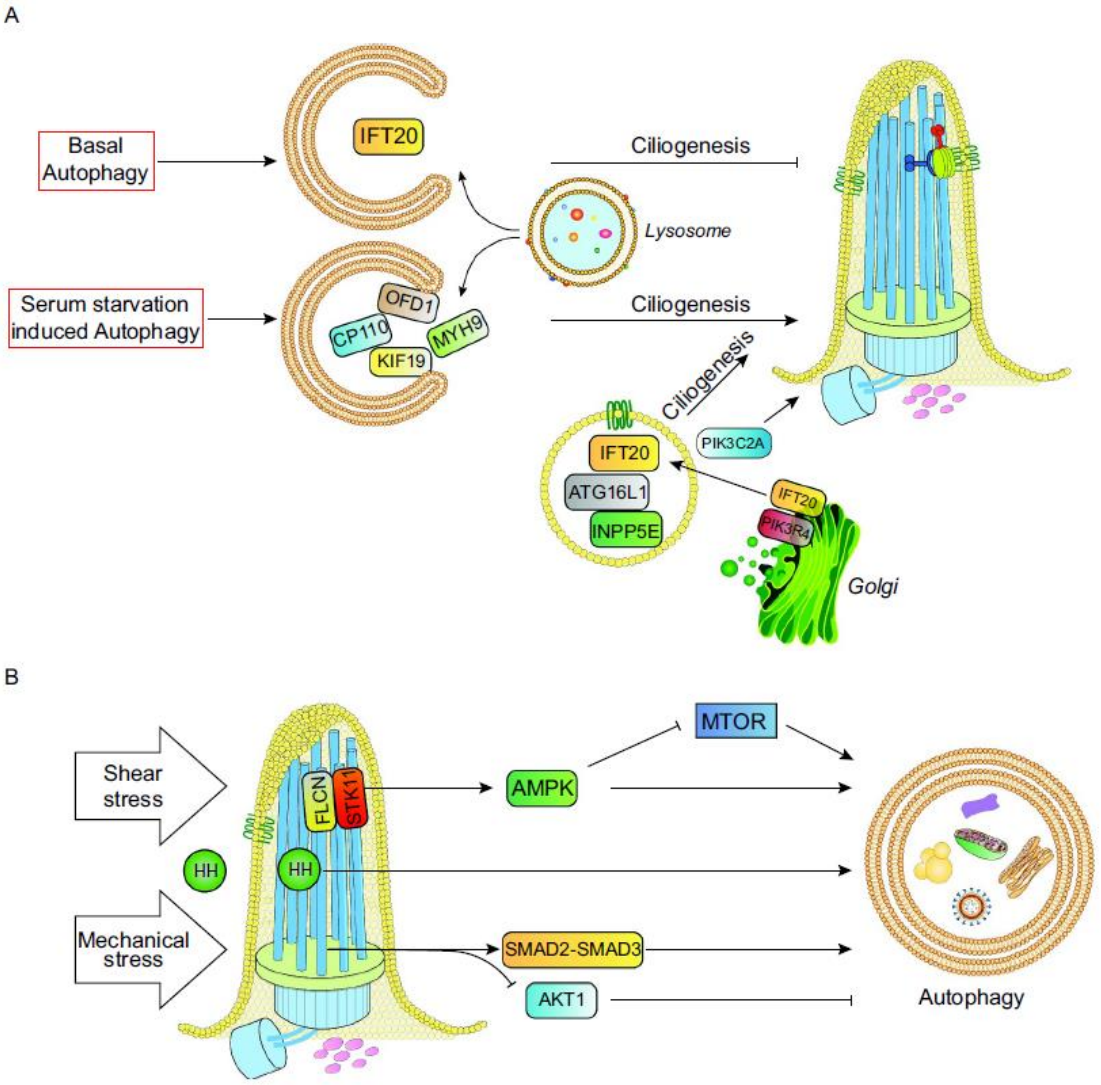

Figure 1.18 Autophagy and cilia. *A) Basal autophagy and serum starvation autophagy have opposite effects on ciliogenesis, through degradation of different ciliary proteins. B) Cilia regulate autophagy in response to shear stress, HH signalling, and mechanical stress (Morleo et al., 2023).*

New insight into the involvement of mitochondria in the crosstalk between cilia and autophagy has been recently shown. Indeed, inducing in dopaminergic neurons a mitochondrial stress as mitochondrial fission through the inactivation of OPA1, which normally drives mitochondrial fusion, leads to the increase of reactive oxygen species (ROS) and activation of AMPK. This promotes the inhibition of mTOR and consequently the activation of autophagy, which leads to ciliogenesis through the degradation of OFD1, even under nutrient complete condition (**Fig. 1.19 A**) (Bae *et al*, 2019; Morleo *et al.*, 2023). This finding reveals that the mitochondrial dysfunction could stimulate ciliogenesis through the activation of autophagy. Reversely, also cilia can affect mitochondrial function in terms of energy production. Indeed, cilia of renal epithelial cells could regulate mitochondrial biogenesis and lipophagy (which is the process of degradation of lipid droplets through autophagy), which together promote ATP production, by their capability to activate AMPK through shear stress sensing (**Fig. 1.19 B**) (Miceli *et al*, 2020; Morleo *et al.*, 2023). In conclusion, cilia and autophagy display a complex crosstalk, since autophagy could promote ciliogenesis and cilia through their structural components or their signalling pathways could affect autophagy.

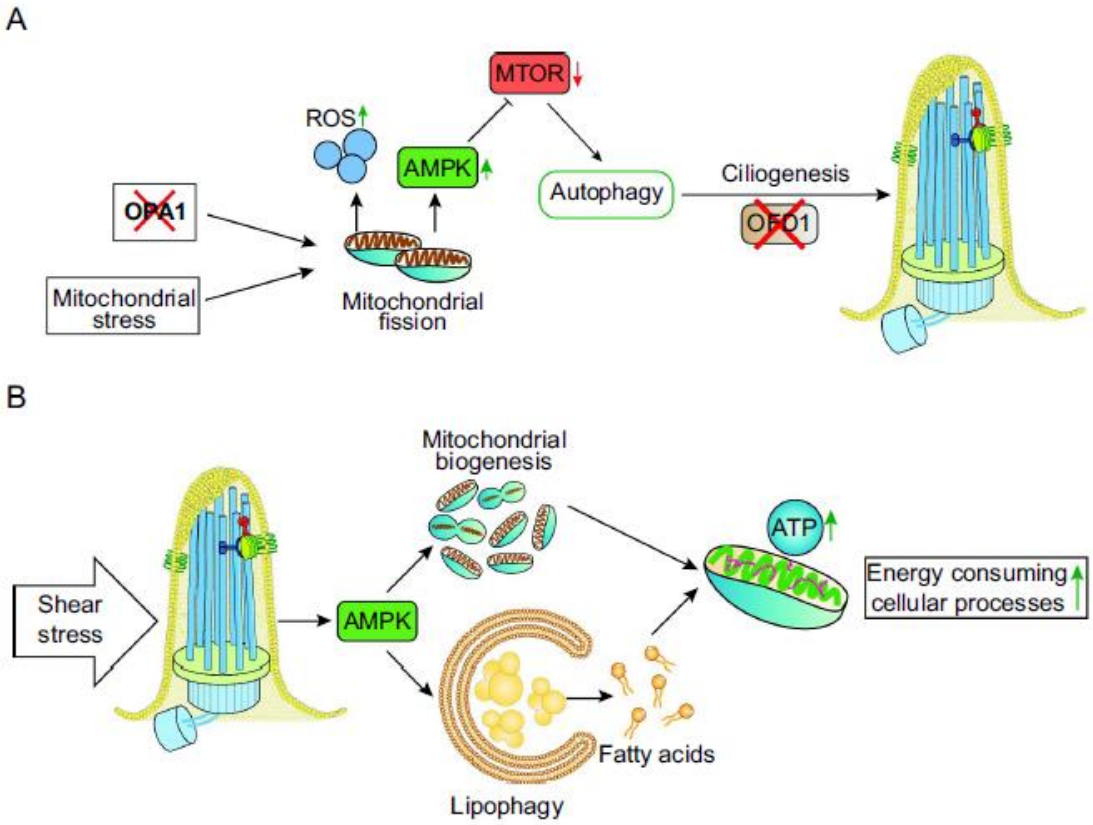

Figure 1.19 Mitochondria, autophagy, and cilia. *A) Mitochondrial fission unduced by OPA1 inactivation or mitochondrial stress generates reactive oxygen species (ROS) and AMPK activation, which inhibits mTOR and drives autophagic degradation of OFD1 leading to ciliogenesis. B) Shear stress sensed by cilia induces AMPK activation and subsequent mitochondrial biogenesis and fatty acids release through lipophagy leading to ATP production by mitochondria. This enhances energy consuming processes (Morleo et al., 2023)*

1.2 Ciliopathies

Ciliopathies are the group of disorders due to dysfunction of cilia. In general, ciliopathies affect different tissues and organs, usually leading to polydactyly, obesity, neurodevelopmental defects, and renal cystogenesis (Hildebrandt *et al*, 2011; Reiter & Leroux, 2017). Indeed, ciliopathies could give rise to multiple abnormalities or to single-organ malformations. These disorders could be divided into motile ciliopathies, due to the dysfunction of motile cilia, and immotile or sensory ciliopathies, caused by alterations in primary cilia (**Fig. 1.20**) (Reiter & Leroux, 2017). Furthermore, ciliopathies are classified in other two main cathegories: first-order and second-order ciliopathies. First-order ciliopathies include the ciliopathies due to the dysfunction of ciliary components that mediate direct impairment of structure, assembly, maintenance, motility (for motile cilia), and signalling. Second-order ciliopathies are caused by the impairment of extra-ciliary components that indirectly drive abnormalities in cilia machineries and pathways (Reiter & Leroux, 2017).

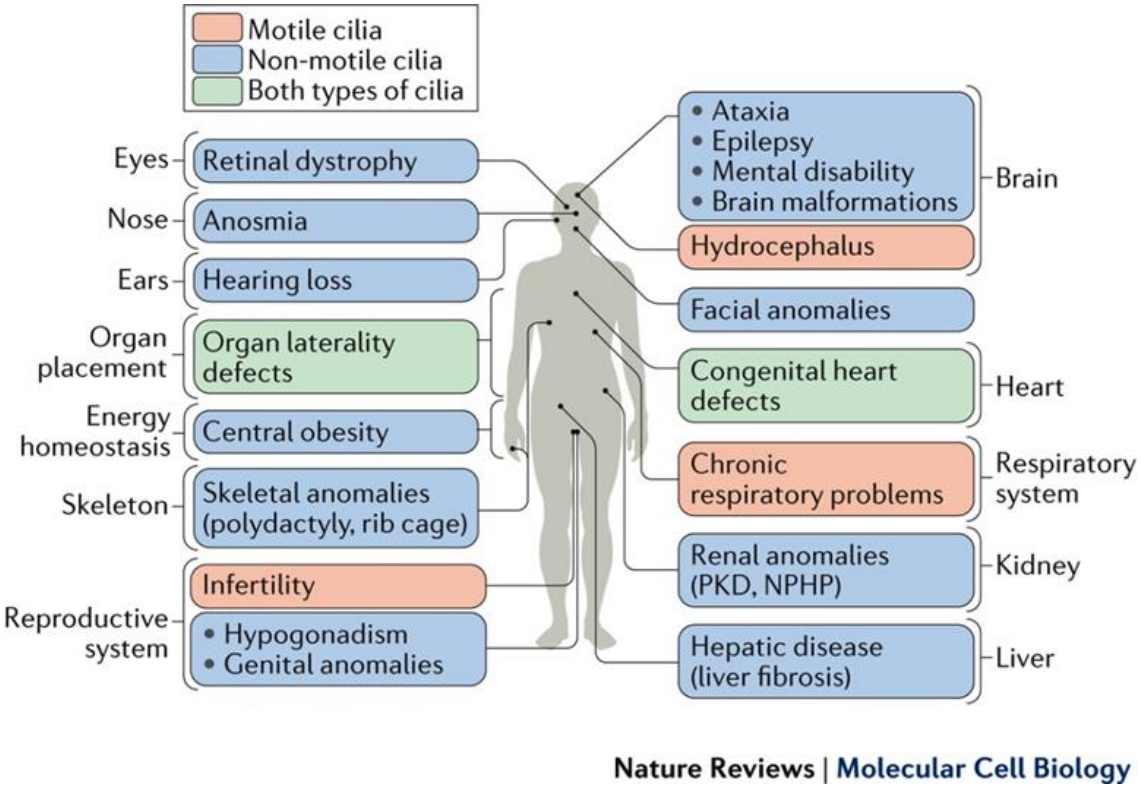

Figure 1.20 Schematic representation of motile and sensory ciliopathies. *Ciliopathies cause abnormalities in several tissuea and organs. Orange boxes represent pathological defects induced by motile cilia dysfunction. Blue boxes represent pathological defects induced by non-motile cilia. Green boxes represent pathological defects induced by both motile and immotile cilia (Reiter & Leroux, 2017).*

1.2.1 Motile ciliopathies

Motile ciliopathies are caused by dysfunction of motile cilia. Primary ciliary dyskinesia (PCD) is characterized by *situs inversus* (due to abnormal left-right asymmetry), sinusitis, atelectasis, and chronic bronchitis (caused by impaired motility of cilia for mucus clearance in the airways), and male infertility (due to defects in the locomotion of sperm cells). Female decreased fertility (caused by improper propelling of the oocyte through the oviducts) and hydrocephalus (due to altered movement of the cerebrospinal fluid) represent less common features of PCP (Horani *et al*, 2016). Generally, PCP is caused by mutations in ciliary components that directly drive cilia motility (first-order ciliopathies), but there are cases where this disease is due to mutations in genes encoding for proteins that are responsible of the pre-assembly of dynein complexes before their trafficking to cilia, as *DYX1C1* and *DNAAF2-3* (second-order ciliopathies) (Mitchison *et al*, 2012; Tarkar *et al*, 2013).

1.2.2 Sensory ciliopathies

1.2.2.1 Autosomal Dominant Polycystic Kidney Disease: the most common ciliopathy

Autosomal Dominant Polycystic Kidney Disease (ADPKD) is the most common ciliopathy, with a frequency of 1:500-1:1000 (Torres *et al*, 2007). ADPKD pathogenesis is characterized by progressive renal cystogenesis leading to kidney function failure leading to chronic kidney disease (CKD) and end-stage renal disease (ESRD) (Torres *et al.*, 2007). Renal cysts derive from all the segments of the nephron and liver and bile ducts cysts have been described in ADPKD patients. Hypertension and intracranial aneurysms are other features of ADPKD. This disease is due to loss-of-function mutations in *PKD1* (85% of cases) and *PKD2* (15% of cases) genes, which encode for polycystin-1 and polycystin-2, respectively (**Fig. 1.21**) (Bergmann *et al*, 2018).

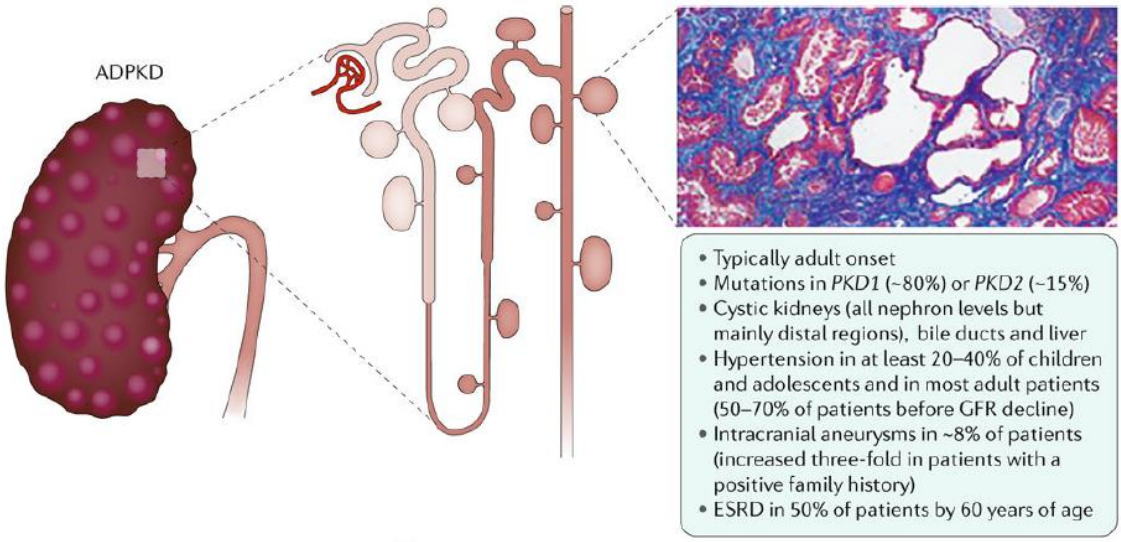

Figure 1.21 Pathological features of ADPKD. *Adapted from (Bergmann et al., 2018).*

Polycystins form a complex that localizes in different cellular compartments, including primary cilia, and that is reported to prevent cystogenesis (Boletta & Germino, 2003). Polycystins are described to play a role in modulating the activity of cAMP, mTOR, WNT, Ca^{2+}, Hippo, and vascular endothelial growth factor (VEGF) signalling pathways (Bergmann *et al.*, 2018). Although ADPKD is inherited as a dominant genetic disease, its molecular behaviour resembles the one of a recessive disease. Indeed, since the inactivation of one allele has been reported to be not sufficient to give rise to the disease, it has been proposed the presence of a "second hit", which leads to the inactivation of the second *PKD* allele or to the decrease of polycystins activity under a certain threshold (**Fig. 1.22**) (Pei, 2001; Wallace, 2011).

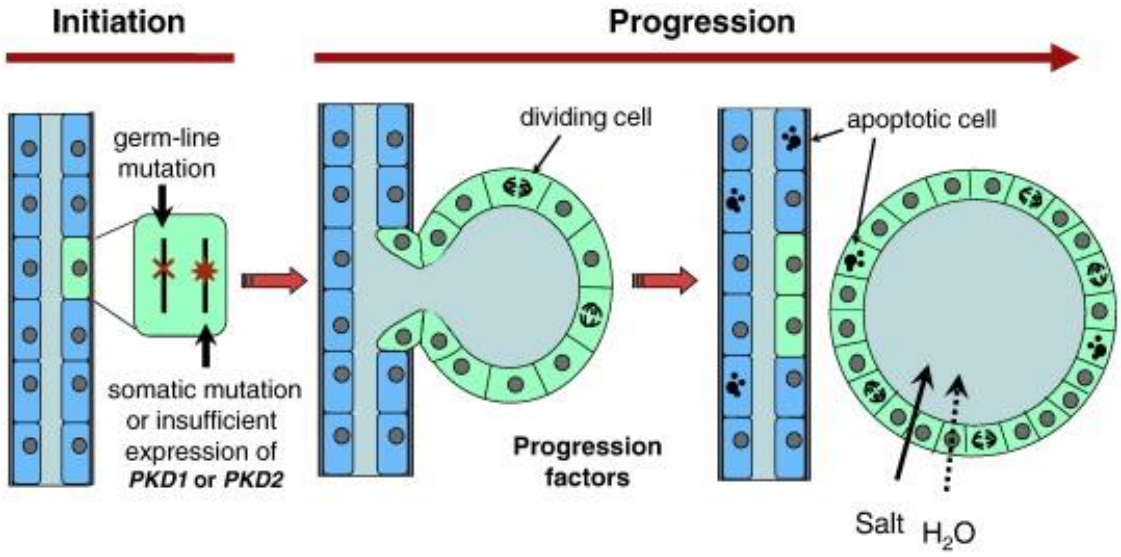

Figure 1.22 Schematic representation of ADPKD progression steps. *The initiation of the disease is due to a second hit that is represented by a somatic mutation on the second PKD allele or by insufficient expression of PKD1 or PKD2. Progression of the disease is characterized by the formation of focal cysts that become fluid-filled and characterized by highly proliferative and apoptotic cells (Wallace, 2011)*

1.2.2.1.1 Cilia-dependent cyst activation pathway in ADPKD

Cilia ablation through the inactivation of genes encoding for IFT proteins, such as IFT88 (Pazour *et al*, 2000; Yoder *et al.*, 2002), IFT20 (Jonassen *et al*, 2008), and KIF3a (Lin *et al*, 2003) is reported to induce renal cystogenesis, even at a lower level compared to ADPKD. These findings shed light for the first time on the relevance of cilia in ADPKD progression. Indeed, the disruption of cilia is supposed to induce renal cystogenesis by causing the removal of polycystins at this compartment. Nevertheless, the concomitant disruption of cilia and polycystins ameliorates ADPKD phenotype in term of renal cystogenesis (**Fig. 1.23**) (Ma *et al*, 2013; Shao *et al*, 2020). Indeed, in mice where either *Kif3a* or *Ift20* were conditionally inactivated in the segments of the renal tubules concomitanly with *Pkd1* or *Pkd2*, kidney to body weight ratio, cystic index, and serum urea nitrogen concentration resulted to be decreased compared to *Pkd1*and *Pkd2* mutant mice (Ma *et al.*, 2013). Thus, the presence of a cilia-dependent cyst activation (CDCA) pathway has been hypothesized to be restricted to cilia and to be normally suppressed by polycystins (Ma *et al*, 2017). Upon polycystins inactivation, this pathway has been proposed to be activated leading to renal cystogenesis. The eradication of this pathway through the disruption of cilia ameliorates PKD phenotype. Studies showing that the chemical ablation of primary cilia through ganetespib, an inhibitor of heat shock protein 90 (HSP90), ameliorates cystogenesis in ADPKD, support the hypothesis of the CDCA pathway existence (Nikonova *et al*, 2018). However, the molecular players that belong to this pathway are still elusive and cAMP, mTOR, and MAPK/ERK signalling seem not to be involved (Ma *et al.*, 2013).

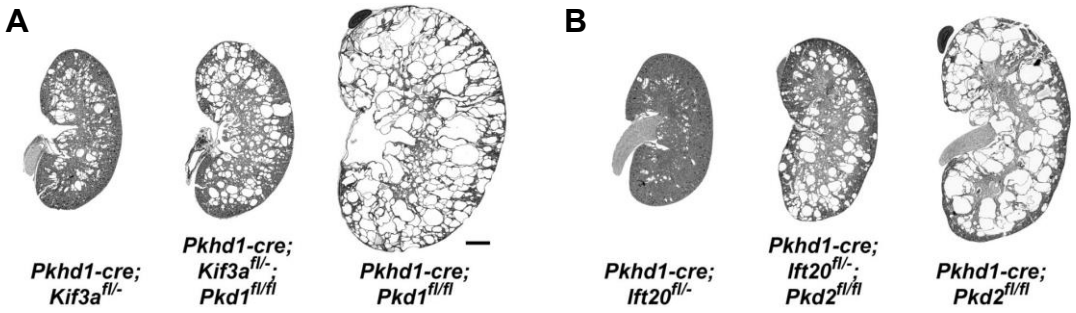

Figure 1.23 Loss of cilia ameliorates PKD cystogenesis. *A) Representative images of kidneys of Pkhd1-cre;Kif3a$^{fl/-}$ (mild cystogenesis), Pkhd1-cre;Kif3a$^{fl/-}$;Pkd1$^{fl/fl}$ (medium cystogenesis), and Pkhd1-cre;Pkd1$^{fl/fl}$ (high cystogenesis) mice. B) Representative images of kidneys of Pkhd1-cre;Ift20$^{fl/-}$ (mild cystogenesis), Pkhd1-cre;Ift20$^{fl/-}$;Pkd2$^{fl/fl}$ (medium cystogenesis), and Pkhd1-cre;Pkd2$^{fl/fl}$ (high cystogenesis) mice. (Ma et al., 2013).*

1.2.2.2 Autosomal Recessive Polycystic Kidney Disease

Autosomal Recessive Polycystic Kidney Disease (ARPKD) is mostly due to missense and truncating mutations in the polycystic kidney and hepatic disease 1 (*PKHD1*). *PKHD1* encodes for fibrocystin/polydactin, which is a around 4000 residue protein consisting of one transmembrane domain with a large N-terminal tail and a short C-terminal domain (Onuchic *et al*, 2002; Ward *et al*, 2002). Fibrocystin is localized at the apical side of plasma membrane and at cilia because of the presence of a ciliary targeting motif at its C-terminal domain (Follit *et al*, 2010; Ward *et al.*, 2003). Fibrocystin is expressed during embryogenesis and it is crucial for kidney development, since it is involved in the correct branching of the ureteric bud. In the adult fibrocystin is expressed in the kidney and, at a lower level, in the liver and in the pancreas. Furthermore, fibrocystin has been reported to interact with PC2 within its complex with PC1 (Wang *et al*, 2007). ARPKD usually manifests perinatally or during infancy and is characterized by the development of renal cysts and bile ducts malformations, causing CKD and ESRD (**Fig. 1.24**) (Bergmann *et al.*, 2018). Renal cysts of ARPKD derive from distal tubules and collecting duct, while congenital hepatic fibrosis is caused by ductal plate malformation, which is a feature of other ciliopathies, such as Joubert syndrome, Bardet Biedl syndrome, and nephronophtisis (Bergmann, 2015). Hypetension is extensively reported in ARPKD patients, while intracranial aneurysms are found with low rate in ARPKD patients (Guay-Woodford & Desmond, 2003; Perez *et al*, 2018). Neonatal infants affected by ARPKD die after delivery for pulmonary dysplasia in the 20% of cases (Bergmann *et al.*, 2018). Some cases with a mild phenotype of ARPKD present mutations in the DAZ-interacting protein 1-like protein (DZIP1L), which encodes for a TZ protein (Lu *et al*, 2017). As in ADPKD, cAMP, MYC, and mTOR signalling pathways are upregulated (Fischer *et al*, 2009).

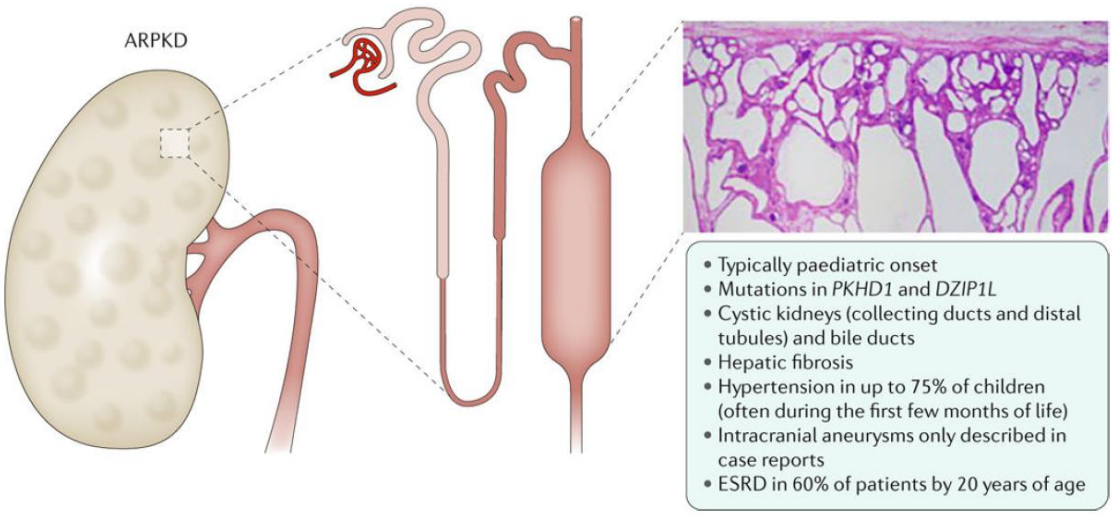

Figure 1.24 Pathological features of ARPKD. *Adapted from (Bergmann et al., 2018).*

1.2.2.3 Joubert syndrome

Joubert syndrome (JS) is a ciliopathy caused by mutations in around 40 genes related to primary cilia, whose products are localized in different ciliary compartments, including the ciliary tip, the basal body, and the TZ (**Fig. 1.25**) (Van De Weghe *et al*, 2022).

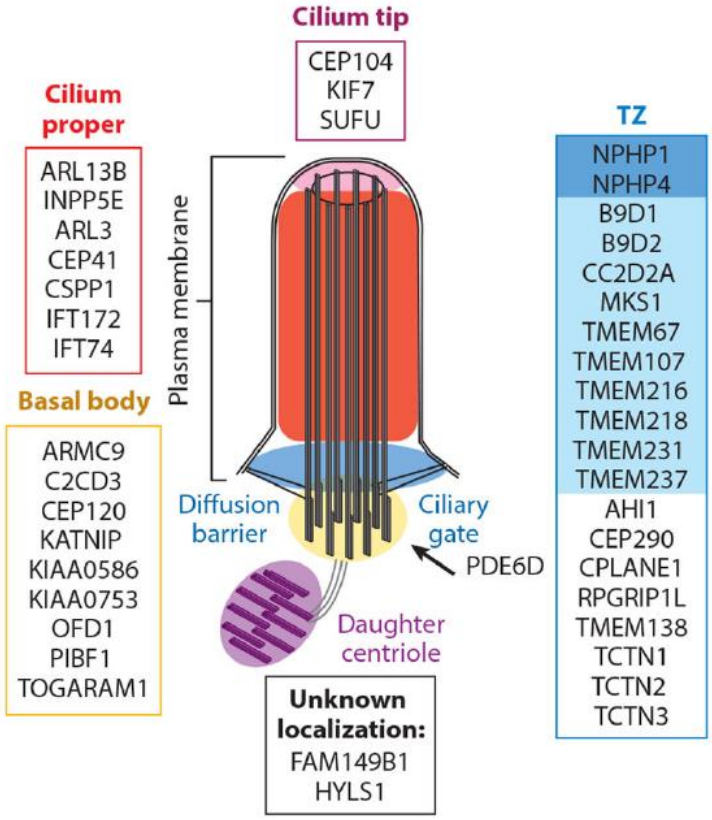

Figure 1.25 Schematic representation of Joubert syndrome-associated proteins. *Joubert syndrome-associated proteins include proteins localized at the cilium proper, at the cilium tip, at the basal bosy, and at the transition zone (TZ). Only FAM149B1 and HYLS1 are of unknown localization. Adapted from (Van De Weghe et al., 2022).*

JS is characterized by multi-organ malformations that affect brain, eye, kidneys, liver, and skeleton. JS is usually prenatally diagnosed by magnetic resonance imaging (MRI) through the appearance of a peculiar mid-hindbrain malformation named “molar tooth sign” (MTS) (Maria *et al*, 1997). The MTS is represented by cerebellar vermis hypoplasia or aplasia, deep interpeduncular fossae, and thick and horizontally oriented superior cerebellar peduncles (**Fig. 1.26**) (Van De Weghe *et al.*, 2022).

Figure 1.26 Magnetic nuclear resonance image of Joubert syndrome molar tooth sign. *The molar tooth sign (in red circle) is a mid-hindbrain malformation that represents a diagnostic feature of Joubert syndrome. Adapted from (Van De Weghe et al., 2022).*

Conditional knockout mice of the ciliary genes *Arl13b*, *Inpp5e*, and *Talpid3* (a centrosomal protein involved in the cilium assembly) recapitulate axonal tract malformations and alterations of superior cerebellar peduncles decussation similar to the one observed in human JS related diseases (JSRD) (**Fig. 1.27**) (Bashford & Subramanian, 2019; Guo *et al*, 2019).

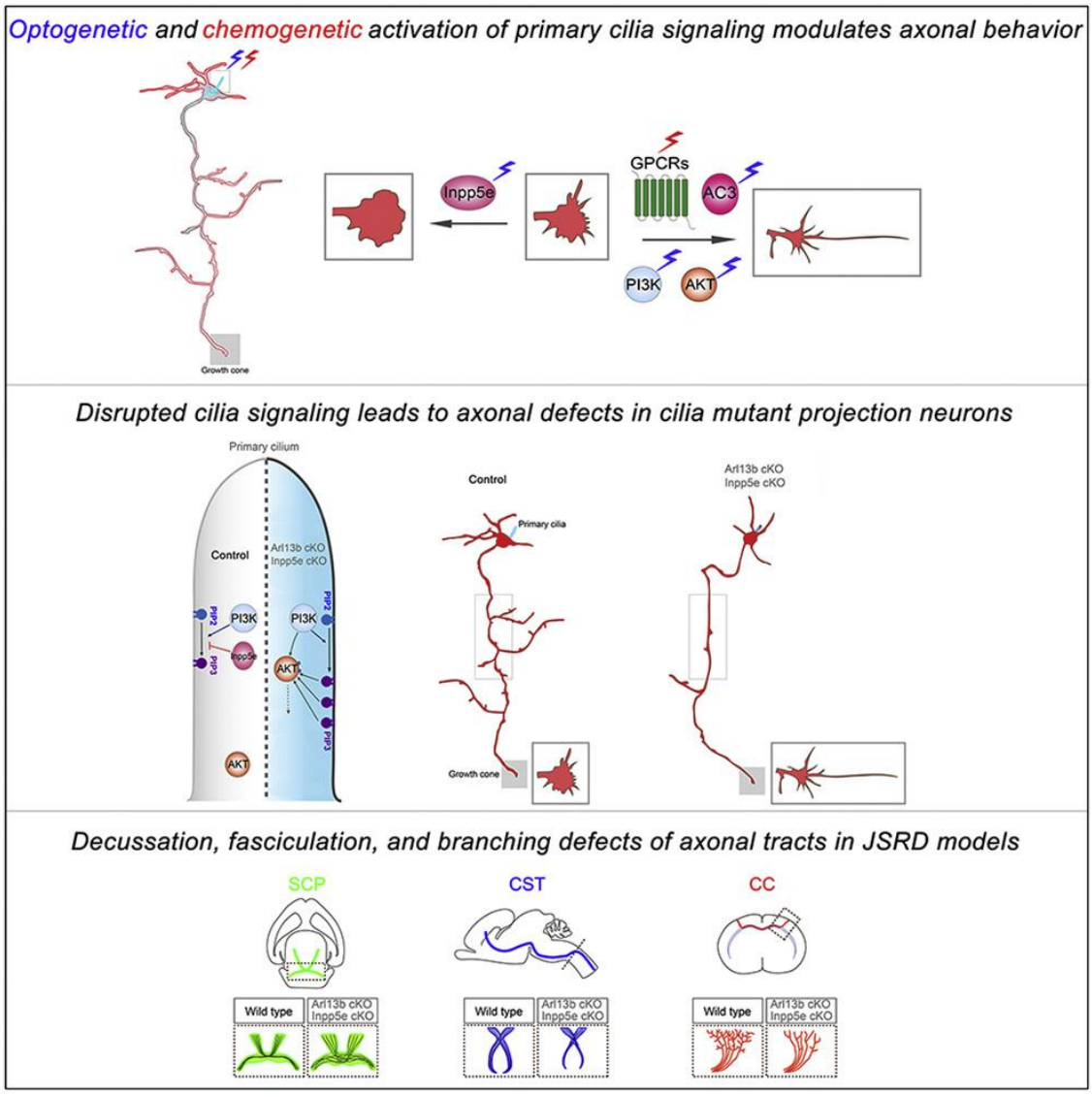

Figure 1.27 Schematic representation of axonal behavior regulation by cilia in physiology and in disease. *Axonal behavior is modulated by ciliary signalling, which is altered by the conditional inactivation of Arl13b and Inpp5e ciliary genes. Conditional knockout mice for these genes recapitulate axonal tracts malformations of Joubert syndrome related diseases (JSRD) (Guo et al., 2019)*

Generally, during infancy JS manifestations comprehend hypotonia, tachypnea and apnea, and eye movement anomalies. In some individuals these symptoms coexist with ataxia and mental retardation. The 15% of JS patients could be affected by polydactyly, liver fibrosis, or an eye malformation called coloboma, while retinal dystrophy and renal cystogenesis and fibrosis occur in the 30% and 20% of cases, respectively (Van De Weghe *et al.*, 2022). Of note, the severity of this disease has been associated with the type of the two mutations: protein-truncating mutations cause severe manifestation of the disease, with early onset and abnormalities in multiple organs, while missense mutations induce a mild phenotype, with a late onset and restricted organ manifestations (Hildebrandt *et al.*, 2011).

1.2.2.4 Meckel syndrome

Meckel syndrome (MKS) has been described for the first time in the XIX century by Johann Friedrich Meckel in two siblings with occipital encephalocele, polydactyly, and polycystic kidneys. This recessive disorder is classified as a ciliopathy, since it is due to mutations in ciliary genes (reported in **Fig. 1.28**) (Van De Weghe *et al.*, 2022).

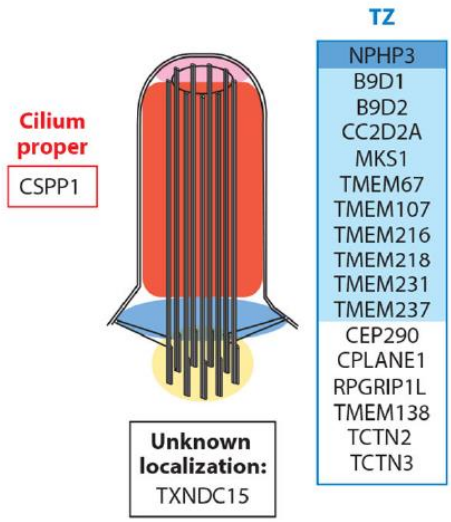

Figure 1.28 Schematic representation of Meckel syndrome-associated proteins. *The majority of Meckel syndrome (MKS)-associated proteins are transition zone (TZ) proteins. Adapted from (Van De Weghe et al., 2022)*

Like in JS, also in MKS different combinations of mutations lead to a plethora of phenotypes with different severity. Although some cases of survival during infancy have been reported, MKS is usually pre- or peri-natal lethal. Other features of this recessive multi-organ disorder are represented by congenital hepatic fibrosis and *situs inversus*. Additional brain malformation (as hydroencephalus), eye abnormalities (coloboma, anophthalmia, microphthalmia), skeletal dysplasia, cleft lip and palate, congenital heart disease, lung hypoplasia, oral hamartomas, and ambiguous genitalia, are associated with this ciliopathy (Barisic *et al*, 2015).

1.2.2.5 Bardet-Biedl syndrome

Bardet-Biedl syndrome (BBS) is a autosomal recessive disease classified as a ciliopathy. Indeed, it is caused by mutations in 22 genes, including the ones encoding the BBSome core proteins (BBS1, BBS2, BBS4, BBS5, BBS7, BBS8, BBS9, BBS18/BBIP10) (see **Chapter 1.1.1.2**). In particular BBS1 mutations are associated with the majority of BBS cases. The main manifestations of this syndrome include cognitive retardation, retinal degeneration, cystic kidneys, polydactyly, anosmia, and infertility. Other BBS features consist of systemic metabolism alterations, leading to diabetes mellitus and obesity. These findings have contributed to demonstrate an interplay between cilia and systemic metabolism (see **Chapter 1.3**) (Hildebrandt *et al.*, 2011; McConnachie *et al*, 2021).

1.2.2.6 Nephronophthisis

Nephronophthisis (NPH) is the most frequent cause of end-stage renal disease (ESRD) in children (Hildebrandt & Zhou, 2007). Three different subtypes of autosomal recessive kidney disorder have been classified: infantile, juvenile, and adult NPH. Infantile NPH is characterized by the onset of ESRD before the 5 years of age, with enlarged kidneys and severe hypertension. Juvenile NPH represent the most common form leading to marked tubulointerstitial fibrosis and the development of renal cysts in the cortical part of kidney medulla from distal. The juvenile form of NPH is also characterized by polyuria, polydipsia, and proteinuria. Extra-renal abnormalities have been described in some NPH patients. Among them, retinal dystrophy, polydactyly, cerebellar vermis hypoplasia, and cranio-ectodermal aplasia are encounted. The adult NPH displays similar features compared to the juvenile form driving the onset of the disease later than 15 years of age (Stokman *et al*, 2021). This disease is due to mutations in 22 genes, most of which encode for ciliary proteins. The latter have been found in different centrosome-cilium complex compartment: basal body, distal appendages, transition zone, and inversin compartment. Others are reported to be involved in the IFT trafficking (reported in **Fig. 1.29**) (Stokman *et al.*, 2021).

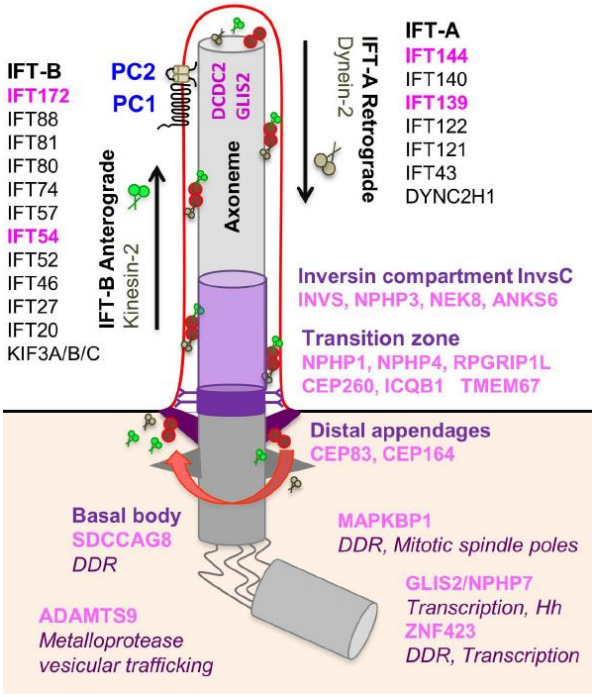

Figure 1.29 Schematic representation of nephronophtisis-associated proteins. *Most nephronophtisis-associated proteins are localized at the centrosome-cilium complex. Adapted from (Stokman et al., 2021).*

1.2.2.7 Alström syndrome

Alström syndrome (ALMS) is a rare autosomal recessive disorder affecting less than 1:1,000,000 individuals (Girard & Petrovsky, 2011). ALMS is caused by mutations in ALMS1, most of which induces a truncated protein. Up to 100 mutations in ALMS1 have been described (Joy *et al*, 2007). Main features of ALMS are obesity, type 2 diabetes mellitus, and neurosensory defects (Collin *et al*, 2002). Differently from BBS, this ciliopathy does not manifest with polydactyly and cognitive retardation. Hypertriglyceridemia, which leads to acute pancreatitis, liver abnormalities, hypothyroidism, growth hormone deficiency, and infertility are frequent features of ALMS (Girard & Petrovsky, 2011). ALMS1 is a centrosome protein of 461 kDa, ubiquitously expressed. ALMS1 presence in different tissues is in line with the multiorgan defects that this disease induces (Girard & Petrovsky, 2011). Although its function has still not been completely elucidated, ALMS1 appeared to be involved in primary cilia morphology, since its inactivation results in longer cilia, and in altered TGFβ/BMP signalling (Alvarez-Satta *et al*, 2021; Massague, 2012) (see **Chapter 1.1.2.4**).

1.3 Cilia, obesity, and diabetes

The evidence that a subset of ciliopathies, such as the BBS, MKS, and ALMS, are characterized by the development of obesity, has suggested a possible role of cilia in the regulation of appetite and hunger signalling. The removal of cilia through *Kif3a* and *Ift88* ubiquitous inactivation in mice was reported to induce increase in food intake and subsequently in body weight, showing that cilia could possibly be involved in the regulation of satiety. Indeed, when the mice without cilia were subjected to the diet of the relative controls, they did not develop obesity, suggesting that cilia restrict food intake (Davenport *et al*, 2007). Neuronal ablation of cilia confirms that these organelles are required for the regulation of satiety, since mice lacking cilia in neurons became obese. Since hypothalamic anorexigenic propiomelanocortin (POMC) and orexigenic agouti-related peptide (AgRP)-expressing neurons mediate appetite signalling, cilia were ablated from these neurons *in vivo* to test whether cilia are involved in driving obesity. The removal of cilia in POMC-expressing neurons led to increased food intake and obesity (Davenport *et al.*, 2007). Furthermore, cilia lacking POMC-expressing neurons displayed increased leptin, insulin, and serum glucose levels. However, when mice were subjected to the restricted diet of the controls, they did not increase suggesting that they were secondary to obesity (Berbari *et al*, 2013). Fat Mass and Obesity-Associated (FTO) gene is nearby the TZ protein RPGRIP1L gene, whose heterozygous inactivation leads to hyperphagia and body weight increase. Moreover, it appears that *Rpgrip1l* heterozygous mice display reduced AC3-positive neuronal cilia, suggesting that the lowering of *Rpgrip1l* expression could alter neuronal cilia (Stratigopoulos *et al*, 2014). Furthermore, one of the SNPs of FTO overlaps with cut-like homeobox 1 (CUX1) gene, which is a transcriptional regulator of RPGRIP1L, further strengthening the involvement of this ciliary protein in obesity development (Stratigopoulos *et al*, 2011; Vadnais *et al*, 2013). Among the ciliary GPCRs that appear to regulate energy homeostasis and body weight, NPY2R is able to mediate the satiety signalling and it has been described that its ciliary localization, mediated by BBSome interacting protein (BBIP10), is required to drive its anorexigenic activity, although different *Npy2r* KO mice are reported to display opposed phenotypes with some showing reduced body weight to some that were mild obese with an increased fat pad size compared to the relative controls (Naveilhan *et al*, 1999; Sainsbury *et al*, 2002). Another ciliary GPCR implicated in satiety signalling is

represented by melanin-concentrating hormone receptor 1 (MCHR1), whose activation drives increased food intake, while inhibition promotes anorexigenic effects (Borowsky *et al*, 2002; Qu *et al*, 1996; Shimada *et al*, 1998). Other examples of GPCR proteins localized at cilia, which are involved in the regulation of satiety and energy homeostasis, are dopamine receptor 1 (DRD1), kiss-peptin receptor 1 (KISS1R), somatostatin receptor 3 (SSTR3), and serotonin receptor 6 (5HTR6) (**Fig. 1.30**) (Vaisse *et al*, 2017).

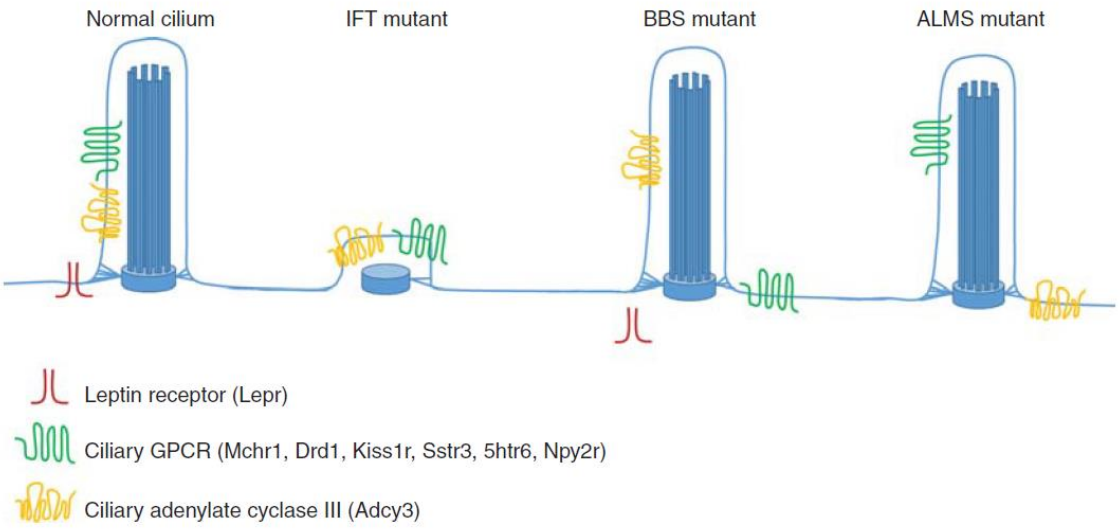

Figure 1.30 Scheme of signalling for the regulation of energy homeostasis orchestrated by cilia. *Upon mutations of ciliary proteins related to intraflagellar transport (IFT), Bardet-Biedl syndrome (BBS), and Alström syndrome (ALMS), the components of the signalling for the regulation of energy homeostasis display an altered localization. Mchr1: melanin-concentrating hormone receptor 1; Drd1: dopamine receptor 1; Kiss1r: kiss-peptin receptor 1; Sstr3: somatostatin receptor 3; 5htr6: serotonin receptor 6 (Vaisse et al., 2017).*

Furthermore, it has been published that cilia play a crucial role in the differentiation of preadipocytes into adipocytes. Other than IGF1R upon insulin binding, also the free fatty fatty acid receptor 4 (FFAR4) has been reported to drive adipogenesis through AC3-driven cAMP increase and consequent exchange protein directly activated by cAMP (EPAC) signalling to drive chromatin remodelling and adipogenic genes expression (**Fig 1.31**) (Hilgendorf *et al*, 2019).

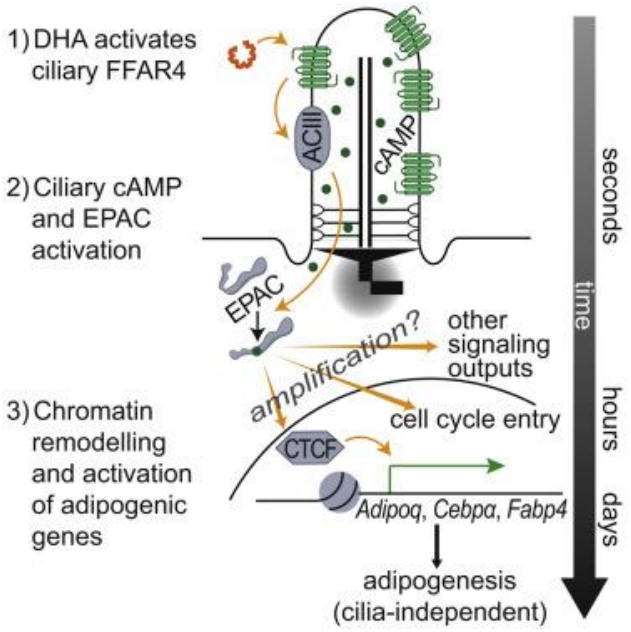

Figure 1.31 Scheme of ciliary FFAR4-induced signalling to promote adipogenesis. *Docosahexaenoic acid (DHA) leads to ciliary FFAR4 activation, which promotes ciliary cAMP and exchange protein directly activated by cAMP (EPAC) signalling to drive chromatine remodeling and adipogenic genes activation. (Hilgendorf et al., 2019).*

Diabetes is driven by the incapability of the organism to drive the transmembrane transport of glucose inside the cells upon insulin signalling. This phenomenon is known as insulin resistance and could be associated to obesity. The possible role of cilia in regulation of glucose metabolism is suggested by the evidence that type 2 diabetes mellitus often affect BBS patients and, in some cases, also ALMS patients. Cilia disruption through *Ofd1* and *Bbs4* inactivation in pancreatic islets is reported to impair the signalling of IR (Gerdes *et al*, 2014), which has been detected in a database for cilia together with another diabetes-susceptibility gene, calcium/calmodulin dependent protein kinase 1D (CAMK1D) (Arnaiz *et al*, 2014). This finding further supports the hypothesis of a possible regulation of systemic metabolism by cilia. In conclusion, although the precise mechanisms leading to this regulation are not completely uncovered, some key findings shed light on the role of cilia in both obesity and diabetes.

1.4 Cellular Metabolism

The cellular metabolism consists of either catabolic or anabolic pathways, which comprise chemical reactions catalyzed by enzymes. Catabolic pathways lead to the breackdown of metabolites to generate energy in the form of ATP, while anabolic pathways drive the production of macromolecules starting from simpler units with energy expenditure. In the following chapters we report the main pillars of cellular metabolism giving insights into the metabolic reprogramming occurring in ADPKD.

1.4.1 Glycolysis

Glycolysis is the multistep process of ten reactions leading to the production of pyruvate, ATP and NADH starting from glucose. Upon normoxia, the pyruvate produced through glycolysis is converted into acetyl-CoA to fuel the tricarboxylic acid (TCA) cycle and to drive oxidative phosphorylation (OXPHOS). During this process, the TCA cycle generates the the electron donors (NADH and $FADH_2$) necessary for the electron transport chain (ETC), where electrons pass through the mitochondrial respiratory chain complexes (complex I, II, III, IV) to be pumped into the intermembrane space of mitochondria. The flow back of protons through the ATP synthase (complex V) induces the synthesis of ATP and oxygen is the final electron acceptor leading to the production of H_2O. Thus, the production of 36-38 moles of ATP occurs from 1 mole of glucose. Upon hypoxia, anaerobic glycolysis promotes the conversion of pyruvate to lactate through lactate dehydrogenase (LDH), since O_2 is not available to support the OXPHOS. Despite this process is less efficient in terms of ATP production as compared to OXPHOS, in the 1920s, Otto Warburg discovered that cancer cells upon normoxia exploit preferentially glycolysis rather than OXPHOS to produce energy (**Fig. 1.32**) (Vander Heiden *et al,* 2009; Warburg *et al,* 1927). This effect is known as aerobic glycolysis or the "Warburg effect" and was supposed to occur in cells with impaired mitochondrial function. However, subsequent studies showed that some tumors do not display impaired mitochondrial respiration, suggesting that the reason why the Warburg effect occurs should be different. Indeed, this process involve also the upregulation of glucose transporters, such as GLUT, to compensate for the reduced efficiency in energy production of aerobic glycolysis compared to OXPHOS (Vander Heiden *et al.*, 2009). Furthermore, increasing the expression of the glycolytic enzymes, such as hexokinase 2

(HK2) and pyruvate kinase (PKM2) represents a complementary strategy for cancerous cells to undergo aerobic glycolysis instead of OXPHOS to promote proliferation.

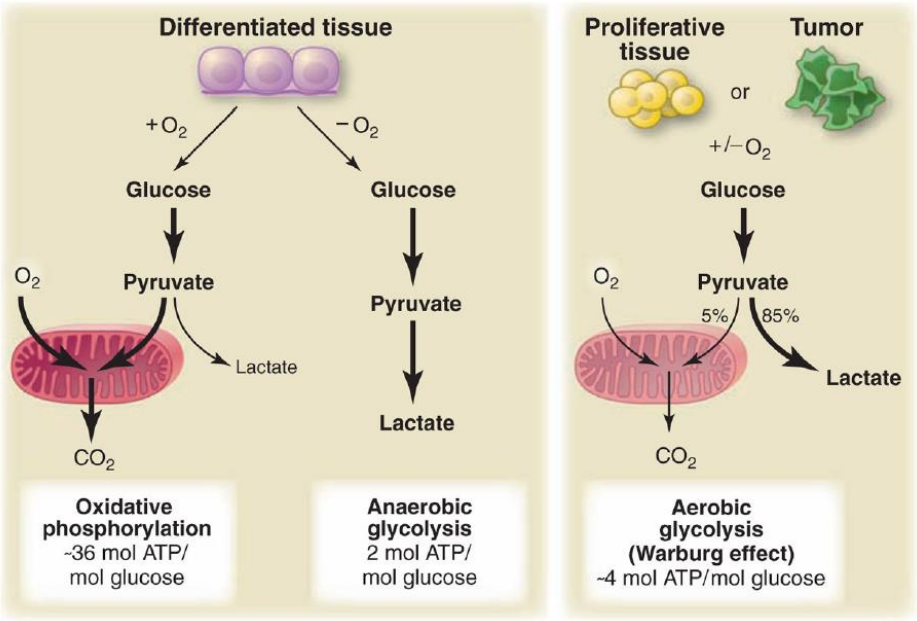

Figure 1.32 Scheme of glycolytic pathways. *Glycolysis is the process of oxidation of glucose to pyruvate. Upon normoxia, glucose-derived pyruvate undergoes oxidative phosphorylation (OXPHOS). Upon hypoxia, glucose-derived pyruvate undergoes anaerobic glycolysis with the production of lactate. Proliferative tissues and tumors are characterized by the Warburg effect or aerobic glycolysis, since cells use glycolysis instead of OXPHOS to produce energy with the production of lactate (Vander Heiden et al., 2009).*

1.4.2 Lipid metabolism

Lipid metabolism mainly consists of fatty acid synthesis (FAS) and fatty acid oxidation (FAO). FAS is required for cell proliferation, since fatty acids are the building blocks of cellular membranes. Indeed, this anabolic pathway is upregulated in cancer, where tumor cells are highly proliferative (DeBerardinis *et al*, 2008). FAS is responsible for the synthesis of fatty acids starting from acetyl-CoA, which could derive by citrate or acetate. As regard as the citrate generated by the TCA cycle, ATP citrate lyase (ACLY) is able to covert the citrate into acetyl-CoA and oxaloacetate in the cytosol. Then, acetyl-CoA is carboxylated by acetyl-CoA carboxylase (ACC) to form malonyl-CoA. ACC displays two isoforms: ACC1 and ACC2. ACC1 allows the production of malonyl-CoA as the substrate for FAS and is preferentially expressed in lipogenic tissues, while ACC2 is expressed in oxidative tissues and produce malonyl-CoA to inhibit carnitine palmitoyl transferase 1 (CPT1), which is the bottleneck enzyme for FAO (Currie *et al*, 2013). Fatty acid synthetase (FASN) produces mainly palmitate by catalysing sequential condentation steps from malonyl-CoA and acetyl-CoA. Fatty acid elongases (ELOVL) and stearoyl-CoA desaturases (SCD) are responsible for palmitate elongation and desaturation at the Δ9 position, respectively. These reactions lead to mono- or poly-unsaturated fatty acids synthesis (Rohrig & Schulze, 2016). FAO represents the catabolic process by which fatty acids shortening leads to the generation of acetyl-CoA, NADH, and $FADH_2$ through repetitive series of reactions. Acetyl-CoA generated by FAO could be used to fuel the TCA cycle to produce energy. As regard as energy production, fatty acids are able to provide the double of ATP compared to carbohydrates. Indeed, FAO rate is upregulated upon nutrient deprived conditions to sustain the production of energy (**Fig. 1.33**). The limiting step for FAO is the entry of fatty acids into the mitochondria, where the oxidation reactions occur. Indeed, fatty acids with a carbon chain longer than 14 carbons require transporters to enter into the mitochondrial interspace and then into the mitochondrial matrix. First, long-chain fatty acids are activated by the long-chain acyl-CoA synthases (ACSLs), which generate acyl-CoAs that are transported into the mitochondrial intermembrane space through CPT1. The latter catalyzes the conversion of acyl-CoAs into acylcarnitines. Then, acylcarnitines are allowed to pass across the inner mitochondrial membrane by the activity of the carnitine-acylcarnitine translocases. In the mitochondrial matrix CPT2 regenerates acyl-CoA from acylcarnitine. At this step, acyl-

CoAs undergo the oxidative removal of successive two carbons to generate acetyl-CoA, which fuels the TCA cycle. Furthermore, NADH and $FADH_2$ produced during FAO are used to generate ATP through the electron transport chain (Houten *et al*, 2016).

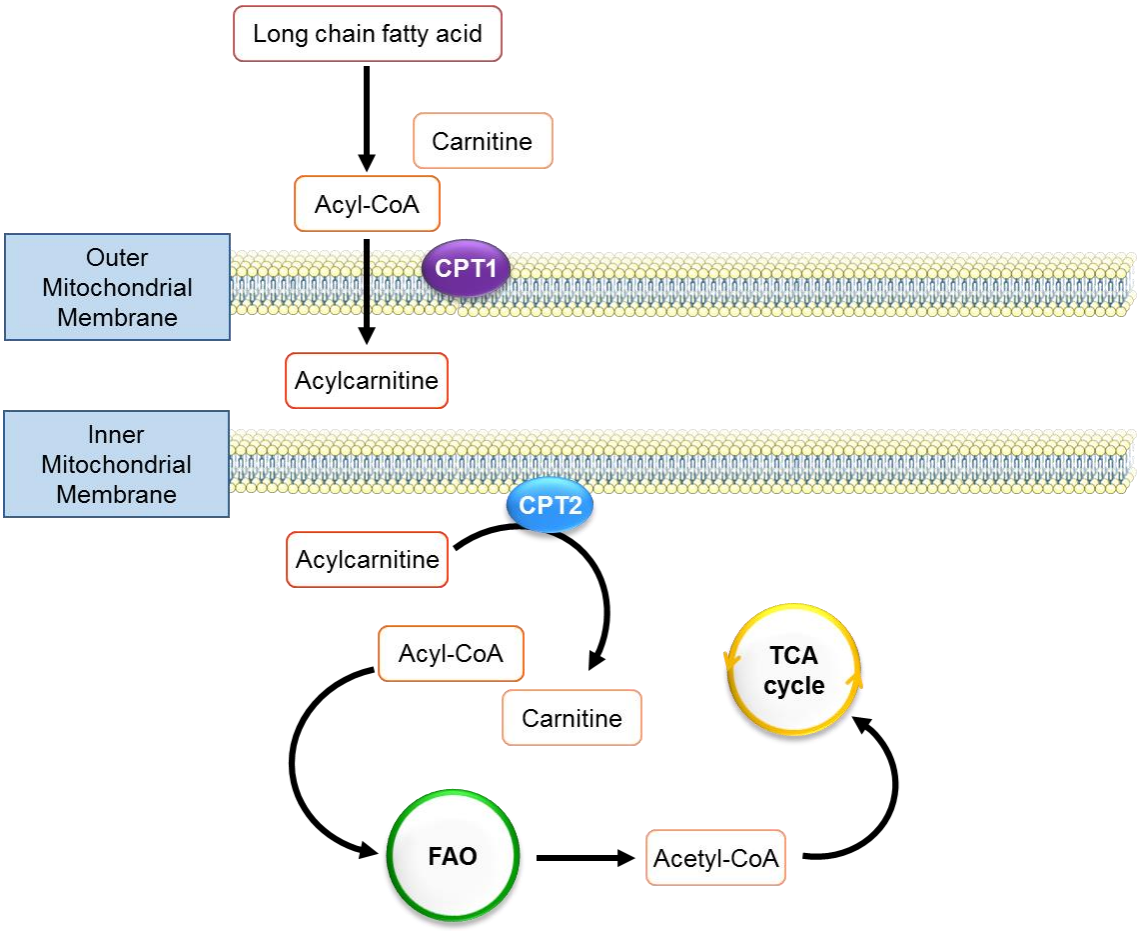

Figure 1.33 Scheme of fatty acid import and oxidation into mitochondria. *Fatty acid oxidation consists of shortening of fatty acids to produce acetyl-CoA, which could be used to fuel the TCA cycle.*

1.4.3 Glutamine metabolism

Glutamine is a non-essential aminoacid that is synthetize by the cells throught the glutamine synthetase enzyme (GS). Nevertheless, the demand of this aminoacid could exceed its production making glutamine essential for the survival of the cell. Indeed, glutamine is a source of both carbon and nitrogen for the synthesis of other non-essential aminoacids, hexosamines, and nucleotides. Glutamine-derived nitrogen could also be released as ammonia. At the systemic level, glutamine represents an inter-organ shuttle, where some organs, such as the lung or the skeletal muscle, produce and secrete glutamine that is consumed by others, such as the kidney, which uses it for the acid-base regulation. Indeed, upon aciduria, glutamine-derived ammonia is excreted together with organic acids to restore the physiological pH (**Fig. 1.34**) (Hensley *et al*, 2013).

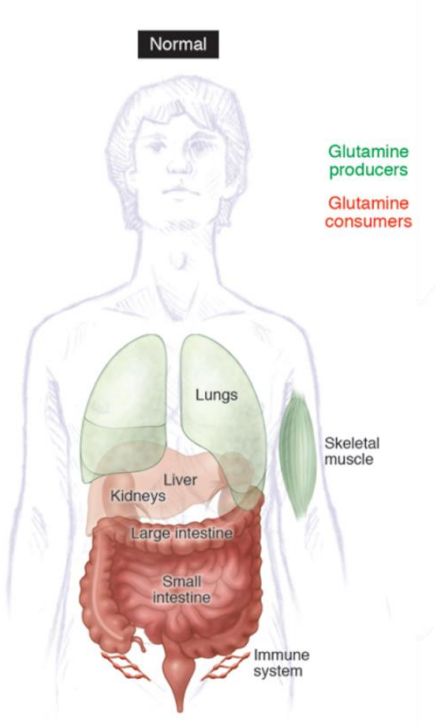

Figure 1.34 Scheme of glutamine producers and consumers organs. *Glutamine is an inter-organ shuttle: lungs and skeletal muscle are glutamine producers, while kidneys, liver, intestine and the immune system are glutamine consumers. Adapted from (Hensley et al., 2013).*

At the cellular level, glutamine is usually converted into glutamate by glutaminase (GLS) with released of ammonia.

Glutamate is the precursor of glutathione, which is a ROS scavenger, and of other non-essential aminoacids as alanine, serine, glycine, and aspartate (DeBerardinis *et al.*, 2008). Furthermore, glutamine-derived glutamate is able to be converted into α-KG, a TCA cycle intermediate, by transaminases, when glucose is available, or by glutamate dehydrogenase (GDH), upon glucose deprivation, leading to the release of ammonia. At this step, glutamine-derived α-KG could be used either to fuel the TCA cycle and produce ATP through OXPHOS by a process named glutaminolysis, or to undergo reductive carboxylation to generate citrate, which is then employed by ACLY to produce acetyl-CoA for FAS (**Fig. 1.35**) (DeBerardinis *et al.*, 2008). Importantly, when glucose is scarce, glutamine becomes the preferential carbon source to fuel the TCA cycle through anaplerosis and, as a consequence, to sustain the cell survival upon metabolic stress (DeBerardinis *et al*, 2007; Yang *et al*, 2014; Zhang *et al*, 2017b). Another piece of evidence of the glutamine role in cell survival is represented by the finding that glutamine, as well as leucine, is a key activator of the serine/threonine kinase mTORC1, which is deeply involved in cell growth and protein translation (Jewell *et al*, 2015). All these findings reveal the role of glutamine as a key metabolite involved in several processes essential for the cell. In highly proliferative cells, such as the cancerous ones, glutaminolysis is upregulated leading to consider it as a hallmark of cancer (DeBerardinis *et al.*, 2008).

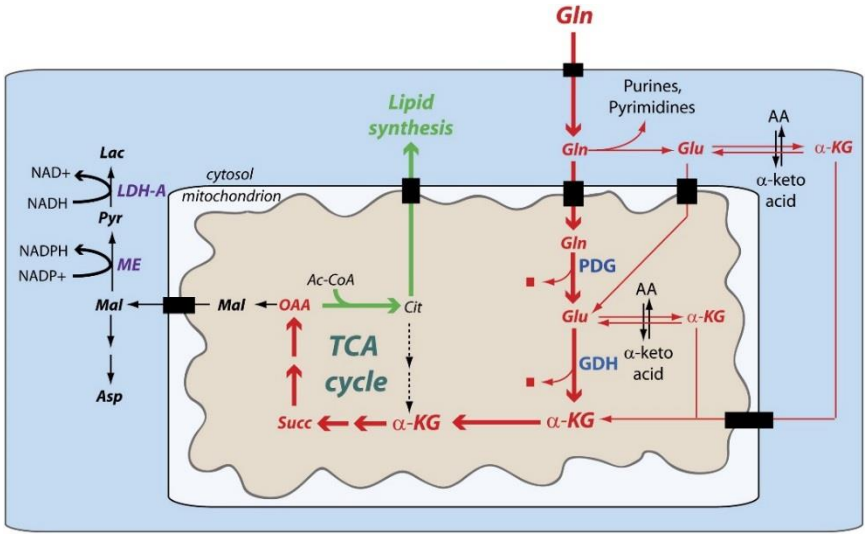

Figure 1.35 Scheme of glutamine metabolism. *Glutamine is a preferential carbon and nitrogen source for the cell. This aminoacid is involved in the synthesis of purines and pyrimidines and is able to fuel the TCA cycle through anaplerosis. Furthermore, glutamine can promote lipid synthesis through the generation of citrate by reductive carboxylation (DeBerardinis et al., 2008).*

1.4.4 Metabolic rewiring in ADPKD

An important feature of ADPKD is represented by the metabolic reprogramming involving several cellular metabolic pathways. Our group found out that this rewiring includes enhanced aerobic glycolysis, which in the cancer field is known as the Warburg effect. This process, described by Otto Warburg, drives the production of lactate from pyruvate upon normoxia. Indeed, our group found that *Pkd1* mutant cells display decreased glucose and increased lactate levels in their conditioned medium. However, the efficiency in terms of ATP production of aerobic glycolysis is dramatically lower than the one reached through the conversion of pyruvate into acetyl-CoA to fuel the tricarboxylic acid (TCA) cycle in mitochondria. Thus, cells that undergo the Warburg effect try to improve ATP production by increasing glucose uptake and utilization. Indeed, tracing with labelled $^{13}C_6$-glucose in *Pkd1* mutant cells revealed a higher glucose uptake that resulted in increased lactate (Podrini *et al*, 2018; Rowe *et al*, 2013). To further support the evidence of aerobic glycolysis in ADPKD, upregulation of the glycolytic key enzymes such as hexokinase 1 (*Hk1*) (which catalyzes the conversion of glucose in glucose-6-phosphate), lactate dehydrogenase (*Ldha*) (responsible of the conversion of pyruvate into lactate), and pyruvate kinase muscle isoform M2 (*Pkm2*) (which converts phosphoenolpyruvate (PEP) into pyruvate) was reported in *Pkd1* mutant cells (**Fig. 1.36**) (Rowe & Boletta, 2014).

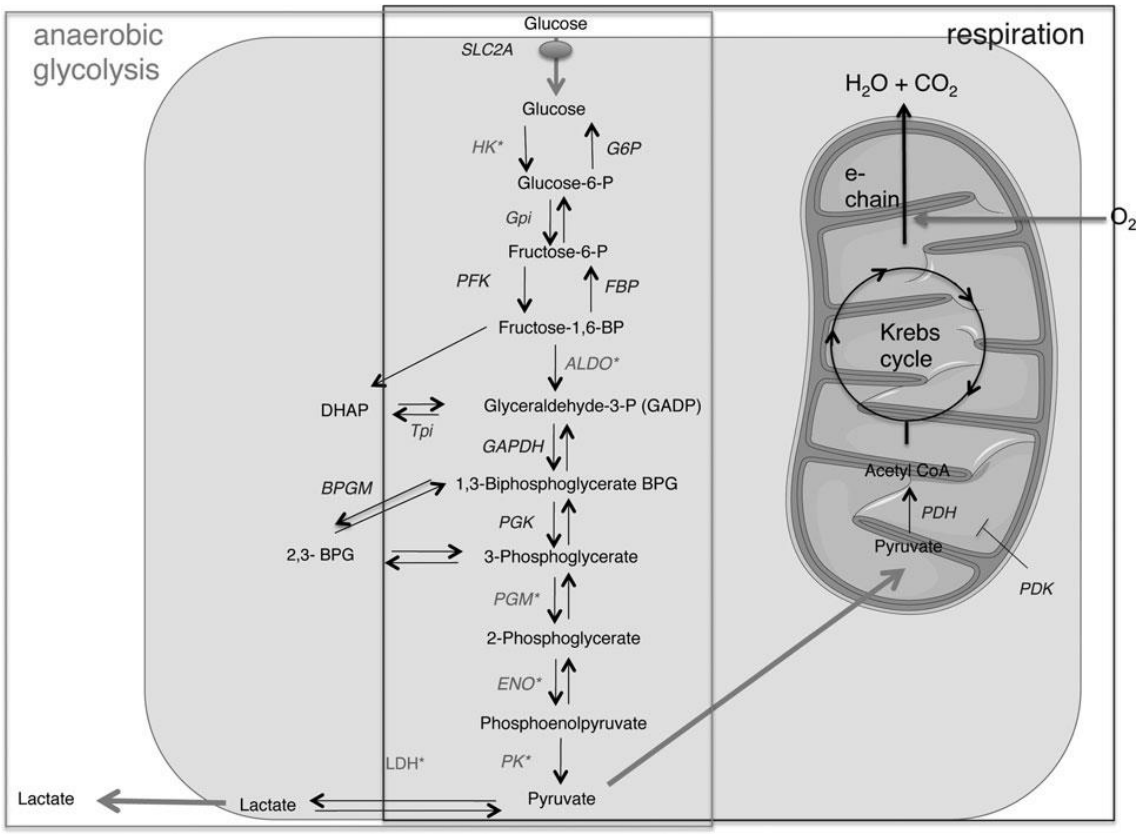

Figure 1.36 Schematic representation of glycolysis reactions. *Aerobic glycolysis drives the oxidation of glucose through different steps to produce pyruvate that once in mitochondria is converted into acetyl-CoA to fuel the Krebs (TCA) cycle. ALDO: aldolase (gene); BGP: biphosphoglycerate; 2,3-BPG: 2,3-biphosphoglycerate; BPGM: biphosphoglycerate mutase (gene); DHAP: dihydroxyacetone phosphate; ENO: enolase (gene); FBP: fructose-1,6-biphosphate; GADP: glyceraldehyde-3-phosphate; GAPDH: glyceraldehyde-3-phosphate dehydrogenase (gene); G6P: glucose-6-phosphate; Gpi: glucose phosphate isomerase (gene); HK: hexokinase (gene); LDH: lactate dehydrogenase (gene); PDH: pyruvate dehydrogenase (gene); PDK: pyruvate dehydrogenase kinase (gene); PFK: phosphofructokinase (gene); PGK: phosphoglycerate kinase (gene); PGM: phosphoglycerate mutase (gene); PK: pyruvate kinase (gene); SLC2A: solute carrier family 2A; Tpi: triose phosphate isomerase (gene). Genes of glycolytic enzymes differentially expressed in cystic kidneys of patients carrying Pkd1 mutations compared to normal kidneys are expressed with asterisks (Rowe & Boletta, 2014).*

Another key feature of the ADPKD metabolic reprogramming is the defective oxidative phosphorylation (OXPHOS), revealed by accumulated α-ketoglutarate (α-KG), decreased glucose-derived TCA cycle intermediates, as succinate, fumarate, and malate, and reduced mitochondrial respiration in *Pkd1 in vitro* models (**Fig. 1.37**) (Podrini *et al*, 2020; Podrini *et al.*, 2018).

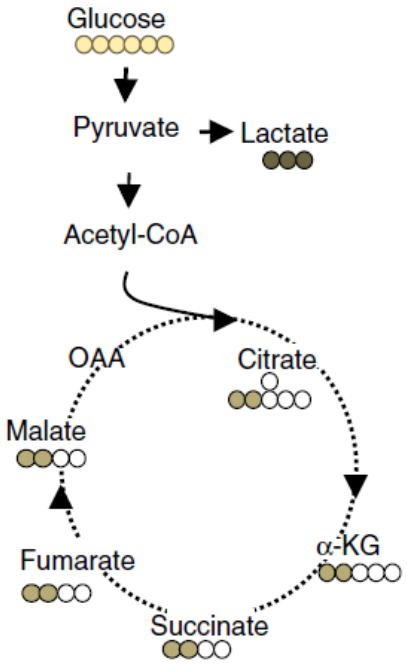

Figure 1.37 Scheme of labelled $^{13}C_6$-glucose tracing of lactate and TCA cycle intermediates. *Coloured dots: $^{13}C_6$ carbon atoms (yellow: glucose m+6; dark brown: lactate m+3; light brown: TCA cycle intermediates m+2). White dots: unlabelled carbons. α-KG: α-ketoglutarate; OAA: oxaloacetate. Adapted from (Podrini et al., 2018)*

Glutaminolysis is upregulated in ADPKD, since glutamine uptake and glutamine-derived TCA cycle intermediates are reported to be upregulated (Podrini *et al.*, 2018). Together with glucose, glutamine is a key carbon source for the energy prodution that is preferentially used to promote OXPHOS (DeBerardinis *et al.*, 2007; Yang *et al.*, 2014; Zhang *et al.*, 2017b). Glutamine is able to be converted into glutamate and to fuel the TCA cycle through the production of α-KG and the downstream TCA cycle intermediates (**Fig. 1.38**) (Podrini *et al.*, 2018).

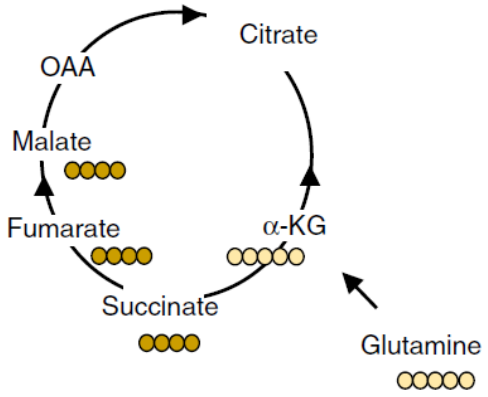

Figure 1.38 Scheme of labelled $^{13}C_5$-glutamine tracing of TCA cycle intermediates. *Coloured dots: $^{13}C_5$ carbon atoms (yellow: glutamine m+5, α-KG m+5; orange: TCA cycle intermediates m+4). White dots: unlabelled carbons. α-KG: α-ketoglutarate; OAA: oxaloacetate. Adapted from (Podrini et al., 2018)*

Glucose and glutamine deprivation promotes cell death in *Pkd1* inactivated cells, suggesting that interfering with carbon metabolism could represent a therapeutic strategy for ADPKD (Podrini *et al.*, 2018). A key role in glutamine usage in ADPKD is played by asparagine synthetase (ASNS) (Podrini *et al.*, 2018). This enzyme catalyzes the conversion of glutamine and aspartate into glutamate and asparagine and is upregulated upon amino acid depletion (Kilberg *et al*, 2012) and endoplasmic reticulum stress (Kilberg *et al*, 2009). Indeed, both these cellular stress pathways promote the phosphorylation of eukaryotic translation elongation 2 subunit α (eIF2α) through general control non derepressable 2 (GCN2) and PRK–like endoplasmic reticulum kinase (PERK), respectively, and subsequent mRNA transcription upregulation. ASNS transcription is activated through the binding of the transcription factor ATF4 to an enhancer at the promoter of this gene (**Fig. 1.39**) (Lomelino *et al*, 2017).

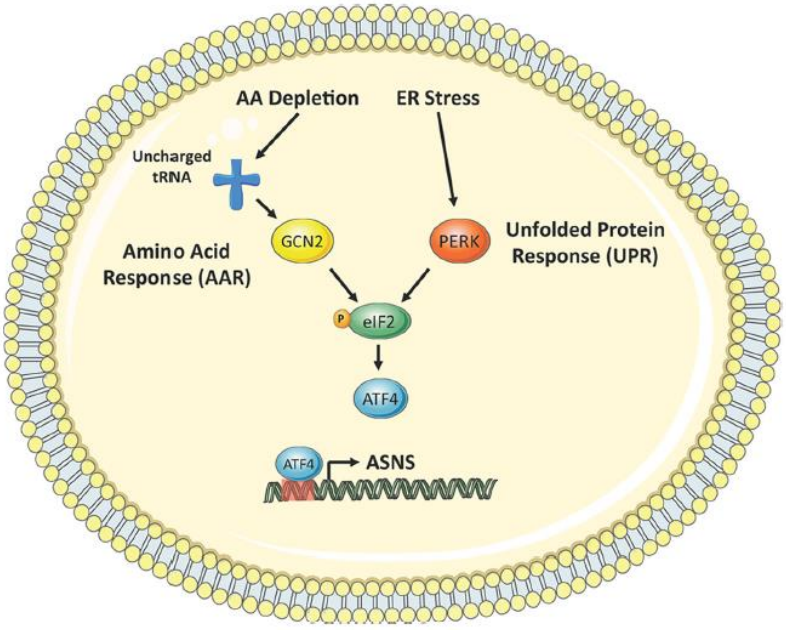

Figure 1.39 Schematic representation of ASNS transcriptional regulation. *Aminoacid (AA) depletion or ER stress drive phosphorylation of eIF2 by GCN2 and PERK, respectively. Then, ATF4 binds an enhancer in the promoter of ASNS to drive its expression (Lomelino et al., 2017).*

Indeed, *Asns* resulted to be upregulated in *Pkd1 in vitro* and *in vivo* models, leading to increased levels of asparagine and decreased aspartate levels (**Fig. 1.40**) (Podrini *et al.*, 2018).

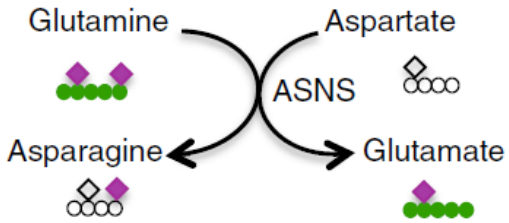

Figure 1.40 Schematic representation of $^{13}C_5$-$^{15}N_2$-glutamine tracing referred to ASNS activity. *ASNS coverts glutamine and aspartate into asparagine and glutamate. Green dots: $^{13}C_5$-glutamine derived carbons. Purple squares: $^{15}N_2$-glutamine derived nitrogens (Podrini et al., 2018)*

Our group propose that ASNS could be a new therapeutic target for ADPKD treatment, since interfering with *Asns* reduces the TCA cycle fuelling driven by glutamine and impairs cell survival especially upon glucose deprivation in *Pkd1* mutant cells at least *in*

vitro (Podrini *et al.*, 2018). Glutamine undergoes reductive carboxylation in *Pkd1* models. Reductive carboxylation is the process by which glutamine is able to produce citrate and subsequently lipogenic acetyl-CoA resulting in fatty acid synthesis. Indeed, *Pkd1* mutant cells display increased glutamine-derived palmitate levels and upregulated expression of fatty acid synthase (*Fasn*), which is a key enzyme involved in fatty acid synthesis (FAS) (Podrini *et al.*, 2018). This upregulation of FAS appears to be causative of the ADPKD decreased fatty acid oxidation (FAO) (Menezes *et al*, 2016), which is a key catabolic process to produce energy, especially during fasting, by degrading long chain fatty acids (Houten *et al.*, 2016). Long chain fatty acids are activated by acyl-CoA synthetase and subsequently are imported into the mitochondrion by carnitine palmitoyl transferase 1 (CPT1) in the form of acylcarnitines. Then, carnitine-acylcarnitine translocase transport them into the mitochondrial matrix, where CPT2 reconvertes acylcarnitines in acyl-CoA. The latter undergo different steps of degradation to produce acetyl-CoA and acyl-CoA shortened of 2 carbons. At this point acetyl-CoA could fuel the TCA cycle to produce ATP or undergo the ketone body synthesis (Houten *et al.*, 2016). In ADPKD models decreased expression of the carnitine palmitoyl transferase 1 a (*Cpt1a*), the isoform expressed in different tissues including liver and kidney, has been described as a consequence of increased FAS, which drives increased malonyl-CoA levels that inhibit CPT1. Interestingly, fenofibrate, an agonist of the Peroxisome proliferator-activated receptor α (PPARα) that is able to increase FAO, is reported to ameliorate PKD phenotype (Lakhia *et al*, 2018). To sum up, ADPKD is characterized by enhanced glycolysis, glutaminolysis, FAS, and decreased OXPHOS and FAO (**Fig. 1.41**) (Podrini *et al.*, 2018), which allows to consider this monogenic disorder also as a metabolic issue.

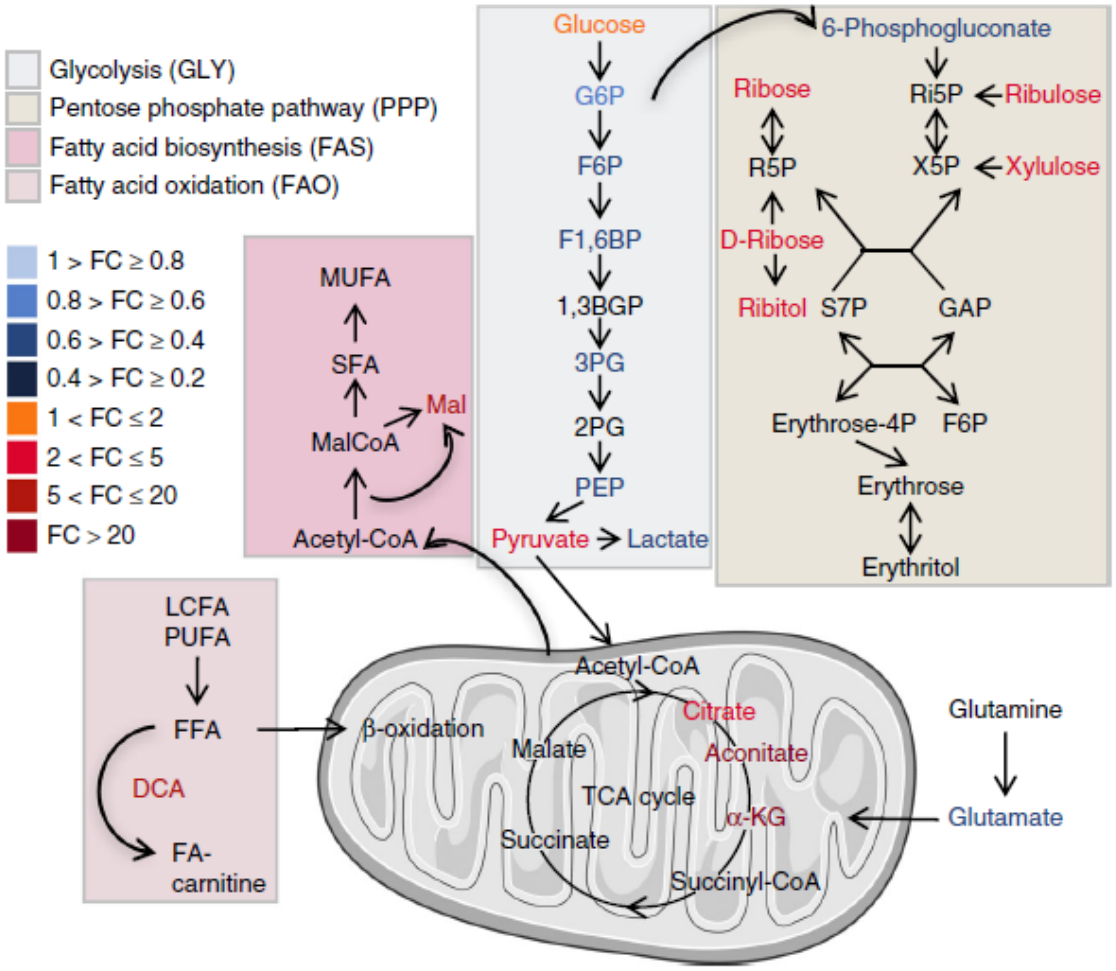

Figure 1.41 Representation of the main pathways involved in the metabolic reprogramming of ADPKD. *G6P: glucose-6-phosphate; F6P: fructose-6-phosphate; F1,6BP: fructose-1,6-bisphosphate; 1,3BGP: 1,3-bisphophoglycerate; 3PG: 3-phosphoglycerate; PEP: phosphoenolpyruvate; Ri5P: Ribulose-5-phosphate; X5P: xylulose-5-phosphate; R5P: ribose-5-phosphate; S7P: sedoeptulose-7-phosphate; GAP:glyceraldehyde-3-phosphate; MUFA: monounsaturated fatty acid; SFA:saturated fatty acid; MalCoA: malonyl-CoA; LCFA: long chain fatty acid; FFA: free fatty acid; α-KG: alpha-ketoglutarate. Metabolites are written with the colors related to the calculated fold change (FC) between cystic and control kidneys. Red coloured metabolites: abundant in cystic versus control kidneys. Blue coloured metabolites: less abundant in cystic versus control kidneys. Adapted from (Podrini et al., 2018)*

AMPK pathway has been found to play a crucial role in ADPKD metabolic reprogramming, since its downregulation in PKD promotes glycolysis upregulation and mTOR pathway activation (Rowe *et al.*, 2013). The strong interconnection between metabolism and ADPKD is further supported by several studies showing that interfering

with altered metabolic pathways ameliorates ADPKD phenotype. Our group showed that chronic treatment with 2-deoxy-D-glucose (2-DG), a fasting-mimetic glucose analog, ameliorates renal cystogenesis *in vivo* in a *Pkd1* inactivated mouse model (Chiaravalli *et al*, 2016). Furthermore, fasting has been found beneficial in slowing PKD progression, since *Pkd1* mutant mice undergone to calorie-restriction displayed an ameliorated phenotype through the activation of the AMPK pathway (Warner *et al*, 2016). This finding supports the evidence of the beneficial effects of metformin (Takiar *et al*, 2011), rapamycin (Shillingford *et al*, 2010), and 2-DG (Chiaravalli *et al.*, 2016) in retarding PKD progression. ADPKD enhanced glutaminolysis has been targeted for therapeutic treatments. In particular some studies have investigated the therapeutic potential of CB-839, a glutamilase (GLS) inhibitor, but its efficacy remains controversial, since it seems to have beneficial effects in two *Pkd1* models (Flowers *et al*, 2018; Soomro *et al*, 2018), but not in another one (Soomro *et al.*, 2018). All these findings reveal that new therapeutic targets for ADPKD treatment could find targets in the altered metabolism of this disease.

2. AIM OF THE WORK

The present thesis aims to investigate a possible crosstalk between primary cilia and cellular metabolism. Based on the evidence that ADPKD, which is the most common ciliopathy, is characterized by a wide metabolic rewiring occurring at the cellular level that affects glycolysis, glutaminolysis, fatty acid synthesis, fatty acid oxidation, and oxidative phosphorylation, we hypothesized that cilia could regulate the responses to the metabolic demands of the cells. Although it is already known that some ciliopathies, such as BBS, MKS, and ALMS, are characterized by defective systemic metabolism leading to obesity and diabetes, the novelty of this work is that cilia display a crucial role in metabolism at the cellular level. Thus, our work aims to uncover the still not completely elucidated function of the primary cilium in the context of cellular metabolism regulation, since shedding light on the role of this cellular *antenna* in physiological and pathological contexts could reveal new therapeutic strategies to treat the ciliopathies.

3. RESULTS

3.1 Primary cilia sense nutrient availability

To investigate whether primary cilia could be involved in the regulation of cellular responses to their metabolic demands, we exposed cilia-proficient cells to nutrient deprivation using HBSS medium. To exclude artefacts due to fixation, we performed live imaging on Mouse Embryonic Fibroblasts (MEFs) transduced with lentiviral vectors carrying the ciliary marker ARL13B tagged with GFP. As expected, serum starvation led to increased ciliary length compared to complete medium condition (**Fig. 3.1.1 A,B**), since serum starvation induces ciliogenesis by synchronising cells in G0/G1 phase (Zhao *et al.*, 2023). Indeed, the percentage of ciliated cells, which is a readout of cell cycle arrest, increased significantly under serum starvation compared to complete serum, as expected (**Fig. 3.1.1 B**). Interestingly, we observed that nutrient deprivation further increased the length of cilia compared to serum starvation (**Fig. 3.1.1 A,B**). We found that this effect is not due to a further exit from the cell cycle compared to serum starvation, since the percentage of ciliated cells did not dramatically change between nutrient deprivation and serum starvation (**Fig. 3.1.1 B**). Of note, we observed that the nutrient deprivation-driven elongation of cilia occurred in different cell lines extensively used for studies on cilia, such as human Retinal Pigment Epithelial (hRPE) cells, mouse Inner Medullary Collecting Duct 3 (mIMCD3) cells, and Madin-Darby Canine Kidney (MDCK) type II cells (**Fig. 3.1.1 A,B**). These results show that the capability of cilia to sense nutrient availability is shared by different cell types both fibroblasts and epithelial cells from different species (human, mouse, and dog) and with different tissue expression (embryo, retina, and renal epithelia), suggesting that the effect of ciliary elongation induced by nutrient deprivation is related to the primary cilium structure *per se*, and does not seem to be dependent on the features of the cell type.

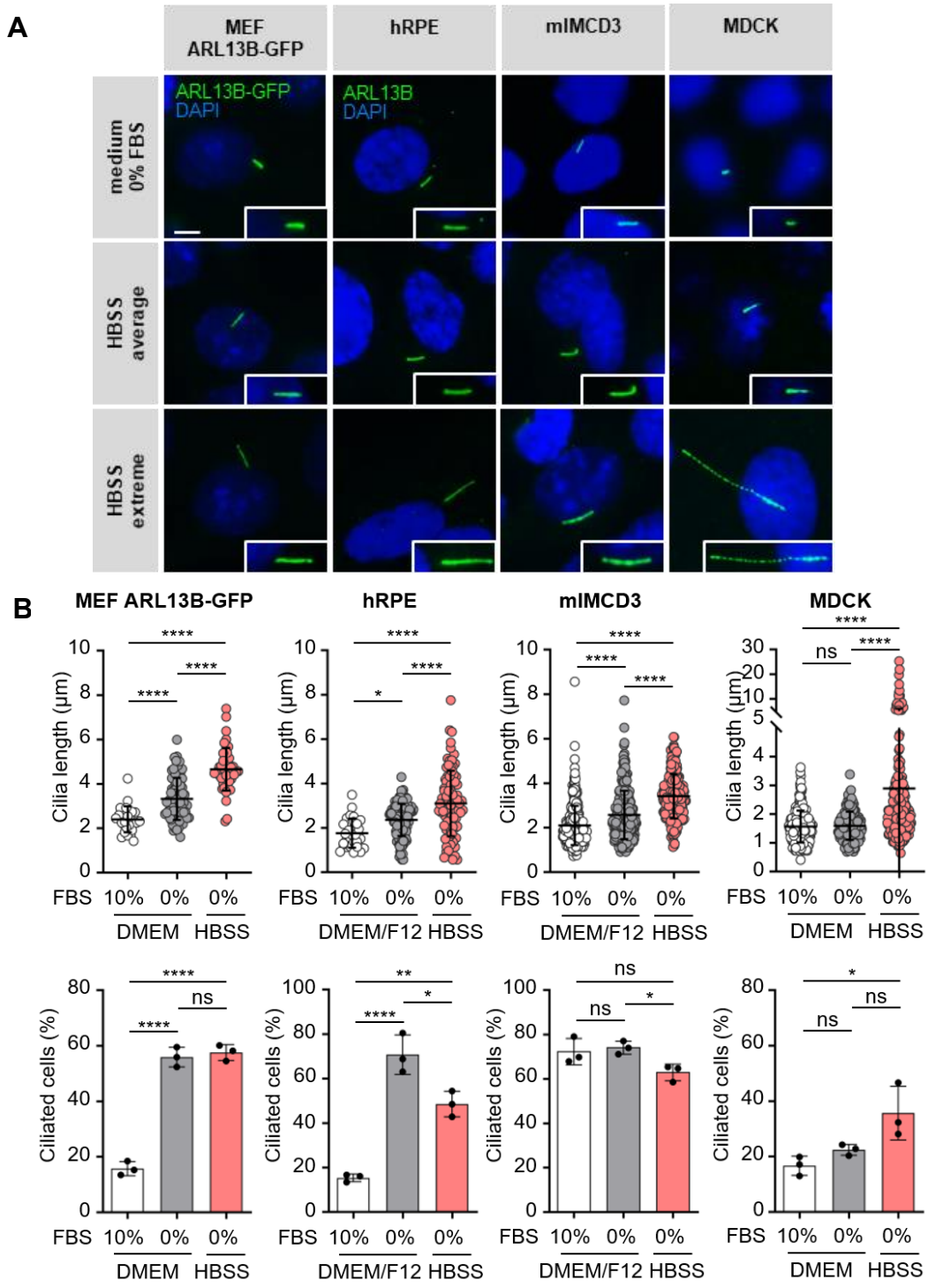

Figure 3.1.1 Nutrient deprivation elongates cilia. *A) Representative fluorescence and immunofluorescence images of primary cilia of different cell lines (MEF ARL13B-GFP, hRPE, mIMCD3, MDCK) under complete medium conditions (10%FBS), serum starvation (0%FBS), and nutrient deprivation (HBSS) (ARL13B, green: cilium; DAPI, blue: nucleus). Scale bar: 10 µm. Insets show the magnification of cilia. Scale bar: 10 µm. B) Quantification of cilia length and percentage of ciliated cells in the different cell lines, in the indicated conditions. Data in dot and bar plots are mean ± SD. For statistical analysis one-way ANOVA, followed by Tukey's multiple comparisons test, was used; ns: not significant, *p < 0.05, **p < 0.01, ****p < 0.0001.*

Thus, we wondered whether nutrient deprivation-driven elongation of primary cilia could occur at earlier time points compared to 24 hours, which is reported in literature to be sufficient to drive ciliogenesis and consequently to promote ciliary elongation upon serum starvation compared to serum complete condition (Pampliega *et al*, 2013; Tang *et al*, 2013). Thus, we performed a time-course analysis by exposing cells to nutrient-deprived medium (HBSS) for short time points (4-8 hours) and long time-points (24 hours). Of note, although the elongation of cilia induced by nutrient deprivation at early time points was significantly reduced compared to late time points, we found that nutrient deprivation elongated cilia starting from 4 hours (**Fig. 3.1.2**) compared to serum deprivation both at early (8 hours) and at late time points (24 hours).

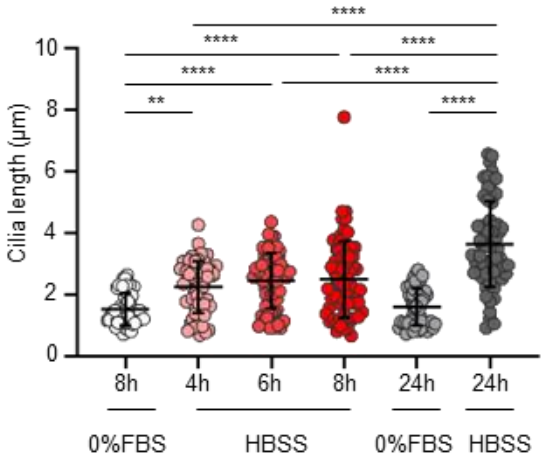

Figure 3.1.2 Nutrient deprivation drives cilia elongation at early time points. *Quantification of cilia length in mIMCD3 cultured for either 8 or 24 h in serum deprivation (0% FBS) or 4,6,8,24 h in nutrient deprivation (HBSS). Data in dot plots are mean ± SD. For statistical analysis, one-way ANOVA, followed by Tukey's multiple comparisons test, was used; **p < 0.01, ****p < 0.0001.*

3.2 Cilia-deficient cells display altered glucose and glutamine metabolism

Since we found that cilia sense nutrient availability and elongate upon nutrient deprivation, we wondered whether the ablation of primary cilia could affect cellular metabolism. For this purpose, we generated by CRISPR/Cas9 technology cilia-deficient MEF and mIMCD3 cells by knocking out the *Ift88* gene, which encodes for an IFT-B protein essential for ciliogenesis (Pazour *et al.*, 2000). Thus, to confirm the disruption of cilia by *Ift88* inactivation, we verified by western blot analysis the absence of the IFT88 protein and by IF using anti-ARL13B antibodies the lack of cilia in *Ift88* KO cells compared to the relative controls, which displayed, as expected, IFT88 expression and cilia (**Fig. 3.2.1 A,B**).

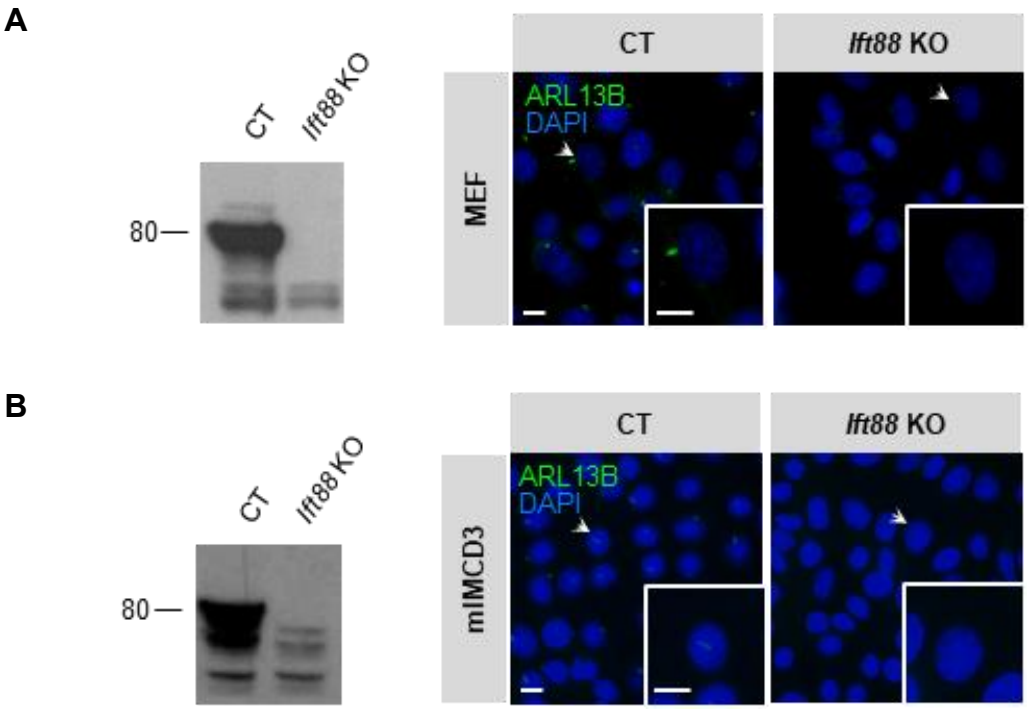

Figure 3.2.1 Ift88 KO cells generated by CRISPR/Cas9 technology do not display cilia. *A) Left: western blot analysis for IFT88 protein expression in cellular lysates from Ift88 KO and control (CT) MEF. Right: Representative immunofluorescence images of primary cilia in Ift88 KO and control (CT) MEF (ARL13B, green: cilium; DAPI, blue: nucleus). Scale bar: 10 µm. Insets show a magnification of the cell indicated by the arrow. Scale bar: 10 µm. B) Left: western blot analysis for IFT88 protein expression in cellular lysates from Ift88 KO and control (CT) mIMCD3. Right: Representative immunofluorescence images of primary cilia in Ift88 KO and control (CT) mIMCD3 (ARL13B: cilium; DAPI: nucleus). Scale bar: 10 µm. Insets show a magnification of the cell indicated by the arrow. Scale bar: 10 µm.*

First, we tested whether cilia-deficient (*Ift88* KO) cells displayed differences in their growth compared to controls upon complete (both nutrient and serum-rich) medium condition. No overt differences were detectable between cilia-deficient and cilia-proficient cells (**Fig. 3.2.2**).

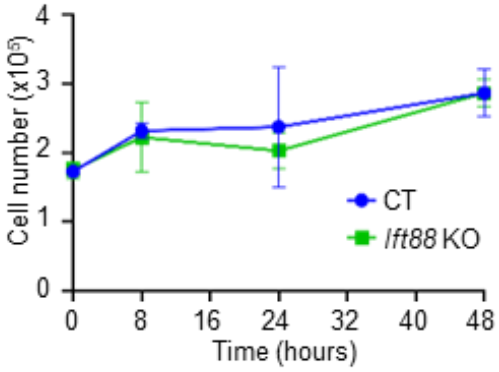

Figure 3.2.2 Cilia-deficient cells do not display overt alterations in growth under complete medium. *Growth curves of Ift88 KO (green) and CT (blue) MEF under complete (both nutrient and serum-rich) medium condition. The cellular growth was measured at 8, 24, and 48 hours for both Ift88 KO and CT cells.*

Since nutrients are metabolized by the cell to fuel the TCA cycle and produce energy within mitochondria, we wondered whether *Ift88* KO and control cells could present differences in their mitochondrial respiration, which is a readout of mitochondrial function. Thus, we measured oxygen consumption rate (OCR) during time in basal conditions and after sequential injection of oligomycin (mitochondrial respiratory chain complex V inhibitor that switches off the ATP-production coupled respiration), FCCP (uncoupler of the proton flux that induces mitochondrial maximal respiration), and a mixture of antimycin A and rotenone (mitochondrial respiratory chain complex III and I inhibitors that completely shut down mitochondrial respiration) by Mito Stress Test, according to Agilent protocols. We noticed that upon both serum complete (10% FBS) and serum depleted (0% FBS) conditions mIMCD3 control cells showed that their maximal respiration (induced by the injection of FCCP) was comparable to the basal one, which was lower compared to the one displayed by MEF control cells. Indeed, IMCD cells are reported to be glycolytic. Interestingly, like the growth curves, cilia-deficient cells did not display dramatic differences in their mitochondrial respiration compared to

their relative controls under nutrient-rich medium either with or without serum (**Fig. 3.2.3 A,B**).

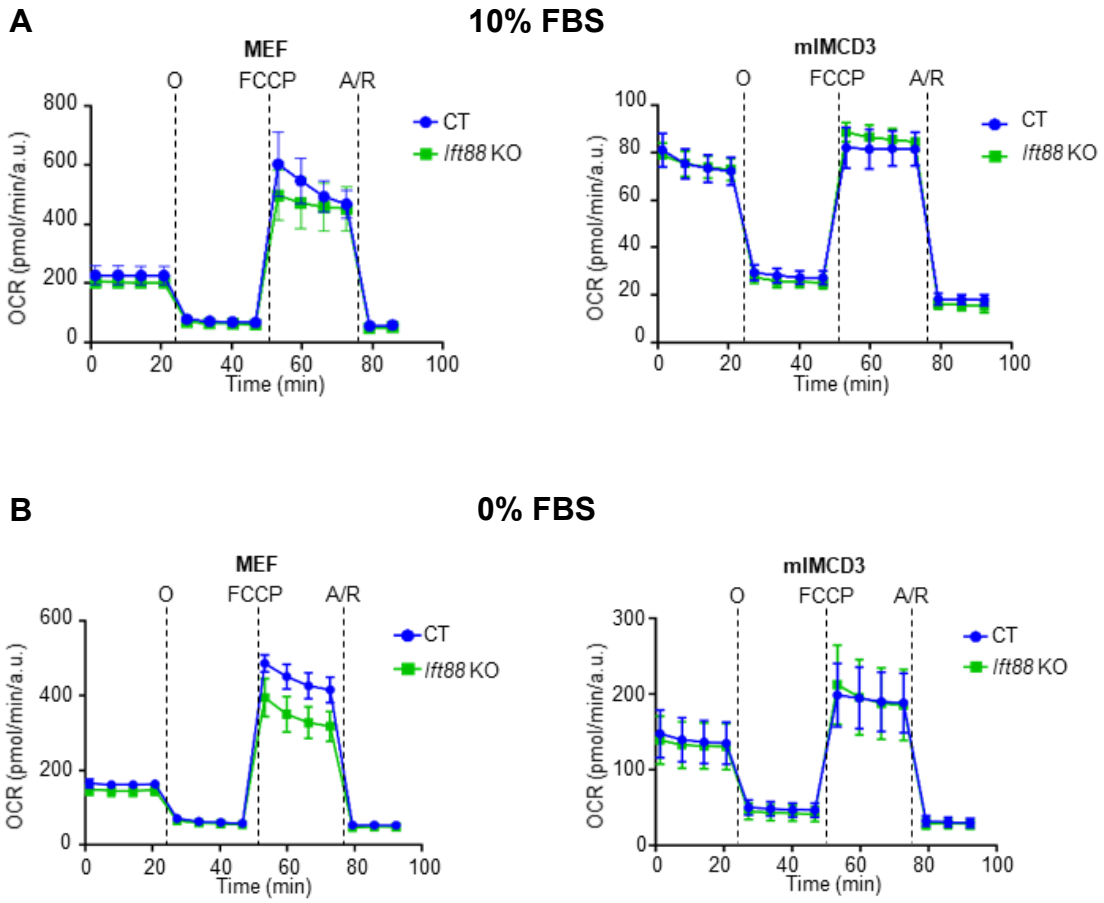

Figure 3.2.3 Cilia-deficient cells do not display overt alterations mitochondrial respiration under nutrient-rich medium either with or without serum. *A) Left: analysis of OCR measurement during time in Ift88 KO (green) and CT (blue) MEF under complete medium conditions (10% FBS) for 24 h, in basal condition and after sequential injection of oligomycin (O), FCCP, and antimycin/rotenone (A/R). Right: analysis of OCR measurement during time in Ift88 KO (green) and CT (blue) mIMCD3 under complete medium conditions for 24 h, in basal condition and after sequential injection of O, FCCP, and A/R. B) Left: analysis of OCR measurement during time in Ift88 KO (green) and CT (blue) MEF under serum starvation (0% FBS) for 24 h, in basal condition and after sequential injection of O, FCCP, and A/R. Right: analysis of OCR measurement during time in Ift88 KO (green) and CT (blue) mIMCD3 under serum starvation (0% FBS) for 24h, in basal condition and after sequential injection of O, FCCP, and A/R.*

However, when we exposed *Ift88* KO and control MEF cells to serum starvation and we performed NMR spectroscopy metabolomics profiling on their conditioned media, we observed a clear separation between their clusters through principal component analysis (PCA) (**Fig. 3.2.4 A,B**).

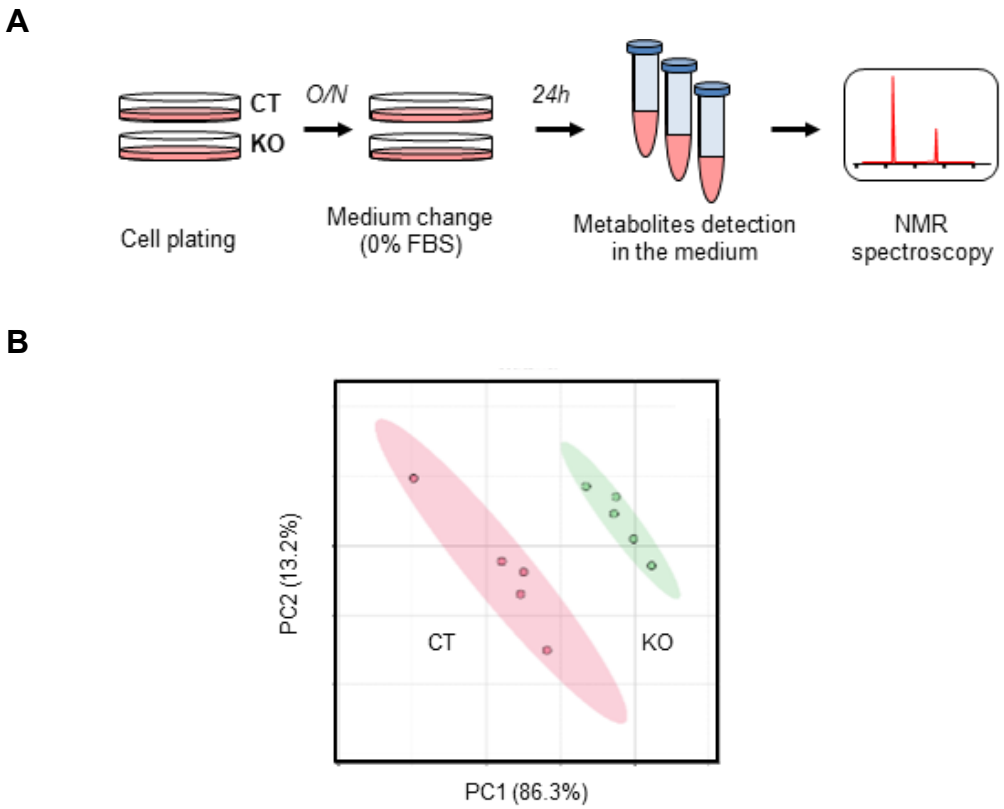

Figure 3.2.4 NMR spectroscopy reveals that cilia-deficient cells show a clear separation in their exometabolome upon serum deprivation. *A) Schematic representation of NMR spectroscopy exometabolome experimental design. B) Principal Component Analysis (PCA) of extracellular metabolites of Ift88 KO (green) and CT (red) MEF measured by NMR spectroscopy as in A.*

This result is due to significant differences between *Ift88* KO and CT conditioned media in the levels of several metabolites belonging to both carbon and aminoacid metabolism (**Table 3.1,3.2; Fig. 3.2.5 A,B**).

	MO (mM)			IFT88 $^{-/-}$ KO cells (mM)					CTR cells (mM)				
	MO1	MO2	MO3	KO1	KO2	KO3	KO4	KO5	CTR1	CTR2	CTR3	CTR4	CTR5
2'Hydroxybutyrate	0.025	0.009	0.024	0.087	0.090	0.100	0.094	0.106	0.075	0.094	0.083	0.078	0.080
Acetate	0.059	0.038	0.002	0.189	0.183	0.164	0.186	0.169	0.111	0.116	0.090	0.129	0.147
Alanine	0.000	0.007	0.008	0.257	0.285	0.264	0.280	0.252	0.134	0.157	0.174	0.151	0.134
Arginine	0.204	0.173	0.225	0.253	0.205	0.217	0.178	0.241	0.202	0.153	0.305	0.172	0.278
Ethanol	0.962	0.970	0.941	0.911	0.960	0.925	0.956	1.009	0.862	0.932	1.029	0.929	0.972
Formate	0.015	0.015	0.015	0.353	0.355	0.347	0.348	0.342	0.211	0.208	0.228	0.211	0.207
Glucose	21.930	23.033	22.152	16.690	18.086	17.517	17.623	17.797	11.468	15.103	16.520	15.940	15.764
Glutamate	0.009	0.007	0.042	0.319	0.236	0.288	0.236	0.263	0.573	0.707	0.720	0.559	0.545
Glutamine	1.347	1.596	1.602	0.513	0.654	0.615	0.643	0.561	0.327	0.455	0.529	0.416	0.416
Glycine	0.369	0.370	0.353	0.720	0.730	0.722	0.720	0.702	0.645	0.662	0.712	0.653	0.648
Histidine	0.128	0.176	0.170	0.197	0.161	0.157	0.168	0.198	0.184	0.178	0.223	0.149	0.136
Isoleucine	0.666	0.603	0.677	0.620	0.635	0.596	0.609	0.579	0.572	0.615	0.648	0.559	0.613
Lactate	0.065	0.051	0.001	4.398	4.509	4.391	4.374	4.151	6.992	7.145	7.707	7.040	7.366
Leucine	0.682	0.596	0.546	0.538	0.510	0.635	0.482	0.558	0.388	0.557	0.668	0.490	0.511
Lysine	0.436	0.609	0.529	0.784	0.355	0.608	0.503	0.554	0.583	0.552	0.726	0.580	0.535
Methionine	0.228	0.187	0.179	0.201	0.204	0.200	0.201	0.223	0.176	0.157	0.169	0.171	0.177
Niacinamide	0.027	0.030	0.030	0.032	0.026	0.024	0.028	0.030	0.000	0.025	0.024	0.029	0.022
Phenylalanine	0.372	0.393	0.377	0.384	0.375	0.362	0.365	0.359	0.314	0.362	0.405	0.357	0.342
Pyridoxine	0.017	0.018	0.014	0.008	0.015	0.015	0.027	0.007	0.012	0.000	0.015	0.014	0.007
Pyroglutamate	1.523	1.551	1.398	1.318	1.339	1.543	1.528	1.512	1.263	1.660	1.717	1.532	1.510
Pyruvate	0.006	0.012	0.018	0.143	0.153	0.146	0.150	0.138	0.069	0.075	0.093	0.069	0.065
Threonine	0.611	0.685	0.659	0.614	0.724	0.716	0.751	0.692	0.720	0.753	0.757	0.712	0.713
Tryptophan	0.071	0.062	0.075	0.076	0.072	0.077	0.069	0.056	0.062	0.064	0.058	0.062	0.048
Tyrosine	0.428	0.411	0.412	0.405	0.404	0.405	0.415	0.395	0.217	0.377	0.410	0.378	0.408
Valine	0.692	0.697	0.674	0.608	0.613	0.607	0.609	0.594	0.562	0.581	0.613	0.567	0.565

Table 3.1 List of NMR identified and quantified metabolites. *Concentration of each metabolite is expressed in mM for unconditioned medium (MO) and for media conditioned by Ift88 KO and CTR MEF cells. For MO, 3 replicates have been used. For KO and CTR, 5 replicates have been used.*

	IFT88 $^{-/-}$ KO cells		CTR cells		Student t -test		Fold change (KO/CTR)
	Average (nM/num of cells)	**stdev**	**Average (nM/num of cells)**	**stdev**	**p-value**	**sign**	
2'Hydroxybutyrate	0.00742	0.00051	0.00603	0.00603	0.003	*	1.231(↑)
Acetate	0.01390	0.00112	0.00879	0.00879	0.001	*	1.581(↑)
Alanine	0.02087	0.00181	0.01010	0.01010	0.000005	*	2.066(↑)
Arginine	0.01700	0.00187	0.01548	0.01548	0.816	NS	1.098(=)
Ethanol	0.07415	0.00387	0.06965	0.06965	0.183	NS	1.065(=)
Formate	0.02718	0.00118	0.01568	0.01568	0.0000001	*	1.734(↑)
Glucose	1.36705	0.07747	1.10325	1.10325	0.011	*	1.239(↑)
Glutamate	0.02086	0.00224	0.04560	0.04560	0.000009	*	0.457(↓)
Glutamine	0.04662	0.00604	0.03152	0.03152	0.003	*	1.479(↑)
Glycine	0.05600	0.00253	0.04890	0.04890	0.001	*	1.145(=)
Histidine	0.01366	0.00125	0.01275	0.01275	0.414	NS	1.072(=)
Isoleucine	0.04737	0.00299	0.04432	0.04432	0.166	NS	1.069(=)
Lactate	0.34013	0.01981	0.53440	0.53440	0.000004	*	0.636(↓)
Leucine	0.04235	0.00386	0.03847	0.03847	0.310	NS	1.101(=)
Lysine	0.04340	0.01108	0.04373	0.04373	0.952	NS	0.992(=)
Methionine	0.01602	0.00072	0.01252	0.01252	0.000278	*	1.280(↑)
Niacinamide	0.00219	0.00022	0.00147	0.00147	0.100	NS	1.493(↑)
Phenylalanine	0.02873	0.00131	0.02620	0.02620	0.053	NS	1.097(=)
Pyridoxine	0.00115	0.00065	0.00070	0.00070	0.234	NS	1.649(↑)
Pyroglutamate	0.11274	0.00880	0.11314	0.11314	0.954	NS	0.996(=)
Pyruvate	0.01138	0.00083	0.00544	0.00544	0.000002	*	2.092(↑)
Threonine	0.05454	0.00546	0.05384	0.05384	0.796	NS	1.013(=)
Tryptophan	0.00545	0.00071	0.00431	0.00431	0.012	*	1.263(↑)
Tyrosine	0.03154	0.00144	0.02643	0.02643	0.116	NS	1.193(=)
Valine	0.04722	0.00202	0.04254	0.04254	0.005	*	1.110(=)

Table 3.2 List of NMR identified and relatively quantified metabolites and the corresponding univariate analysis. *Average and standard deviation is calculated for each metabolite for KO and CTR MEF samples. Fold change (FC), considered as the ratio between the mean value of the two groups KO and CTR: metabolites with a FC>1.2 (↑): increase of metabolite level, FC<0.7 (↓): decrease of metabolite level, 0.7<FC<1.2 (=): metabolite level is not different. p-value is calculated using unpaired Student's two-tailed t-test, (fourth column). Statistically significant differences in metabolites in KO vs CTR are expressed in bold and with asterisk (*), NS: not significant; *p < 0.05.*

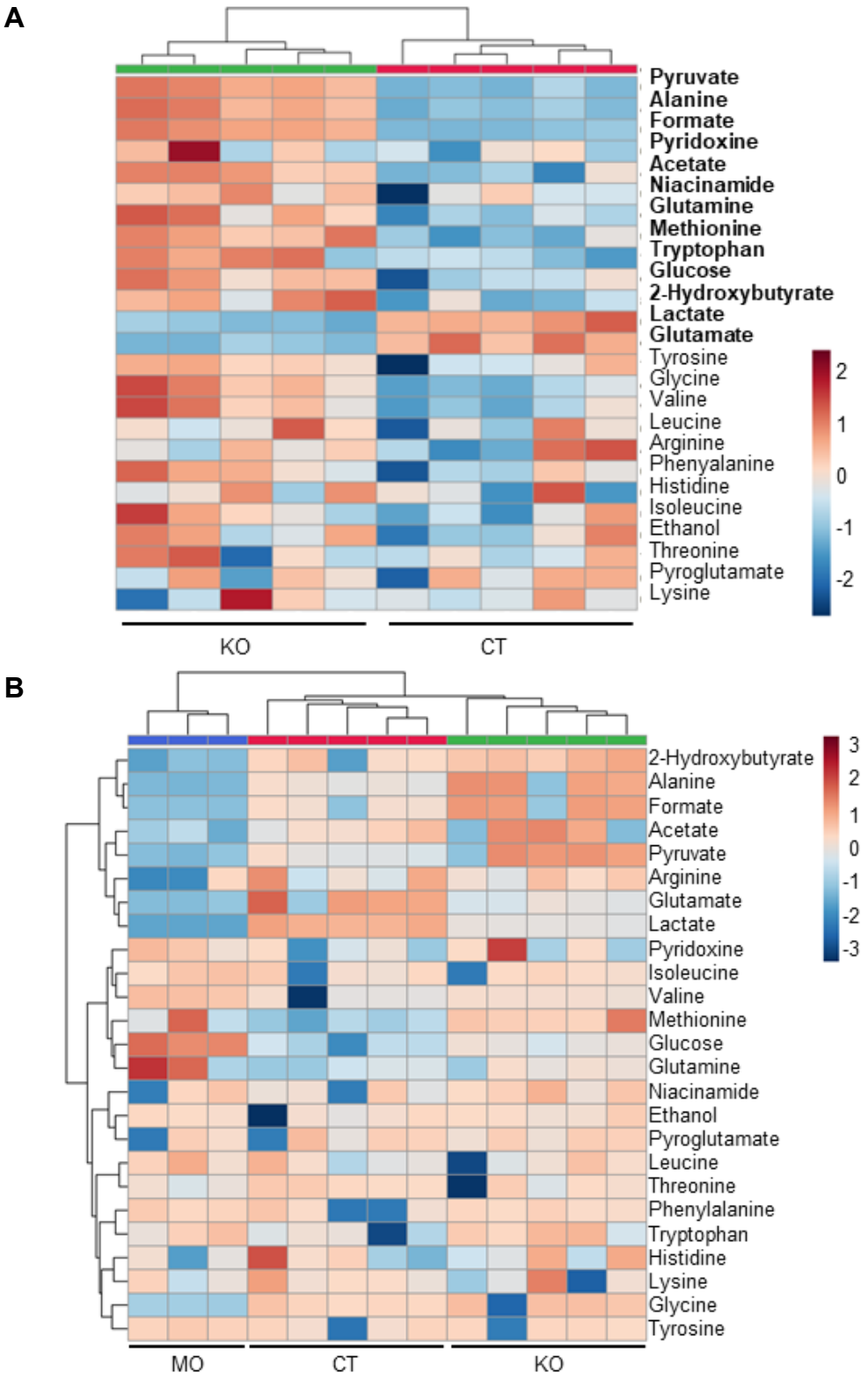

Figure 3.2.5 Cilia-deficient cells show impaired nutrient utilization upon serum deprivation. *A) Hierarchical clustering of extracellular metabolites of Ift88 KO (green) and CT (red) MEF by NMR spectroscopy as in 3.2.4 A. The metabolites in bold are significantly different between Ift88 KO (green) and CT (red). B) Hierarchical clustering of extracellular metabolites of unconditioned medium (MO), Ift88 KO (green) and CT (red) by NMR spectroscopy as in 3.2.4 A.*

Of note, among the metabolites that changed, *Ift88* KO MEF cells displayed decreased levels of glutamine and glucose uptake, mirrored by reduced glutamate and lactate production compared to the relative controls (**Fig. 3.2.6**), suggesting a possible impairment of cilia-deficient cells in the utilization of the two main carbon sources for the cell.

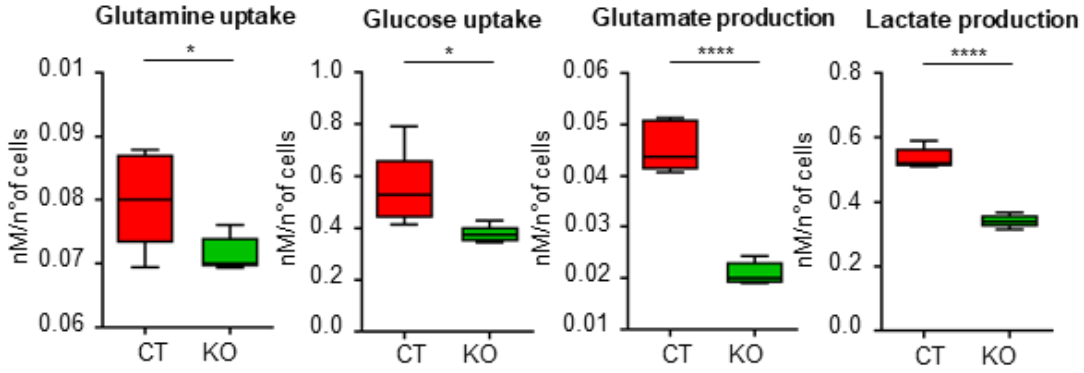

Figure 3.2.6 Cilia-deficient cells display impaired glucose and glutamine metabolism upon serum deprivation. *Box and whisker plots of glutamine and glucose uptake, and glutamate and lactate production in Ift88 KO (green) and CT (red) MEF assessed by NMR spectroscopy as in 3.2.4 A. Box and whisker plots are represented with median and min to max. For statistical analysis, Student's unpaired two-tailed t-test was used; *p < 0.05, ****p < 0.0001.*

Next, we confirmed these results by LC-MS targeted endometabolomics on *Ift88* KO and control cells cultured for 24 hours in partial serum starvation (DMEM + 0.5% FBS), which is comparable to total serum deprivation (**Fig. 3.2.7 A**). Indeed, from the enriched pathway analysis we found that the metabolites that changed between *Ift88* KO and control MEF cells belonged to glutamine metabolism and TCA cycle (**Fig. 3.2.7 B**). Since glutamine is reported to be preferentially used for TCA cycle fuelling by its capability to be converted into glutamate and then into α-ketoglutarate (α-KG) to promote mitochondrial respiration and energy production production (DeBerardinis *et al.*, 2007; Yang *et al.*, 2014; Zhang *et al.*, 2017b), these data suggested that the alteration in glutaminolysis could be causative of the alteration in the TCA cycle uncovered by enriched pathway analysis. Furthermore, as NMR spectroscopy analysis revealed, also LC-MS metabolomics corroborated the evidence that *Ift88* KO cells displayed a general impairment of aminoacids metabolism, since, other than glutamine and glutamate

metabolism, also alanine, aspartate and arginine metabolism, together with aminoacyl-tRNA biosynthesis, were found to be altered by loss of cilia (**Fig. 3.2.7 B**).

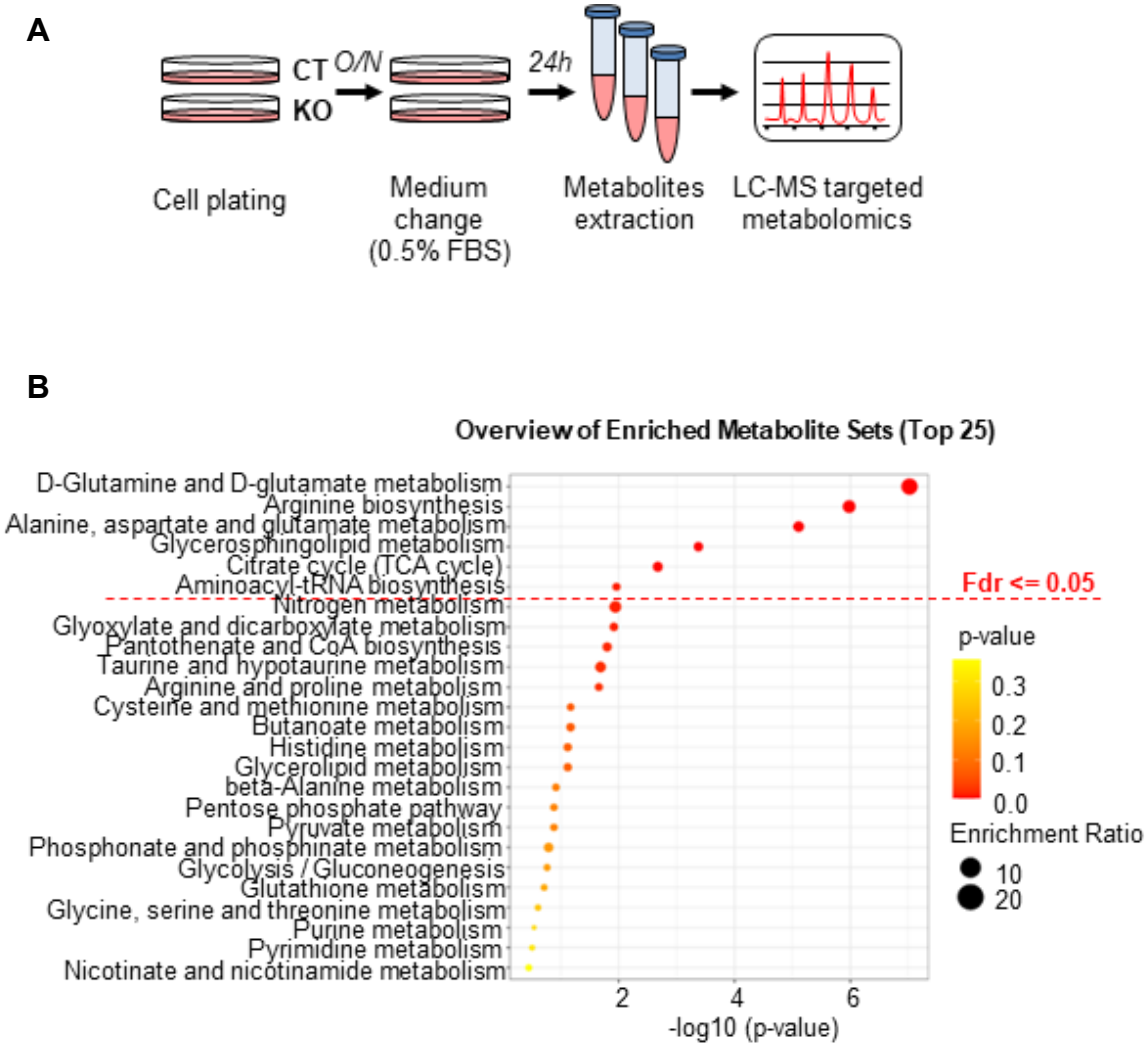

Figure 3.2.7 Cilia-deficient cells show altered aminoacid metabolism upon partial serum deprivation. *A) Schematic representation of LC-MS targeted metabolomics experimental design. B) Enrichment pathway analysis of LC-MS targeted metabolomics as in A.*

Interestingly, the analysis showed that, other than intracellular glutamine and glutamate decrease, also aspartate and asparagine levels are significantly different between *Ift88* KO and control cells. In particular, we appreciated increased levels of aspartate and decreased levels of asparagine in cilia-deficient cells compared to their relative controls (**Fig. 3.2.8**).

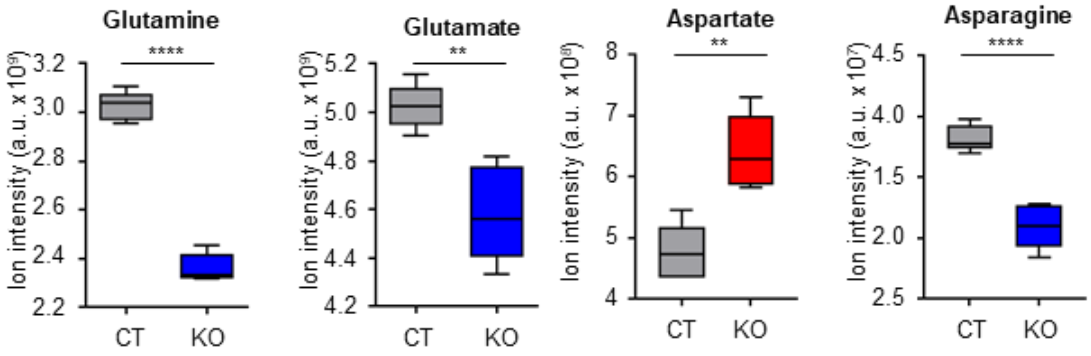

Figure 3.2.8 Cilia-deficient cells show altered glutamine and aspartate metabolism upon partial serum deprivation. *Box and whisker plots of intracellular levels of glutamine, glutamate, aspartate and asparagine in Ift88 KO and CT MEF assessed by LC-MS targeted metabolomics as in 3.2.7 A. Box and whisker plots are represented with median and min to max. For statistical analysis, Student's unpaired two-tailed t-test was used; **p < 0.01, ****p < 0.0001.*

Collectively, these data show that cilia-deficient cells present a general impairment of nutrient utilization, involving reduced glucose and glutamine utilization to produce lactate and glutamate, and defective aminoacids metabolism with increased levels of aspartate and decreased levels of asparagine in the *Ift88* KO MEF cells. Of note, our results revealed that also the TCA cycle is impaired in cilia-deficient cells possibly as a consequence of defective glutamine conversion into glutamate induced by disruption of cilia.

3.3 Glutamine, but not glucose, shortens primary cilia through mitochondrial respiration fuelling

Since cilia-deficient cells displayed altered glutamine and glucose uptake and utilization, we wondered whether these metabolites could have an effect on cilia. Thus, we supplemented HBSS, which causes ciliary elongation, with either glutamine or glucose and we measured ciliary length. Interestingly, glutamine, but not glucose, was able to induce the shortening of primary cilia (**Fig. 3.3.1**).

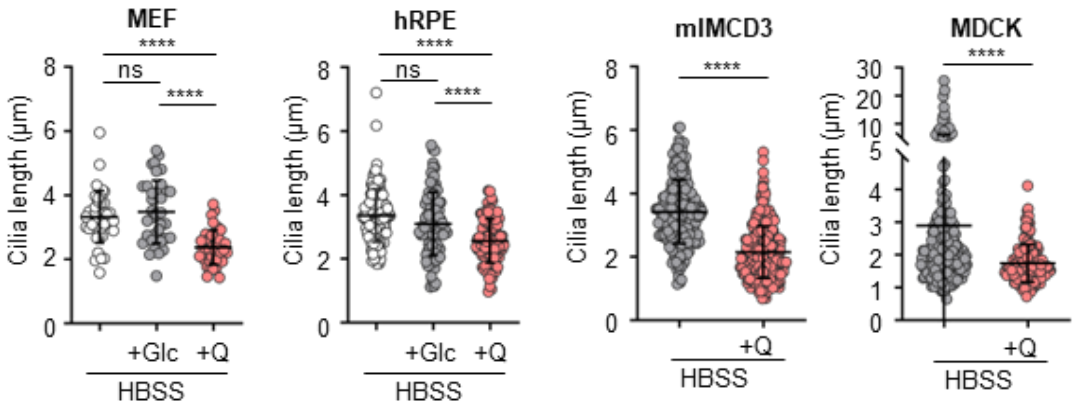

Figure 3.3.1 Glutamine, but not glucose, shortens cilia. *Quantification of cilia length of different cell lines (MEF, hRPE, mIMCD3, MDCK) cultured for 24 h in HBSS supplemented with either Glucose (Glc) or Glutamine (Q). Data in dot plots are mean with ± SD. For statistical analysis, Student's unpaired two-tailed t-test or one-way ANOVA, followed by Tukey's multiple comparisons test, were used; ns: not significant, ****p < 0.0001.*

Furthermore, we found that cilia respond not only to supra-physiological levels of glutamine (2-4 mM), usually present in commercial media, but also to physiological concentrations starting from 0.2 mM (**Fig. 3.3.2**), suggesting that cilia sensing of glutamine could be physiologically relevant.

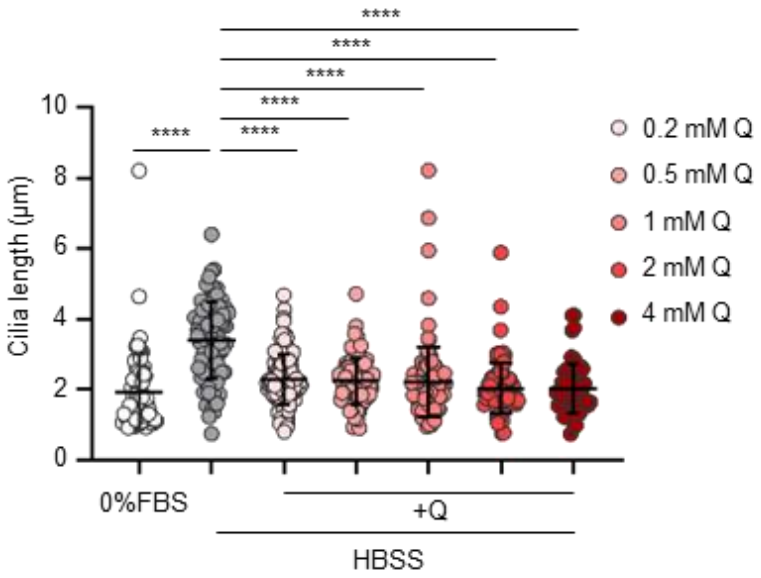

Figure 3.3.2 Physiological and supra-physiological levels of glutamine shorten cilia. *Quantification of cilia length in mIMCD3 cells cultured for 24 h in HBSS supplemented with different concentrations of Q (0.2, 0.5, 1, 2, 4 mM). Data in dot plots are mean with ± SD. For statistical analysis, one-way ANOVA, followed by Tukey's multiple comparisons test, was used; ****p < 0.0001.*

We wondered whether this effect of glutamine was able to shorten cilia or to prevent their elongation. To test this hypothesis, we cultured the mIMCD3 cells under nutrient deprivation and then we supplemented HBSS with glutamine. Interestingly, we found that the cilia shortened upon glutamine replenishment for 4-6 hours (**Fig. 3.3.3**). As for ciliary elongation by nutrient deprivation, also glutamine-induced shortening of primary cilia occurs at early time-points.

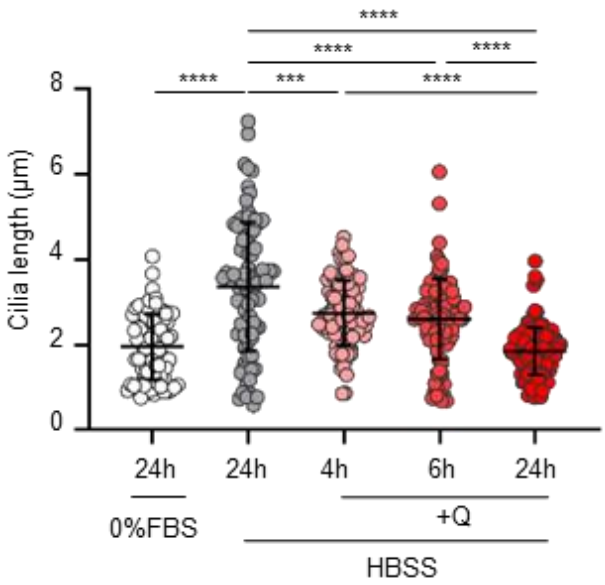

Figure 3.3.3 Glutamine replenishment after nutrient deprivation induces the shortening of primary cilia. *Quantification of cilia length in mIMCD3 cultured for 24 h in either serum starvation (0% FBS) or HBSS and with glutamine replenishment for 4, 6, 24 h. Data in dot plots are mean with ± SD. For statistical analysis one-way ANOVA, followed by Tukey's multiple comparisons test, was used; ***p < 0.001, ****p < 0.0001.*

Since glutamine can be converted into glutamate and then α-KG to fuel the TCA cycle to drive oxidative phosphorylation (OXPHOS) and mitochondrial respiration (**Fig. 3.3.4 A**), we wondered whether this could be the driver of ciliary shortening upon glutamine supplementation. Upon acute injection of glutamine after 4 hours of nutrient deprivation, cells displayed a decreased maximal respiration compared to the basal one in all the culture conditions, suggesting that cells did not cope with the injection of FCCP in terms of promoting mitochondrial maximal respiration. Nevertheless, cells cultured for either 4 or 16 hours under glutamine supplementation showed a dramatical increase of maximal respiration compared to the basal one, suggesting that upon these conditions FCCP injection was well tolerated by the cells. As expected, we observed that glutamine, but not glucose, is able to induce a significant increase in mitochondrial respiration compared to the relative control upon glutamine acute injection, or supplementation to HBSS for either 4 or 16 hours, driving ATP-production coupled respiration (**Fig. 3.3.4 B-D**).

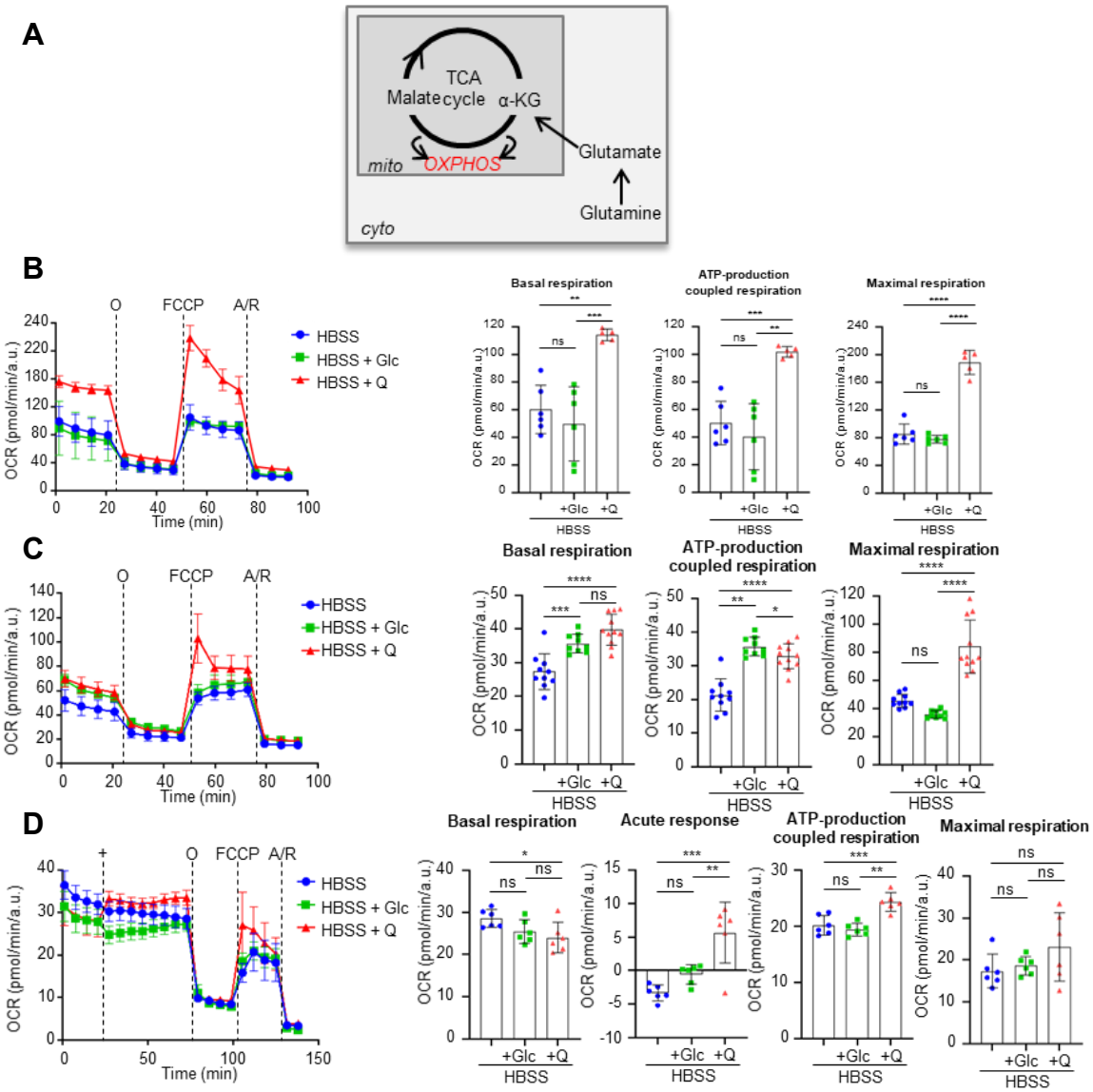

Figure 3.3.4 Glutamine supplementation induces mitochondrial respiration upon nutrient deprivation. *A) Schematic representation of glutamine anaplerosis through its conversion into glutamate and then α-ketoglutarate (α-KG) to fuel the TCA cycle and drive oxidative phosphorylation (OXPHOS). B) Left: analysis of OCR measurement during time in MEF under HBSS (blue) or HBSS supplemented with either Glucose (Glc) (green) or Glutamine (Q) (red) for 4h, in basal condition and after sequential injection of oligomycin (O), FCCP, and antimycin/rotenone (A/R). Right: Quantification of basal respiration, ATP-production coupled respiration, and maximal respiration as in Left. C) Left: analysis of OCR measurement during time in MEF under HBSS or HBSS (blue) supplemented with either Glc (green) or Q (red) for 16h, in basal condition and after sequential injection of O, FCCP, and A/R. Right: Quantification of basal respiration, ATP-production coupled respiration, and maximal respiration as in Left. D) Left: analysis of OCR measurement during time in MEF under HBSS (blue) or HBSS supplemented with either Glc (green) or Q (red) for 4h, in basal condition and after sequential injection of Q, O, FCCP, and A/R. Right: Quantification of basal respiration, acute response, ATP-production coupled respiration, and maximal respiration as in Left. Data in columns are mean with ± SD. For statistical analysis, one-way ANOVA, followed by Tukey's multiple comparisons test, was used; ns: not significant, *p < 0.05, **p < 0.01, ***p < 0.001, ****p < 0.0001.*

As a control, we measured extracellular acidification rate (ECAR) upon glutamine and glucose supplementation. As expected, glucose, but not glutamine, caused an increased ECAR compared to HBSS, rejecting the hypothesis that glutamine-driven shortening of cilia is caused by variations in pH (**Fig. 3.3.5**).

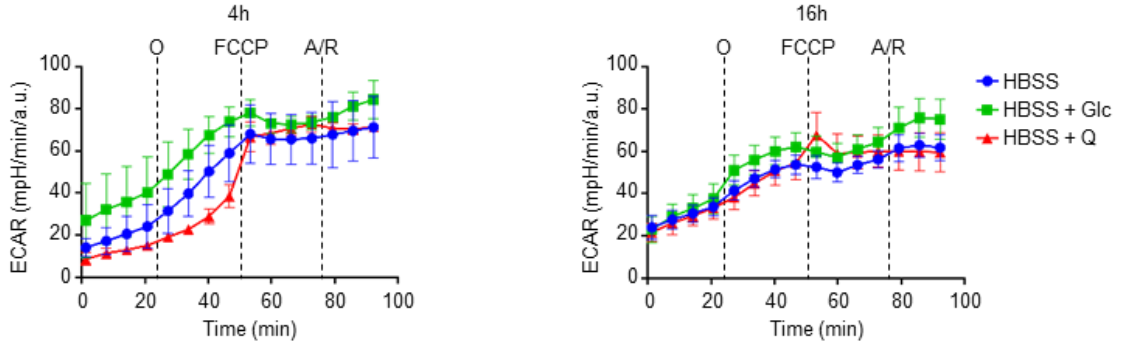

Figure 3.3.5 Glucose, but not glutamine, acidifies the medium. *Left: Analysis of ECAR measurement during time referred to 3.3.4 B. Right: Analysis of ECAR measurement during time referred to 3.3.4 C.*

These results suggested that primary cilia respond to glutamine for its capability to fuel the TCA cycle and drive mitochondrial respiration.

3.4 Cilia sense mitochondrial function impairment and energy crisis of the cell

Since glutamine shortened cilia possibly by TCA fueling, we wondered whether cilia could sense mitochondrial function and, as a consequence, the energy status of the cell. With this purpose, we treated MEF and hRPE cells with inhibitors of the mitochondrial respiratory chain complexes (**Fig. 3.4.1 A**) and we measured cilia length. We appreciated a significant increase of ciliary length in cells treated with either antimycin/rotenone or oligomycin compared to the relative controls (**Fig. 3.4.1 B**), suggesting that cilia sense mitochondrial dysfunction. This is in line with previous findings that interfering with mitochondrial function causes ciliary elongation in neurons (Bae *et al.*, 2019).

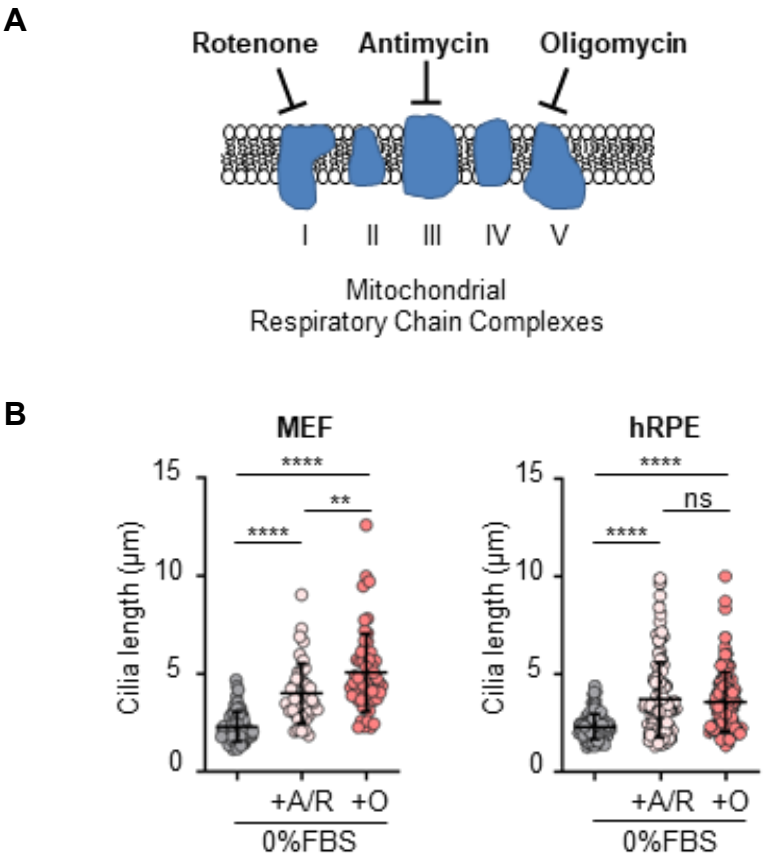

Figure 3.4.1 Mitochondrial dysfunction leads to cilia elongation. *A) Schematic representation of Mitochondrial Respiratory Chain Complexes targets of Oligomycin, Antimycin, and Rotenone. B) Quantification of cilia length in MEF (left) and hRPE (right) cultured for 24h in serum starvation (0% FBS) ± either Antimycin/Rotenone (A/R) or Oligomycin (O). Data in dot plots are mean with ± SD. For statistical analysis, one-way ANOVA, followed by Tukey's multiple comparisons test, was used; ns: not significant, **p < 0.01, ****p < 0.0001.*

Since mitochondria are the center of energy production and their dysfunction is sensed by cilia, we hypothesized that cilia could sense the energy status of the cell. First of all, we verified upon nutrient deprivation the activation of AMPK, which is a central regulator of energy homeostasis activated upon an energetic crisis to restore the energy balance of the cell (Mihaylova & Shaw, 2011). AMPK is also reported to mediate shear stress responses by being activated by LKB1, which is localized at the centrosome-cilium complex (Boehlke *et al*, 2010; Miceli *et al*, 2020). We appreciated increased levels of AMPK phosphorylation at Threonine 172 (pAMPK^{T172}), which is a read-out of the activation of AMPK induced by an energy imbalance of the cell, upon nutrient deprivation, without affecting the expression levels of total AMPK protein (**Fig. 3.4.2**).

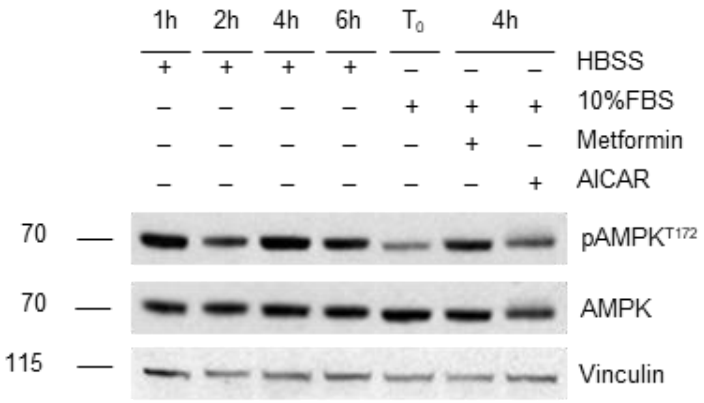

Figure 3.4.2 AMPK activation by nutrient deprivation and AICAR. *Western blot analysis for pAMPK^{T172} and total AMPK protein expression in cellular lysates from MEF under either HBSS for 1, 2, 4, 6h or complete medium condition (10% FBS) for 4h ± either Metformin or AICAR. Vinculin was used as loading control.*

To investigate whether cilia could sense the energy status of the cell, we mimicked an energetic crisis by chemical activation of AMPK through AICAR, an allosteric activator of this kinase. Strikingly, we appreciated a statistically significant elongation of primary cilia of cells treated with AICAR compared to the relative controls treated with DMSO, without affecting the percentage of ciliated cells (**Fig. 3.4.3 A,B**). This result suggests that cilia sense energetic crisis upon nutrient deprivation through AMPK activation. Collectively, our findings show that cilia sense the energetic imbalance induced by nutrient deprivation, which drives the activation of AMPK. This result is also supported

by the evidence that disrupting mitochondrial respiration, which leads to decreased energy production, is able to drive ciliary elongation.

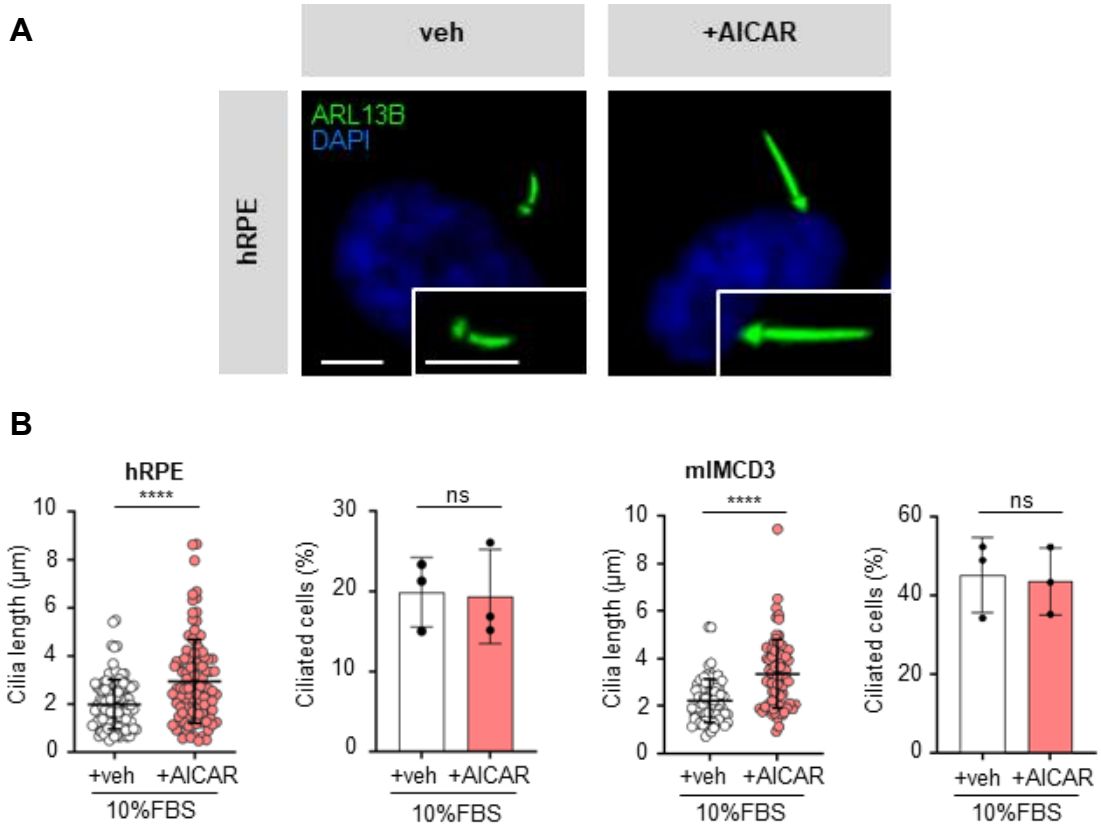

Figure 3.4.3 AMPK activation by AICAR elongates cilia. *A) Representative immunofluorescence images of primary cilia (ARL13B, green: cilia; DAPI, blue; nucleus) in hRPE under complete medium condition ± vehicle (veh) or AICAR. Scale bar: 5 µm. B) Left: quantification of cilia length and percentage of ciliated cells in hRPE in complete medium condition (10% FBS) ± vehicle (veh) or AICAR. Right: quantification of cilia length and percentage of ciliated cells in mIMCD3 in complete medium condition (10% FBS) ± vehicle (veh) or AICAR. Data in dot plots are mean with ± SD. For statistical analysis, Student's unpaired two-tailed t-test was used; ns: not significant, ****p < 0.0001.*

Indeed, these data suggest that the capability of primary cilia to sense nutrient availability by elongating upon nutrient deprivation and by shortening upon glutamine supplementation could be due to the mitochondrial activity and, as a consequence, the energy status of the cell.

3.5 Glutamine supplementation upon nutrient deprivation partially rescues metabolic stress

To investigate how glutamine affects the metabolism upon nutrient deprivation, we performed LC-MS targeted metabolomics in wild type MEF cells exposed for 24 hours to partial serum deprivation (DMEM + 0.5% FBS), nutrient deprivation (HBSS), and glutamine supplementation (HBSS +4 mM Q) (**Fig. 3.5.1 A**). Interestingly, we found that glutamine was able to rescue, at least partially, the metabolic crisis induced by exposing cells to nutrient deprived medium. Indeed, 67 metabolites, upon 137, differed significantly between HBSS + Q and HBSS. Interestingly, not only glutamine and glutamate, but also asparagine and aspartate levels were rescued by glutamine supplementation, as expected by previuos findings (Alkan *et al*, 2018). (**Fig. 3.5.1 B,C**). Furthermore, also metabolites belonging to the TCA cycle, such as α-KG and malate, were rescued by glutamine supplementation (**Fig. 3.5.1 B,C**). These results strengthen the evidence that glutamine is the privileged source of carbon used by the cell to drive mitochondrial respiration and ultimately ATP production (DeBerardinis *et al.*, 2007; Yang *et al.*, 2014; Zhang *et al.*, 2017b).

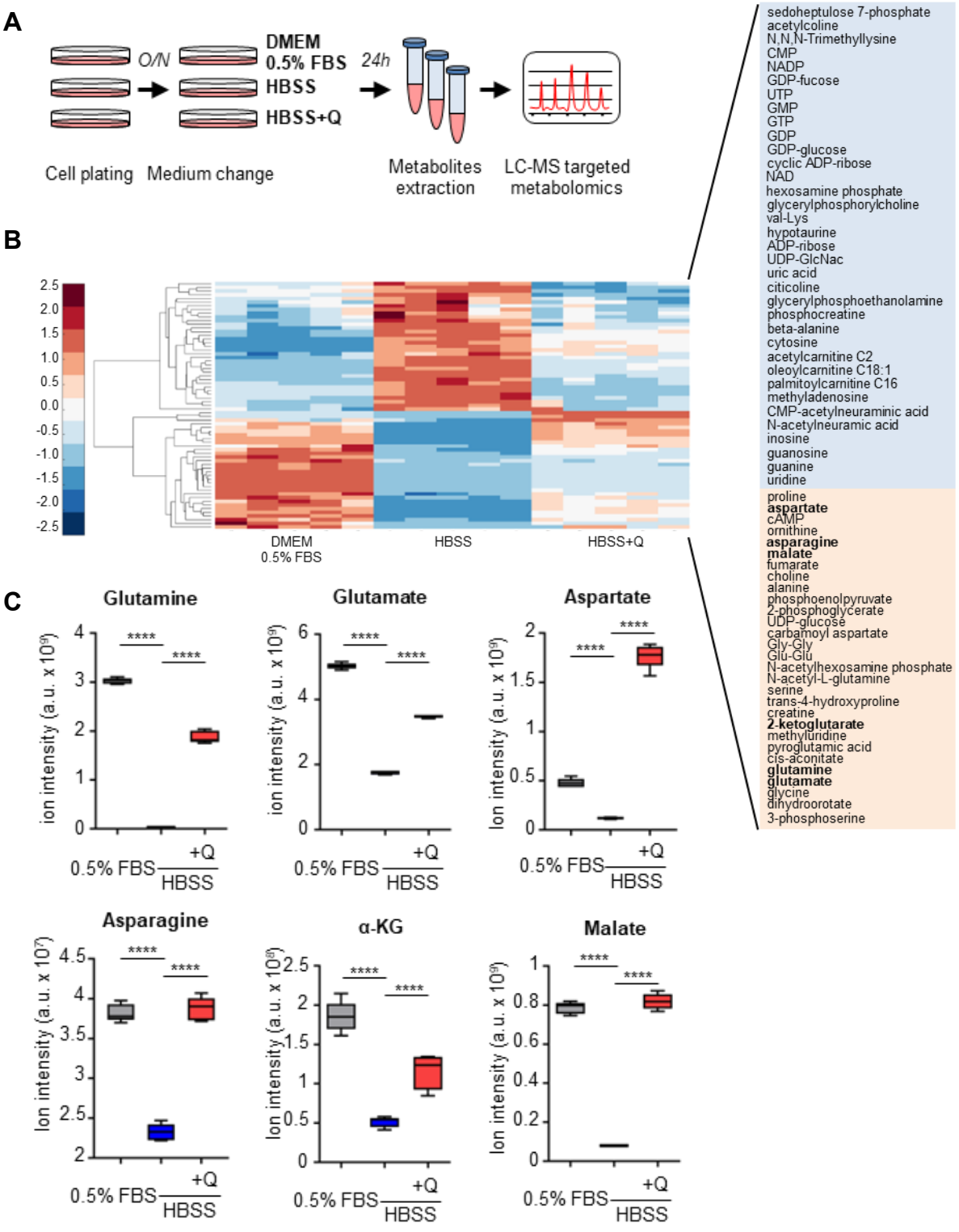

Figure 3.5.1 Glutamine partially rescues metabolic stress induced by nutrient deprivation. *A) Schematic representation of LC-MS targeted metabolomics experimental design. B) Hierarchical clustering of metabolites assessed by LC-MS targeted metabolomics on MEF cells as in A. n = 5. C) Box and whisker plots of intracellular levels of glutamine, glutamate, aspartate, asparagine, α-KG, and malate assessed by LC-MS targeted metabolomics as in A. n = 5. Box and whisker plots are represented with median and min to max. For statistical analysis, one-way ANOVA, followed by Tukey's multiple comparisons test, was used; ****p < 0.0001.*

3.6 Cilia-deficient cells show decreased energy charges and fatty acid oxidation under metabolic stress

Since we found that cilia respond to nutrient deprivation by elongating and to glutamine supplementation by shortening, we exposed cilia-deficient MEF cells to these conditions and we performed LC-MS analysis to verify whether the absence of cilia could have an effect on metabolism upon nutrient deprivation and glutamine supplementation (**Fig. 3.6.1 A**). As shown in the volcano plot, differences in the energy metabolism were detected between cilia-deficient and cilia-proficient cells upon nutrient deprivation (**Fig. 3.6.1 B**). Indeed, cilia-deficient cells revealed a significant reduction in energy charges in terms of nucleotide triphosphate to nucleotide monophosphate ratio (**Fig. 3.6.1 C**), suggesting that the absence of the primary cilium induces an impairment in the energy homeostasis regulation. This finding corroborates our results showing that cilia sense the energetic imbalance of the cell induced by nutrient deprivation and at least partially rescued by glutamine through TCA cycle fuelling to drive OXPHOS and ATP production.

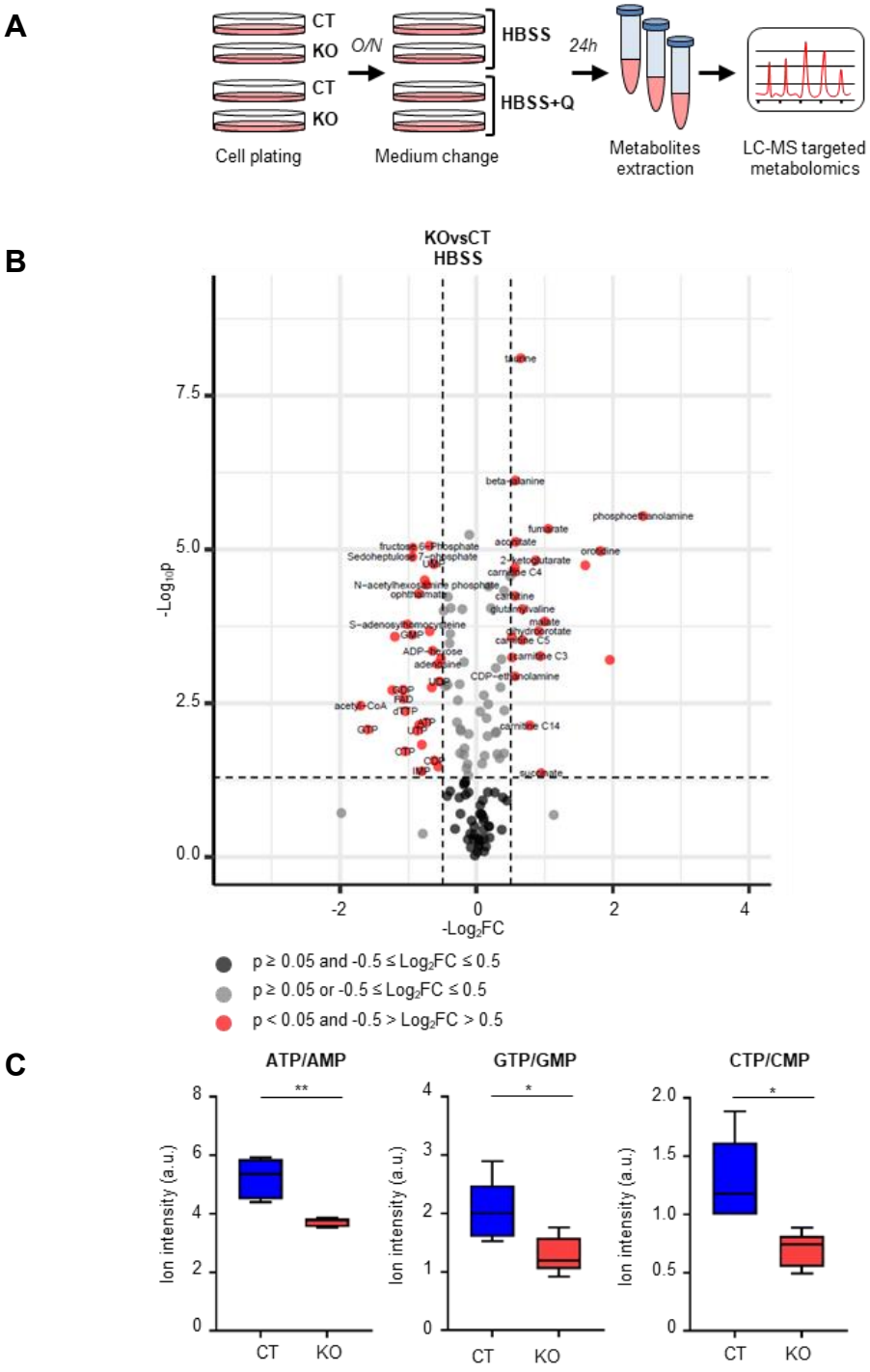

Figure 3.6.1 Cilia-deficient cells show impaired energetic metabolism under nutrient deprivation. *A) Schematic representation of LC-MS targeted metabolomics in Ift88 KO and CT MEF in HBSS ± glutamine (Q) for 24h. B) Volcano plot of metabolites in Ift88 KO vs CT MEF in HBSS for 24 hours as assessed by LC-MS targeted metabolomics as in A. FC = fold change. Black dots: p ≥ 0.05 and -0.5 ≤ Log2FC ≤ 0.5; grey dots: p ≥ 0.05 or -0.5 ≤ Log2FC ≤ 0.5; red dots: p < 0.05 and -0.5 > Log2FC > 0.5.C). C) Box and whisker plots of energy charges expressed as ATP/AMP, GTP/GMP, and CTP/CMP in Ift88 KO (red) and CT (blue) MEF assessed by LC-MS targeted metabolomics as in A. Box and whisker plots are represented with median and min to max. For statistical analysis, Student's unpaired two-tailed t-test was used; *p < 0.05, **p < 0.01.*

Interestingly, we found that upon 4 hours of nutrient deprivation *Ift88* KO MEF cells display an accumulation of carinitines and decreased acylcarnitines levels (**Fig. 3.6.2 A,B**), uncovering a possible impairment of fatty acid oxidation (FAO), which is one of the main drivers of energy production for the cell (Houten *et al.*, 2016). Since acyl-CoA activated long chain fatty acids are imported into the mitochondria through the carnitine palmitoyltransferase 1 (CPT1) as acylcarnitines, we wondered whether it could be altered in cilia-deficient cells.

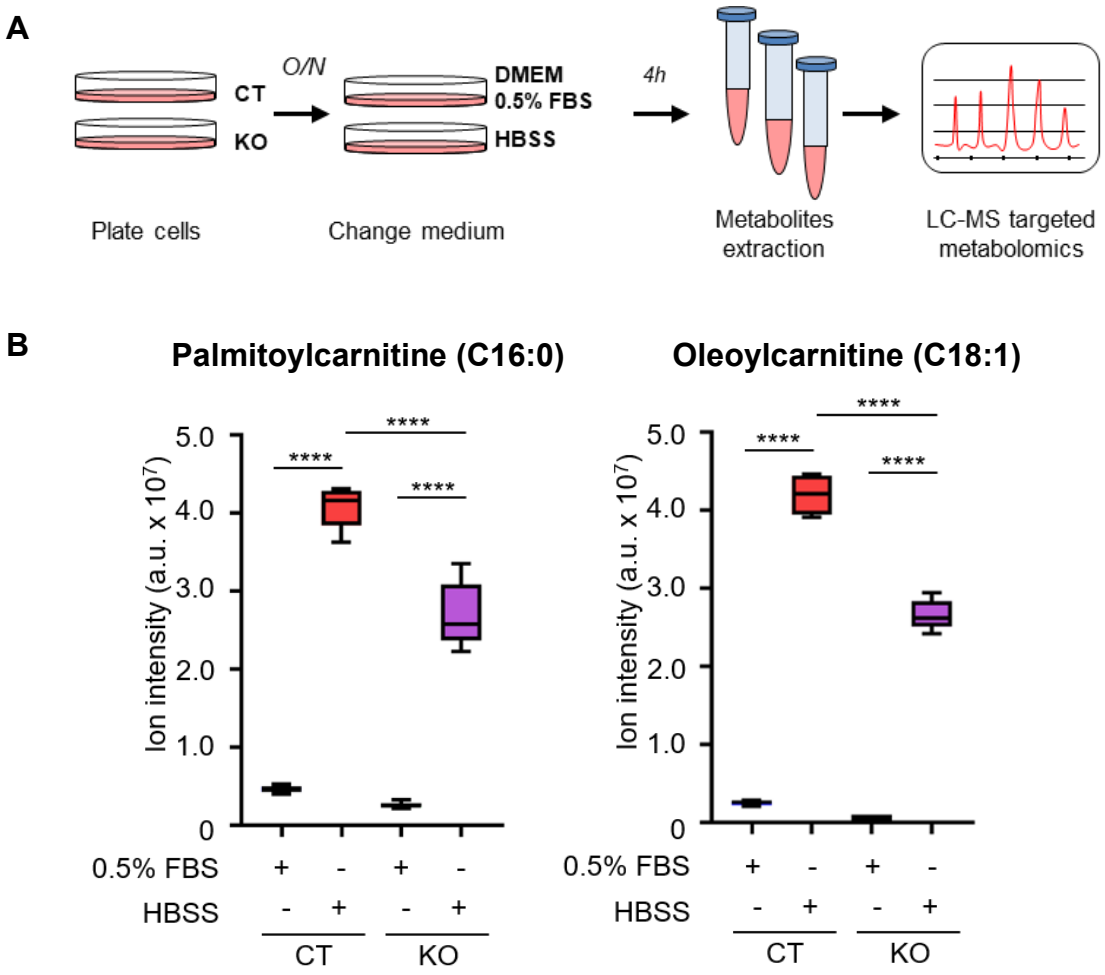

Figure 3.6.2 Cilia-deficient cells display decreased acylcarnitines under nutrient deprivation. *A) Schematic representation of LC-MS targeted metabolomics in Ift88 KO and CT MEF in either partial serum starvation (0.5% FBS) or HBSS for 4h. n = 5 B) Box and whisker plots of palmitoylcarnitine C16:0 and oleoylcarnitine C18:1 in Ift88 KO and CT MEF assessed by LC-MS targeted metabolomics as in A. n = 5 Box and whisker plots are represented with median and min to max. For statistical analysis, one-way ANOVA, followed by Tukey's multiple comparisons test, was used; ****p < 0.0001.*

Strikingly, we detected downregulated transcriptional levels of the isoform *Cpt1a* (expressed also in the kidney) upon nutrient deprivation both in *Ift88* KO MEF and mIMCD3 cells (**Fig. 3.6.3**).

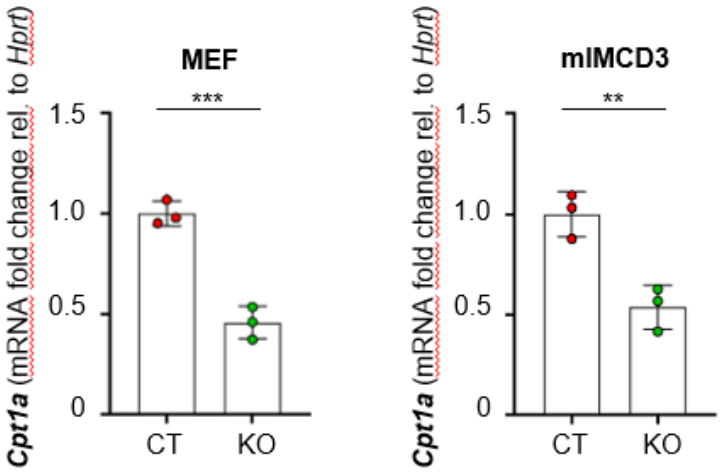

Figure 3.6.3 Cilia-deficient cells display decreased Cpt1a expression under nutrient deprivation. *qRT-PCR of Cpt1a mRNA expression (fold change relative to Hprt) in Ift88 KO and CT MEF (left) and mIMCD3(right) under HBSS. Data in columns are mean ± SD. Statistical analysis: Student's unpaired two-tailed t-test; **p < 0.01, ***p < 0.001.*

Furthermore, we verified the transcriptional expression of *Cpt1a* and *Cpt2*, which reconverts acylcarnitines into carnitine and acyl-CoAs in the mitochondrial matrix, in the kidneys of a mouse model where *Ift88* is conditionally inactivated in renal tubules (*Ift88*$^{flox/flox}$*;KspCre*) at P35, when renal cystogenesis occurred (**Fig. 3.6.4 A,B**). We observed that both *Cpt1a* and *Cpt2* are transcriptionally downregulated (**Fig. 3.6.4 C**), suggesting that the ablation of primary cilia induces a general impairment of FAO both *in vitro* and *in vivo*.

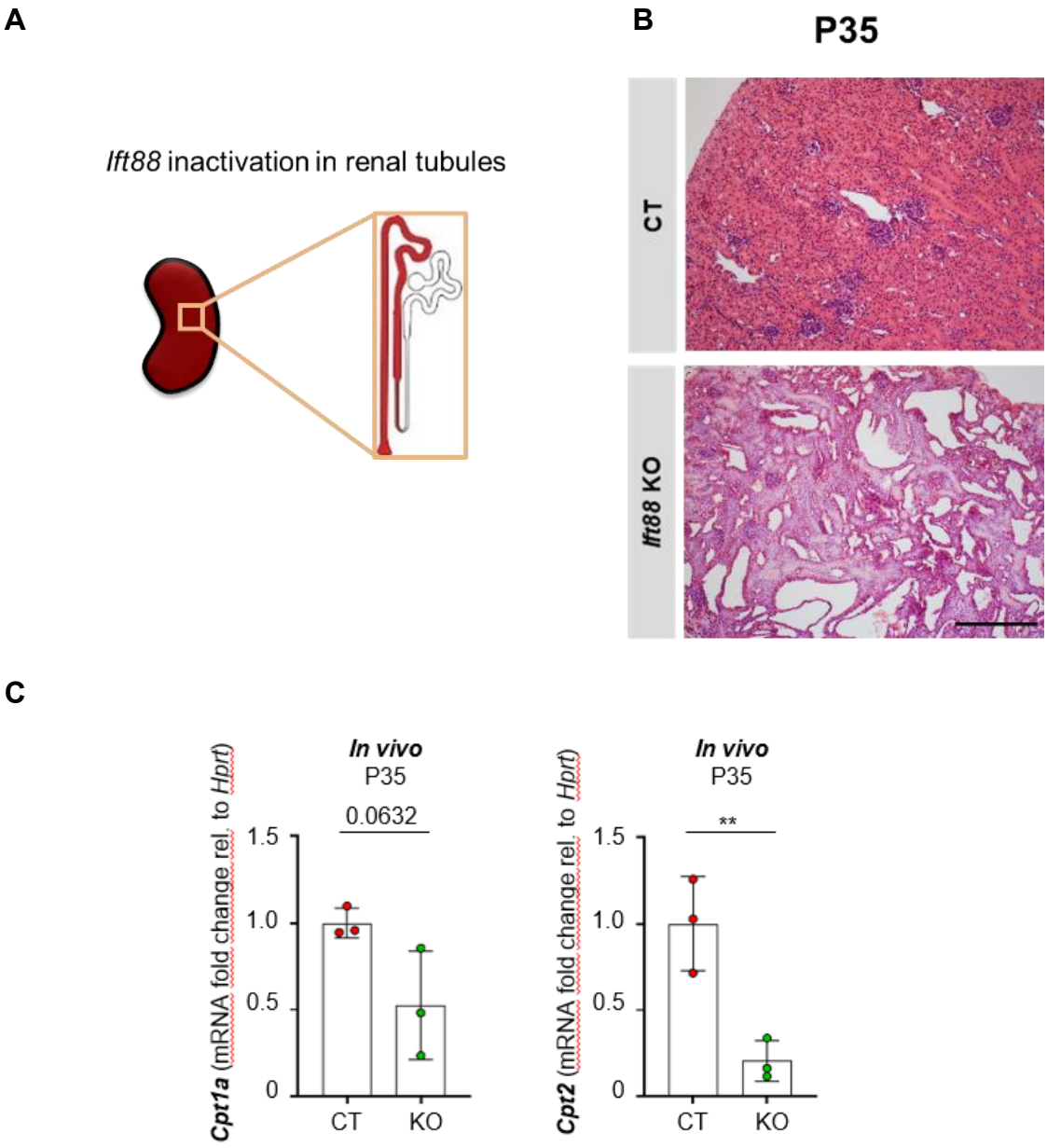

Figure 3.6.4 Absence of cilia in mouse kidneys reduces Cpt1 and 2 expression. *A) Schematic representation of conditional inactivation of Ift88 in renal tubules by KspCre recombinase. B) Representative hematoxylin and eosin staining for kidney tissues of* $Ift88^{flox/flox}$*;KspCre and* $Ift88^{flox/flox}$ *(CT) at P35. C) qRT-PCR of Cpt1a and Cpt2 mRNA expression (fold change relative to Hprt) in* $Ift88^{flox/flox}$*;KspCre and CT kidney lysates. Data in columns are mean ± SD. For statistical analysis, Student's unpaired two-tailed t-test was used; **p < 0.01.*

Taken together, these results reveal that cilia-deficient cells display decreased energy charges and FAO, suggesting a general impairment of energy homeostasis regulation due to absence of cilia.

3.7 Cilia-deficient cells show impaired glutamine utilization and decreased asparagine production

Since our analyses revealed that glutamine is able to drive the shortening of primary cilia possibly through the fueling of the TCA cycle, we wondered whether the ablation of cilia could have an effect on glutamine utilization for mitochondrial respiration. Interestingly, we observed that cilia-deficient MEF cells showed a decreased mitochondrial respiration compared to the relative controls upon glutamine supplementation (**Fig. 3.7.1**). Similarly to both control and *Ift88* KO cells under nutrient-deprived condition, cilia-deficient cells upon glutamine supplementation did not well tolerate FCCP injection as compared to their relative controls. The evidence that cilia loss impairs the capability of cells to drive mitochondrial respiration suggest that primary cilia facilitate glutamine utilization into the TCA cycle to produce ATP and restore the energy status of the cell.

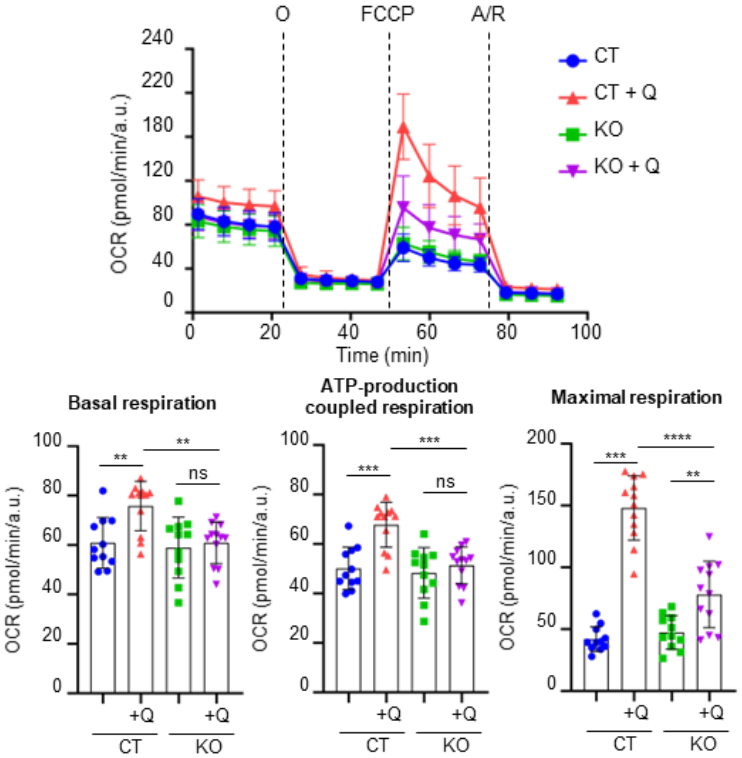

Figure 3.7.1 Cilia-deficient cells display reduced utilization of glutamine to drive mitochondrial respiration. *Top: analysis of OCR measurement during time in Ift88 KO and CT MEF under HBSS (CT: blue; KO: green) or HBSS supplemented with Glutamine (Q) (CT: red; KO: purple) for 4h, in basal condition and after sequential injection of oligomycin (O), FCCP, and antimycin/rotenone (A/R). Bottom: Quantification of basal respiration, ATP-production coupled respiration, and maximal respiration as in Top. Data in columns are mean with ± SD. For statistical analysis, one-way ANOVA, followed by Tukey's multiple comparisons test, was used; ns: not significant, **p < 0.01, ***p < 0.001, ****p < 0.0001.*

LC-MS targeted metabolomics revealed that 51 metabolites out of 137 significantly changed between *Ift88* KO and CT MEF upon glutamine supplementation (**Fig. 3.7.2 A**). The calculation of the fold change of glutamine supplementation (HBSS+Q) *versus* HBSS in *Ift88* KO and CT cells showed that cilia-deficient cells displayed not only decreased glutamine levels upon HBSS+Q *versus* HBSS compared to the relative controls, but also reduced asparagine levels upon HBSS+Q *versus* HBSS as compared to the relative controls (**Fig. 3.7.2 A-C**). These results are in line with our results obtained upon partial serum deprivation showing that glutamine and asparagine levels were decreased in *Ift88* KO cells (**Fig. 3.2.8**).

A

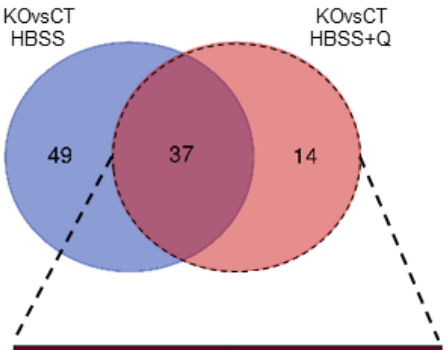

CT	KO	
Inf	175.6	**3-phosphoserine**
81.08	40.26	glutamine
12.2	7.17	fumarate
10.61	4.39	carbamoyl aspartate
10.27	6.18	malate
4.85	3.81	N-acetyl-L-glutamine
4.39	2.78	phosphocholine
2.88	2.78	proline
2.28	1.88	**alanine**
1.81	1.2	**trans-4-hydroxyproline**
1.67	1.32	**asparagine**
1.66	2.26	butyrylcarnitine C4
1.48	2.28	**phosphoenolpyruvate**
1.35	1.26	carnitine
1.31	1.94	**2-phosphoglycerate**
1.27	1.63	N-acetylhexosamine phosphate
1.23	1.1	UDP-glucose
1.14	1.83	**3-phosphoglycerate**
1.13	0.93	2-hydroxyglutarate
1.07	0.7	propionylcarnitine C3
1.05	0.79	isovalerylcarnitine C5
1.04	1.07	AMP
1.03	0.86	taurine
1	0.8	**dimethylarginine**
0.96	1.19	**glucuronic acid**
0.94	0.81	glycerophosphoinositol
0.93	0.86	N-acetyl-L-aspartate
0.91	1.04	propionycholine
0.89	0.79	**IMP**
0.88	0.92	UMP
0.88	0.84	hypotaurine
0.82	0.7	UDP-GlcNac
0.81	0.9	UDP
0.76	0.57	uridine
0.75	1.09	lactate
0.73	0.83	GMP
0.64	0.72	glycerophosphoethanolamine
0.64	0.58	GDP-glucose
0.63	0.66	Beta-alanine
0.58	0.72	fructose-6-phosphate
0.55	0.63	NADPH
0.52	0.38	**inosine**
0.5	0.75	adonitol
0.46	0.37	**cytosine**
0.46	0.48	N,N,N-trimethyllysine
0.39	0.28	**methyladenosine**
0.38	0.46	acetylcarnitine C2
0.34	0.35	uric acid
0.29	0.58	**dihydroxyacetone phosphate**
0.27	0.42	glutathione
0.11	0.14	N-acetylneuramic acid

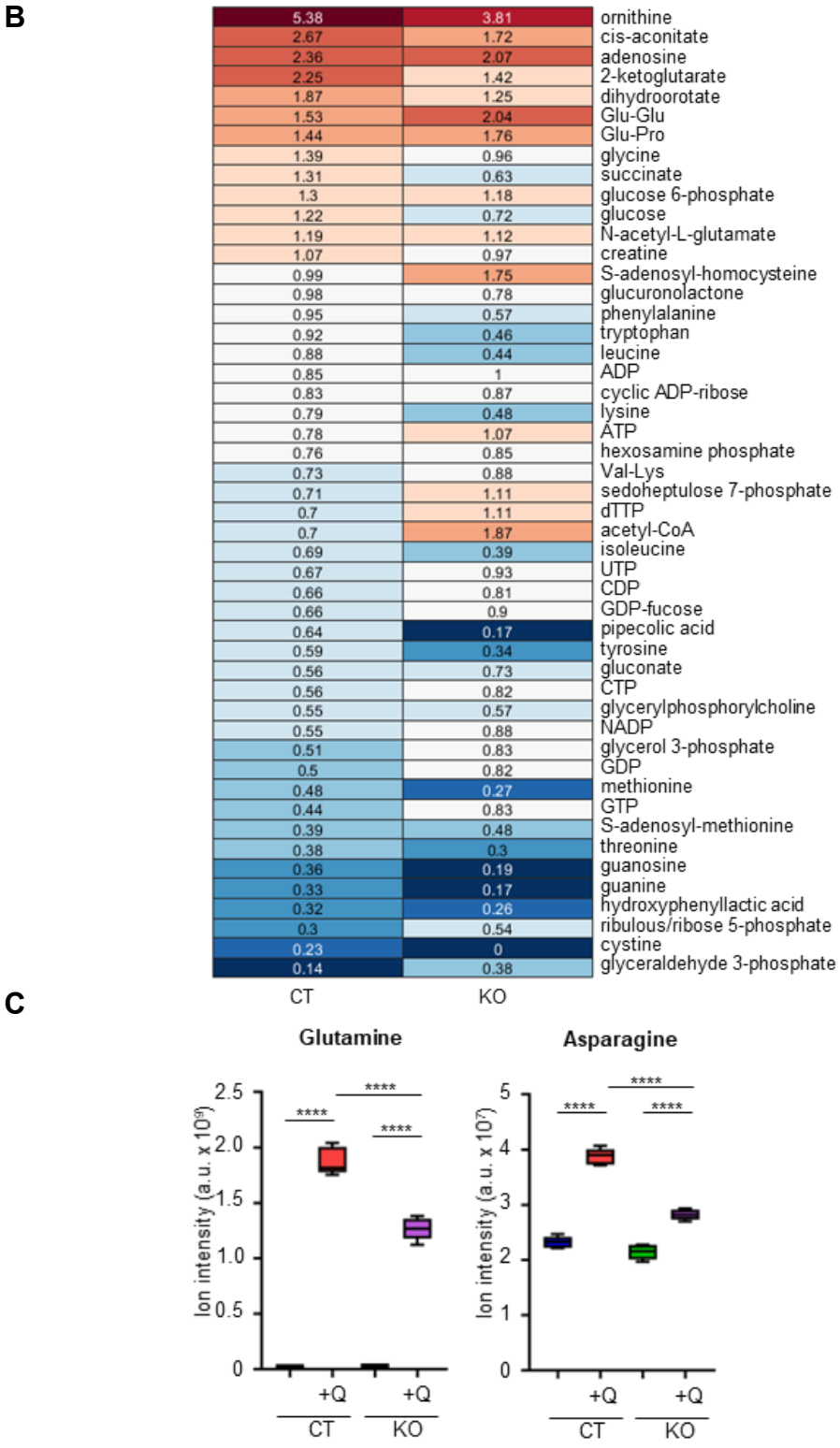

Figure 3.7.2 Cilia-deficient cells display reduced glutamine usage. *A) Top: Venn diagram representing the number of metabolites significantly changing in Ift88 KO vs CT MEF in HBSS and HBSS + Q. Light blue: 49 metabolites that change in KO vs CT only in HBSS. Rose: 14 metabolites changing in Ift88 KO vs CT MEF only in HBSS + Q. Purple: 37 metabolites changing in Ift88 KO vs CT MEF in HBSS and HBSS + Q. Bottom: Heat-map showing the Fold Change (FC) of HBSS + Q vs HBSS, in CT and KO, of the statistically different 51 metabolites in HBSS*

*+ Q (rose and purple in the Venn diagram). The 14 metabolites expressed in bold are the ones that change in Ift88 KO vs CT MEF in HBSS + Q. B) Heat-map showing the Fold Change (FC) of HBSS + Q vs HBSS, in CT and KO, of the statistically different 49 metabolites in HBSS (light blue in the Venn diagram). C) Box and whisker plots of glutamine and asparagine in Ift88 KO and CT MEF assessed by LC-MS targeted metabolomics as in 3.6.1A. Box and whisker plots are represented with median and min to max. For statistical analysis, one-way ANOVA, followed by Tukey's multiple comparisons test, was used; ****p < 0.0001.*

This piece of evidence, together with the results shown above (**Fig. 3.2.8**), prompted us to hypothesize a possible impairment of asparagine synthetase (ASNS), an enzyme able to convert glutamine and aspartate into glutamate and asparagine and upregulated upon nutrient deprivation (Lomelino *et al.*, 2017), in *Ift88* KO MEF cells (**Fig. 3.7.3 A**). $^{15}N_2$-glutamine-labelled tracing on *Ift88* KO and CT cells confirmed that intracellular levels of glutamine and asparagine release were decreased in cilia-deficient cells (**Fig. 3.7.3 B**), reinforcing our pieces of evidence that ASNS could be impaired in cilia-deficient cells.

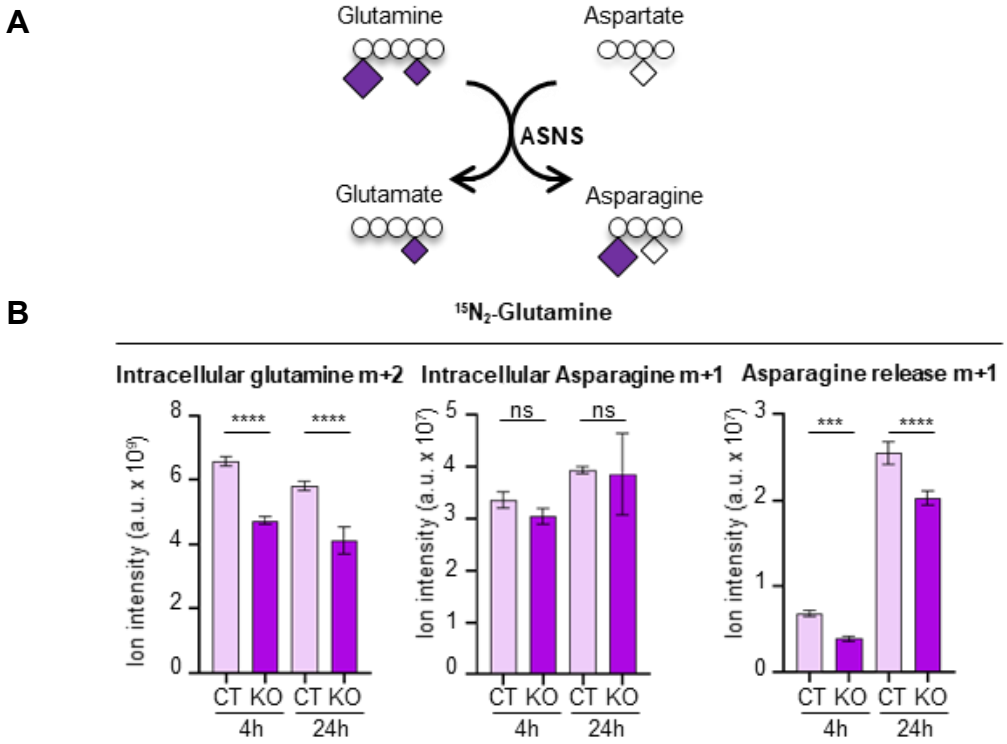

Figure 3.7.3 Absence of cilia impaires asparagine release. *A) Schematic representation of nitrogen-labelled ($^{15}N_2$) glutamine utilization by asparagine synthetase (ASNS). B) Levels of intracellular glutamine (m+2) and asparagine (m+1), and asparagine release (m+1) assessed by nitrogen-labelled $^{15}N_2$-glutamine LC-MS targeted metabolomics in Ift88 KO vs CT MEF in HBSS and HBSS + Q for either 4 or 24h. Data in dot plots are mean with ± SD. For statistical analysis, one-way ANOVA, followed by Tukey's multiple comparisons test, was used; ns: not significant, ***p < 0.001, ****p < 0.0001.*

Thus, we performed qRT-PCR to detect the transcriptional expression of *Asns* in cilia-deficient MEF and mIMCD3 cells and we found a reduction in its mRNA expression upon nutrient deprivation in *Ift88* KO cells compared to controls (**Fig. 3.7.4**).

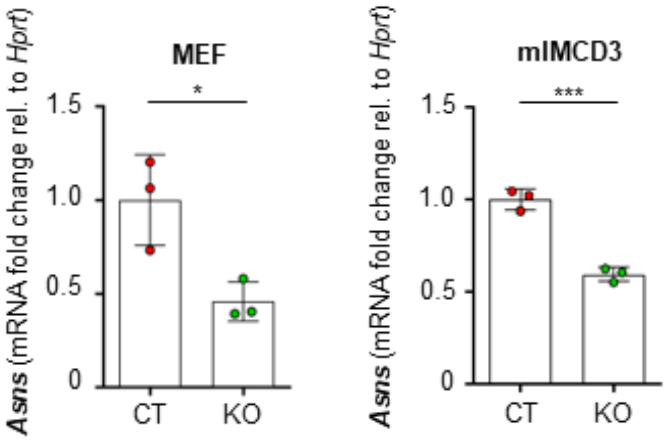

Figure 3.7.4 Absence of cilia reduces Asns expression. *Left: qRT-PCR of Asns mRNA expression (fold change relative to Hprt) in Ift88 KO (green) and CT (red) MEF upon HBSS. Right: qRT-PCR of Asns mRNA expression (fold change relative to Hprt) in Ift88 KO (green) and CT (red) mIMCD3 upon HBSS. Data in dot plots are mean with ± SD. For statistical analysis, Student's unpaired two-tailed t-test was used; *p < 0.05, ***p < 0.001.*

3.8 Cilia facilitate glutamine utilization through asparagine synthetase (ASNS)

Considering our results, we wondered what could be the driver of glutamine-induced shortening of cilia. Since glutamine is known to activate mTOR (Jewell *et al.*, 2015), we tested whether this kinase could be involved in the glutamine effect on primary cilia. We found that, as expected, under glutamine supplementation to nutrient deprived medium mTOR was activated leading to the downstream phosphorylation of S6 ribosomal protein (S6RP) in mIMCD3 cells (**Fig. 3.8.1 A**). However, we observed that rapamycin, an inhibitor of mTOR, did not abrogate the ciliary shortening induced by glutamine, suggesting that this effect is mTOR-independent (**Fig. 3.8.1 B**). Furthermore, we found that leucine, the other aminoacid able to activate mTOR (Jewell *et al.*, 2015), did not induce a decrease in the length of cilia as glutamine did (**Fig. 3.8.1 C,D**).

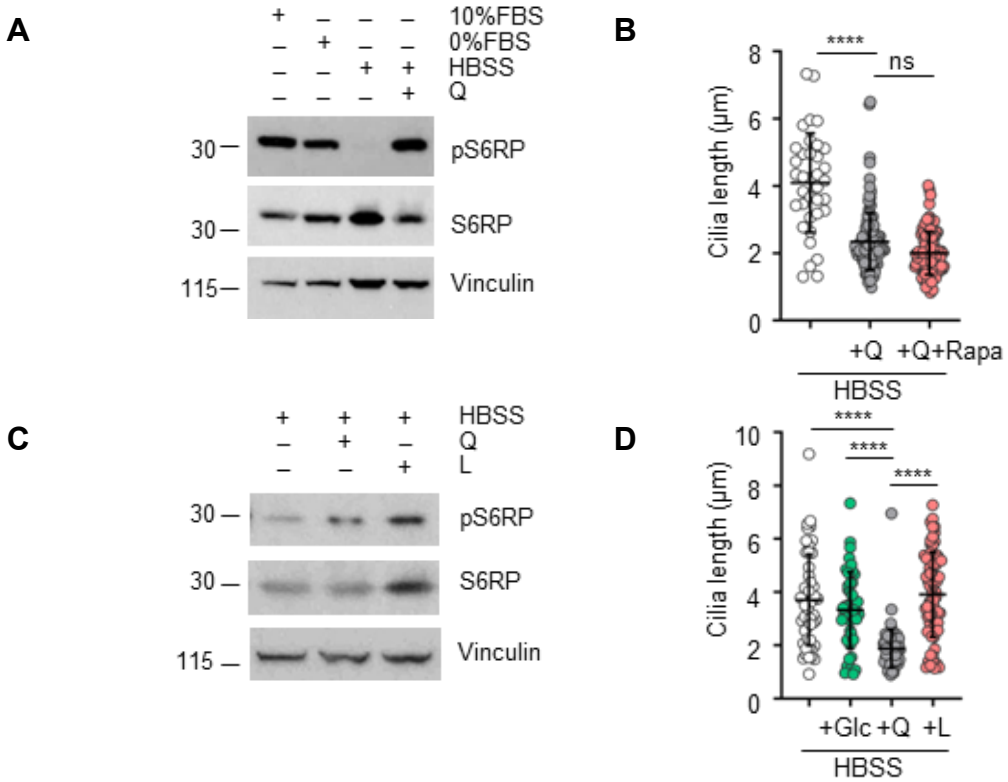

Figure 3.8.1 Glutamine shortens cilia independently of mTOR. *A) Western blot analysis for pS6RP and total S6RP protein expression in cellular lysates from mIMCD3 under either complete medium condition (10% FBS), serum starvation (0% FBS), HBSS ± glutamine (Q) for 24h. Vinculin was used as loading control. B) Quantification of cilia length in mIMCD3 in HBSS ± Q or HBSS+Q+Rapamycin (Rapa) for 24h. C) Western blot analysis for pS6RP and total S6RP protein expression in cellular lysates from mIMCD3 in HBSS ± Q or leucine (L) for 24h. Vinculin was used as loading control. D) Quantification of cilia length in mIMCD3 in HBSS ± Glucose (Glc), Q, or L for 24h. Data in dot plots are mean with ± SD. For statistical analysis, one-way ANOVA, followed by Tukey's multiple comparisons test, was used; ns: not significant, ****p < 0.0001.*

Since ASNS seemed to be impaired in cilia-deficient cells, we investigated whether this enzyme could instead be involved in the cilia shortening induced by glutamine. To test this hypothesis, we silenced *Asns* through siRNA and we found that ASNS protein expression was drastically reduced in si*Asns* mIMCD3 cells (**Fig. 3.8.2 A,B**).

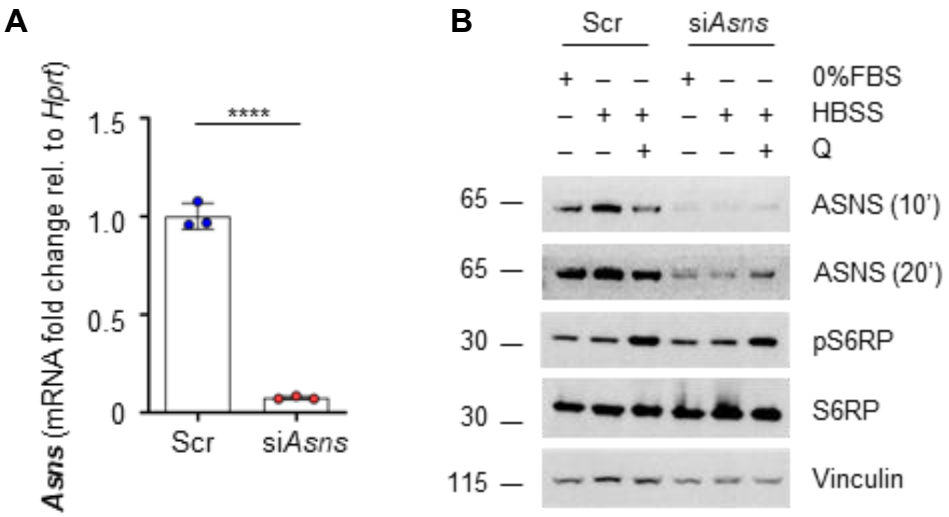

Figure 3.8.2 Silencing of Asns does not dramatically affect mTOR pathway. *A) qRT-PCR of Asns mRNA expression (fold change relative to Hprt) in Asns transiently knockdown (siAsns, red) and scramble (Scr, blue) mIMCD3. B) Western blot analysis for ASNS, pS6RP, and total S6RP protein expression in cellular lysates from mIMCD3 under either serum starvation (0% FBS) and HBSS ± glutamine (Q) for 24h. Vinculin was used as loading control. Different exosures of ASNS are reported in branchets. Data in columns are mean with ± SD. For statistical analysis, Student's unpaired two-tailed t-test was used; ****p < 0.0001.*

While cilia of cells treated with the negative siRNA (scramble) elongated upon nutrient deprivation and shortened upon glutamine supplementation, cilia of cells treated with the si*Asns* siRNA showed increased length upon both serum and glutamine supplementation to nutrient starvation for 24 hours, as already reported in another unbiased study for the detection of siRNA involved in ciliary length regulation (Wheway *et al*, 2015). Even more interestingly, silencing of *Asns* severily impaired the shortening of cilia upon glutamine supplementation compared to the scramble cells, suggesting that ASNS could mediate the cilia shortening induced by glutamine (**Fig. 3.8.3**). Of note, we found that *Asns* silencing did not affect mTOR activation upon glutamine supplementation, reinforcing the finding that the effect was mTOR-independent (**Fig. 3.8.2 B**).

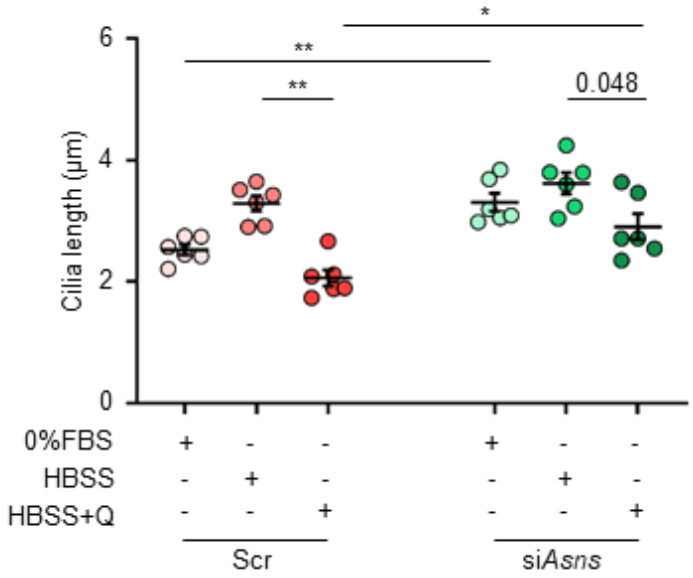

Figure 3.8.3 Silencing of Asns elongates cilia and impaires the shortening of cilia upon glutamine supplementation. *Average cilia length values from 6 independent experiments in mIMCD3 transiently knocked down for Asns (siAsns) compared to control (Scr) in either serum starvation (0% FBS) or HBSS ± glutamine (Q) for 24h. Data in dot plots are mean with ± SEM. For statistical analysis, one-way ANOVA, followed by Bonferroni's multiple comparisons test, was used; *p < 0.05, **p < 0.01.*

Furthermore, a more detailed analysis of the distribution of cilia lengths clearly showed a different shape between cilia lengths of scramble cells upon glutamine supplementation compared the ones of scramble cells upon nutrient deprivation, while the distribution of cilia lengths of si*Asns* cells is similar between nutrient deprivation and glutamine supplementation (**Fig. 3.8.4 A,B**). Indeed, scramble cells upon glutamine supplementation displayed the peak of cilia lengths at 1-2 µm compared to the one at 3-4 µm upon nutrient deprivation, while si*Asns* cells showed the peak of cilia lengths upon glutamine supplementation at 2-3 µm, which was similar to the one at 3-4 µm upon nutrient deprivation (**Fig. 3.8.4 A,B**).

A

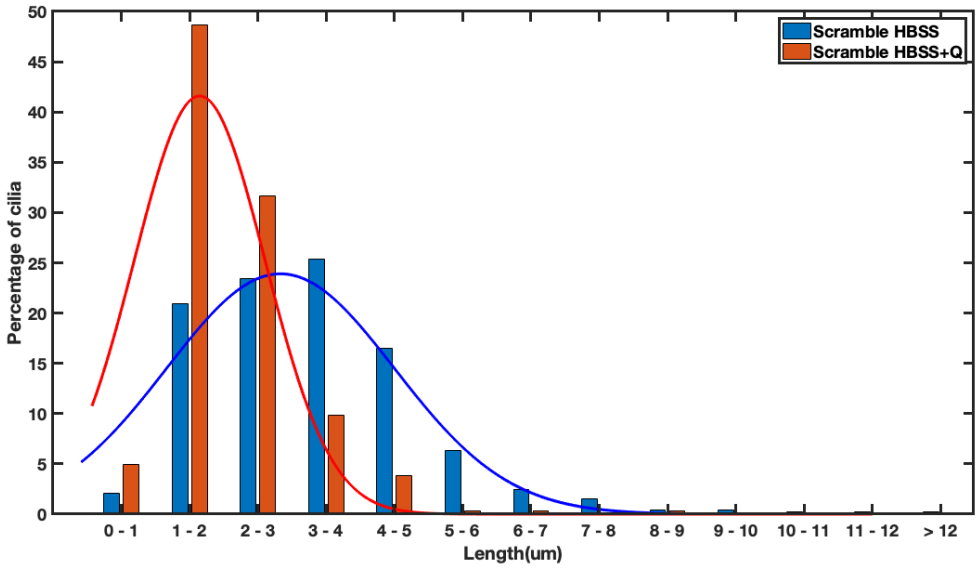

B

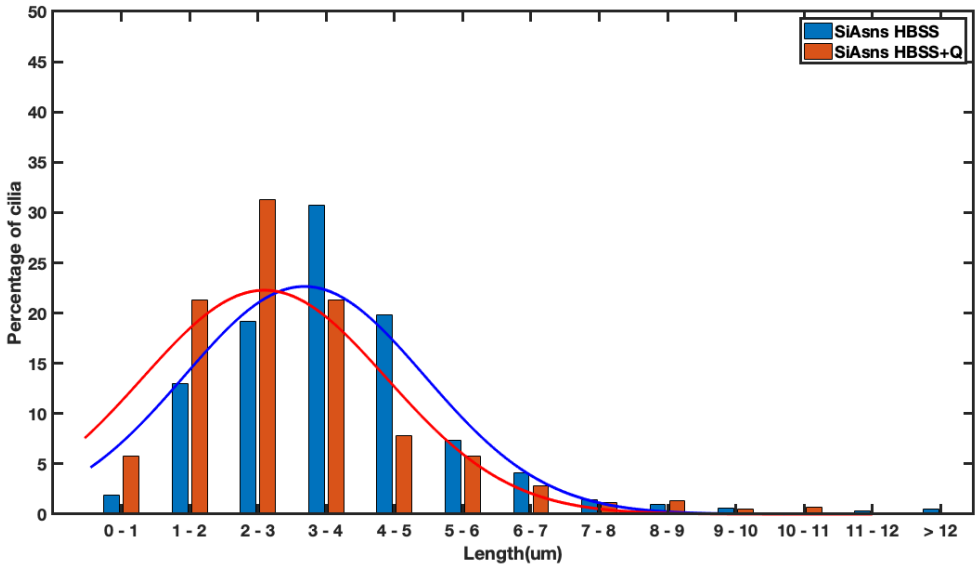

Figure 3.8.4 Silencing of Asns upon glutamine supplementation displays a similar distribution of cilia lengths compared to nutrient deprivation. *A) Distribution of cilia lengths of 6 independent experiments in scramble (Scr) mIMCD3 in HBSS ± glutamine (Q) for 24h. B) Distribution of cilia lengths of 6 independent experiments in Asns transiently knocked down mIMCD3 (siAsns) in HBSS ± Q for 24h. Cilia lengths were divided in cathegories of 1 µm each.*

Furthermore, we observed that silencing of *Asns* completely abrogated the glutamine-driven shortening of cilia after 8 hours of culture in either nutrient deprivation or glutamine supplementation, suggesting that the si*Asns* cells are less able to utilize glutamine at shorter time points compared to scramble cells (**Fig. 3.8.5**).

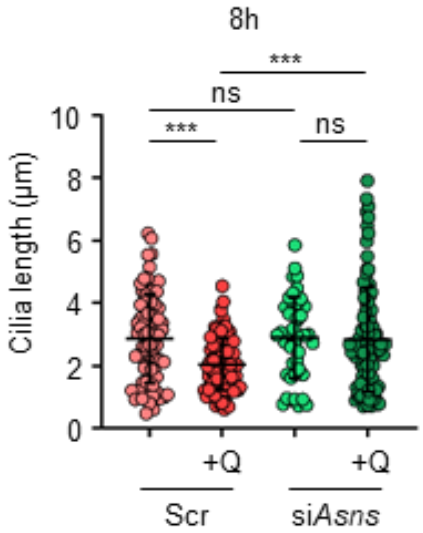

Figure 3.8.5 Silencing of Asns abrogates cilia shortening upon glutamine supplementation at early time-points. *Quantification of cilia length in mIMCD3 transiently knocked down for Asns (siAsns) compared to control (Scr) in HBSS ± glutamine (Q) for 8h. Data in dot plots are mean with ± SD. For statistical analysis, one-way ANOVA, followed by Tukey's multiple comparisons test, was used; ns: not significant, ***p < 0.001.*

Since asparagine, together with glutamate, is the product of ASNS, we tested whether the effect of glutamine on cilia was driven by the synthesis of asparagine. However, asparagine supplementation was not able to shorten cilia at the same extent as glutamine, suggesting that asparagine synthesis is not the key player in the effect induced by glutamine (**Fig. 3.8.6**). Furthermore, to corroborate our results, we treated mIMCD3 cells with asparaginase (ASNase), an enzyme able to degrade asparagine, to investigate whether the absence of asparagine could affect ciliary length. Consistently with previous results, we appreciated that this treatment did not affect ciliary length upon glutamine supplementation compared to the relative controls, suggesting that ASNS drives glutamine induced shortening of cilia not via asparagine synthesis (**Fig. 3.8.6**).

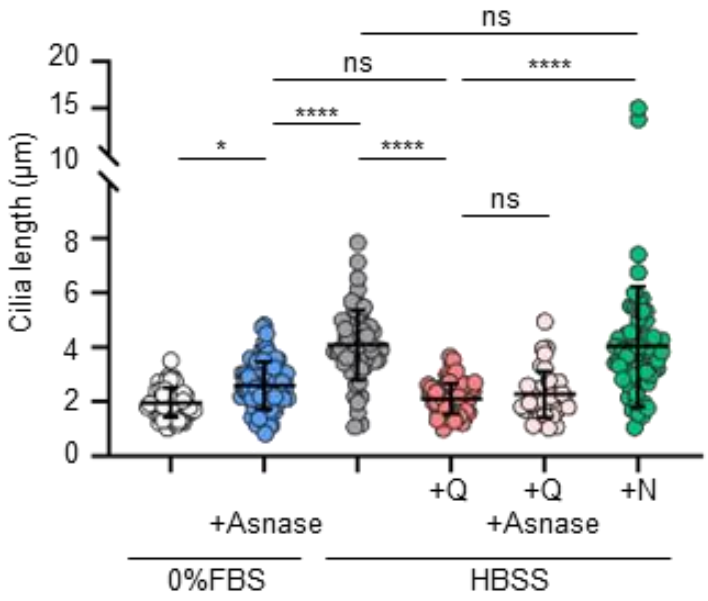

Figure 3.8.6 Asparagine supplementation or degradation does not affect cilia length upon metabolic stress. *Quantification of cilia length in mIMCD3 in either serum starvation (0% FBS) ± asparaginase (ASNase), or HBSS ± glutamine (Q) (4 mM), or HBSS + Q + ASNase, or HBSS + asparagine (N) (0.1 mM) for 24h. Data in dot plots are mean with ± SD. For statistical analysis, one-way ANOVA, followed by Tukey's multiple comparisons test, was used; ns: not significant, *p < 0.05, ****p < 0.0001.*

We also confirmed that both physiological and supra-physiological levels of asparagine (0.1 and 1 mM) did not dramatically shorten primary cilia compared to physiological and supra-physiological levels of glutamine (0.5 and 4 mM) (**Fig. 3.8.7**).

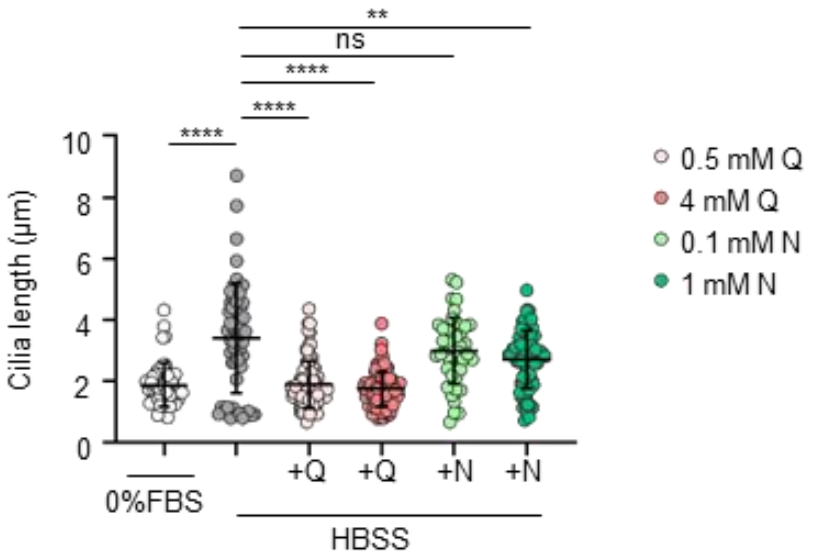

Figure 3.8.7 Physiological and supra-physiological levels of asparagine supplementation do not affect cilia length upon metabolic stress. *Quantification of cilia length in mIMCD3 in either serum starvation (0% FBS) or HBSS ± Q (0.5 or 4 mM), or or HBSS + N (0.1 or 1 mM) for 24h. Data in dot plots are mean with ± SD. For statistical analysis, one-way ANOVA, followed by Tukey's multiple comparisons test, was used; ns: not significant, **p < 0.01, ****p < 0.0001.*

Thus, we wondered whether this effect could be due to ASNS-driven glutamate fueling of the TCA cycle. Strikingly, si*Asns* cells displayed decreased acute response to glutamine in terms of mitochondrial respiration compared to the relative controls. Overall, both si*Asns* and controls did not well tolerated the FCCP injection to drive maximal respiration. The finding that silencing of *Asns* significantly reduced the acute response to glutamine suggested that ASNS mediates glutamine-driven shortening of cilia by producing glutamate to fuel the TCA cycle (**Fig. 3.8.8 A,B**).

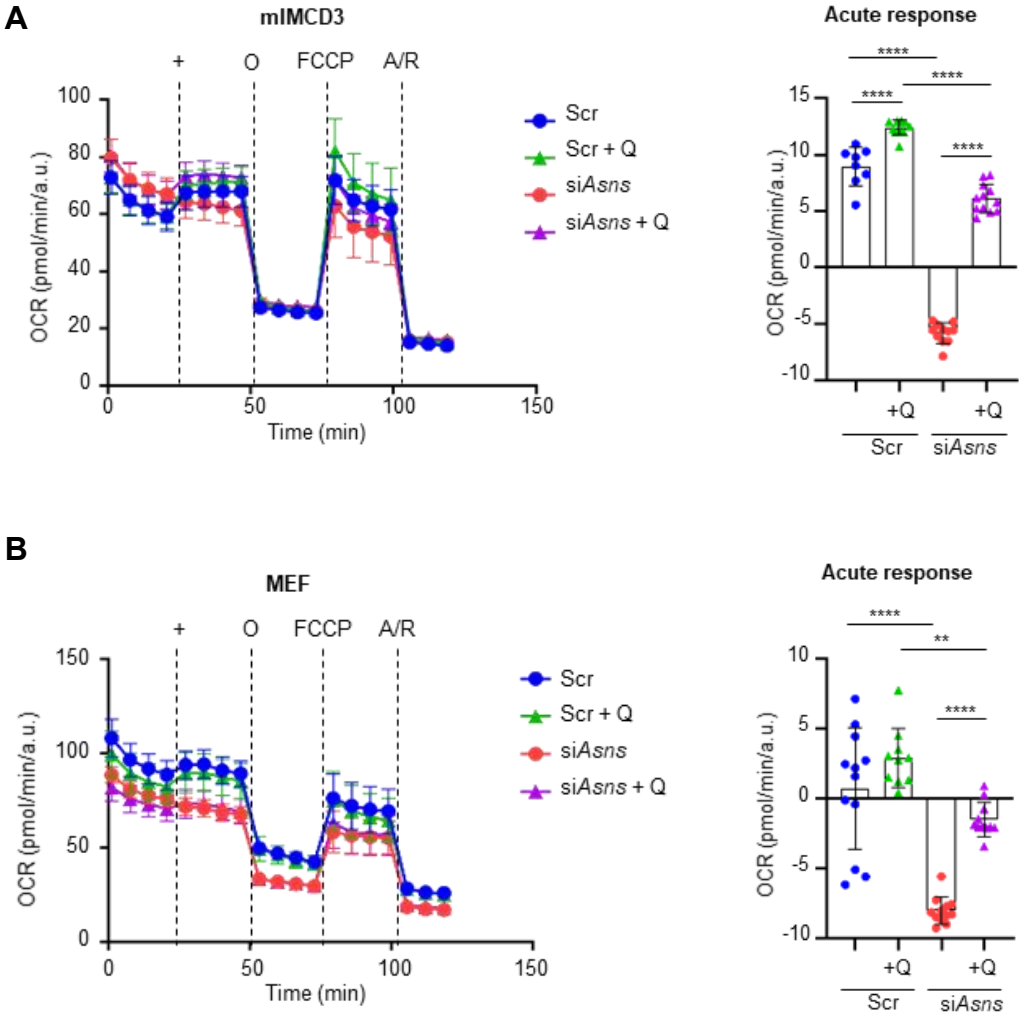

Figure 3.8.8 Silencing of Asns impaires glutamine usage into mitochondrial respiration upon metabolic stress. *A). Left: analysis of OCR measurement during time in Asns transiently knocked down (siAsns) and scramble (Scr) mIMCD3 under HBSS (siAsns: red; Scr: blue) or HBSS supplemented with glutamine (Q) (siAsns: purple; Scr: green) for 4h, in basal condition and after sequential injection of Q, oligomycin (O), FCCP, and antimycin/rotenone (A/R). Right: Quantification of acute response as in Left. B) Left: analysis of OCR measurement during time in Asns transiently knocked down (siAsns) and scramble (Scr) MEF cells under HBSS (siAsns: red; Scr: blue) or HBSS supplemented with glutamine (Q) (siAsns: purple; Scr: green) for 4h, in basal condition and after sequential injection of Q, oligomycin (O), FCCP, and antimycin/rotenone (A/R). Right: Quantification of acute response as in Left. Data in columns are mean with ± SD. For statistical analysis, one-way ANOVA, followed by Tukey's multiple comparisons test, was used; **p < 0.01, ****p < 0.0001.*

In conclusion, our findings reveal that cilia facilitate glutamine utilization through ASNS capability to produce glutamate to fuel the TCA cycle.

3.9 ASNS localizes at the centrosome-cilium complex

Since our results revealed a prominent role of ASNS in the capability of cilia to facilitate glutamine utilization to fuel the TCA cycle, we hypothesized that this enzyme could localize at the centrosome-cilium complex. Thus, we starved the cells from serum to facilitate ciliogenesis and we "deciliated" cells with a previously described buffer (see Materials and Methods, **Chapter 5.11**) (Ishikawa *et al*, 2012; Kim *et al*, 2014). Then, we performed sequential centrifugations to obtain subcellular fractions containing cytosol, organelles, and cilia (**Fig. 3.9.1 A**). Interestingly, we found that the ciliary fraction (fraction 3), enriched for IFT88 protein, showed an amount of ASNS protein, suggesting a possible localization of ASNS at cilia (**Fig. 3.9.1 B**).

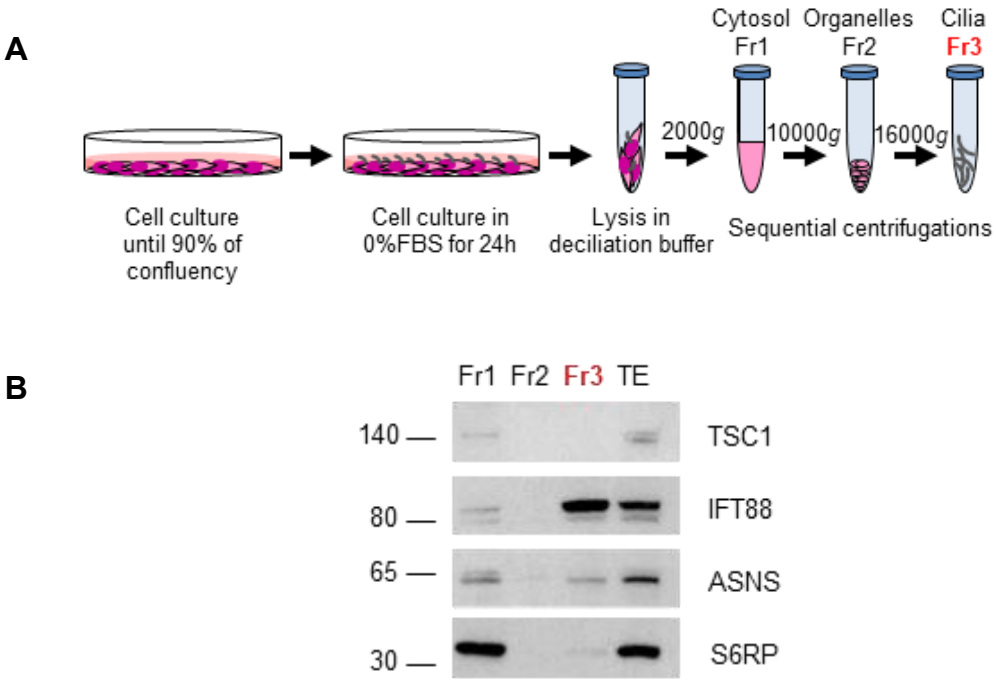

Figure 3.9.1 ASNS localizes in the ciliary fraction obtained by subcellular fractionation assay. *A) Scheme of cilia enrichment by subcellular fractionation. B) Western blot for TSC1, IFT88, ASNS, and S6RP of Fraction 1 (Fr1: cytoplasmic), Fraction 2 (Fr2: organelles), Fraction 3 (Fr3: cilia enriched) and total extract (TE) from mIMCD3 as in A.*

To better corroborate our results, we tried to localize ASNS at cilia by IF. Unfortunately, the antibodies available gave non-specific signal in cilia of si*Asns* cells. Thus, we performed transient transfection with ASNS tagged with either GFP or mCherry at either N- or C-terminus using Lipofectamine. Next, we performed IF for ARL13B to stain cilia in mIMCD3 cells after 8 hours of serum starvation, and we found that GFP-ASNS signal localized at the base of cilia (**Fig. 3.9.2**).

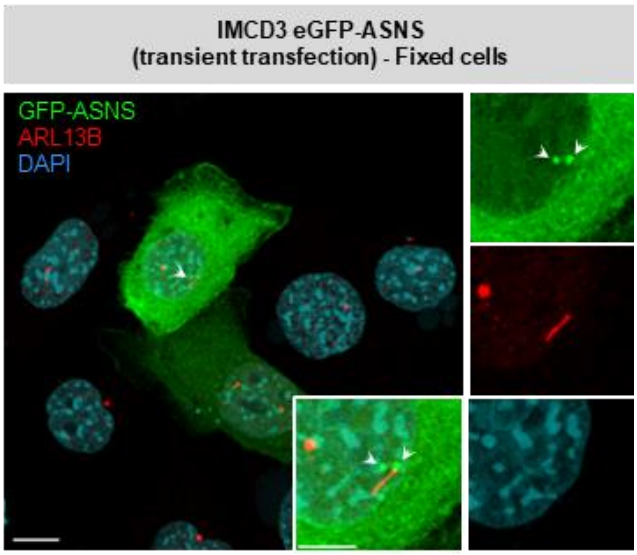

Figure 3.9.2 ASNS is enriched at the base of cilia. *Representative IF images of mIMCD3 transiently transfected with eGFP-ASNS in serum starvation (0% FBS) for 8h. eGFP-ASNS (green), cilia (ARL13B, red), nuclei (DAPI, blue). Scale bar: 10 µm. Arrows indicate the localization of eGFP-ASNS at the base of cilia. The magnification of the localization of eGFP-ASNS at the base of cilia (merged and single channels) is shown in the insets. Scale bar: 5 µm.*

To further verify the colocalization of ASNS at centrosome, we performed IF costaining for ARL13B and the centrosome marker γ-tubulin on mIMCD3 cells transiently transfected with either GFP-ASNS or mCherry-ASNS (**Fig. 3.9.3 A,B**). Strikingly, we found that tagged ASNS costained with γ-tubulin. Taken together, these results show that ASNS localizes at the centrosome-cilium complex, suggesting that this enzyme could have this peculiar localization to fill a specific function in this compartment.

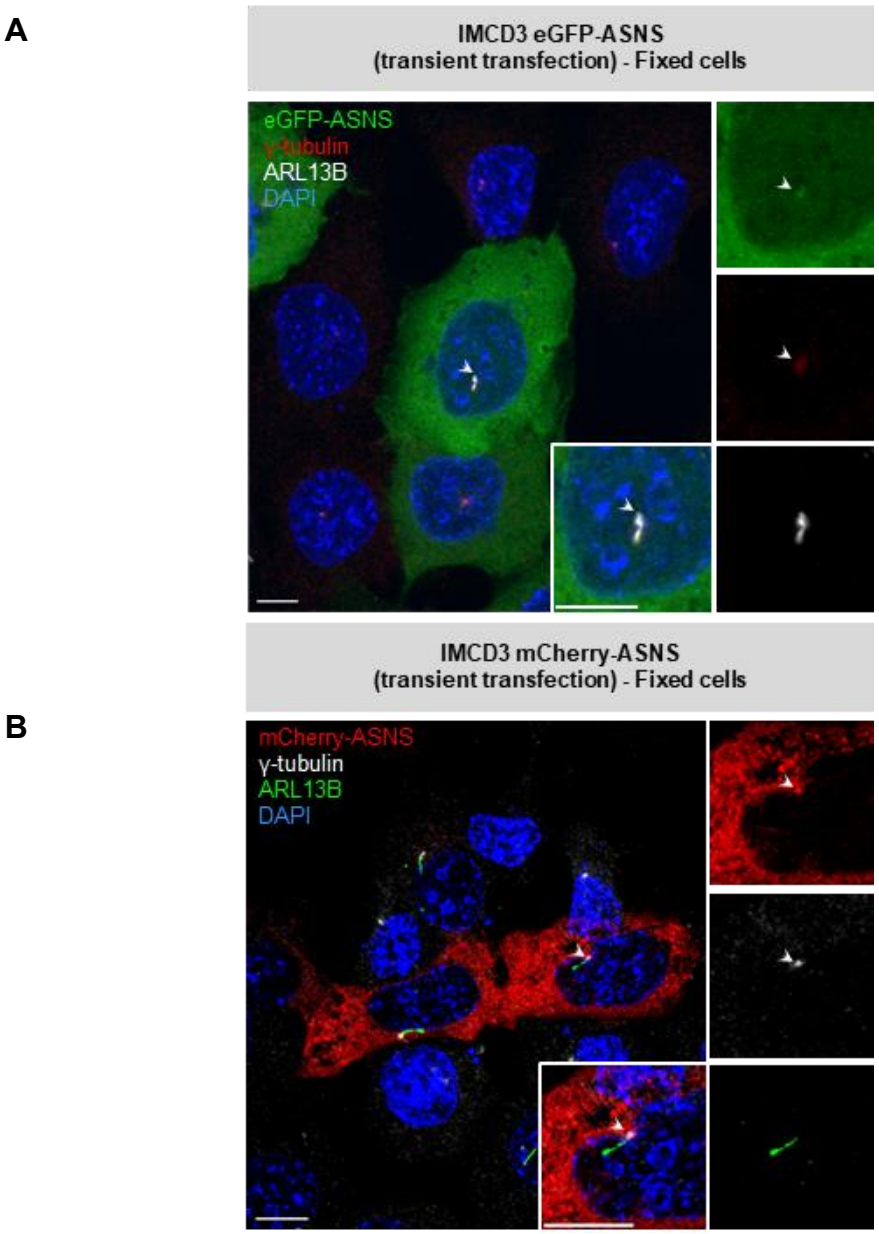

Figure 3.9.3 ASNS localizes at centrosome-cilium complex. *A) Representative IF images of mIMCD3 transiently transfected with eGFP-ASNS in serum starvation (0% FBS) for 8h. eGFP-ASNS (green), centrosomes (γ-tubulin, red), cilia (ARL13B, white), nuclei (DAPI, blue). Scale bar: 10 µm. Arrows indicate the localization of eGFP-ASNS at the base of cilia. The magnification of the localization of eGFP-ASNS at the base of cilia (merged and single channels) is shown in the insets. Scale bar: 10 µm. B) Representative IF images of mIMCD3 transiently transfected with mCherry-ASNS in HBSS for 8h. mCherry-ASNS (red), centrosomes (γ-tubulin, white), cilia (ARL13B, green), nuclei (DAPI, blue). Scale bar: 10 µm. Arrows indicate the localization of mCherry-ASNS at the base of cilia. The magnification of the localization of mCherry-ASNS at the base of cilia (merged and single channels) is shown in the insets. Scale bar: 10 µm.*

4. DISCUSSION

In this thesis we show a new role of primary cilia in sensing nutrient availability and in favouring glutamine utilization through asparagine synthetase (ASNS). Of interest, we found that exposing cells to nutrient deprivation drives cilia elongation, which is rescued by glutamine, but not by glucose. We show that glutamine-driven shortening is due to the capability of glutamine to promote energy production by fuelling the TCA cycle in the mitochondria. ASNS resulted to play a key role in this context, since it mediates the conversion of glutamine into glutamate to drive oxidative phosphorylation (OXPHOS) and cilia shortening. Although the sensory function of primary cilia is well established, their role in sensing and possibly regulating cellular responses to metabolic demands at the cellular level was still uncovered. Indeed, obesity and diabetes are recurrent alterations of the systemic metabolism reported to be features of some ciliopathies revealing the importance of these cellular *antennae* in the regulation of systemic metabolism at the whole body level. In this context, also some studies about the differentiation of preadipocytes into mature adipocytes reported cilia as the key players in promoting adipogenesis (Hilgendorf *et al.*, 2019), but the importance of the ciliary function in the regulation of cellular metabolism was still uncovered. Interestingly, recent work of our group showed that Autosomal Dominant Polycystic Kidney Disease (ADPKD), the most common monogenic disorder and ciliopathy, displays a wide cellular metabolic reprogramming (Podrini *et al.*, 2018; Rowe *et al.*, 2013), resembling the one observed in cancer. Thus, this finding led us to hypothesize that cilia could play a crucial role in the regulation of the metabolism at the cellular level by sensing metabolites and prompted us to initiate the studies contained herein. Based on our results, we propose that cilia sense nutrient availability by elongating under nutrient deprivation and by shortening under glutamine supplementation. We also propose that glutamine is able to shorten cilia by fueling the TCA cycle and driving ATP production. We found out that cilia facilitate glutamine usage into the TCA cycle via ASNS, which we found to be enriched in the centrosome-cilium complex (**Fig. 4.1**).

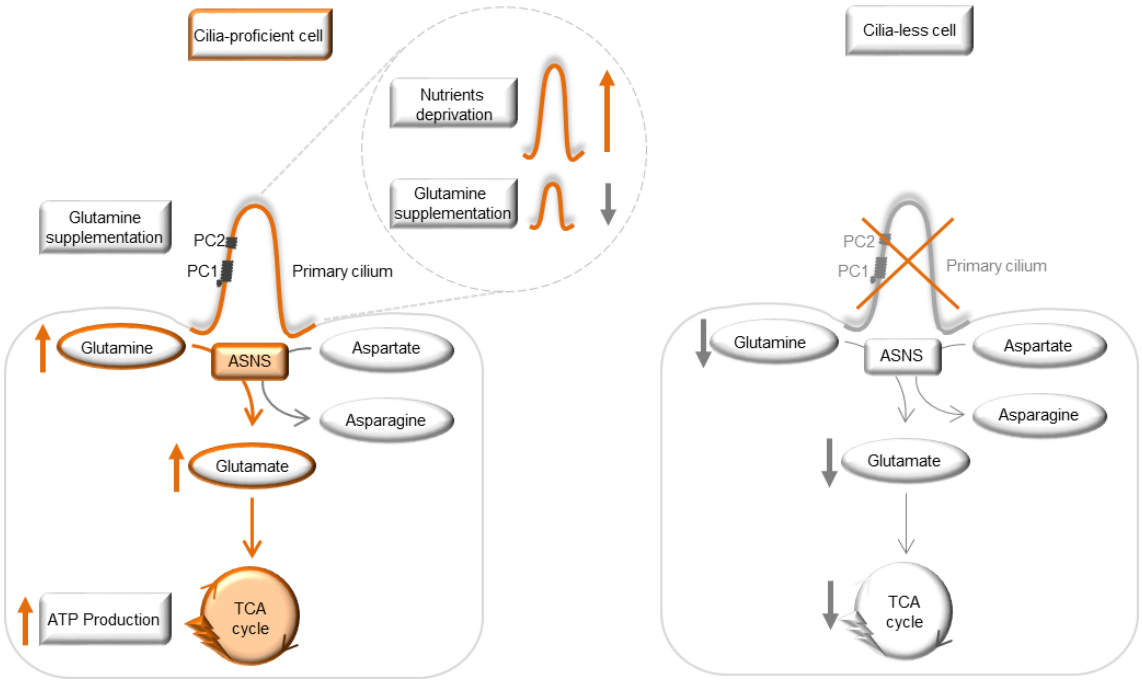

Figure 4.1 Proposed model of cilia-driven response to glutamine. *Schematic representation of the proposed model by which primary cilia sense nutrient availability and facilitate glutamine utilization through ASNS into the TCA cycle to drive ATP production. This mechanism is impaired in cilia-deficient cells.*

Primary cilia sense nutrient availability

In this thesis, we show that nutrient deprivation elongates primary cilia compared to serum starvation in multiple cell lines (MEF, hRPE, mIMCD3, MDCK) that are extensively used for ciliary studies. Serum starvation is known to drive ciliogenesis by synchronizing cells in a reversible cell cycle arrest (G0/G1 phase) (Zhao *et al.*, 2023). Therefore, the percentage of ciliated cells is used as a readout of cell cycle arrest. Of note, we found that nutrient deprivation does not affect the percentage of ciliated cells compared to serum starvation, suggesting that the nutrient deprivation-driven elongation is not caused by a further percentage of cells exiting the cell cycle compared to serum starvation. Since ciliary elongation induced by nutrient deprivation is not restricted to a specific cell line, but is shared by several cell types (ranging from fibroblasts to epithelial cells, deriving from different species, and normally present in different tissues), this piece of evidence reveals that the elongation driven by nutrient deprivation should be due to the

cilium *per se* and not be dependent on cell type features. Although the physiological relevance of the elongation of cilia has already to be clarified, here we propose that primary cilia are sensors of nutrient availability at the cellular level and therefore elongate upon nutrient deprivation. Of note, in this thesis we propose that cilia sense the imbalance of the energy status of the cells induced by nutrient deprivation. Despite the relvance of the ciliary function in the regulation of systemic metabolism is already known, our finding that cilia are sensors of nutrient availability at the cellular level uncovers a new role of cilia as regulators of cellular metabolism, in line with the previous evidence of our group that *Pkd1* mutant cells are characterized by a wide cellular metabolic reprogramming (Podrini *et al.*, 2018; Rowe *et al.*, 2013).

Primary cilia preferentially sense glutamine

Of interest, we found that glutamine, but not glucose, shortens cilia upon nutrient deprivation. An important result of our work is that glutamine is able to promote cilia retraction when it is replenished after cells exposure to nutrient deprivation. We found that both elongation and retraction of cilia occur at early time points (4-8 hours). Since the concentration of glutamine in commercial media is 10-fold higher than the physiological one reported to be present in the serum, we treated cells with increasing doses of glutamine from a physiological range of concentration (0.2-0.5 mM) to a supraphysiological one (2-5 mM). We found that the ciliary shortening is achieved with physiological concentrations of glutamine, suggesting that this effect could be physiologically relevant to drive the regulation of cellular responses to glutamine availability. This evidence is particularly relevant, since a physiological medium called Plasmax has been proposed to improve the metabolic fidelity of *in vitro* models of cancer by mimicking better than the commercial media the physiological metabolic environment to which cells are exposed (Vande Voorde *et al*, 2019). Nevertheless, further investigation about the molecular mechanism involved in the ciliary elongation and shortening process upon nutrient deprivation and glutamine replenishment is required. Indeed, identifying a transporter or receptor (GPCR) able to sense glutamine would better corroborate the finding that cilia sense nutrients, and in particular glutamine, not only for the intracellular responses generated by their utilization, but also for sensing of their presence in the extracellular compartment. Furthermore, since the processes of assembly and disassembly of cilia involve tiny regulated machineries, such as the intraflagellar

transport (IFT), revealing their role in our conditions could shed light on the molecular players underpinning our findings. Other processes that merit to be investigated are represented by post-translational modifications of ciliary microtubules. Indeed, it is possible that glutamine supplementation regulates the assembly and stability of the axoneme through glutamylation of ciliary tubulin (Yang *et al.*, 2021).

Cilia sense and respond to the energetic status of the cell induced by nutrient availability

The evidence that interfering with mitochondrial morphology and activity plays a role in regulating ciliary length has been already described in neurons (Bae *et al.*, 2019). Likewise, in our work we found that inhibition of mitochondrial respiratory chain complexes through oligomycin (complex V inhibitor) and antimycin A/rotenone (complex III and I inhibitors) promotes the elongation of primary cilia, suggesting that the disruption of mitochondrial respiration and consequent reduction of energy production are the drivers of the elongation of cilia observed upon nutrient deprivation. AMPK, which is a central regulator of energy homeostasis (Mihaylova & Shaw, 2011), is activated by an energetic imbalance that could be induced also by nutrient deprivation Upon nutrient deprivation, AMPK resulted to be activated, suggesting that it could be a molecular player involved in the process of ciliary elongation driven by nutrient deprivation. Furthermore, we show that allosteric activation of AMPK through AICAR elongates cilia without affecting the percentage of ciliated cells, suggesting that this effect is not due to an increased cell cycle exit. Thus, we conclude from these results that nutrient deprivation elongates cilia by inducing an energetic crisis involving the activation of AMPK. The other important finding revealing that primary cilia sense the energy status of the cell driven by different nutrient availability conditions is represented by the evidence that cilia-deficient (*Ift88* KO or inactivated) cells display decreased energy charges in terms of reduced triphosphate nucleotides to monophosphate nucleotide ratio. Their impaired energetic metabolism is showed by an altered fatty acid oxidation (FAO). LC-MS analysis revealed that upon 4 hours of nutrient deprivation, acylcarnitines derived from long chain fatty acids, such as palmitoylcarnitine and oleoylcarnitine, are decreased in *Ift88* KO cells compared to their relative controls upon nutrient deprivation. FAO is the catabolic process responsible for the degradation of fatty acids to produce acetyl-CoA to fuel the TCA cycle and, consequently, to drive ATP production (Houten

et al., 2016). A bottle-neck enzyme of FAO is carnitine palmitoyl transferase 1 (CPT1), which is responsible for the entry of acyl-CoA activated long chain fatty acid into mitochondria in the form of acylcarnitines, which are reconverted into carnitines and acyl-CoA by CPT2. In cilia-deficient cells the mRNA expression of the almost ubiquitous isoform expressed also in the kidney *Cpt1a* is significantly downregulated upon serum and nutrient deprivation, suggesting a possible impairment of FAO in cells lacking cilia. We confirmed these results *in vivo* in a mouse model (*Ift88*$^{flox/flox}$*;KspCre*) where *Ift88* is conditionally inactivated in the distal tubules and collecting ducts of the renal tubules. In the renal tissues of these mice at P35, when renal cystogenesis already occurred, we found decreased transcriptional expression of both *Cpt1a* and *Cpt2*. Overall, these findings show that cilia could display a crucial role in sensing the energy status of the cell to possibly orchestrate the cellular metabolic responses to restore the energy homeostasis imbalance due to nutrient deprivation. In this thesis, we propose that glutamine rescues ciliary length by restoring the mitochondrial respiration and, as a consequence, the energetic status of the cell. Indeed, glutamine, together with glucose, is one of the main sources of carbon for the cell and is reported to be preferentially used to drive mitochondrial respiration and, as a consequence, ATP production. This property of glutamine is due to its capability to be converted into glutamate to promote the anaplerosis of the TCA cycle intermediate α-ketoglutarate (α-KG) (DeBerardinis *et al.*, 2007; Yang *et al.*, 2014; Zhang *et al.*, 2017b). We found by LC-MS analysis that glutamine supplementation is able to rescue at least partially the levels of several metabolites involved in the TCA cycle, other than in glutaminolysis and asparagine synthesis, suggesting another time that glutamine is preferentially used to drive ATP production within mitochondria. In line with this, our data reveal that glutamine is able to rescue the ciliary elongation driven by nutrient deprivation by promoting ATP production through TCA cycle fuelling. Indeed, upon glutamine supplementation the ATP-production coupled respiration dramatically increases compared to both nutrient deprived and glucose supplemented conditions. While glucose supplementation drives acidification of the medium, glutamine does not compared to nutrient deprived medium, suggesting that glutamine-induced shortening of cilia is not due to pH acidification. Furthermore, although cilia-deficient cells do not display dramatic differences in both growth and mitochondrial respiration upon nutrient rich condition, we found that *Ift88* KO cells

display decreased mitochondrial respiration upon glutamine supplementation, suggesting that cilia favor glutamine utilization to fuel the TCA cycle, and therefore produce energy. Overall, we found that cilia sense the energetic status of the cell induced by nutrient deprivation through AMPK activation. Although shear stress sensing by cilia was already reported to activate AMPK by LKB1 (Boehlke *et al*, 2010; Miceli *et al*, 2020), which is localized at the centrosome-cilium complex, we found that AMPK activation could be also induced by the capability of cilia to sense nutrient availability. As a result, loss of cilia determines decreased energy charges and impaired FAO, revealing a decreased capability of cilia-deficient cells to respond to an energetic crisis by inducing energy ptoduction. Alternatively, we found that glutamine, which represents the preferential source to drive ATP production upon nutrient depletion, induces the shortening of cilia by restoring, at least partially, the energy homeostasis of the cell.

Cilia favor glutamine utilization via ASNS and independently of mTOR

In this work, we found that cilia facilitate glutamine usage to promote ATP production within mitochondria. Thus, we investigated for a molecular player driving this phenomenon. Since mTOR is described to be regulated by cilia and glutamine is reported to activate mTOR (Jewell *et al.*, 2015), we wondered whether mTOR could be a key molecular player in glutamine sensing by primary cilia. Indeed, in our condition glutamine drives the phosphorylation of S6 ribosomal protein (S6RP), a downstream target of mTOR involved in protein translation. However, the inhibition of mTOR through rapamycin does not abrogate the ciliary shortening induced by glutamine. Furthermore, supplementation with leucine, another aminoacid able to activate mTOR, induces the phosphorylation of S6RP without affecting ciliary length compared to the relative controls upon nutrient deprivation. Taken together, these findings reveal that glutamine shortens cilia independently of mTOR. Of note, metabolomics analyses by NMR and LC-MS revealed that a wide metabolic reprogramming occurs in cilia-deficient cells. In particular, decreased glutamine and glucose uptake, reflected by reduced glutamate and lactate production, are appreciable in *Ift88* KO cells, suggesting that cilia promote the utilization of the two main carbon sources for the cell. Interestingly, we found by LC-MS that, other than reduced glutamine levels, also total asparagine levels are reduced in *Ift88* inactivated cells, while aspartate levels are upregulated. $^{15}N_2$-labelled glutamine tracing upon nutrient deprivation revealed a reduction in the release of

glutamine-derived asparagine in cilia-deficient cells compared to the relative controls. Asparagine is an aminoacid involved in cell survival upon glutamine depletion and could be synthesized together with glutamate from glutamine and aspartate by asparagine synthetase (ASNS) (Lomelino *et al.*, 2017). This enzyme is upregulated upon aminoacid depletion or ER stress and is increased in *Pkd1* mutant cells, as previously reported by our group (Podrini *et al.*, 2018). Of note, we show that ASNS orchestrates the cilia-promoted glutamine usage into the TCA cycle. Indeed, we found that cilia-deficient cells display decreased *Asns* transcriptional expression, in line with the reduced levels of asparagine observed by LC-MS analysis. Furthermore, we appreciated that silencing of *Asns* elongates primary cilia as already reported in an unbiased siRNA screening aimed to identify ciliogenesis regulators (Wheway *et al.*, 2015). Besides this finding, we found that interfering with the expression of this enzyme drastically affects the response to glutamine in terms of ciliary shortening. In particular we observe that cells silenced for *Asns* (si*Asns*) upon glutamine supplementation are not able to shorten their cilia at the same extent of the controls and display an almost overlapping distribution of ciliary length compared to the one exposed to nutrient deprivation. In contrast, cilia of the scramble controls show completely different shapes of the distribution of cilia length with many short cilia upon glutamine supplementation compared to nutrient deprivation. Indeed, exposing cells transiently silenced for *Asns* and their relative controls to nutrient deprivation and glutamine supplementation shows that *Asns* silencing completely abrogates the ciliary shortening induced by glutamine. We found that ASNS mediates glutamine-driven shortening by promoting glutamine usage in mitochondrial respiration instead of asparagine synthesis. Indeed, in this work we show that asparagine is not responsible for the ciliary shortening induced by glutamine. Indeed, supplementation with both physiological (0.1 mM) and supraphysiological (1 mM) asparagine does not induce ciliary shortening at the same extent of glutamine. Consistently with this finding, asparagine degradation through asparaginase (ASNase) does not abrogate the ciliary shortening observed upon glutamine supplementation. Alternatively, we found that upon acute injection of glutamine si*Asns* MEF and mIMCD3 cells show decreased acute response in terms of mitochondrial respiration compared to scramble control cells. Collectively, these results provide evidence that cilia mediate glutamine utilization to fuel mitochondrial respiration through the capability of ASNS to produce glutamate instead

of asparagine. Of interest, we found that ASNS is localized at the centrosome-cilium complex, since subcellular fractionation assay (Ishikawa *et al.*, 2012; Kim *et al.*, 2014) on mIMCD3 revealed an enrichment of this enzyme in the cilia fraction enriched in IFT88 protein. The other approach that we used is the detection by immunofluorescence. Due to the aspecific signals given by antibodies for immunofluorescence detection of this enzyme, we coped with this technical issue by transfecting cells transiently with eGFP and mCherry-tagged ASNS. In these *in vitro* systems we appreciated an enrichment of the fluorescent protein at the base of the cilia. Using γ-tubulin as a marker of centrosomes, we found that ASNS signal colocalizes with it, suggesting that ASNS is present in the centrosome-cilium complex. However, further investigation about its enrichment at the base of cilia should be pursued. Indeed, it is possible that localization of ASNS at the centrosome-cilium complex is required to increase local production of glutamate, since form our data asparagine appeared not to be involved in the ASNS-driven glutamine utilization orchestrated by cilia. We could speculate that local production of glutamate could be involved in the glutamylation of the microtubules of the axoneme that is a process known to regulate microtubules assembly and stability. Alternatively, since we found that ASNS production of glutamate is facilitated by cilia to drive mitochondrial respiration, another reason for local production of glutamate at the base of cilia could be a more efficient way to fuel the TCA cycle in mitochondria near to the primary cilium. However, despite some studies described the regulation of the mitochondrial migration to sites where ATP levels are reduced (Lee *et al*, 2022), we should investigate whether upon nutrient deprivation and glutamine supplementation mitochondria display different localization in the cell, possibly driven by ASNS-produced glutamate.

Implications for disease

The results shown in this thesis shed light on the role of primary cilia in physiology, but also in pathology. Indeed, our proposal of cilia as sensors of nutrient availability and as regulators of cellular responses to metabolic requirements uncovers that cilia are not only involved in the regulation of systemic metabolism (since ciliopathies manifestations frequently include obesity and diabetes), but also display a crucial role in metabolism regulation at the cellular level. Previous findings of our group show that inactivation of polycystins causative of ADPKD leads to a wide metabolic reprogramming characterized by increased glycolysis, glutaminolysis, fatty acid synthesis, and decreased FAO and

oxidative phosphorylation (OXPHOS) at the cellular level. Of note, our results suggest that disruption of cilia drive an energetic metabolism impairment opposite to the one observed in ADPKD. Indeed, while *Pkd1* mutants are characterized by enhanced glycolysis and glutaminolysis (Podrini *et al.*, 2018), *Ift88* inactivated cells display decreased levels in the key metabolites involved in these metabolic pathways, suggesting another time opposite metabolic behaviour between *Ift88* and *Pkd1* mutant cells (Podrini et al., 2018). Although these results appear to be counterintuitive, since both polycystins and IFT proteins disruption leads to renal cystogenesis, they are in line with the hypothesis of the presence of the cilia-dependent cyst activation pathway (CDCA). Indeed, this still uncovered pathway has been proposed to be procystogenic, limited to cilia, and normally repressed by polycystins (Ma *et al.*, 2013). Since cilia disruption concomitantly to polycystins inactivation ameliorates the ADPKD phenotype, it is plausible that the loss of cilia promotes opposite effects that at least partially rescue or slower PKD altered pathways. Of note, we found that *Asns* expression is slightly, but significantly, downregulated in cilia-deficient cells and that both total levels of asparagine and release of $^{15}N_2$-glutamine-derived asparagine are decreased in *Ift88* inactivated cells. By contrast, *Pkd1* mutant cells display increased asparagine levels due to increased *Asns* expression. Thus, the finding that cilia facilitate glutamine utilization through the activity of ASNS is in line with the amelioration of ADPKD phenotype due to loss of cilia. Indeed, since the disruption of cilia impaires ASNS activity, leading to decreased synthesis of aparagine and reduced mitochondrial respiration, this would counterbalance the abnormally upregulated ASNS activity found by our group in *Pkd1* mutants (Podrini et al., 2018). This is in line with previous findings of our group that show that silencing of *Asns* impaires cell survival in *Pkd1* mutants *in vitro*. From the other side, we appreciated that FAO is impaired in cilia-deficient cells, as in ADPKD. This suggests that possibly cilia display a dualistic role in by positively or negatively regulating renal cystogenesis. From this point of view, we could classify ciliary pro-cystogenic pathways (positively/negatively regulated by both polycystins and cilia) and ciliary anti-cystogenic pathways (oppositively regulated by polycystins and cilia). Among the ciliary pro-cystogenic pathways, we could include FAO, which is downregulated by both ciliary loss and polycystins inactivation. Alternatively, among the ciliary anti-cystogenic pathways

(CDCA-related), we could include glutaminolysis via ASNS, which is downregulated by loss of cilia and upregulated by polycystins inactivation (**Fig. 4.2**).

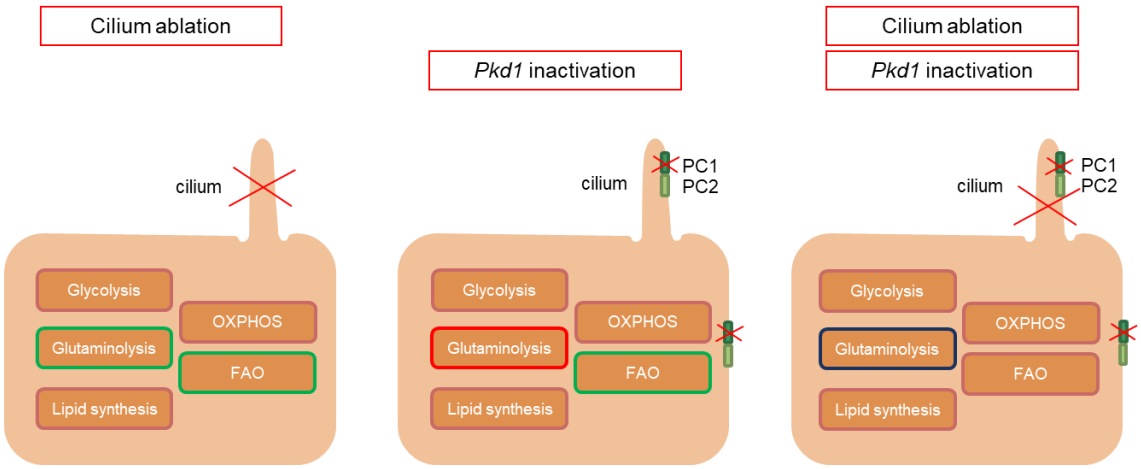

Figure 4.2 Proposed model of ciliary pro-cystogenic and anti-cystogenic pathways. *Schematic representation of the proposed model by which primary cilia regulate pro-cystogenic (FAO) and anti-cystogenic pathways (glutaminolysis). Green boxes: downregulated pathways. Red boxes: upregulated pathways. Blue box: putative CDCA pathway. FAO: fatty acid oxidation; OXPHOS: oxidative phosphorylation.*

Other than in ADPKD and renal diseases, cilia are reported to play a role in cancer, where these organelles appear to upregulate or downregulate proliferation depending on the context (Wong *et al*, 2009). Cancer is characterized by upregulated glutaminolysis as PKD. Thus, since we found that cilia sense and respond to glutamine via ASNS, we can propose that a ciliary gain-of-function could be observed in the afore-mentioned diseases. By contrast, a ciliary loss-of-function could be found in diseases characterized by decreased glutamine uptake and utilization. Another relevant finding of this work is that ASNS localizes at the centrosome-cilium complex and that its activity is downregulated by ciliary disruption. The evidence that ASNS deficiency is a disorder characterized by microcephaly and intellectual disability (Lomelino *et al.*, 2017; Ruzzo *et al*, 2013), features shared by ciliopathies, raises the hypothesis that diseases characterized by downregulation of ASNS could be classified as ciliopathies.

Concluding remarks

In conclusion, in this thesis we propose a novel role of cilia as sensors of nutrient availability that favour glutamine usage through ASNS to restore, at least in part, the energetic status of the cell. Despite a lack of a precise mechanism by which cilia properly sense nutrients and in particular glutamine, our findings could give insight in the function of primary cilia in the regulation of cellular responses to metabolic requests. Indeed, although cilia were already known to mediate the regulation of systemic metabolism ata the body level (proofed by the evidence that obesity and diabetes are recurrent features of ciliopathies), the function of cilia in cellular metabolism was still uncovered. In this work, we uncover a new role of cilia as regulators of cellular metabolism by revealing that cilia are sensors of nutrients availability and favor glutamine utilization at the cellular level.

5. MATERIALS AND METHODS

5.1 Cell lines and conditioning media

Mouse Embryonic Fibroblasts (MEFs) used are described in (Distefano *et al*, 2009). Madin-Darby Canine Kidney type II (MDCK) cells are described in (Boletta *et al*, 2000). Murine Inner Medullary Collecting Duct (mIMCD3) cells were kindly provided by Dr. Miriam Schmidts (Freiburg University, Freiburg, Germany). Human Retinal Pigment Epithelial (hRPE) cells were kindly provided by Dr. Nicoletta Landsberger (San Raffaele Scientific Institute, Milan, Italy). *Ift88* KO MEFs (MEF^{Ift88}) and mIMCD3 ($mIMCD^{Ift88}$) were generated by CRISPR/Cas9 technology (see below). MEFs were stably transduced with ARL13B-GFP plasmid (Larkins *et al*, 2011) (Addgene, #40879) using lentiviral vectors. MEFs and MDCK cell lines were grown in 37°C, 5% CO_2 incubators, in high glucose DMEM medium (Thermo Fisher Scientific, #41965062). mIMCD3 cells were cultured in DMEM/F12 medium with GlutaMAX (Thermo Fisher Scientific, #31331093), supplemented with 10% FBS, 1% Penicillin-Streptomycin (PenStrep) (Thermo Fisher Scientific, #15070-063) and 1% Sodium Pyruvate (Thermo Fisher Scientific, #11360-039) or DMEM/F12 medium without L-Glutamine (Thermo Fisher Scientific, #21331046) supplemented with 2.5 mM L-Glutamine (Thermo Fisher Scientific, #25030-024), 10% FBS, 1% PenStrep. hRPE cells were cultured in DMEM/F12 medium without L-Glutamine (Thermo Fisher Scientific, #21331046) supplemented with 10% FBS, 1% PenStrep. mNeonGreen-ASNS stable mIMCD3 cells were cultured in high glucose, pyruvate DMEM medium (Thermo Fisher Scientific**,** #41966029) and Ham's F-12 Nutrient Mix (Thermo Fisher Scientific, #21765029) (1:1), supplemented with 10% FBS, 400 µg/ml Hygromycin (Sigma-Aldrich, #H0654), and 1% Sodium Pyruvate.

5.2 CRISPR/Cas9 generation of *Ift88* KO MEFs and mIMCD3

To generate *Ift88* KO MEFs (MEF^{Ift88}), U6gRNA-Cas9-2A-GFP plasmids (Sigma-Aldrich) carrying three distinct custom-designed gRNA sequences targeting exons 5, 11 and 14 were used (gRNA#1: GATCTGATCTAAGGCCATTCGG; gRNA#2: CAAAAGACGCTTCGATCACAGG; gRNA#3: CAATGGGAAGACCGATGACAGG). For mIMCD3 cells the most efficient guide (gRNA#1) was employed. Cells were plated on 150 mm^2 plates the day before the transfection. Transfection was performed using Lipofectamine 3000 (Thermo Fisher Scientific, #L3000015) following the manufacturer's instructions. 5 µg of plasmid DNA

per dish with 1:3 DNA/Lipofectamine ratio were used. The CMV-Cas9-2A-RFP scrambled gRNA was used as a control. Three days after transfection cells were sorted by FACS for GFP (potential MEF^{Ift88} or mIMCD^{Ift88}) or RFP (control MEFs or mIMCD3) and plated as single cells into 96-wells plates. The vital clones were sequentially expanded and screened for the absence of the protein by western blot. Immunofluorescence staining for ARL13B confirmed the absence of cilia in *Ift88* KO MEFs or mIMCD3. 10 out of 18 vital clones *Ift88* KO were established for MEFs, and 5 *Ift88* KO out of 11 vital clones were generated for mIMCD3 cells. Clones were kept in culture separately. To perform the experiments fresh pools of three different clones for both *Ift88* control and KO cells (MEFs and mIMCD3) were used. Each pool was prepared with an equal proportion (1:3) of each single clone (out of three). For *Ift88* KO MEFs pools each clone was generated by each of the three different guides. For mIMCD3 cells that are more subject to clonality problems most experiments were also conducted with individual clones (not shown in the manuscript).

5.3 *In vitro* treatments

To induce ciliogenesis, cells were starved from serum for 24 hours. To induce nutrients deprivation, cells were treated with HBSS (Thermo Fisher Scientific, #14025-050) for 24 hours. To analyse primary cilium response to nutrients, HBSS was supplemented with 0.2, 0.5, 1, 2, 4 mM L-Glutamine (Thermo Fisher Scientific, #25030-024), 20 mM D-(+)-Glucose (Sigma-Aldrich, #G7021), 0.5 or 5 mM L-Leucine (Sigma-Aldrich, #L8000), or 0.1 or 1 mM L-Asparagine (Sigma-Aldrich, #A4159). For AICAR treatment, complete medium was supplemented with 1 mM AICAR (Sigma-Aldrich, #A9978) or DMSO (Sigma-Aldrich, #D2650) either for 24 hours (for immunofluorescence) or 4 hours (for western blot analysis). For Metformin treatment, complete medium was supplemented with 2 mM Metformin (Sigma-Aldrich, #317240) for 4 hours (for western blot analysis). For mitochondrial respiratory chain complexes inhibition, cells were treated with 1 µM oligomycin (Agilent Technologies) and 0.5 µM antimycin A/rotenone (Agilent Technologies) for 24 hours. For rapamycin treatment, cells were treated with 100 nM rapamycin (LC Laboratories, #R-5000) for 24 hours. For asparaginase treatment, cells were treated with 5 U/mL asparaginase (Sigma-Aldrich, #A3809) for 24 hours.

5.4 Antibodies and Inhibitors

For immunofluorescence analysis the following antibodies were used: rabbit ARL13B (Proteintech, #17711-1-AP; 1:250), mouse Acetylated alpha-Tubulin (Sigma-Aldrich, #T6793; 1:1000), rabbit Pericentrin (Covance, #PRB-432C; 1:750); mouse γ-tubulin (Sigma-Aldrich, #T6557; 1:5000). Fluorochrome-conjugated secondary antibodies were the following: goat anti-rabbit AlexaFluor 488 (Thermo Fisher Scientific, #A-21441; 1:1000), goat anti-mouse AlexaFluor 546 (Thermo Fisher Scientific, #A-11003; 1:1000); chicken anti-mouse AlexaFluor 594 (Thermo Fisher Scientific, #A-21201; 1:1000), and goat anti-rabbit Alexa Fluor 647 (Thermo Fisher Scientific, #A-21244; 1:1000). For nuclear staining we used DAPI (Santa Cruz Biotechnology, #sc-3598; 1:5000 or 1:10000). For Dolichos Biflorus Agglutinin positive (DBA-positive) renal epithelial cells staining DBA Rhodamine (Vector Laboratories, # RL-1032-2; 1:100) was used. For western blot analysis the following antibodies were used: p-AMPK (Thr172) (Cell Signalling Technology, 2535S; 1:1000), AMPK (Cell Signalling Technology, #2532; 1:1000), ASNS (abcam, #ab111873), p-S6RP (s235/236) (Cell Signalling Technology, #2211s; 1:1000), S6RP (Cell Signalling Technology, #2217; 1:1000), Hamartin/TSC1 (Cell Signalling Technology, #4906; 1:1000), IFT88 (Proteintech, #13967-1-AP; 1:1000), Acetylated alpha-Tubulin (Sigma-Aldrich, #T6793; 1:750). For housekeeping protein expression Vinculin V284 antibody (Millipore, #05-386; 1:15000) was used. HRP-conjugated secondary antibodies were from GE Healthcare: anti-rabbit IgG HRP linked (#934V), anti-mouse IgG HRP linked (#NA9310V), and anti-rat IgG HRP linked (#NA935V).

5.5 Immunofluorescence on cells

For immunofluorescence (IF) analysis, cells were plated on glass coverslips. Coating of coverslips with Fibronectin (Sigma-Aldrich, #11051407001; 1 μg/mL in PBS) was performed befor plating mIMCD3 and MDCK cell lines. Cells were fixed for 10 min in cold Methanol or 4% Paraformaldehyde (PFA) (Electron Microscopy Sciences, #157-4) followed by permeabilization in 0.1% Triton X-100 (Sigma-Aldrich, #T8787) in PBS. Blocking in 3% BSA (Sigma-Aldrich, #A7906) in PBS was performed for 1 hour at Room Temperature (RT) and incubation with primary antibody diluted in 3% BSA in PBS was carried out for 1 hour at RT or overnight at 4°C. Then incubation with secondary antibody

diluted in 3% BSA in PBS was performed for 1 hour at RT and nuclei were stained with DAPI or with Hoechst 33342 (Thermo Fisher Scientific, # H3570) for live imaging analysis. Glasses were then mounted with Fluorescence Mounting medium (Dako, #S3023). Images were obtained using Zeiss Axio Observer.Z1, GE Healthcare DeltaVision Ultra, and Olympus FluoVIEW 3000 RS microscopes. Quantification of both ciliary length and ciliated cells frequency was performed manually using FIJI (FIJI Is Just ImageJ) software.

5.6 Western blot analysis

For western blot analysis, as already described by out group in (Nigro *et al*, 2019), a lysis buffer solution of 150 mM NaCl (Sigma-Aldrich, #s9625), 20 mM Na_2HPO_4 (BDH, #10494L)/NaH_2PO_4 (BDH, #102455S), 10% Glycerol (Sigma-Aldrich, #G7757), 1% Triton X-100 (pH 7.2), complete protease inhibitor cocktail (Roche, #11836145001) and phosphatase inhibitors [1 mM final concentration of glycerophosphate (Sigma-Aldrich, #G9891), sodium orthovanadate (Sigma-Aldrich, #S6508), and sodium fluoride (Sigma-Aldrich, #S6521)] was used to lyse cells or kidneys. Quantification of total lysates was performed using Biorad Protein Assay Dye reagent (Bio-Rad Laboratories, #500-0006) and Laemmli buffer at a final concentration 2x was added to the samples. Tris-Glycine gradient gels (Life Technologies, #NP0335BOX) were used to resolve proteins, which were transferred onto Immobilon-P polyvinylidene fluoride (PVDF) membranes (Millipore, #IPVH00010). Blocking of membranes was performed with 5% milk in Tris-buffered saline, Tween 20 (Sigma-Aldrich, #P1379) (TBS-T). Primary antibodies were diluted in 3% BSA in TBS-T. HRP-conjugated secondary antibodies were diluted 1:10000 in 5% milk in TBS-T and detection was made with ECL (GE Healthcare, #RPN2106) alone or supplied with 10% SuperSignal West Femto (Thermo Fisher Scientific, #34095) when necessary.

5.7 Real-Time PCR analysis

RNAspin Mini kit (GE Healthcare, #25-0500-72) was used to isolate total RNA from cells or kidneys. Reverse transcription of extracted RNA using $Oligo(dT)_{15}$ primers (Promega, #C1101) or Random Primers (Promega, #C1181) and ImProm-II Reverse Transcriptase (Promega, #A3802) was used to obtain cDNA. Quantitative Real Time PCR

analysis was performed on technical duplicates using iTaq Univer SYBR Green (Bio-Rad Laboratories, #1725125) on CFX96 Touch Real-Time PCR Detection System (Bio-Rad Laboratories). Primer sequences for qRT-PCR are reported below:

mHprt fw 5'-TTATGTCCCCCGTTGACTGA-3'
mHprt rev 5'-ACATTGTGGCCCTCTGTGTG-3'
mAsns fw 5'-GGTTTTCTCGATGCCTCCTT-3'
mAsns rev 5'-TGTGGCTCTGTTACAATGGTG-3'
mCpt1a fw 5'-GGTCTTCTCGGGTCGAAAGC-3'
mCpt1a rev 5'-TCCTCCCACCAGTCACTCAC-3'
mCpt1a fw 5'- AGTGGCCTCACAGACTCCAG-3'
mCpt1a rev 5'-GCCCATGTTGTACAGCTTCC-3'
mCpt2 fw 5'-CAATGAGGAAACCCTGAGGA-3'
mCpt2 rev 5'-GATCCTTCATCGGGAAGTCA-3'

5.8 *Asns* transient knockdown

For transient *Asns* gene silencing in mIMCD3 cells 20 nM *Asns* siRNA (Thermo Fisher Scientific, #AM16704/188316) and scramble (Scr) siNegative n. 1 (Thermo Fisher Scientific, #AM4611) or n. 2 (Thermo Fisher Scientific, #AM4613) for controls were used following manufacturer's instructions. As previously described in (Podrini *et al.*, 2018), the transfections were performed two times over 2 days using Lipofectamine 3000 or Lipofectamine RNAiMAX Transfection Reagent (Thermo Fisher Scientific, #13778150) following the manufacturer's protocol. After transfections, cells were plated for total RNA extraction, protein extraction, IF, and Seahorse analysis.

5.9 eGFP-ASNS and mCherry-ASNS transient transfection

The plasmids for expression of ASNS (p-ASNS) and N-terminally tagged eGFP-ASNS (p-eGFP-ASNS) and mCherry-ASNS (p-mCherry-ASNS) recombinant proteins were generated by Genscript Biotech Corp. For transient transfection of p-eGFP-ASNS and p-mCherry-ASNS, mIMCD3 cells were plated in 12-wells plates. Transfection was performed using Lipofectamine 3000 (Thermo Fisher Scientific, #L3000015) following the manufacturer's instructions. 1 μg of plasmid DNA per well with 1:2 DNA/Lipofectamine ratio were used. After transfections, cells were used for IF staining.

5.10 Seahorse Metabolic Flux Analysis

The Mito Stress Test (Agilent Technologies) was performed by seeding 20,000 cells/well in a 96-wells Seahorse cell culture microplates and incubating them in a 5% CO_2 incubator at 37°C overnight, as already described by our group in (Cassina *et al*, 2020). Then, culture medium was changed with pH-adjusted (pH = 7.4 ± 0.1) with 2 mM HEPES bicarbonate-free HBSS, and pH-adjusted with 2mM HEPES HBSS supplemented either with 20 mM D-(+)-Glucose or 4 mM L-Glutamine for 4, 16, and 24 hours. The plate was incubated at 37°C for 1 hour in a non-CO_2 incubator before starting the assay. Oxygen Consumption Rate (OCR) was measured using the Seahorse XF Mito Stress Test Kit (Agilent Technologies, #103015-100) on an XFe96 Analyzer (Agilent Technologies) following the manufacturer's instructions. Briefly, cells were sequentially injected with 1 µM oligomycin, 1.5 µM FCCP, 0.5 µM antimycin A/rotenone. For measuring OCR in response to acute injection of nutrients, Mito Stress Test was performed on cells treated for 4 hours in pH-adjusted with 2mM HEPES HBSS and acutely injected with 20 mM D-(+)-Glucose or 4 mM L-Glutamine. For measuring OCR of *Ift88* control and KO MEFs and mIMCD3 in nutrient-rich condition cells either with or without FBS cells were cultured for 24 hours in DMEM or DMEM/F12 ± 10% FBS. Then, culture medium was changed with Seahorse XF DMEM medium (Agilent Technologies, #103575-100) and the plate was incubated at 37°C for 1 hour in a non-CO_2 incubator before starting the assay. Cell numbers were normalized using CyQuant Cell Proliferation Assay (Thermo Fisher Scientific, #C35011). All the analyses were performed with the Agilent Seahorse Wave software (Agilent Technologies).

5.11 Cilia Enrichment

Cells were seeded on 150 mm^2 dish at 90% confluence. Cells were starved for 24 hours or 48 hours in DMEM/F12 with GlutaMAX supplemented with 0% FBS and 1% PenStrep. After 10 min incubation in PBS supplemented with 1 mM of EDTA cells were scraped, centrifuged at 200 x g for 5 minutes, and washed with HBS [25 nM HEPES, 137 mM NaCl, 5 mM KCl, 0.7 mM Na_2HPO_4 2 H_2O, 6 mM D-(+)-Glucose pH 7.05]. Pellet was resuspended in 1 mL of Deciliation solution [20 mM HEPES pH 7, 112 mM NaCl, 3.4 mM KCl, 10 mM $CaCl_2$, 2.4 mM $NaHCO_3$, 20% ethanol] with 10 µg/mL cytochalasin D and 1% protease inhibitor cocktail for 15 minutes at 4°C rotating. After a centrifugation

at 1000 x g for 5 minutes at 4°C, sequential centrifugations for 30 minutes at 4°C were performed. The first centrifugation was performed at 2000 x g to collect the first cytoplasmic fraction. The second centrifugation was performed at 10000 x g to collect the second organelles fraction. The third centrifugation was performed at 16000 x g to collect the third cilia enriched fraction. This protocol has been adapted from (Ishikawa *et al.*, 2012; Kim *et al.*, 2014).

5.12 NMR exometabolome analysis

Ift88 control and KO MEFs were seeded in 100 mm^2 plates in complete medium. Then, the culture medium was replaced overnight with high glucose DMEM medium supplemented with 0.5% FBS and 1% PenStrep. The day after, the culture medium was replaced with high glucose DMEM medium supplemented with 0% FBS and 1% PenStrep for 24 hours. A blank control with non-conditioned medium was used to calculate the metabolites relative quantification and consumption. For NMR analysis of the extracellular medium, 530 µl of cell culture medium were mixed with 60 µl of deuterated sodium phosphate (Na_3PO_4) solution containing 4,4-dimethyl-4-silapentane-1-sulfonic acid (DSS), as a chemical shift reference for proton dimension, and 10 µl of 1.2% NaN_3 water solution. The final sample volume was 600 µl and contained 50 mM sodium phosphate (Na_3PO_4), 0.02% NaN_3 and 50 µM DSS. NMR spectra were recorded at 298 K on a Bruker Avance 600 Ultra Shield TM Plus 600 MHz spectrometer equipped with triple resonance cryoprobe (TCI), pulsed field gradients and refrigerated autosampler (SampleJet). Samples were stored at 4°C until data collection. 1D ^{1}H NMR spectra (noesypr1d) were recorded with an acquisition time of 3s, 128 transients and a relaxation delay of 6s. Spectral window was set to 14 ppm. 1D ^{1}H NMR spectra were typically processed with zero filling to 128k points, and apodized with an unshifted Gaussian and a 1 Hz line broadening exponential using Mnova 14.1 (MestreLab Research S.L, Santiago de Compostela). Metabolites were identified and quantified using Chenomx NMR Suite 8.6 (Chenomx, Alberta, Canada). Relative quantification (Rel.Quant.) was calculated using the following equation:

$$Rel.\,Quant. = \frac{[Meta]x - [Meta]mo}{[Meta]mo}$$

Where [Meta]x represents the concentration of metabolites in the medium conditioned by *Ift88* control and KO MEFs; [Meta]mo represents the concentration of metabolites in the non-conditioned medium. Negative values corresponded to metabolites up-taken from the medium, whereas positive values corresponded to metabolites released in the medium.

Metabolite concentration, expressed in mM, was normalized for the total number of cells. The reported concentration of the metabolites is expressed as nM/number of cells.

Glucose or glutamine consumption was calculated using the following equation:

$$Consumption = \frac{[Meta]mo - [Meta]x}{finalnumberofcells}$$

where [Meta]x is the concentration of glucose or glutamine in the medium conditioned by *Ift88* control and KO MEFs, [Meta]mo represents the concentration of metabolites in the non-conditioned medium.

Principal component analysis (PCA) was performed using the 25 identified and quantified metabolites in the exometabolome samples.
Raw data of NMR exometabolome analysis are reported in Table 3.1.

5.13 Targeted metabolomic analysis in *Ift88* KO MEFs

For unlabelled targeted metabolomics *Ift88* control and KO MEF cells were plated in quintuplicate. Cell were exposed to either HBSS or HBSS supplemented with 4 mM Glutamine for 24 hours. Cell pellets were extracted with 1 mL extraction solution, i.e. Methanol for highly pure liquid chromatography (Sigma-Aldrich): acetonitrile gradient grade for liquid chromatography (Merck): ultrapure water (Sigma-Aldrich), 50:30:20 with 100 ng ml−1 of HEPES (Sigma-Aldrich) per million cells. Extracellular metabolites were extracted with 750 µl of extraction solution to 50 µl cell culture medium (spinned). Samples were incubated at 4°C for 15 minutes, centrigued at 13000 r.p.m, and the supernatant transferred into autosampler vials was stored at −80 °C. Separation of metabolites by LC-MS chromatography was performed using a Millipore Sequant ZIC-pHILIC analytical column (5 µm, 2.1 × 150 mm) equipped with a 2.1 × 20 mm guard column (both 5 mm particle size) and a binary solvent system. Solvent A was: 20 mM ammonium carbonate, and 0.05% ammonium hydroxide; Solvent B was acetonitrile. The

column oven was kept at 40°C and the autosampler tray at 4°C. The gradient for chromatographic separation run at a flow rate of 0.200 mL/min: 0–2 min: 80% B; 2-17 min: linear gradient from 80% B to 20% B; 17-17.1 min: linear gradient from 20% B to 80% B; 17.1-22.5 min: hold at 80% B. Next, samples were randomized and analysed by LC–MS injecting a volume of 5 µl. An equal mixture of all individual samples was used to generate pooled samples next analysed interspersed at regular intervals within sample sequence as a quality control. Metabolites were measured using a Thermo Scientific Q Exactive Hybrid Quadrupole-Orbitrap Mass spectrometer (HRMS) that was coupled to a Dionex Ultimate 3000 UHPLC. The full-scan, polarity-switching modewas used to opearate the mass spectrometer, using the spray voltage set to +4.5 kV/-3.5 kV. Furthremore, the heated capillary was held at 320°C, while the auxiliary gas heater at 280°C. The sheath gas flow was set to 35 units, the auxiliary gas flow to 10 units, and the sweep gas flow was set to 0 unit. HRMS data acquisition was performed in a range of m/z = 70–900, with the resolution set at 70,000, the AGC target at 1 × 106, and the maximum injection time (Max IT) at 120 ms. The identities of the metabolites was confirmed as follows: (1) using precursor ion m/z was matched within 5 ppm of theoretical mass predicted by the chemical formula; (2) using a retention time of metabolites within 5% of the retention time of a purified standard thatb was run in identical chromatographic conditions. The review of the chromatogram and that of the peak area integration were performed using the Thermo Fisher software Tracefinder 5.0. The area of the peak for each detected metabolite was normalized using the total ion count (TIC) of the same sample to correct for any variations that had been introduced by sample handling and instrument analysis. All the normalized areas were used as variables for further statistical data analysis. For glutamine tracing experiments, Ift88 control and KO MEFs were cultured in HBSS supplemented with 4 mM $^{15}N_2$-Glutamine (Cambridge Isotope Laboratories) for 4 hours or 24 hours. Cells were seeded in parallel plates and protein content was determined by the Bradford method at 0 and 24 hours post medium change. The extraction of intracellular and extracellular metabolites was carried out in the same way as the un-labelled metabolomics. The theoretical masses of ^{15}N-isotopologues for each metabolite were calculated and added to a library of predicted isotopologues. These masses were then searched within a 5 ppm tolerance and integrated only if the peak showed less than 1% difference in retention time from the [U-14N] monoisotopic mass

in the same chromatogram. Natural isotope abundances were corrected using the AccuCor algorithm (https://github.com/lparsons/accucor). Percentage of intracellular pool from each isotopologue was calculated respective of the control (for each metabolite).

$$\overline{m}_x log_2 \overline{m}_{HBSS+Q} < \overline{m}_{HBSS} log_2 \overline{m}_{HBSS+Q} > \overline{m}_{HBSS}$$

5.14 Metabolite Analysis

We applied fold-change and *t*-test analysis in order to identify dysregulated metabolites in the different conditions. For each *p*-value resulting from *t*-test, a False Discovery Rate (*FDR*) has been computed by applying the Benjamini and Hochberg procedure as in (Podrini *et al.*, 2018). Then, only metabolites having *FDR* < 0.05 have been considered as statistically significant deregulated. Heatmaps have been created by applying the Matlab (Sobie, 2011) heatmap function with colormap represented in logarithmic scale. Volcano plots have been obtained by a homemade Matlab function.

5.15 Metabolite Set Enrichment Analysis

Over Representation Analysis has been employed, by using MetaboAnalyst 5.0 (Chong *et al*, 2019), to identify pathways that are significantly enriched in KEGG database (Kanehisa & Goto, 2000) starting from an input list of metabolites. We applied the hyper-geometric test to compute a statistical significance (*p-value*) for each pathway having at least three compounds captured in the input list. Hyper-geometric test scores have been computed based on cumulative binominal distribution, while *FDR* have been obtained by applying the Benjamini and Hochberg procedure.

5.16 *Ift88;KspCre* Murine Model

For the genetic ablation of *Ift88* in the kidney, *Ift88*$^{flox/flox}$ mice (purchased from Jackson Laboratory) and KspCre mice (kindly provided by Dr. Peter Igarashi, University of Minnesota, Minneapolis, USA) were inter-crossed to generate *Ift88*$^{flox/flox}$:*KspCre* experimental mice in a pure C57BL/6N genetic background. As controls, intra-litter *Ift88*$^{flox/flox}$ were used.

5.17 Hematoxylin and eosin staining

Kidneys of *Ift88*$^{flox/flox}$*;KspCre* and relative controls (*Ift88*$^{flox/flox}$) were collected at P35 and washed in PBS. 4% paraformaldehyde (Sigma-Aldrich, #P6148) was used to fix the samples. Incubation in 70% of ethanol (Sigma-Aldrich, St. Louis, MO, US) was performed. Samples underwent passages in ethanol ascending scale up to 100% and were then embedded in paraffin blocks. Formalin-fixed paraffin-embedded consecutive sections (4 mm) were dewaxed and hydrate through graded decrease alcohol series and stained for histology. For histological analysis in bright-field microscopy, standard protocols for Hematoxylin and Eosin using Mayer's Hematoxylin (BioOptica, #05-06002/L) and Eosin (BioOptica, #05-10002/L) were applied.For bright-field imaging, Zeiss Axio Imager M2m was employed.

5.18 Statistical analysis

Student's t-test or one-way ANOVA analysis of variance were used to establish differences between averages, as indicated in the figure legends; Tukey's or Bonferroni's post-test were employed for multiple comparisons.

6. REFERENCES

Abdelhamed ZA, Natarajan S, Wheway G, Inglehearn CF, Toomes C, Johnson CA, Jagger DJ (2015) The Meckel-Gruber syndrome protein TMEM67 controls basal body positioning and epithelial branching morphogenesis in mice via the non-canonical Wnt pathway. *Dis Model Mech* 8: 527-541

Alkan HF, Walter KE, Luengo A, Madreiter-Sokolowski CT, Stryeck S, Lau AN, Al-Zoughbi W, Lewis CA, Thomas CJ, Hoefler G *et al* (2018) Cytosolic Aspartate Availability Determines Cell Survival When Glutamine Is Limiting. *Cell Metab* 28: 706-720 e706

Alvarez-Satta M, Lago-Docampo M, Bea-Mascato B, Solarat C, Castro-Sanchez S, Christensen ST, Valverde D (2021) ALMS1 Regulates TGF-beta Signaling and Morphology of Primary Cilia. *Front Cell Dev Biol* 9: 623829

Anvarian Z, Mykytyn K, Mukhopadhyay S, Pedersen LB, Christensen ST (2019) Cellular signalling by primary cilia in development, organ function and disease. *Nat Rev Nephrol* 15: 199-219

Arnaiz O, Cohen J, Tassin AM, Koll F (2014) Remodeling Cildb, a popular database for cilia and links for ciliopathies. *Cilia* 3: 9

Arora K, Lund JR, Naren NA, Zingarelli B, Naren AP (2020) AC6 regulates the microtubule-depolymerizing kinesin KIF19A to control ciliary length in mammals. *J Biol Chem* 295: 14250-14259

Arrighi N, Lypovetska K, Moratal C, Giorgetti-Peraldi S, Dechesne CA, Dani C, Peraldi P (2017) The primary cilium is necessary for the differentiation and the maintenance of human adipose progenitors into myofibroblasts. *Sci Rep* 7: 15248

Asante D, Stevenson NL, Stephens DJ (2014) Subunit composition of the human cytoplasmic dynein-2 complex. *J Cell Sci* 127: 4774-4787

Ascenzi MG, Blanco C, Drayer I, Kim H, Wilson R, Retting KN, Lyons KM, Mohler G (2011) Effect of localization, length and orientation of chondrocytic primary cilium on murine growth plate organization. *J Theor Biol* 285: 147-155

Awan A, Oliveri RS, Jensen PL, Christensen ST, Andersen CY (2010) Immunoflourescence and mRNA analysis of human embryonic stem cells (hESCs) grown under feeder-free conditions. *Methods Mol Biol* 584: 195-210

Awata J, Takada S, Standley C, Lechtreck KF, Bellve KD, Pazour GJ, Fogarty KE, Witman GB (2014) NPHP4 controls ciliary trafficking of membrane proteins and large soluble proteins at the transition zone. *J Cell Sci* 127: 4714-4727

Badgandi HB, Hwang SH, Shimada IS, Loriot E, Mukhopadhyay S (2017) Tubby family proteins are adapters for ciliary trafficking of integral membrane proteins. *J Cell Biol* 216: 743-760

Bae JE, Kang GM, Min SH, Jo DS, Jung YK, Kim K, Kim MS, Cho DH (2019) Primary cilia mediate mitochondrial stress responses to promote dopamine neuron survival in a Parkinson's disease model. *Cell Death Dis* 10: 952

Bakkebo M, Huse K, Hilden VI, Forfang L, Myklebust JH, Smeland EB, Oksvold MP (2012) SARA is dispensable for functional TGF-beta signaling. *FEBS Lett* 586: 3367-3372

Balogh P, Katz S, Kiss AL (2013) The role of endocytic pathways in TGF-beta signaling. *Pathol Oncol Res* 19: 141-148

Bangs F, Anderson KV (2017) Primary Cilia and Mammalian Hedgehog Signaling. *Cold Spring Harb Perspect Biol* 9

Barisic I, Boban L, Loane M, Garne E, Wellesley D, Calzolari E, Dolk H, Addor MC, Bergman JE, Braz P *et al* (2015) Meckel-Gruber Syndrome: a population-based study on prevalence, prenatal diagnosis, clinical features, and survival in Europe. *Eur J Hum Genet* 23: 746-752

Barnes BG (1961) Ciliated secretory cells in the pars distalis of the mouse hypophysis. *J Ultrastruct Res* 5: 453-467

Bashford AL, Subramanian V (2019) Mice with a conditional deletion of Talpid3 (KIAA0586) - a model for Joubert syndrome. *J Pathol* 248: 396-408

Berbari NF, Pasek RC, Malarkey EB, Yazdi SM, McNair AD, Lewis WR, Nagy TR, Kesterson RA, Yoder BK (2013) Leptin resistance is a secondary consequence of the obesity in ciliopathy mutant mice. *Proc Natl Acad Sci U S A* 110: 7796-7801

Bergmann C (2015) ARPKD and early manifestations of ADPKD: the original polycystic kidney disease and phenocopies. *Pediatr Nephrol* 30: 15-30

Bergmann C, Guay-Woodford LM, Harris PC, Horie S, Peters DJM, Torres VE (2018) Polycystic kidney disease. *Nat Rev Dis Primers* 4: 50

Bishop GA, Berbari NF, Lewis J, Mykytyn K (2007) Type III adenylyl cyclase localizes to primary cilia throughout the adult mouse brain. *J Comp Neurol* 505: 562-571

Boehlke C, Kotsis F, Patel V, Braeg S, Voelker H, Bredt S, Beyer T, Janusch H, Hamann C, Godel M *et al* (2010) Primary cilia regulate mTORC1 activity and cell size through Lkb1. *Nat Cell Biol* 12: 1115-1122

Boletta A, Germino GG (2003) Role of polycystins in renal tubulogenesis. *Trends Cell Biol* 13: 484-492

Boletta A, Qian F, Onuchic LF, Bhunia AK, Phakdeekitcharoen B, Hanaoka K, Guggino W, Monaco L, Germino GG (2000) Polycystin-1, the gene product of PKD1, induces resistance to apoptosis and spontaneous tubulogenesis in MDCK cells. *Mol Cell* 6: 1267-1273

Borgal L, Habbig S, Hatzold J, Liebau MC, Dafinger C, Sacarea I, Hammerschmidt M, Benzing T, Schermer B (2012) The ciliary protein nephrocystin-4 translocates the canonical Wnt regulator Jade-1 to the nucleus to negatively regulate beta-catenin signaling. *J Biol Chem* 287: 25370-25380

Borowsky B, Durkin MM, Ogozalek K, Marzabadi MR, DeLeon J, Lagu B, Heurich R, Lichtblau H, Shaposhnik Z, Daniewska I *et al* (2002) Antidepressant, anxiolytic and anorectic effects of a melanin-concentrating hormone-1 receptor antagonist. *Nat Med* 8: 825-830

Boukhalfa A, Roccio F, Dupont N, Codogno P, Morel E (2021) The autophagy protein ATG16L1 cooperates with IFT20 and INPP5E to regulate the turnover of phosphoinositides at the primary cilium. *Cell Rep* 35: 109045

Breslow DK, Koslover EF, Seydel F, Spakowitz AJ, Nachury MV (2013) An in vitro assay for entry into cilia reveals unique properties of the soluble diffusion barrier. *J Cell Biol* 203: 129-147

Cabail MZ, Li S, Lemmon E, Bowen ME, Hubbard SR, Miller WT (2015) The insulin and IGF1 receptor kinase domains are functional dimers in the activated state. *Nat Commun* 6: 6406

Carvalho-Santos Z, Azimzadeh J, Pereira-Leal JB, Bettencourt-Dias M (2011) Evolution: Tracing the origins of centrioles, cilia, and flagella. *J Cell Biol* 194: 165-175

Cassina L, Chiaravalli M, Boletta A (2020) Increased mitochondrial fragmentation in polycystic kidney disease acts as a modifier of disease progression. *FASEB J* 34: 6493-6507

Chavez M, Ena S, Van Sande J, de Kerchove d'Exaerde A, Schurmans S, Schiffmann SN (2015) Modulation of Ciliary Phosphoinositide Content Regulates Trafficking and Sonic Hedgehog Signaling Output. *Dev Cell* 34: 338-350

Cheung HO, Zhang X, Ribeiro A, Mo R, Makino S, Puviindran V, Law KK, Briscoe J, Hui CC (2009) The kinesin protein Kif7 is a critical regulator of Gli transcription factors in mammalian hedgehog signaling. *Sci Signal* 2: ra29

Chiaravalli M, Rowe I, Mannella V, Quilici G, Canu T, Bianchi V, Gurgone A, Antunes S, D'Adamo P, Esposito A *et al* (2016) 2-Deoxy-d-Glucose Ameliorates PKD Progression. *J Am Soc Nephrol* 27: 1958-1969

Chong J, Wishart DS, Xia J (2019) Using MetaboAnalyst 4.0 for Comprehensive and Integrative Metabolomics Data Analysis. *Curr Protoc Bioinformatics* 68: e86

Christensen ST, Morthorst SK, Mogensen JB, Pedersen LB (2017) Primary Cilia and Coordination of Receptor Tyrosine Kinase (RTK) and Transforming Growth Factor beta (TGF-beta) Signaling. *Cold Spring Harb Perspect Biol* 9

Clement CA, Ajbro KD, Koefoed K, Vestergaard ML, Veland IR, Henriques de Jesus MP, Pedersen LB, Benmerah A, Andersen CY, Larsen LA *et al* (2013) TGF-beta signaling is associated with endocytosis at the pocket region of the primary cilium. *Cell Rep* 3: 1806-1814

Cole DG (1999) Kinesin-II, coming and going. *J Cell Biol* 147: 463-466

Cole DG, Chinn SW, Wedaman KP, Hall K, Vuong T, Scholey JM (1993) Novel heterotrimeric kinesin-related protein purified from sea urchin eggs. *Nature* 366: 268-270

Collin GB, Marshall JD, Ikeda A, So WV, Russell-Eggitt I, Maffei P, Beck S, Boerkoel CF, Sicolo N, Martin M *et al* (2002) Mutations in ALMS1 cause obesity, type 2 diabetes and neurosensory degeneration in Alstrom syndrome. *Nat Genet* 31: 74-78

Corbit KC, Shyer AE, Dowdle WE, Gaulden J, Singla V, Chen MH, Chuang PT, Reiter JF (2008) Kif3a constrains beta-catenin-dependent Wnt signalling through dual ciliary and non-ciliary mechanisms. *Nat Cell Biol* 10: 70-76

Criswell PS, Ostrowski LE, Asai DJ (1996) A novel cytoplasmic dynein heavy chain: expression of DHC1b in mammalian ciliated epithelial cells. *J Cell Sci* 109 (Pt 7): 1891-1898

Currie E, Schulze A, Zechner R, Walther TC, Farese RV, Jr. (2013) Cellular fatty acid metabolism and cancer. *Cell Metab* 18: 153-161

Davenport JR, Watts AJ, Roper VC, Croyle MJ, van Groen T, Wyss JM, Nagy TR, Kesterson RA, Yoder BK (2007) Disruption of intraflagellar transport in adult mice leads to obesity and slow-onset cystic kidney disease. *Curr Biol* 17: 1586-1594

De Robertis E (1956) Morphogenesis of the retinal rods; an electron microscope study. *J Biophys Biochem Cytol* 2: 209-218

DeBerardinis RJ, Lum JJ, Hatzivassiliou G, Thompson CB (2008) The biology of cancer: metabolic reprogramming fuels cell growth and proliferation. *Cell Metab* 7: 11-20

DeBerardinis RJ, Mancuso A, Daikhin E, Nissim I, Yudkoff M, Wehrli S, Thompson CB (2007) Beyond aerobic glycolysis: transformed cells can engage in glutamine metabolism that exceeds the requirement for protein and nucleotide synthesis. *Proc Natl Acad Sci U S A* 104: 19345-19350

Distefano G, Boca M, Rowe I, Wodarczyk C, Ma L, Piontek KB, Germino GG, Pandolfi PP, Boletta A (2009) Polycystin-1 regulates extracellular signal-regulated kinase-dependent phosphorylation of tuberin to control cell size through mTOR and its downstream effectors S6K and 4EBP1. *Mol Cell Biol* 29: 2359-2371

Dyson JM, Conduit SE, Feeney SJ, Hakim S, DiTommaso T, Fulcher AJ, Sriratana A, Ramm G, Horan KA, Gurung R *et al* (2017) INPP5E regulates phosphoinositide-dependent cilia transition zone function. *J Cell Biol* 216: 247-263

Egorova AD, Khedoe PP, Goumans MJ, Yoder BK, Nauli SM, ten Dijke P, Poelmann RE, Hierck BP (2011) Lack of primary cilia primes shear-induced endothelial-to-mesenchymal transition. *Circ Res* 108: 1093-1101

Ehnert S, Sreekumar V, Aspera-Werz RH, Sajadian SO, Wintermeyer E, Sandmann GH, Bahrs C, Hengstler JG, Godoy P, Nussler AK (2017) TGF-beta(1) impairs mechanosensation of human osteoblasts via HDAC6-mediated shortening and distortion of primary cilia. *J Mol Med (Berl)* 95: 653-663

Ehrlich M (2016) Endocytosis and trafficking of BMP receptors: Regulatory mechanisms for fine-tuning the signaling response in different cellular contexts. *Cytokine Growth Factor Rev* 27: 35-42

Fisch C, Dupuis-Williams P (2011) Ultrastructure of cilia and flagella - back to the future! *Biol Cell* 103: 249-270

Fischer DC, Jacoby U, Pape L, Ward CJ, Kuwertz-Broeking E, Renken C, Nizze H, Querfeld U, Rudolph B, Mueller-Wiefel DE *et al* (2009) Activation of the AKT/mTOR pathway in autosomal recessive polycystic kidney disease (ARPKD). *Nephrol Dial Transplant* 24: 1819-1827

Flowers EM, Sudderth J, Zacharias L, Mernaugh G, Zent R, DeBerardinis RJ, Carroll TJ (2018) Lkb1 deficiency confers glutamine dependency in polycystic kidney disease. *Nat Commun* 9: 814

Follit JA, Li L, Vucica Y, Pazour GJ (2010) The cytoplasmic tail of fibrocystin contains a ciliary targeting sequence. *J Cell Biol* 188: 21-28

Franco I, Gulluni F, Campa CC, Costa C, Margaria JP, Ciraolo E, Martini M, Monteyne D, De Luca E, Germena G *et al* (2014) PI3K class II alpha controls spatially restricted endosomal PtdIns3P and Rab11 activation to promote primary cilium function. *Dev Cell* 28: 647-658

Garcia-Gonzalo FR, Corbit KC, Sirerol-Piquer MS, Ramaswami G, Otto EA, Noriega TR, Seol AD, Robinson JF, Bennett CL, Josifova DJ *et al* (2011) A transition zone complex regulates mammalian ciliogenesis and ciliary membrane composition. *Nat Genet* 43: 776-784

Garcia-Gonzalo FR, Phua SC, Roberson EC, Garcia G, 3rd, Abedin M, Schurmans S, Inoue T, Reiter JF (2015) Phosphoinositides Regulate Ciliary Protein Trafficking to Modulate Hedgehog Signaling. *Dev Cell* 34: 400-409

Garcia G, 3rd, Raleigh DR, Reiter JF (2018) How the Ciliary Membrane Is Organized Inside-Out to Communicate Outside-In. *Curr Biol* 28: R421-R434

Gencer S, Oleinik N, Kim J, Panneer Selvam S, De Palma R, Dany M, Nganga R, Thomas RJ, Senkal CE, Howe PH *et al* (2017) TGF-beta receptor I/II trafficking and signaling at primary cilia are inhibited by ceramide to attenuate cell migration and tumor metastasis. *Sci Signal* 10

Gerdes JM, Christou-Savina S, Xiong Y, Moede T, Moruzzi N, Karlsson-Edlund P, Leibiger B, Leibiger IB, Ostenson CG, Beales PL *et al* (2014) Ciliary dysfunction impairs beta-cell insulin secretion and promotes development of type 2 diabetes in rodents. *Nat Commun* 5: 5308

Gibbons BH, Asai DJ, Tang WJ, Hays TS, Gibbons IR (1994) Phylogeny and expression of axonemal and cytoplasmic dynein genes in sea urchins. *Mol Biol Cell* 5: 57-70

Girard D, Petrovsky N (2011) Alstrom syndrome: insights into the pathogenesis of metabolic disorders. *Nat Rev Endocrinol* 7: 77-88

Grillo MA, Palay SL (1963) Ciliated Schwann cells in the autonomic nervous system of the adult rat. *J Cell Biol* 16: 430-436

Guay-Woodford LM, Desmond RA (2003) Autosomal recessive polycystic kidney disease: the clinical experience in North America. *Pediatrics* 111: 1072-1080

Guo J, Otis JM, Suciu SK, Catalano C, Xing L, Constable S, Wachten D, Gupton S, Lee J, Lee A *et al* (2019) Primary Cilia Signaling Promotes Axonal Tract Development and Is Disrupted in Joubert Syndrome-Related Disorders Models. *Dev Cell* 51: 759-774 e755

Guo X, Wang XF (2009) Signaling cross-talk between TGF-beta/BMP and other pathways. *Cell Res* 19: 71-88

Han S, Miyoshi K, Shikada S, Amano G, Wang Y, Yoshimura T, Katayama T (2019) TULP3 is required for localization of membrane-associated proteins ARL13B and INPP5E to primary cilia. *Biochem Biophys Res Commun* 509: 227-234

Han SJ, Jung JK, Im SS, Lee SR, Jang BC, Park KM, Kim JI (2018) Deficiency of primary cilia in kidney epithelial cells induces epithelial to mesenchymal transition. *Biochem Biophys Res Commun* 496: 450-454

He M, Subramanian R, Bangs F, Omelchenko T, Liem KF, Jr., Kapoor TM, Anderson KV (2014) The kinesin-4 protein Kif7 regulates mammalian Hedgehog signalling by organizing the cilium tip compartment. *Nat Cell Biol* 16: 663-672

Heldin CH, Moustakas A (2016) Signaling Receptors for TGF-beta Family Members. *Cold Spring Harb Perspect Biol* 8

Hensley CT, Wasti AT, DeBerardinis RJ (2013) Glutamine and cancer: cell biology, physiology, and clinical opportunities. *J Clin Invest* 123: 3678-3684

Hildebrandt F, Benzing T, Katsanis N (2011) Ciliopathies. *N Engl J Med* 364: 1533-1543

Hildebrandt F, Zhou W (2007) Nephronophthisis-associated ciliopathies. *J Am Soc Nephrol* 18: 1855-1871

Hilgendorf KI, Johnson CT, Jackson PK (2016) The primary cilium as a cellular receiver: organizing ciliary GPCR signaling. *Curr Opin Cell Biol* 39: 84-92

Hilgendorf KI, Johnson CT, Mezger A, Rice SL, Norris AM, Demeter J, Greenleaf WJ, Reiter JF, Kopinke D, Jackson PK (2019) Omega-3 Fatty Acids Activate Ciliary FFAR4 to Control Adipogenesis. *Cell* 179: 1289-1305 e1221

Hirokawa N, Tanaka Y, Okada Y (2012) Cilia, KIF3 molecular motor and nodal flow. *Curr Opin Cell Biol* 24: 31-39

Horani A, Ferkol TW, Dutcher SK, Brody SL (2016) Genetics and biology of primary ciliary dyskinesia. *Paediatr Respir Rev* 18: 18-24

Houten SM, Violante S, Ventura FV, Wanders RJ (2016) The Biochemistry and Physiology of Mitochondrial Fatty Acid beta-Oxidation and Its Genetic Disorders. *Annu Rev Physiol* 78: 23-44

Hu Q, Milenkovic L, Jin H, Scott MP, Nachury MV, Spiliotis ET, Nelson WJ (2010) A septin diffusion barrier at the base of the primary cilium maintains ciliary membrane protein distribution. *Science* 329: 436-439

Huang P, Schier AF (2009) Dampened Hedgehog signaling but normal Wnt signaling in zebrafish without cilia. *Development* 136: 3089-3098

Huangfu D, Liu A, Rakeman AS, Murcia NS, Niswander L, Anderson KV (2003) Hedgehog signalling in the mouse requires intraflagellar transport proteins. *Nature* 426: 83-87

Hubbard SR (2013) The insulin receptor: both a prototypical and atypical receptor tyrosine kinase. *Cold Spring Harb Perspect Biol* 5: a008946

Humke EW, Dorn KV, Milenkovic L, Scott MP, Rohatgi R (2010) The output of Hedgehog signaling is controlled by the dynamic association between Suppressor of Fused and the Gli proteins. *Genes Dev* 24: 670-682

Hurley JH (2015) ESCRTs are everywhere. *EMBO J* 34: 2398-2407

Insinna C, Lu Q, Teixeira I, Harned A, Semler EM, Stauffer J, Magidson V, Tiwari A, Kenworthy AK, Narayan K *et al* (2019) Investigation of F-BAR domain PACSIN proteins uncovers membrane tubulation function in cilia assembly and transport. *Nat Commun* 10: 428

Ishikawa H, Thompson J, Yates JR, 3rd, Marshall WF (2012) Proteomic analysis of mammalian primary cilia. *Curr Biol* 22: 414-419

Jacoby M, Cox JJ, Gayral S, Hampshire DJ, Ayub M, Blockmans M, Pernot E, Kisseleva MV, Compere P, Schiffmann SN *et al* (2009) INPP5E mutations cause primary cilium signaling defects, ciliary instability and ciliopathies in human and mouse. *Nat Genet* 41: 1027-1031

Jekely G, Arendt D (2006) Evolution of intraflagellar transport from coated vesicles and autogenous origin of the eukaryotic cilium. *Bioessays* 28: 191-198

Jensen VL, Li C, Bowie RV, Clarke L, Mohan S, Blacque OE, Leroux MR (2015) Formation of the transition zone by Mks5/Rpgrip1L establishes a ciliary zone of exclusion (CIZE) that compartmentalises ciliary signalling proteins and controls PIP2 ciliary abundance. *EMBO J* 34: 2537-2556

Jewell JL, Kim YC, Russell RC, Yu FX, Park HW, Plouffe SW, Tagliabracci VS, Guan KL (2015) Metabolism. Differential regulation of mTORC1 by leucine and glutamine. *Science* 347: 194-198

Jia J, Kolterud A, Zeng H, Hoover A, Teglund S, Toftgard R, Liu A (2009) Suppressor of Fused inhibits mammalian Hedgehog signaling in the absence of cilia. *Dev Biol* 330: 452-460

Jin H, White SR, Shida T, Schulz S, Aguiar M, Gygi SP, Bazan JF, Nachury MV (2010) The conserved Bardet-Biedl syndrome proteins assemble a coat that traffics membrane proteins to cilia. *Cell* 141: 1208-1219

Jonassen JA, San Agustin J, Follit JA, Pazour GJ (2008) Deletion of IFT20 in the mouse kidney causes misorientation of the mitotic spindle and cystic kidney disease. *J Cell Biol* 183: 377-384

Joy T, Cao H, Black G, Malik R, Charlton-Menys V, Hegele RA, Durrington PN (2007) Alstrom syndrome (OMIM 203800): a case report and literature review. *Orphanet J Rare Dis* 2: 49

Kanehisa M, Goto S (2000) KEGG: kyoto encyclopedia of genes and genomes. *Nucleic Acids Res* 28: 27-30

Kaneshiro ES, Matesic DF, Jayasimhulu K (1984) Characterizations of six ethanolamine sphingophospholipids from Paramecium cells and cilia. *J Lipid Res* 25: 369-377

Kawasaki M, Ezura Y, Hayata T, Notomi T, Izu Y, Noda M (2015) TGF-beta Suppresses Ift88 Expression in Chondrocytic ATDC5 Cells. *J Cell Physiol* 230: 2788-2795

Kiesel P, Alvarez Viar G, Tsoy N, Maraspini R, Gorilak P, Varga V, Honigmann A, Pigino G (2020) The molecular structure of mammalian primary cilia revealed by cryo-electron tomography. *Nat Struct Mol Biol* 27: 1115-1124

Kilberg MS, Balasubramanian M, Fu L, Shan J (2012) The transcription factor network associated with the amino acid response in mammalian cells. *Adv Nutr* 3: 295-306

Kilberg MS, Shan J, Su N (2009) ATF4-dependent transcription mediates signaling of amino acid limitation. *Trends Endocrinol Metab* 20: 436-443

Kim H, Xu H, Yao Q, Li W, Huang Q, Outeda P, Cebotaru V, Chiaravalli M, Boletta A, Piontek K *et al* (2014) Ciliary membrane proteins traffic through the Golgi via a Rabep1/GGA1/Arl3-dependent mechanism. *Nat Commun* 5: 5482

Kim J, Hsia EY, Brigui A, Plessis A, Beachy PA, Zheng X (2015) The role of ciliary trafficking in Hedgehog receptor signaling. *Sci Signal* 8: ra55

Kinnebrew M, Iverson EJ, Patel BB, Pusapati GV, Kong JH, Johnson KA, Luchetti G, Eckert KM, McDonald JG, Covey DF *et al* (2019) Cholesterol accessibility at the ciliary membrane controls hedgehog signaling. *Elife* 8

Koefoed K, Skat-Rordam J, Andersen P, Warzecha CB, Pye M, Andersen TA, Ajbro KD, Bendsen E, Narimatsu M, Vilhardt F *et al* (2018) The E3 ubiquitin ligase SMURF1 regulates cell-fate specification and outflow tract septation during mammalian heart development. *Sci Rep* 8: 9542

Kozminski KG, Johnson KA, Forscher P, Rosenbaum JL (1993) A motility in the eukaryotic flagellum unrelated to flagellar beating. *Proc Natl Acad Sci U S A* 90: 5519-5523

Labour MN, Riffault M, Christensen ST, Hoey DA (2016) TGFbeta1 - induced recruitment of human bone mesenchymal stem cells is mediated by the primary cilium in a SMAD3-dependent manner. *Sci Rep* 6: 35542

Lakhia R, Yheskel M, Flaten A, Quittner-Strom EB, Holland WL, Patel V (2018) PPARalpha agonist fenofibrate enhances fatty acid beta-oxidation and attenuates polycystic kidney and liver disease in mice. *Am J Physiol Renal Physiol* 314: F122-F131

Lancaster MA, Louie CM, Silhavy JL, Sintasath L, Decambre M, Nigam SK, Willert K, Gleeson JG (2009) Impaired Wnt-beta-catenin signaling disrupts adult renal homeostasis and leads to cystic kidney ciliopathy. *Nat Med* 15: 1046-1054

Larkins CE, Aviles GD, East MP, Kahn RA, Caspary T (2011) Arl13b regulates ciliogenesis and the dynamic localization of Shh signaling proteins. *Mol Biol Cell* 22: 4694-4703

Lechtreck KF (2015) IFT-Cargo Interactions and Protein Transport in Cilia. *Trends Biochem Sci* 40: 765-778

Lechtreck KF, Johnson EC, Sakai T, Cochran D, Ballif BA, Rush J, Pazour GJ, Ikebe M, Witman GB (2009) The Chlamydomonas reinhardtii BBSome is an IFT cargo required for export of specific signaling proteins from flagella. *J Cell Biol* 187: 1117-1132

Lee SE, Kang YC, Kim Y, Kim S, Yu SH, Park JH, Kim IH, Kim HY, Han K, Lee HK *et al* (2022) Preferred Migration of Mitochondria toward Cells and Tissues with Mitochondrial Damage. *Int J Mol Sci* 23

Lemmon MA, Schlessinger J (2010) Cell signaling by receptor tyrosine kinases. *Cell* 141: 1117-1134

Li A, Saito M, Chuang JZ, Tseng YY, Dedesma C, Tomizawa K, Kaitsuka T, Sung CH (2011) Ciliary transition zone activation of phosphorylated Tctex-1 controls ciliary resorption, S-phase entry and fate of neural progenitors. *Nat Cell Biol* 13: 402-411

Li Y, Wei Q, Zhang Y, Ling K, Hu J (2010) The small GTPases ARL-13 and ARL-3 coordinate intraflagellar transport and ciliogenesis. *J Cell Biol* 189: 1039-1051

Liem KF, Jr., He M, Ocbina PJ, Anderson KV (2009) Mouse Kif7/Costal2 is a cilia-associated protein that regulates Sonic hedgehog signaling. *Proc Natl Acad Sci U S A* 106: 13377-13382

Lienkamp S, Ganner A, Boehlke C, Schmidt T, Arnold SJ, Schafer T, Romaker D, Schuler J, Hoff S, Powelske C *et al* (2010) Inversin relays Frizzled-8 signals to promote proximal pronephros development. *Proc Natl Acad Sci U S A* 107: 20388-20393

Lin F, Hiesberger T, Cordes K, Sinclair AM, Goldstein LS, Somlo S, Igarashi P (2003) Kidney-specific inactivation of the KIF3A subunit of kinesin-II inhibits renal ciliogenesis and produces polycystic kidney disease. *Proc Natl Acad Sci U S A* 100: 5286-5291

Liu M, Zhang W, Li M, Feng J, Kuang W, Chen X, Yang F, Sun Q, Xu Z, Hua J *et al* (2021) NudCL2 is an autophagy receptor that mediates selective autophagic degradation of CP110 at mother centrioles to promote ciliogenesis. *Cell Res* 31: 1199-1211

Liu P, Lechtreck KF (2018) The Bardet-Biedl syndrome protein complex is an adapter expanding the cargo range of intraflagellar transport trains for ciliary export. *Proc Natl Acad Sci U S A* 115: E934-E943

Loktev AV, Zhang Q, Beck JS, Searby CC, Scheetz TE, Bazan JF, Slusarski DC, Sheffield VC, Jackson PK, Nachury MV (2008) A BBSome subunit links ciliogenesis, microtubule stability, and acetylation. *Dev Cell* 15: 854-865

Lomelino CL, Andring JT, McKenna R, Kilberg MS (2017) Asparagine synthetase: Function, structure, and role in disease. *J Biol Chem* 292: 19952-19958

Long H, Zhang F, Xu N, Liu G, Diener DR, Rosenbaum JL, Huang K (2016) Comparative Analysis of Ciliary Membranes and Ectosomes. *Curr Biol* 26: 3327-3335

Lu H, Galeano MCR, Ott E, Kaeslin G, Kausalya PJ, Kramer C, Ortiz-Bruchle N, Hilger N, Metzis V, Hiersche M *et al* (2017) Mutations in DZIP1L, which encodes a ciliary-transition-zone protein, cause autosomal recessive polycystic kidney disease. *Nat Genet* 49: 1025-1034

Ma M, Gallagher AR, Somlo S (2017) Ciliary Mechanisms of Cyst Formation in Polycystic Kidney Disease. *Cold Spring Harb Perspect Biol* 9

Ma M, Tian X, Igarashi P, Pazour GJ, Somlo S (2013) Loss of cilia suppresses cyst growth in genetic models of autosomal dominant polycystic kidney disease. *Nat Genet* 45: 1004-1012

Maria BL, Hoang KB, Tusa RJ, Mancuso AA, Hamed LM, Quisling RG, Hove MT, Fennell EB, Booth-Jones M, Ringdahl DM *et al* (1997) "Joubert syndrome" revisited: key ocular motor signs with magnetic resonance imaging correlation. *J Child Neurol* 12: 423-430

Marshall WF, Nonaka S (2006) Cilia: tuning in to the cell's antenna. *Curr Biol* 16: R604-614

Massague J (2012) TGFbeta signalling in context. *Nat Rev Mol Cell Biol* 13: 616-630

McConnachie DJ, Stow JL, Mallett AJ (2021) Ciliopathies and the Kidney: A Review. *Am J Kidney Dis* 77: 410-419

Menezes LF, Lin CC, Zhou F, Germino GG (2016) Fatty Acid Oxidation is Impaired in An Orthologous Mouse Model of Autosomal Dominant Polycystic Kidney Disease. *EBioMedicine* 5: 183-192

Miceli C, Roccio F, Penalva-Mousset L, Burtin M, Leroy C, Nemazanyy I, Kuperwasser N, Pontoglio M, Friedlander G, Morel E *et al* (2020) The primary cilium and lipophagy translate mechanical forces to direct metabolic adaptation of kidney epithelial cells. *Nat Cell Biol* 22: 1091-1102

Mick DU, Rodrigues RB, Leib RD, Adams CM, Chien AS, Gygi SP, Nachury MV (2015) Proteomics of Primary Cilia by Proximity Labeling. *Dev Cell* 35: 497-512

Mihaylova MM, Shaw RJ (2011) The AMPK signalling pathway coordinates cell growth, autophagy and metabolism. *Nat Cell Biol* 13: 1016-1023

Milenkovic L, Weiss LE, Yoon J, Roth TL, Su YS, Sahl SJ, Scott MP, Moerner WE (2015) Single-molecule imaging of Hedgehog pathway protein Smoothened in primary cilia reveals binding events regulated by Patched1. *Proc Natl Acad Sci U S A* 112: 8320-8325

Mitchison HM, Schmidts M, Loges NT, Freshour J, Dritsoula A, Hirst RA, O'Callaghan C, Blau H, Al Dabbagh M, Olbrich H *et al* (2012) Mutations in axonemal dynein assembly factor DNAAF3 cause primary ciliary dyskinesia. *Nat Genet* 44: 381-389, S381-382

Monnich M, Borgeskov L, Breslin L, Jakobsen L, Rogowski M, Doganli C, Schroder JM, Mogensen JB, Blinkenkjaer L, Harder LM *et al* (2018) CEP128 Localizes to the Subdistal Appendages of the Mother Centriole and Regulates TGF-beta/BMP Signaling at the Primary Cilium. *Cell Rep* 22: 2584-2592

Montesano R (1979) Inhomogeneous distribution of filipin-sterol complexes in the ciliary membrane of rat tracheal epithelium. *Am J Anat* 156: 139-145

Morleo M, Vieira HLA, Pennekamp P, Palma A, Bento-Lopes L, Omran H, Lopes SS, Barral DC, Franco B (2023) Crosstalk between cilia and autophagy: implication for human diseases. *Autophagy* 19: 24-43

Mukhopadhyay S, Wen X, Chih B, Nelson CD, Lane WS, Scales SJ, Jackson PK (2010) TULP3 bridges the IFT-A complex and membrane phosphoinositides to promote trafficking of G protein-coupled receptors into primary cilia. *Genes Dev* 24: 2180-2193

Mukhopadhyay S, Wen X, Ratti N, Loktev A, Rangell L, Scales SJ, Jackson PK (2013) The ciliary G-protein-coupled receptor Gpr161 negatively regulates the Sonic hedgehog pathway via cAMP signaling. *Cell* 152: 210-223

Nachury MV, Loktev AV, Zhang Q, Westlake CJ, Peranen J, Merdes A, Slusarski DC, Scheller RH, Bazan JF, Sheffield VC *et al* (2007) A core complex of BBS proteins cooperates with the GTPase Rab8 to promote ciliary membrane biogenesis. *Cell* 129: 1201-1213

Nachury MV, Mick DU (2019) Establishing and regulating the composition of cilia for signal transduction. *Nat Rev Mol Cell Biol* 20: 389-405

Nager AR, Goldstein JS, Herranz-Perez V, Portran D, Ye F, Garcia-Verdugo JM, Nachury MV (2017) An Actin Network Dispatches Ciliary GPCRs into Extracellular Vesicles to Modulate Signaling. *Cell* 168: 252-263 e214

Najafi M, Maza NA, Calvert PD (2012) Steric volume exclusion sets soluble protein concentrations in photoreceptor sensory cilia. *Proc Natl Acad Sci U S A* 109: 203-208

Naveilhan P, Hassani H, Canals JM, Ekstrand AJ, Larefalk A, Chhajlani V, Arenas E, Gedda K, Svensson L, Thoren P *et al* (1999) Normal feeding behavior, body weight and leptin response require the neuropeptide Y Y2 receptor. *Nat Med* 5: 1188-1193

Nechipurenko IV (2020) The Enigmatic Role of Lipids in Cilia Signaling. *Front Cell Dev Biol* 8: 777

Niewiadomski P, Kong JH, Ahrends R, Ma Y, Humke EW, Khan S, Teruel MN, Novitch BG, Rohatgi R (2014) Gli protein activity is controlled by multisite phosphorylation in vertebrate Hedgehog signaling. *Cell Rep* 6: 168-181

Nigro EA, Distefano G, Chiaravalli M, Matafora V, Castelli M, Pesenti Gritti A, Bachi A, Boletta A (2019) Polycystin-1 Regulates Actomyosin Contraction and the Cellular Response to Extracellular Stiffness. *Sci Rep* 9: 16640

Nikonova AS, Deneka AY, Kiseleva AA, Korobeynikov V, Gaponova A, Serebriiskii IG, Kopp MC, Hensley HH, Seeger-Nukpezah TN, Somlo S *et al* (2018) Ganetespib limits ciliation and cystogenesis in autosomal-dominant polycystic kidney disease (ADPKD). *FASEB J* 32: 2735-2746

Nusse R, Clevers H (2017) Wnt/beta-Catenin Signaling, Disease, and Emerging Therapeutic Modalities. *Cell* 169: 985-999

Nusslein-Volhard C, Wieschaus E (1980) Mutations affecting segment number and polarity in Drosophila. *Nature* 287: 795-801

Nygaard MB, Almstrup K, Lindbaek L, Christensen ST, Svingen T (2015) Cell context-specific expression of primary cilia in the human testis and ciliary coordination of Hedgehog signalling in mouse Leydig cells. *Sci Rep* 5: 10364

Ocbina PJ, Tuson M, Anderson KV (2009) Primary cilia are not required for normal canonical Wnt signaling in the mouse embryo. *PLoS One* 4: e6839

Oh EC, Katsanis N (2013) Context-dependent regulation of Wnt signaling through the primary cilium. *J Am Soc Nephrol* 24: 10-18

Onuchic LF, Furu L, Nagasawa Y, Hou X, Eggermann T, Ren Z, Bergmann C, Senderek J, Esquivel E, Zeltner R *et al* (2002) PKHD1, the polycystic kidney and hepatic disease 1 gene, encodes a novel large protein containing multiple immunoglobulin-like plexin-transcription-factor domains and parallel beta-helix 1 repeats. *Am J Hum Genet* 70: 1305-1317

Orhon I, Dupont N, Zaidan M, Boitez V, Burtin M, Schmitt A, Capiod T, Viau A, Beau I, Kuehn EW *et al* (2016) Primary-cilium-dependent autophagy controls epithelial cell volume in response to fluid flow. *Nat Cell Biol* 18: 657-667

Pampliega O, Orhon I, Patel B, Sridhar S, Diaz-Carretero A, Beau I, Codogno P, Satir BH, Satir P, Cuervo AM (2013) Functional interaction between autophagy and ciliogenesis. *Nature* 502: 194-200

Pazour GJ, Dickert BL, Vucica Y, Seeley ES, Rosenbaum JL, Witman GB, Cole DG (2000) Chlamydomonas IFT88 and its mouse homologue, polycystic kidney disease gene tg737, are required for assembly of cilia and flagella. *J Cell Biol* 151: 709-718

Pazour GJ, San Agustin JT, Follit JA, Rosenbaum JL, Witman GB (2002) Polycystin-2 localizes to kidney cilia and the ciliary level is elevated in orpk mice with polycystic kidney disease. *Curr Biol* 12: R378-380

Pei Y (2001) A "two-hit" model of cystogenesis in autosomal dominant polycystic kidney disease? *Trends Mol Med* 7: 151-156

Perez JL, McDowell MM, Zussman B, Jadhav AP, Miyashita Y, McKiernan P, Greene S (2018) Ruptured intracranial aneurysm in a patient with autosomal recessive polycystic kidney disease. *J Neurosurg Pediatr* 23: 75-79

Phua SC, Chiba S, Suzuki M, Su E, Roberson EC, Pusapati GV, Schurmans S, Setou M, Rohatgi R, Reiter JF *et al* (2017) Dynamic Remodeling of Membrane Composition Drives Cell Cycle through Primary Cilia Excision. *Cell* 168: 264-279 e215

Pigino G, Geimer S, Lanzavecchia S, Paccagnini E, Cantele F, Diener DR, Rosenbaum JL, Lupetti P (2009) Electron-tomographic analysis of intraflagellar transport particle trains in situ. *J Cell Biol* 187: 135-148

Piperno G, Fuller MT (1985) Monoclonal antibodies specific for an acetylated form of alpha-tubulin recognize the antigen in cilia and flagella from a variety of organisms. *J Cell Biol* 101: 2085-2094

Podrini C, Cassina L, Boletta A (2020) Metabolic reprogramming and the role of mitochondria in polycystic kidney disease. *Cell Signal* 67: 109495

Podrini C, Rowe I, Pagliarini R, Costa ASH, Chiaravalli M, Di Meo I, Kim H, Distefano G, Tiranti V, Qian F *et al* (2018) Dissection of metabolic reprogramming in polycystic kidney disease reveals coordinated rewiring of bioenergetic pathways. *Commun Biol* 1: 194

Porter KR (1955) The submicroscopic morphology of protoplasm. *Harvey Lect* 51: 175-228

Prosseda PP, Luo N, Wang B, Alvarado JA, Hu Y, Sun Y (2017) Loss of OCRL increases ciliary PI(4,5)P(2) in Lowe oculocerebrorenal syndrome. *J Cell Sci* 130: 3447-3454

Qu D, Ludwig DS, Gammeltoft S, Piper M, Pelleymounter MA, Cullen MJ, Mathes WF, Przypek R, Kanarek R, Maratos-Flier E (1996) A role for melanin-concentrating hormone in the central regulation of feeding behaviour. *Nature* 380: 243-247

Radhakrishnan A, Rohatgi R, Siebold C (2020) Cholesterol access in cellular membranes controls Hedgehog signaling. *Nat Chem Biol* 16: 1303-1313

Raleigh DR, Sever N, Choksi PK, Sigg MA, Hines KM, Thompson BM, Elnatan D, Jaishankar P, Bisignano P, Garcia-Gonzalo FR *et al* (2018) Cilia-Associated Oxysterols Activate Smoothened. *Mol Cell* 72: 316-327 e315

Rattanasopha S, Tongkobpetch S, Srichomthong C, Siriwan P, Suphapeetiporn K, Shotelersuk V (2012) PDGFRa mutations in humans with isolated cleft palate. *Eur J Hum Genet* 20: 1058-1062

Reiter JF, Blacque OE, Leroux MR (2012) The base of the cilium: roles for transition fibres and the transition zone in ciliary formation, maintenance and compartmentalization. *EMBO Rep* 13: 608-618

Reiter JF, Leroux MR (2017) Genes and molecular pathways underpinning ciliopathies. *Nat Rev Mol Cell Biol* 18: 533-547

Rohrig F, Schulze A (2016) The multifaceted roles of fatty acid synthesis in cancer. *Nat Rev Cancer* 16: 732-749

Rowe I, Boletta A (2014) Defective metabolism in polycystic kidney disease: potential for therapy and open questions. *Nephrol Dial Transplant* 29: 1480-1486

Rowe I, Chiaravalli M, Mannella V, Ulisse V, Quilici G, Pema M, Song XW, Xu H, Mari S, Qian F *et al* (2013) Defective glucose metabolism in polycystic kidney disease identifies a new therapeutic strategy. *Nat Med* 19: 488-493

Ruzzo EK, Capo-Chichi JM, Ben-Zeev B, Chitayat D, Mao H, Pappas AL, Hitomi Y, Lu YF, Yao X, Hamdan FF *et al* (2013) Deficiency of asparagine synthetase causes congenital microcephaly and a progressive form of encephalopathy. *Neuron* 80: 429-441

Sainsbury A, Schwarzer C, Couzens M, Fetissov S, Furtinger S, Jenkins A, Cox HM, Sperk G, Hokfelt T, Herzog H (2002) Important role of hypothalamic Y2 receptors in body weight regulation revealed in conditional knockout mice. *Proc Natl Acad Sci U S A* 99: 8938-8943

Satir P, Christensen ST (2008) Structure and function of mammalian cilia. *Histochem Cell Biol* 129: 687-693

Schneider L, Cammer M, Lehman J, Nielsen SK, Guerra CF, Veland IR, Stock C, Hoffmann EK, Yoder BK, Schwab A *et al* (2010) Directional cell migration and chemotaxis in wound healing response to PDGF-AA are coordinated by the primary cilium in fibroblasts. *Cell Physiol Biochem* 25: 279-292

Schneider L, Clement CA, Teilmann SC, Pazour GJ, Hoffmann EK, Satir P, Christensen ST (2005) PDGFRalphaalpha signaling is regulated through the primary cilium in fibroblasts. *Curr Biol* 15: 1861-1866

Shao L, El-Jouni W, Kong F, Ramesh J, Kumar RS, Shen X, Ren J, Devendra S, Dorschel A, Wu M *et al* (2020) Genetic reduction of cilium length by targeting intraflagellar transport 88 protein impedes kidney and liver cyst formation in mouse models of autosomal polycystic kidney disease. *Kidney Int* 98: 1225-1241

Sheffield VC (2010) The blind leading the obese: the molecular pathophysiology of a human obesity syndrome. *Trans Am Clin Climatol Assoc* 121: 172-181; discussion 181-172

Shi X, Garcia G, 3rd, Van De Weghe JC, McGorty R, Pazour GJ, Doherty D, Huang B, Reiter JF (2017) Super-resolution microscopy reveals that disruption of ciliary transition-zone architecture causes Joubert syndrome. *Nat Cell Biol* 19: 1178-1188

Shillingford JM, Piontek KB, Germino GG, Weimbs T (2010) Rapamycin ameliorates PKD resulting from conditional inactivation of Pkd1. *J Am Soc Nephrol* 21: 489-497

Shim MS, Nettesheim A, Dixon A, Liton PB (2021) Primary cilia and the reciprocal activation of AKT and SMAD2/3 regulate stretch-induced autophagy in trabecular meshwork cells. *Proc Natl Acad Sci U S A* 118

Shimada M, Tritos NA, Lowell BB, Flier JS, Maratos-Flier E (1998) Mice lacking melanin-concentrating hormone are hypophagic and lean. *Nature* 396: 670-674

Shiratori H, Hamada H (2014) TGFbeta signaling in establishing left-right asymmetry. *Semin Cell Dev Biol* 32: 80-84

Simons M, Gloy J, Ganner A, Bullerkotte A, Bashkurov M, Kronig C, Schermer B, Benzing T, Cabello OA, Jenny A *et al* (2005) Inversin, the gene product mutated in nephronophthisis type II, functions as a molecular switch between Wnt signaling pathways. *Nat Genet* 37: 537-543

Sobie EA (2011) An introduction to MATLAB. *Sci Signal* 4: tr7

Soomro I, Sun Y, Li Z, Diggs L, Hatzivassiliou G, Thomas AG, Rais R, Parker SJ, Slusher BS, Kimmelman AC *et al* (2018) Glutamine metabolism via glutaminase 1 in autosomal-dominant polycystic kidney disease. *Nephrol Dial Transplant* 33: 1343-1353

Soriano P (1997) The PDGF alpha receptor is required for neural crest cell development and for normal patterning of the somites. *Development* 124: 2691-2700

Sorkin A, von Zastrow M (2009) Endocytosis and signalling: intertwining molecular networks. *Nat Rev Mol Cell Biol* 10: 609-622

Sorokin S (1962) Centrioles and the formation of rudimentary cilia by fibroblasts and smooth muscle cells. *J Cell Biol* 15: 363-377

Steidl ME, Nigro EA, Nielsen AK, Pagliarini R, Cassina L, Lampis M, Podrini C, Chiaravalli M, Mannella V, Distefano G *et al* (2023) Primary cilia sense glutamine availability and respond via asparagine synthetase. *Nat Metab*

Stoetzel C, Bar S, De Craene JO, Scheidecker S, Etard C, Chicher J, Reck JR, Perrault I, Geoffroy V, Chennen K *et al* (2016) A mutation in VPS15 (PIK3R4) causes a ciliopathy and affects IFT20 release from the cis-Golgi. *Nat Commun* 7: 13586

Stokman MF, Saunier S, Benmerah A (2021) Renal Ciliopathies: Sorting Out Therapeutic Approaches for Nephronophthisis. *Front Cell Dev Biol* 9: 653138

Stratigopoulos G, LeDuc CA, Cremona ML, Chung WK, Leibel RL (2011) Cut-like homeobox 1 (CUX1) regulates expression of the fat mass and obesity-associated and retinitis pigmentosa GTPase regulator-interacting protein-1-like (RPGRIP1L) genes and coordinates leptin receptor signaling. *J Biol Chem* 286: 2155-2170

Stratigopoulos G, Martin Carli JF, O'Day DR, Wang L, Leduc CA, Lanzano P, Chung WK, Rosenbaum M, Egli D, Doherty DA *et al* (2014) Hypomorphism for RPGRIP1L, a ciliary gene vicinal to the FTO locus, causes increased adiposity in mice. *Cell Metab* 19: 767-779

Stuck MW, Chong WM, Liao JC, Pazour GJ (2021) Rab34 is necessary for early stages of intracellular ciliogenesis. *Curr Biol* 31: 2887-2894 e2884

Takiar V, Nishio S, Seo-Mayer P, King JD, Jr., Li H, Zhang L, Karihaloo A, Hallows KR, Somlo S, Caplan MJ (2011) Activating AMP-activated protein kinase (AMPK) slows renal cystogenesis. *Proc Natl Acad Sci U S A* 108: 2462-2467

Tang Z, Lin MG, Stowe TR, Chen S, Zhu M, Stearns T, Franco B, Zhong Q (2013) Autophagy promotes primary ciliogenesis by removing OFD1 from centriolar satellites. *Nature* 502: 254-257

Tarkar A, Loges NT, Slagle CE, Francis R, Dougherty GW, Tamayo JV, Shook B, Cantino M, Schwartz D, Jahnke C *et al* (2013) DYX1C1 is required for axonemal dynein assembly and ciliary motility. *Nat Genet* 45: 995-1003

Torres VE, Harris PC, Pirson Y (2007) Autosomal dominant polycystic kidney disease. *Lancet* 369: 1287-1301

Vadnais C, Awan AA, Harada R, Clermont PL, Leduy L, Berube G, Nepveu A (2013) Long-range transcriptional regulation by the p110 CUX1 homeodomain protein on the ENCODE array. *BMC Genomics* 14: 258

Vaisse C, Reiter JF, Berbari NF (2017) Cilia and Obesity. *Cold Spring Harb Perspect Biol* 9

van Dam TJ, Townsend MJ, Turk M, Schlessinger A, Sali A, Field MC, Huynen MA (2013) Evolution of modular intraflagellar transport from a coatomer-like progenitor. *Proc Natl Acad Sci U S A* 110: 6943-6948

Van De Weghe JC, Gomez A, Doherty D (2022) The Joubert-Meckel-Nephronophthisis Spectrum of Ciliopathies. *Annu Rev Genomics Hum Genet* 23: 301-329

Vande Voorde J, Ackermann T, Pfetzer N, Sumpton D, Mackay G, Kalna G, Nixon C, Blyth K, Gottlieb E, Tardito S (2019) Improving the metabolic fidelity of cancer models with a physiological cell culture medium. *Sci Adv* 5: eaau7314

Vander Heiden MG, Cantley LC, Thompson CB (2009) Understanding the Warburg effect: the metabolic requirements of cell proliferation. *Science* 324: 1029-1033

VanderVorst K, Dreyer CA, Konopelski SE, Lee H, Ho HH, Carraway KL, 3rd (2019) Wnt/PCP Signaling Contribution to Carcinoma Collective Cell Migration and Metastasis. *Cancer Res* 79: 1719-1729

Vasudevan HN, Mazot P, He F, Soriano P (2015) Receptor tyrosine kinases modulate distinct transcriptional programs by differential usage of intracellular pathways. *Elife* 4

Vuolo L, Herrera A, Torroba B, Menendez A, Pons S (2015) Ciliary adenylyl cyclases control the Hedgehog pathway. *J Cell Sci* 128: 2928-2937

Wallace DP (2011) Cyclic AMP-mediated cyst expansion. *Biochim Biophys Acta* 1812: 1291-1300

Wang S, Zhang J, Nauli SM, Li X, Starremans PG, Luo Y, Roberts KA, Zhou J (2007) Fibrocystin/polyductin, found in the same protein complex with polycystin-2, regulates calcium responses in kidney epithelia. *Mol Cell Biol* 27: 3241-3252

Warburg O, Wind F, Negelein E (1927) The Metabolism of Tumors in the Body. *J Gen Physiol* 8: 519-530

Ward CJ, Hogan MC, Rossetti S, Walker D, Sneddon T, Wang X, Kubly V, Cunningham JM, Bacallao R, Ishibashi M *et al* (2002) The gene mutated in autosomal recessive polycystic kidney disease encodes a large, receptor-like protein. *Nat Genet* 30: 259-269

Ward CJ, Yuan D, Masyuk TV, Wang X, Punyashthiti R, Whelan S, Bacallao R, Torra R, LaRusso NF, Torres VE *et al* (2003) Cellular and subcellular localization of the ARPKD protein; fibrocystin is expressed on primary cilia. *Hum Mol Genet* 12: 2703-2710

Warner G, Hein KZ, Nin V, Edwards M, Chini CC, Hopp K, Harris PC, Torres VE, Chini EN (2016) Food Restriction Ameliorates the Development of Polycystic Kidney Disease. *J Am Soc Nephrol* 27: 1437-1447

Wheway G, Schmidts M, Mans DA, Szymanska K, Nguyen TT, Racher H, Phelps IG, Toedt G, Kennedy J, Wunderlich KA *et al* (2015) An siRNA-based functional genomics screen for the identification of regulators of ciliogenesis and ciliopathy genes. *Nat Cell Biol* 17: 1074-1087

Williams CL, Li C, Kida K, Inglis PN, Mohan S, Semenec L, Bialas NJ, Stupay RM, Chen N, Blacque OE *et al* (2011) MKS and NPHP modules cooperate to establish basal body/transition zone membrane associations and ciliary gate function during ciliogenesis. *J Cell Biol* 192: 1023-1041

Wingfield JL, Lechtreck KF, Lorentzen E (2018) Trafficking of ciliary membrane proteins by the intraflagellar transport/BBSome machinery. *Essays Biochem* 62: 753-763

Wong SY, Seol AD, So PL, Ermilov AN, Bichakjian CK, Epstein EH, Jr., Dlugosz AA, Reiter JF (2009) Primary cilia can both mediate and suppress Hedgehog pathway-dependent tumorigenesis. *Nat Med* 15: 1055-1061

Wu CT, Chen HY, Tang TK (2018) Myosin-Va is required for preciliary vesicle transportation to the mother centriole during ciliogenesis. *Nat Cell Biol* 20: 175-185

Xie YF, Shi WG, Zhou J, Gao YH, Li SF, Fang QQ, Wang MG, Ma HP, Wang JF, Xian CJ *et al* (2016) Pulsed electromagnetic fields stimulate osteogenic differentiation and maturation of osteoblasts by upregulating the expression of BMPRII localized at the base of primary cilium. *Bone* 93: 22-32

Yamamoto Y, Chino H, Tsukamoto S, Ode KL, Ueda HR, Mizushima N (2021) NEK9 regulates primary cilia formation by acting as a selective autophagy adaptor for MYH9/myosin IIA. *Nat Commun* 12: 3292

Yang C, Ko B, Hensley CT, Jiang L, Wasti AT, Kim J, Sudderth J, Calvaruso MA, Lumata L, Mitsche M *et al* (2014) Glutamine oxidation maintains the TCA cycle and cell survival during impaired mitochondrial pyruvate transport. *Mol Cell* 56: 414-424

Yang WT, Hong SR, He K, Ling K, Shaiv K, Hu J, Lin YC (2021) The Emerging Roles of Axonemal Glutamylation in Regulation of Cilia Architecture and Functions. *Front Cell Dev Biol* 9: 622302

Ye F, Nager AR, Nachury MV (2018) BBSome trains remove activated GPCRs from cilia by enabling passage through the transition zone. *J Cell Biol* 217: 1847-1868

Yeh C, Li A, Chuang JZ, Saito M, Caceres A, Sung CH (2013) IGF-1 activates a cilium-localized noncanonical Gbetagamma signaling pathway that regulates cell-cycle progression. *Dev Cell* 26: 358-368

Yoder BK, Hou X, Guay-Woodford LM (2002) The polycystic kidney disease proteins, polycystin-1, polycystin-2, polaris, and cystin, are co-localized in renal cilia. *J Am Soc Nephrol* 13: 2508-2516

Zemirli N, Boukhalfa A, Dupont N, Botti J, Codogno P, Morel E (2019) The primary cilium protein folliculin is part of the autophagy signaling pathway to regulate epithelial cell size in response to fluid flow. *Cell Stress* 3: 100-109

Zhang J, Dalbay MT, Luo X, Vrij E, Barbieri D, Moroni L, de Bruijn JD, van Blitterswijk CA, Chapple JP, Knight MM *et al* (2017a) Topography of calcium phosphate ceramics regulates primary cilia length and TGF receptor recruitment associated with osteogenesis. *Acta Biomater* 57: 487-497

Zhang J, Pavlova NN, Thompson CB (2017b) Cancer cell metabolism: the essential role of the nonessential amino acid, glutamine. *EMBO J* 36: 1302-1315

Zhang J, Tian XJ, Xing J (2016) Signal Transduction Pathways of EMT Induced by TGF-beta, SHH, and WNT and Their Crosstalks. *J Clin Med* 5

Zhang R, Tang J, Li T, Zhou J, Pan W (2022) INPP5E and Coordination of Signaling Networks in Cilia. *Front Mol Biosci* 9: 885592

Zhao H, Khan Z, Westlake CJ (2023) Ciliogenesis membrane dynamics and organization. *Semin Cell Dev Biol* 133: 20-31

Zhu D, Shi S, Wang H, Liao K (2009) Growth arrest induces primary-cilium formation and sensitizes IGF-1-receptor signaling during differentiation induction of 3T3-L1 preadipocytes. *J Cell Sci* 122: 2760-2768